

JAXA Special Publication

**Proceedings of International Symposium on  
“SM/MPAC&SEED Experiment”**

March 10-11, 2008

**International Congress Center EPOCHAL TSUKUBA,  
Tsukuba, Ibaraki, Japan**

March 2009

**Japan Aerospace Exploration Agency**

# CONTENTS

*Foreword by M. Suzuki (JAXA)*

*Introduction*     *Chairperson: K. Matsumoto (JAXA)*

**Japan's Materials Space Exposure Experiments before SM/MPAC&SEED**     1  
M. Suzuki, H. Shimamura, K. Imagawa (JAXA)

**SM/MPAC&SEED Experiment Overview**     5  
Y. Kimoto, J. Ishizawa, E. Miyazaki, M. Suzuki (JAXA)

*Space Environment of SM/MPAC&SEED*     *Chairperson: F. Urayama (SED)*

**Post Retrieval Analyses of Space Environment Monitoring Samples: Radiation Effects, UV,  
and Atomic Oxygen Fluence**     11  
Y. Kimoto, K. Yano, J. Ishizawa, E. Miyazaki (JAXA)

**Induced Contamination Predictions for JAXA's Micro-Particles Capturer and Space  
Environment Exposure Devices**     19  
C. Steagall, K. Smith, A. Huang, C. Soares, and R. Mikatariyan (The Boeing Company)

**Contamination Effect on SM/MPAC&SEED Experiment**     27  
N. Baba (JAMSS), Y. Kimoto (JAXA)

*New Polymeric Materials*     *Chairperson: T. Nakamura (Hokkaido University)*

**Thermal and environmental stability of polymeric materials  
- New generation, novel asymmetric aromatic polyimides -**     35  
R. Yokota (JAXA)

**MPAC Experiment**      *Chairperson: Y. Kimoto (JAXA)*

**Overview of the MPAC Experiment - Development of Dust Collector, Hypervelocity Impact Experiments, and Post Flight Analysis –**      49  
Y. Kitazawa (IHI Corporation), A. Fujiwara (Kansai University), T. Kadono (Nagoya University), T. Noguchi (Ibaraki University), R. Yamanaka, Y. Kimoto, M. Suzuki (JAXA)

**Initial Investigation of Silica Aerogel Equipped on SM/MPAC & SEED Recovered from the ISS in 2002, 2004, and 2005**      59  
T. Noguchi (Ibaraki University), T. Nakamura (Kyushu University), Y. Kitazawa (IHI Corporation), R. Yamanaka, Y. Kimoto, M. Suzuki (JAXA)

**Materials in Space -1**      *Chairperson: J. Ishizawa (JAXA)*

**Influence on Polymer Matrix Composite Exposed to Space Environment**      67  
Y. Arakawa (Fuji Heavy Industries LTD.)

**Effects of LEO Environment on Mechanical Properties of PEEK Films under Tensile Stress**      73  
T. Nakamura and O. Fujita (Hokkaido University)

**Effects of LEO Environment on Mechanical Properties of Polyimide Films under Tensile Stress**      81  
H. Shimamura (JAXA)

**Materials in Space -2**      *Chairperson: M. Tagawa (Kobe University)*

**NASA Glenn Research Center's Materials International Space Station Experiments (MISSE 1-7)**      91  
K. K. de Groh (NASA Glenn Research Center), B. A. Banks (Consultant, Alphaport, Inc.), J. A. Dever, D. A. Jaworske, S. K. Miller (NASA Glenn Research Center)

**Materials in Space -3**     *Chairperson: M. Iwaki (JAXA)*

- SM/SEED Space Exposure Experiment of Ball Bearing Lubricated by Tribo-Coating** 121  
K. Adachi (Tohoku University), K. Kato (Nihon University)
- Evaluation of MoS<sub>2</sub> Bonded Film Degradation on ISS SM-SEED Experiment** 127  
M. Akiyama (IHI Aerospace), M. Tagawa (Kobe University), K. Matsumoto (JAXA)
- Evaluation of Solid Lubricative Coatings after Space Environment Exposure Test** 131  
M. Tosa, A. Kasahara, M. Goto (National Institute for Materials Science)

**Materials in Space -4**     *Chairperson: M. Iwata (Kyushu Institute of Technology)*

- SM/SEED Experiments of Carbide and Nitride Ceramics for Three Years** 135  
O. Odawara (Tokyo Institute of Technology)
- Material Aging of Siloxane Coated Polyimide Film and Silicone Based White Paint on SM/SEED Exposure Experiments** 139  
J. Ishizawa (JAXA)
- Evaluation of F-OSR Exposed to Space on SM/SEED Experiment** 149  
E. Miyazaki, J. Ishizawa, H. Shimamura (JAXA)
- Evaluation of Silicone Potting Compound and Silicone Adhesive Exposed to Space on SM/SEED Experiment** 155  
E. Miyazaki, K. Mori, J. Ishizawa, H. Shimamura (JAXA)

**On-going & Future plan**     *Chairperson: M. Tosa (National Institute for Materials Science)*

- MEDET in-Flight Experiment: Description and First Results** 161  
V. Inguibert, S. Duzellier, JM Siguier (ONERA), A. Tighe, M. V. Eesbeek (ESA/ESTEC)
- Status of JEM/MPAC&SEED Experiment Onboard SEDA-AP on Kibo Exposed**



**Facility** 167  
S. Ichikawa, Y. Kimoto, E. Miyazaki, K. Kubo, K. Yano, K. Matsumoto, J. Ishizawa, H. Shimamura, R. Yamanaka, M. Suzuki (JAXA)

**Future Space Exposure Experiment beyond 2011 -Its Problems and New Challenges** 171  
M. Tagawa (Kobe University)



(c)Roskosmos/RSC-Energia

ISS and MPAC&SEED from STS-110 flight (April, 2002)



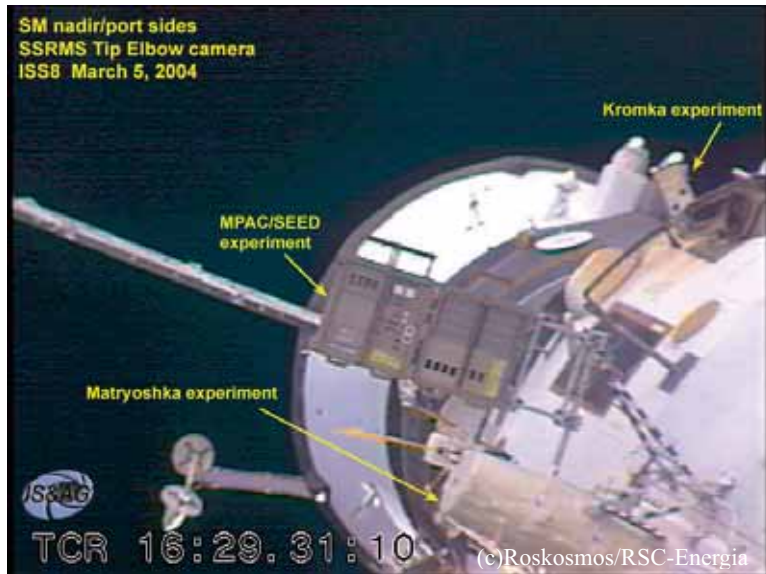
(c)Roskosmos/RSC-Energia

ISS and MPAC&SEED from STS-110 flight (April, 2002)



(c)Roskosmos/RSC-Energia

ISS and MPAC&SEED from STS-113 flight (December, 2002)



(c)Roskosmos/RSC-Energia

Copy of MCC display in Moscow (March, 2004)



(c)Roskosmos/RSC-Energia

MPAC&SEED and Earth in the third EVA (August, 2005)





Participants photo of International Symposium on “SM/MIPAC&SEED Experiment” (March 11, 2008)

## FOREWORD

International Symposium on “SM/MPAC&SEED (Service Module/Micro Particles Capturer and Space Environment Exposure Device) Experiment” was held on March 10-11, 2008 at International Congress Center (Epochal Tsukuba), in Tsuba, Ibaraki, JAPAN. In the Symposium, 22 papers are presented, including three key-note presentations.

The SM/MPAC&SEED, consisted of three identical sample units, was launched to ISS (International Space Station) by Progress on August 2001, and attached on the exterior surface of the Russian Service Module(SM) on October 2001. Each sample unit contained various materials to capture micro-particles and to examine the effects of space environment effects.

The first unit was retrieved into inside the ISS by EVA (Extra-Vehicular Activity) on August 2002, and returned to the Earth on November 2002. The second unit was retrieved on February 2004, and returned to the Earth on April 2004. The final unit was retrieved on August 2005, and returned to the Earth on October 2005. All the units were successfully retrieved, and the analyses of the samples have been conducted. The unique feature of this experiment is that the identical samples were retrieved changing the space exposure duration.

Symposia on SM/MPAC&SEED experiment have been held on March 2004, and on February 2006 for first and second retrieved samples, respectively. In the present, final Symposium, summarizing results of the SM/MPAC&SEED experiment for all the retrieved samples were reported.

Analysis results are sometimes confusing and/or contradicted each other in some cases. One cause of this is that the material degradation process is complex phenomena, in which numerous factors are involved, such as atomic oxygen, ultraviolet rays, radiation, contaminants and so on. To understand the space environment effects exactly based on the limited data, exchange of information and experiences, and discussions among the related researchers are mandatory. In this Symposium, the discussions among the participants were active, and in-depth. I believe the Symposium contributed for the advances in this disciplines.

March, 2008

JAXA, Institute of Aerospace Technology  
Electronic, Mechanical Components and Materials Group

Mineo SUZUKI

## JAPAN'S MATERIALS SPACE EXPOSURE EXPERIMENTS BEFORE SM/MPAC&SEED

Mineo SUZUKI<sup>1</sup>, Hiroyuki SHIMAMURA<sup>1</sup> and Kichiro IMAGAWA<sup>2</sup>

<sup>1</sup> *Institute of Aerospace Technology, Japan Aerospace Exploration Agency, Tsukuba, Ibaraki 305-8505, Japan*

<sup>2</sup> *Human Space Systems and Utilization Mission Directorate, Japan Aerospace Exploration Agency, Tsukuba, Ibaraki 305-8505, Japan*

Overview of Japan's materials space exposure experiments before SM/MPAC&SEED is presented. They are EOIM-3, EFFU and ESEM. EOIM-3 and ESEM experiments were carried out on board the Space Shuttle, while EFFU was mounted on SFU free flyer. In these experiments, there were many valuable findings, but contradictory phenomena were sometimes observed for similar materials, possibly due to the differences of the space environment and the specimens experiment-by-experiment. These experiences greatly contributed to planning and successful completion of SM/MPAC&SEED experiment.

**Keywords:** Materials space exposure experiments, EOIM-3, EFFU, ESEM

### 1. Introduction

Space is harsh environment for materials. Materials might be degraded by space environments such as radiation, ultraviolet (UV) rays, atomic oxygen (AO), thermal cycling and so on. Thus the effects of these environment factors on various materials have been examined in simulated ground-based tests, as well as space exposure experiments.

Space Shuttle opened new era for materials space exposure experiments. The exposed samples can be easily retrieved and detailed analysis is possible on ground. Meanwhile, Space Shuttle demonstrated necessity of materials space exposure experiment: serious AO effect was recognized in Low Earth Orbit (LEO) in early flights (e.g. Ag was blackened by AO during 1 week exposure). Later, combined effect of AO and UV became clear on some materials, but ground simulation technique was not yet established. ISS (International Space Station) program urged evaluation of materials degradation by long duration exposure to LEO environment. Thus a number of materials space exposure experiments were carried out, including EOIM (Evaluation of Oxygen Interaction with Materials), LDEF (Long Duration Exposure Facility) and EURECA (European Retrievable Carrier).

After construction of early phase of ISS, materials space exposure experiments were carried out almost on the ISS, such as MISSE (Materials International Space Station Experiment), and SM/MPAC&SEED (Service Module/ Micro -Particles Capturer and Space Environment Exposure Device). ISS is suitable for long duration experiments.

Japan had conducted three materials space exposure experiments before SM/MPAC&SEED experiment. They are:

- EOIM-3 (Evaluation of Oxygen Interaction with Materials - 3)
- EFFU (Exposed Facility Flyer Unit) on SFU (Space Flyer Unit)
- ESEM (Evaluation of Space Environment and Effects on Materials) on MFD (Manipulator Flight Demonstration)

In this paper, overview of these experiments is presented.

### 2. EOIM-3

Launched on STS-46 (Atlantis) on July 31, 1992, EOIM-3 pallet containing 46 Japan's samples (26 kinds) were exposed to the space environment, and returned to the Earth on Aug.8, 1992. EOIM-3 was Japan's first materials space exposure experiment. EOIM was NASA's materials space exposure project [1], and Japan participated in the NASA project. The objective of Japan's experiment was to confirm the phenomena occurred on the material surface induced by space exposure, and to pursue the degradation mechanisms, mainly due to atomic oxygen.

The overview of EOIM-3 experiment is shown in Fig.1. The samples were typical materials already used for Japanese satellites, and to be used for JEM (Japanese Experiment Module) of ISS. The exposed samples were:

- Thermal control film & paint : 11 kinds, 19 samples
- Structural materials: 3 kinds, 8 samples
- Insulating materials: 4 kinds, 7 samples
- Adhesives: 3 kinds, 5 samples
- Optical materials: 5 kinds, 7 samples

The estimated environments for about 1 week flight were:

- AO Fluence
  - Thermospheric model:  $2.0\text{-}2.2 \times 10^{20}$  atoms/cm<sup>2</sup>
  - Kapton erosion:  $2.3\text{-}2.5 \times 10^{20}$  atoms/cm<sup>2</sup>
  - Mass spectrometer:  $2.2 \pm 0.4 \times 10^{20}$  atoms/cm<sup>2</sup>
- UV Fluence
  - 25 ESH (Equivalent Solar Hours)
- Temperature
  - 5°C-20°C during exposure period
- Contamination
  - 2 nm thickness silicone

Retrieved samples were examined by using surface analysis techniques such as SEM(Scanning Electron Microscope), XPS(X-ray Photoelectron Spectroscopy), AES(Auger Electron Spectroscopy), FTIR(Fourier Transform InfraRed spectroscopy), SIMS(Secondary Ion Mass Spectrometry), focusing on the effect of AO. AO erosion yields of several materials were compared with the reported values.

The observed degradation phenomena were similar with that in



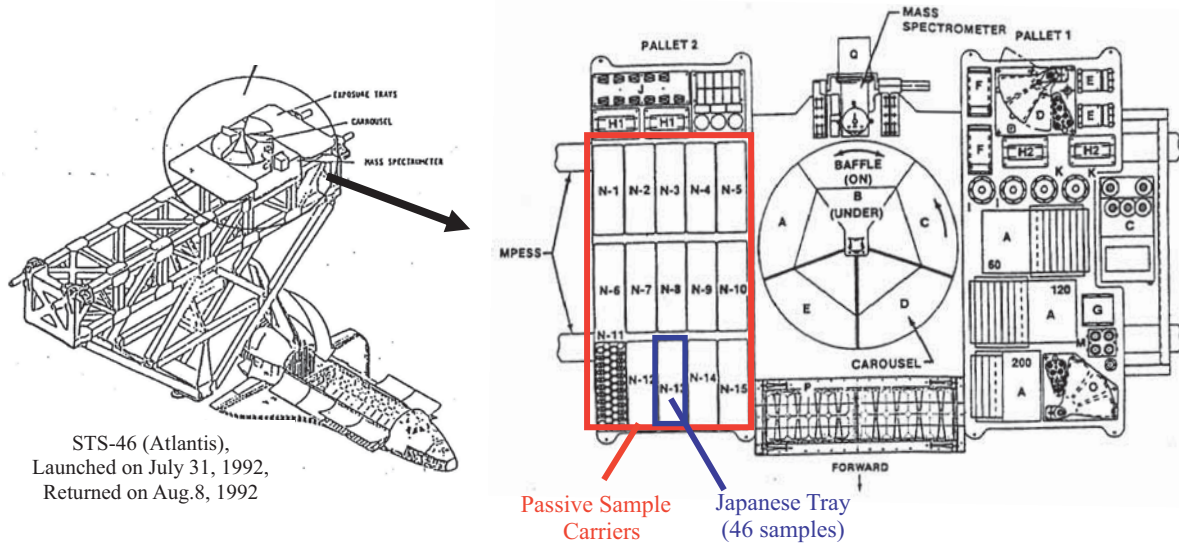


Fig.1 Overview of EOIM-3 experiment

the other EOIM experiments, and with that caused by ground-based atomic oxygen (AO) irradiation. The importance of AO effects on materials was recognized.

The degradation mechanisms were also pursued. But available data were too limited to elucidate the mechanisms. In addition, some samples showed different results from the former experiments. The major findings of the experiment are reported in ref. [2].

3. EFFU

EFFU was attached to exterior of SFU, and launched on March, 1995 by H-2 rocket. After 10 months flight in 482 km orbit, SFU was retrieved into STS-72 (Endeavour) on January, 1996. EFFU was Japan's first long duration materials space exposure experiment. The major purpose of the experiment was to confirm the adequacy of materials design for JEM-EF (Japanese Experiment Module - Exposed Facility) to be jointed to ISS. The overview of EFFU experiment is shown in Fig.2.

EFFU carried following 22 kinds of samples.

- Solid lubricant: 7 kinds
- CFRP: 3 kinds
- Cover glass: 2 kinds
- Anodized aluminum: 4 kinds
- Thermal control film & paint :5 kinds
- Insulating materials: 1 kind

Unique samples were solid lubricant films. JEM-EF has moving mechanical components, which will be partly exposed directly to space environment.

Accumulated fluxes of UV and AO for about 10 month's exposure were estimated by using monitoring materials, as follows:

- AO Fluence
  - +Z:  $2.5 \times 10^{19}$  atoms/cm<sup>2</sup>
  - X:  $4.7 \times 10^{19}$  atoms/cm<sup>2</sup>
- UV Fluence
  - +Z: very small
  - X: 150 ESD (Equivalent Solar Days)

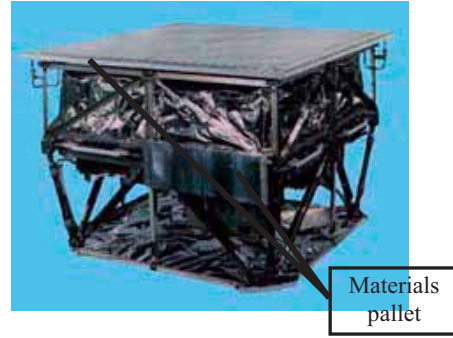
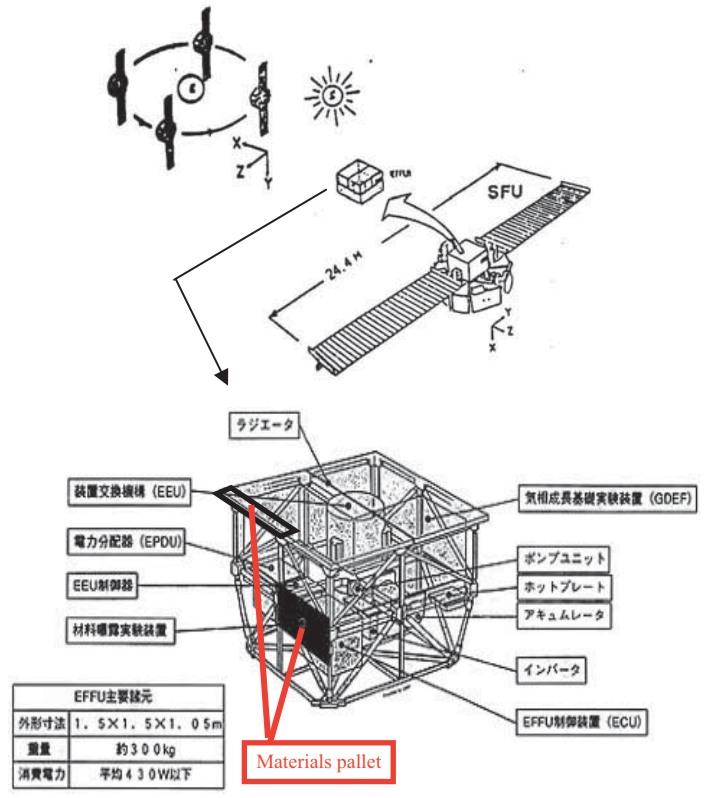


Fig.2 Overview of EFFU experiment

EFFU Sample analysis revealed that the degradation was similar with that in other space exposure experiments, and with that in ground-based simulation experiments (e.g. erosion of PTFE in  $\beta$ -cloth). The degradation was within the design margin, thus the soundness of JEM materials design was confirmed.

The exposed solid lubricant film showed longer wear life, possibly due to hardening of the organic binder material by UV. It was pointed out, however, that further hardening may cause rupture of the film. Contamination of  $\text{SiO}_x$  was identified. It is recognized that effects of the contamination should be included to evaluate the effect of actual space environment on materials.

This experiment gave the first insight of long-term space exposure effect on materials for Japanese researchers. The major findings of the experiment are reported in refs. [3][4].

#### 4. ESEM

ESEM pallet containing 29 kinds of samples was attached on the support structure of MFD, and launched on STS-85 (Discovery) on Aug.7, 1997. After about 12 day's exposure, ESEM was returned to the Earth on Aug.19, 1997. ESEM was a follow-on experiment to confirm soundness of JEM materials design. Figure 3 shows the location of ESEM pallet and the appearance of ESEM sample trays.

The exposed samples were:

- Solid lubricant: 7 kinds
- Solar cell: 2 kinds
- Cover glass: 4 kinds
- Adhesives: 3 kinds
- Thermal control film & paint :9 kinds
- Insulating materials: 1 kind
- Inter-connector materials: 3 kinds

In addition, 6 kinds of samples were attached on the sample tray for the evaluation of the exposed environment such as radiation, atomic oxygen, and ultra violet flux.

Accumulated fluxes of UV and AO for about 12 day's exposure were estimated as follows:

- AO Fluence  
 $3.0 - 9.7 \times 10^{19}$  atoms/cm<sup>2</sup> (depended on the location)
- UV Fluence  
 1.8 -2.7 ESD (depended on the location)

Analysis of the retrieved samples gave similar results with the former space exposure experiments. In a follow-up experiment of solid lubricant films, binder itself was exposed. The binder was eroded away, but never hardened. The effect of space environment might be different between composite materials and their constituents. Contamination of organic materials as well as  $\text{SiO}_x$  was detected.

Detailed analysis results of the retrieved samples are summarized in ref. [5].

#### 5. Concluding remarks

In EOIM-3, SFU/EFFU, and MFD/ESEM experiments, there are many valuable findings. However, the effect of space environment on materials and the degradation mechanism are still obscure, especially for the combined effect (e.g. AO+UV, AO+contaminants). In addition, contradictory phenomena were sometimes observed for similar materials, possibly due to the

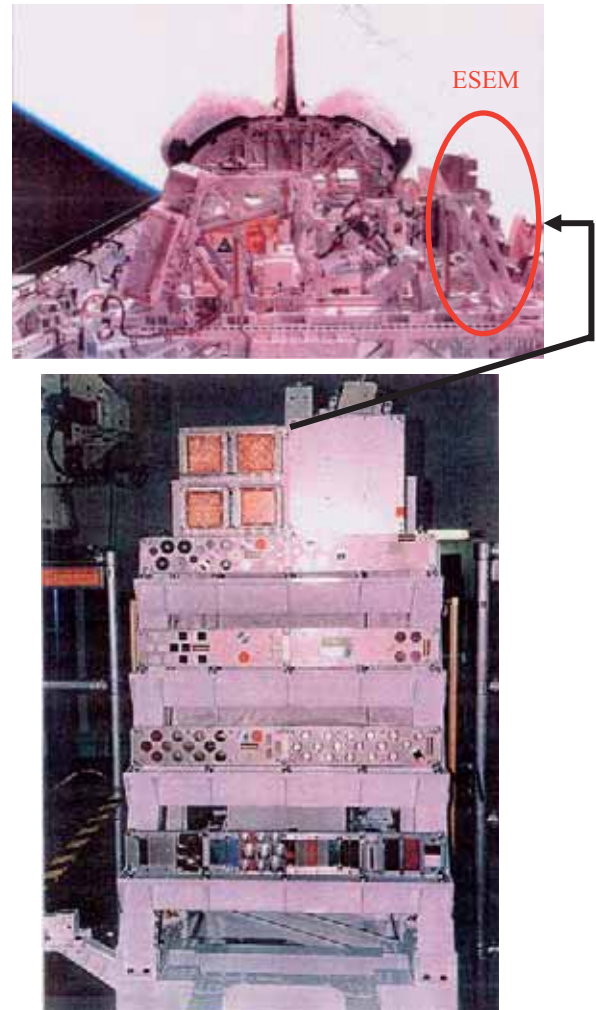


Fig.3 ESEM sample trays and mounted location

difference of space environment experiment-by-experiment (orbit, attitude of the sample tray and duration). Apparently further experiments are needed to fully understand the effect of space environment on materials.

In SM/MPAC&SEED experiment the same 3 sample sets were exposed to the same space environment, but different exposure duration (about 1, 2, and 3 years), to grasp the degradation process more precisely. This method is effective to deduce the degradation process by the space environment. The detailed experimental results of SM/MPAC&SEED are reported in other papers in this proceedings.

ISS is now being utilized for materials space exposure experiments such as MISSE, EuTEF/MEDET (European Technology Exposure Facility/ Material Exposure and Degradation Experiment) and, in the near future, JEM /MPAC&SEED. However, opportunity of materials space exposure experiment is still limited. In these circumstances, cooperation and information exchange among researchers and engineers related to space environment effect on materials will be mandatory.

#### References

- [1] D.E. Brinza et al: Final report on the NASA/JPL Evaluation



- of Oxygen Interactions with Materials-3 (EOIM-3), NASA CR-198865 (1994).
- [2] Analysis of the exposed samples- EOIM-3 experiment, Contractor report, Toshiba SPD15-K93078 (1993). (in Japanese)
- [3] M. Takei, Y. Torii et al.: Space environmental effects on space exposure materials of EFFU, Proc. 47th IAC, IAF-96-1.5.01 (1996)
- [4] T. Fukatsu, Y. Torii, Y. Koyari et al.: Post-flight analysis of the exposed materials on EFFU, Proc. 7th ISMSE, ESA SP-399 (1997) 287.
- [5] Evaluation and Analysis of Parts and Materials installed on MFD-ESEM, NASDA Technical Memorandum NASDA-TMR-000011 (2001)

## SM/MPAC & SEED Experiment Overview

Yugo Kimoto, Junichiro Ishizawa, Eiji Miyazaki, Mineo Suzuki

*Institute of Aerospace Technology, Japan Aerospace Exploration Agency,  
Tsukuba, Ibaraki 305-8505, Japan*

A space materials exposure experiment was performed on the International Space Station (ISS) using the Micro-Particles Capturer and Space Environment Exposure Device (MPAC&SEED) developed by the Japan Aerospace Exploration Agency (JAXA). The experiment was executed on the exterior of the Russian Service Module (SM) of the ISS. The SM/MPAC&SEED consists of the MPAC, which captures space debris, and SEED, which exposes polymeric materials, paint, adhesives, bearings, and compound materials. Three identical MPAC&SEED units were launched on 21 August 2001. The three units were retrieved individually after exposure of 315 days (about 10 months), 865 days (about 28 months), and 1403 days (about 46 months). This paper presents an overview of the SM/MPAC&SEED project and experiment.

**Keywords:** SM/MPAC&SEED, ISS Service Module

### 1. Introduction

Space environment effects on materials are very severe and complex because orbital environments include factors such as high-energy radiation particles, atomic oxygen (AO), micro-level particles, and UV irradiation. In addition, surface degradation associated with contamination can negatively impact optics performance. The space environment and data related to its effects are therefore very important for spacecraft design. The National Space Development Agency of Japan (NASDA), the forerunner of the Japan Aerospace Exploration Agency (JAXA), implemented the space materials exposure experiment on the space shuttle and the ISS. The Russian Service Module (SM)/ Micro-Particle Capturer and Space Environment Exposure Device (MPAC&SEED) experiments were executed on the exterior of the SM of the ISS.

### 2. History of space materials exposure experiments

Since the first space shuttle launch in the 1980s, research of the characteristics of materials in space environments has shifted from evaluation of data collected by telemetry to that of materials exposed in a real space environment and returned to the ground. NASA implemented space materials exposure experiments using both the space shuttle cargo bay and spacecraft launched to space from the space shuttle and retrieved by the space shuttle after a long period. NASA's Long Duration Exposure Facility (LDEF) can gather important results related to the interaction between materials and the space environment because of the large number of deployed samples and the long exposure period [1–3]. The Low Earth Orbit (LEO) space environment is known to have severe effects on spacecraft materials and coatings, so contamination should be an important consideration in spacecraft design.

Japan launched the Exposed Facility Flyer Unit on the Space Flyer Unit (SFU/EFFU) [4], and performed the Evaluation of Oxygen Interaction with Materials-3 (EOIM-3) in 1992 [5] and the Evaluation of Space Environment and Effects on Materials aboard the Manipulator Flight Demonstrator (MFD/ESEM) [6] on space shuttles in 1997. Results of these experiments show that AO irradiation was the most important cause of material

degradation in the LEO environment [7].

### 3. Service Module (SM) / Micro-Particles Capturer and Space Environment Exposure Device (MPAC&SEED)

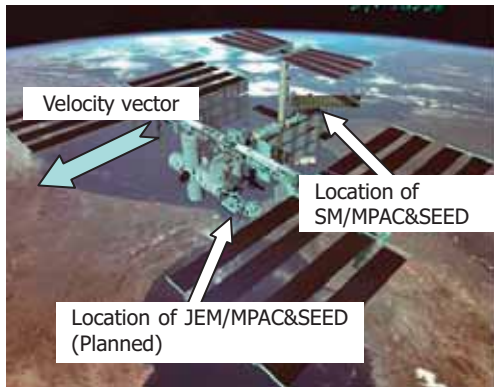
#### 3.1 Overview

The SM/MPAC&SEED experiments are space exposure experiments on the exterior of the Russian Service Module of the ISS. The most unique aspect of the SM/MPAC&SEED experiments is that three identical components were manufactured; the three were exposed simultaneously, and each was retrieved individually after different periods of time. It was the world's first such trial. This method can compare aging deterioration of materials at virtually the same position. Another unique feature is that samples capture micrometeoroid and space debris. This MPAC is a passive experiment designed to sample the micro-meteoroid and space-debris environment and to capture particle residue for later chemical analyses using aerogel, polyimide foam, and 6061-T6 aluminum plate[8]. Another point is that some samples are arranged on both the ram and wake sides. This method should demonstrate the effect of AO, which collides with and erodes materials on the front and back of the spacecraft.

Two MPAC & SEED projects exist. One is for the Japanese Experiment Module Exposed Facility (JEM/EF) on the ISS. The other is for the Service Module (SM) on the ISS [9]. The MPAC & SEED on the JEM/EF (hereinafter JEM/MPAC&SEED) is an instrument of the Space Environment Data Acquisition equipment – Attached Payload (SEDA-AP) [10]. In fact, SEDA-AP has seven sensors that measure neutrons, plasma, heavy ions, high-energy light particles, atomic oxygen, cosmic dust, and their effects. This project began in 1997.

Actually, SM/MPAC&SEED was expected to encounter a different artificial space environment than JEM/MPAC&SEED because the SM is located at the rear of the ISS and JEM is scheduled to be attached at the front (see Fig. 1). Contamination from obstacles and the thruster is expected to be much lower at the front of the ISS than at the rear. Comparing results of the two missions provides a complementary analysis of contamination

effects on material degradation that are dependent on location.



**Fig. 1 Illustration of the ISS and location of both SM/MPAC&SEED and JEM/MPAC&SEED.**

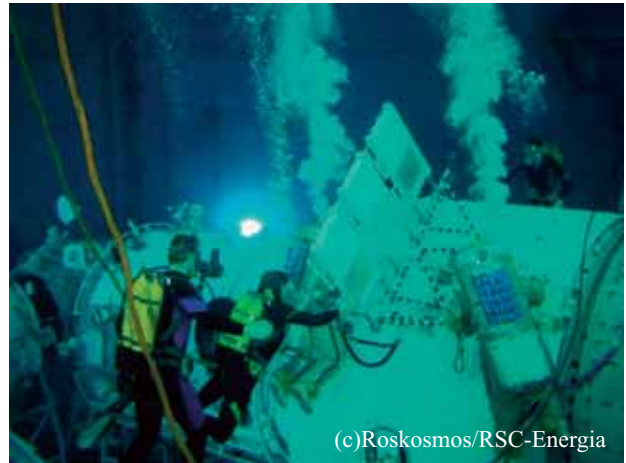
**3.2 History of the SM/MPAC&SEED development**

In September 1998, NASDA began consulting with the Russian Federal Space Agency (Roskosmos) about utilization of the Russian SM as a precursor mission to JEM & JEM/EF. An implementation plan was developed, and a contract for multipurpose experiment projects for MPAC&SEED and High Definition Television (HDTV) was signed in June 1999 [11]. In addition, NASDA began to develop SM/MPAC&SEED in early 1999. Figure 2 presents the schedule of SM/MPAC&SEED development in Russia and Japan.

	1999	2000	2001	2002
Russia			PSR ▲ January EVA Crew training	▲ Launch 21 August ▼ #1 Retrieval ▲ May IVA Crew training
Japan	Specific Design PFM IVA training Model	CDR Manufacture PFT	PSR	Ground support in launch site

**Fig. 2 Schedule of the SM/MPAC&SEED development**

Some photographs of the development phase are shown. Figure 2 shows an External Vehicle Activity (EVA) training scene in Gagarin Cosmonauts Training Center (GCTC) in January 2001. Figure 3 depicts a SM/MPAC&SEED launch container in a sterilization room in the Baikonur Cosmodrome immediately before launch.



**Fig. 3 EVA training in GCTC**



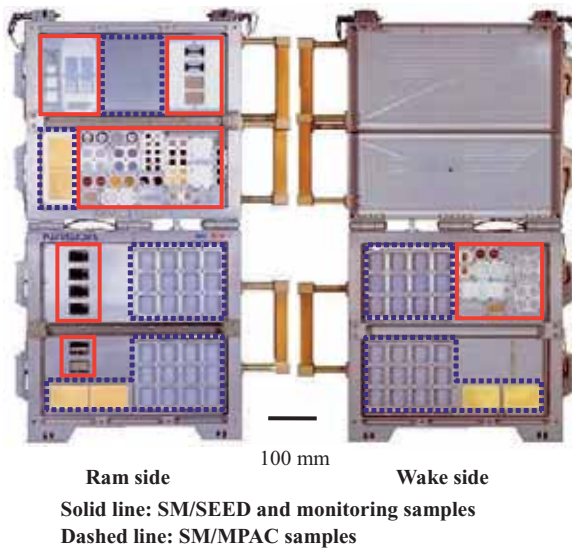
**Fig. 4 A SM/MPAC&SEED launch container in sterilization room immediately before launch**

**3.3 System description in the orbit**

The overall dimensions of a flight SM/MPAC&SEED unit are W570 mm × H900 mm × D158 mm. Figure 5 depicts one unit of SM/MPAC&SEED. Ram and wake sides of the unit correspond to the ram and wake directions of the ISS. Samples are installed on holders stored in the SM/MPAC&SEED. Sample holders can be extracted from the SM/MPAC&SEED to reduce the return weight. The sample holder was packaged by an ISS astronaut and returned to the ground by a Soyuz spacecraft. Three identical SM/MPAC&SEED units (MPAC&SEED #1, #2, and #3) were flown and attached to the SM.

**3.3.1 MPAC experiment**

The MPAC is a passive experiment designed to sample micrometeoroids and space debris. Samples of three types were prepared to capture and measure micro-particles for MPAC. Silica-aerogel (hereinafter, aerogel) is a transparent and porous solid with nanosized holes. It is used for intact capturing of dust particles and also used for estimations of impact parameters (incident direction, particle diameter, and impact velocity) based on the impact track morphology. Polyimide foam was prepared to capture large debris. An aluminum plate was used to record the number of impacts from space debris and micrometeoroids.



**Fig. 5** An SM/MPAC&SEED unit with both front (Ram side) and back (Wake side) shown.

### 3.3.2 SEED experiment

The SEED is a space material exposure experiment. The SEED consists of 28 samples, as outlined in Table 1. Samples were proposed by JAXA, universities, and companies in Japan and were selected by JAXA based on the frequency of use and prospective future use [12–14]. The SEED experiment also includes space environment monitoring samples, which monitor the total dose of AO, UV, space radiation, and temperature [15].

**Table 1** SEED samples

Sample name	Organization	Main Use
CF/polycyanate, PIXA	Fuji Heavy Industries Ltd.	Structural materials
PEEK (loaded & unloaded)	Hokkaido University	Deployable structures
AIN	Tokyo Institute of Technology	Structural and functional materials
SiC (reaction sintering / Hot pressed)		
TiN-coated Al / Al <sub>2</sub> O <sub>3</sub>		
Ball-bearing (3 types)	Tohoku University	Mechanism application
SUS304	National Institute for Materials Science	Lubrication
Cu- / SUS304		
MoS <sub>2</sub> coated Ti alloy	IHI Aerospace	Lubrication
Loaded & unloaded polyimide film (UPILEX-S)	Japan Aerospace Exploration Agency	Deployable structures
Modified polyimide film		Thermal control
Flexible OSR		Thermal control
White paint		Thermal control
Adhesive		Adhesion
Potting compound		Potting

### 3.3.4 SM/MPAC&SEED launch & operation

Three identical SM/MPAC&SEED units (SM/MPAC&SEED #1, #2, and #3) were flown and attached to the SM. The SM/MPAC&SEED was launched aboard a Progress M-45 on 21 August, 2001. The SM/MPAC&SEED was unpacked and constructed during Intra Vehicular Activity (IVA) (see Fig. 6). At 09:17 UT on 15 October 2001, all three units were mounted on the handrail outside the SM by extra-vehicular activity (EVA) (see Fig. 7). On 26 August 2002, the first unit of SM/MPAC&SEED, SM/MPAC&SEED #1, was retrieved by EVA after 315 days of on-orbit exposure. Figure 8 portrays the EVA for deconstructing SM/MPAC&SEED #1. Figure 9 shows

the configuration of the SM/MPAC&SEED after the EVA. Subsequently, SM/MPAC&SEED #2 was retrieved on 26 February 2004 (after 865 days). Later, SM/MPAC&SEED #3 was repositioned to the location that had been occupied by MPAC&SEED #2. Figure 10 depicts the SM/MPAC&SEED configuration after this second EVA. Finally, SM/MPAC&SEED #3 was retrieved on 18 August 2005 (after 1403 days) (see Fig. 11). All SM/MPAC&SEED holders arrived on the ground in the Republic of Kazakhstan and were moved to Moscow. A primary check was performed there before transport to Japan. Figure 12 shows the third primary check out scene in October 2005.



**Fig. 6** IVA for SM/MPAC&SEED construction

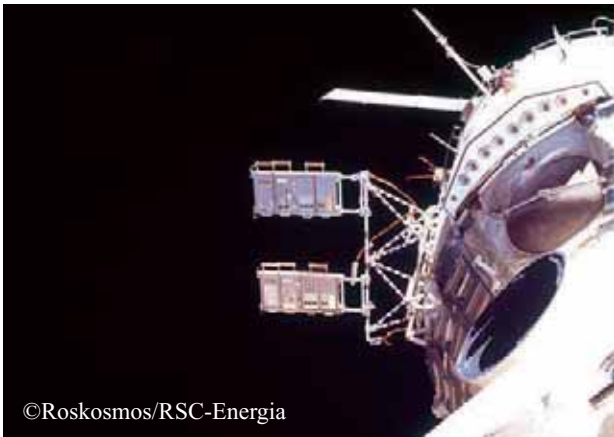


**Fig. 7** Orbit configuration of the entire MPAC&SEED (October 2001)





**Fig. 8** EVA for deconstructing SM/MPAC&SEED #1 (August 2002)



**Fig. 9** Orbit configurations of MPAC& SEED #2 & #3 (August 2002)



**Fig. 10** Orbit configuration of the MPAC& SEED #3 and other external payloads (February 2004)



**Fig. 11** Removal of the MPAC& SEED #3 from the ISS by an astronaut, who is visible on the right. (August 2005).



**Fig. 12** Primary check-out in Moscow after retrieval (October 2005).

Three sets of the retrieved samples were analyzed. The first conference on the post retrieval analysis results was held on 8 March 2004 [16]. The second conference was held on 21 January 2006 [17]. Finally, the third conference, the international symposium for comprehensive analysis for all retrieved samples, was held in 10–11 March 2008.

#### 4. Summary and conclusions

A unique space material exposure experiment, the SM/MPAC&SEED experiment, was conducted. For this experiment, three identical components were manufactured: the three were exposed simultaneously; each was retrieved individually after a different period of time. It was the world's first such trial. This method can compare aging deterioration of materials placed at almost the same position.

Analysis results are reported in this special publication.

#### Acknowledgments

The authors would like to thank Mr. Mitsuyasu Kato in JAXA, Ms. Chie Saito, of JAXA at that time, Mr. Ichiro Yamagata, who is currently in the Japan Atomic Energy Agency and Mr. Akitoshi Yokota of JGC Corp. for their support and

progress on this project. The authors would also like to thank Ms. Yukiko Yamaura in IHI Aerospace Co., Ltd. for development and primary check out. We appreciate the work of all people involved in the development and operation of the SM/MPAC&SEED experiment.

### References

- [1] Stein B. A. and Young P. R, LDEF Materials Data Analysis Workshop, NASA CP-10046, 1990.
- [2] Levine A. S., LDEF-69 Months in Space 1st Post-Retrieval Symposium, NASA CP-3134, 1992.
- [3] Levine A. S., LDEF-69 Months in Space 2nd Post-Retrieval Symposium, NASA CP-3194, 1993.
- [4] Fukatsu Tsutomu et al., “Post-flight Analysis of the exposed materials on the EFFU”, Proc. of the 7th Symposium of Materials in a Space Environment, pp. 287-292, 1997
- [5] Scialdone J. J. et al., “Atomic Oxygen and Space Environment Effects on Aerospace Materials Flown with EOIM-III Experiment”, NASA TM-104636, 1996.
- [6] <http://matdb.jaxa.jp/SpaceExperiment/Image/MFD-ESEM-E.pdf>
- [7] Silverman E.M., “Space Environmental Effects on Spacecraft: LEO Materials Selection Guide”, NASA CP-4661, 1995.
- [8] Michael J. Neish, et al., “Passive Measurement Of Dust Particles on the ISS Using MPAC: Experiment Summary, Particle Fluxes And Chemical Analysis”, Proc. of the Fourth European Conference on Space Debris, Darmstadt, Germany, 18–20 April 2005 (ESA SP-587, August 2005)
- [9] Tachi Y. et al., “Outline of space environment exposure experiment on ISS”, Proc. of the 22nd International Symposium on Space Technology and Space, pp. 1455-1459, 2000.
- [10] Koga K. et al., “Space environment data acquisition equipment – attached payload on the international space station”, COSPAR Colloquia Series Vol. 14, "Solar-Terrestrial Magnetic Activity and Space Environment" Edited by H. Wang, R. Xu, pp. 365-366, 2002.
- [11] Igor Sorokin et al., “Japanese-Russian cooperation on International Space Station now and in the future”, IAC-05-B4.3.03, 56th IAC, 2005.
- [12] Ichiro Yamagata, et al., “Overview of the micro-particles capturer and space environment exposure device (MPAC&SEED) experiment”, Proc. of the 10th International Symposium on “Materials in a Space Environment” (ISMSE) and 8th International Space Conference on “Protection of Materials and Structures from the Space Environment” (ICPMSE), June 2006.
- [13] Imai Fumikazu, Imagawa Kichiro, “NASDA’s Space Environment Exposure Experiment on ISS – First Retrieval of SM/MPAC&SEED –”, Proc. of the 9th Symposium of Materials in a Space Environment, pp. 589–594, June 2003.
- [14] Yugo Kimoto, Ichiro Yamagata, Junichiro Ishizawa, Eiji Miyazaki, Naoko Baba, and Mitsuyasu Kato, “Japanese Space Materials Exposure Experiment Utilizing International Space Station”, IAC-06- B4.3.08, 57th IAC, 2006.
- [15] Yugo Kimoto, Keiichi Yano, Junichiro Ishizawa, Eiji Miyazaki, and Ichiro Yamagata, “Passive measurement of atomic oxygen, UV fluence, and radiation effect on the ISS using the SEED experiment”, Proc. of the 10th International Symposium on “Materials in a Space Environment” (ISMSE) and 8th International Space Conference on “Protection of Materials and Structures from the Space Environment” (ICPMSE), June 2006.
- [16] Proc. on “International Space Station Russian Service Module (SM) / MPAC & SEED 1st Post – Retrieval conference (in Japanese), (2004).
- [17] Proc. on “International Space Station Russian Service Module (SM) / MPAC & SEED 2nd Post – Retrieval conference ((in Japanese), JAXA-SP-06-021 (2007).

**Publications related SM/MPAC&SEED**

Yoshiaki Tachi, Kichiro Imagawa, Youichi Nakayama, and Chiaki Kamakura et al., “Outline of space environment exposure experiment on ISS”, Proc. of the 22nd International Symposium on Space Technology and Space, pp. 1455–1459, 2000.

Imai Fumikazu and Imagawa Kichiro, “NASDA’s Space Environment Exposure Experiment on ISS – First Retrieval of SM/MPAC&SEED –”, Proc. of the 9th Symposium of Materials in a Space Environment, pp. 589–594, June 2003.

Toshihiko Inoue, et al., “Evaluation and Analysis of the First-Retrieved Unit of the Space Environment Exposure Device (SM/MPAC&SEED)”, Proc. of the 24th International Symposium on Space Technology and Space, (CD-ROM), 2004.

Toshihiko Inoue, et al., “Evaluation and Analysis of the First-Retrieved sample of the Space Environment Exposure Device (SM/MPAC&SEED)” (in Japanese), 20th Japan Society of Microgravity Application (JASMAC-20), 2004.

Ichiro Yamagata, et al., “Overview of the micro-particles capturer and space environment exposure device (MPAC&SEED) experiment”, Proc. of the 10th International Symposium on “Materials in a Space Environment” (ISMSE) and 8th International Space Conference on “Protection of Materials and Structures from the Space Environment” (ICPMSE), June 2006.

Kazuyuki Mori, Hiroyuki Shimamura, Takashi Nakamura, and Mineo Suzuki, “Evaluation of Space Materials by Space Environment Exposure Device ” (in Japanese), Transactions of the Japan Society for Aeronautical and Space Sciences, Vol.54, No.633, pp.298-305, 2006.

Ichiro Yamagata, Hiroyuki Shimamura, and Eiji Miyazaki, “Evaluation of 2nd retrieved samples for micro-particles capturer and space environment exposure device on the Russian service module (SM/MPAC&SEED) of the international space station”, (in Japanese), Proc. of the Joint Work Shop of IAT and ISAS in JAXA, 2006.

Yugo Kimoto, Ichiro Yamagata, Junichiro Ishizawa, Eiji Miyazaki, Naoko Baba, and Mitsuyasu Kato, “Japanese Space Materials Exposure Experiment Utilizing International Space Station”, IAC-06- B4.3.08, 57th IAC, 2006.

Yugo Kimoto, Mineo Suzuki, Ichiro Yamagata, Eiji Miyazaki, Junichiro Ishizawa, Naoko Baba, Kazuyuki Mori, and Hiroyuki Himamura, “Overview of SM/MPAC & SEED experiment” (in Japanese), Proc. on “International Space Station Russian Service Module (SM) / MPAC & SEED 2nd Post – Retrieval conference, JAXA-SP-06-021 2007.

Ichiro Yamagata, “Characterization of the Space Environment on Orbit of the International Space Station – Space Dust Environment –” (in Japanese), Journal of the Vacuum Society of Japan, in press, 2008.

## Post Retrieval Analyses of Space Environment Monitoring Samples: Radiation Effects, UV, and Atomic Oxygen Fluence

Yugo Kimoto<sup>1</sup>, Keiichi Yano<sup>2</sup>, Junichiro Ishizawa<sup>1</sup>, Eiji Miyazaki<sup>1</sup>

<sup>1</sup> *Institute of Aerospace Technology, Japan Aerospace Exploration Agency,  
Tsukuba, Ibaraki 305-8505, Japan*

<sup>2</sup> *Space Utilization and Information Technology Division Information Communications Systems Group  
Space Engineering Development Co., Ltd.  
Tsukuba, Ibaraki 305-0032, Japan*

A space materials exposure experiment was performed on the International Space Station (ISS) using the Micro-Particles Capturer and Space Environment Exposure Device (MPAC&SEED) developed by the Japan Aerospace Exploration Agency (JAXA). The experiment was executed on the exterior of the Russian Service Module (SM) of the ISS. The monitoring samples on SEED yield space-environment data such as AO, UV, fluence and space radiation dose data. The exposure and monitoring samples were retrieved after 315 days (about 10 months) and 865 days (about 28 months) and 1403 days (about 46 months) of exposure. This paper presents an analysis result of monitoring samples and orbital and attitude flight information of ISS during the SM/MPAC&SEED mission.

**Keywords:** MPAC&SEED, ISS Service Module, Space Environment Monitoring Samples, AO, UV, TID

### 1. Introduction

The SM/MPAC&SEED was a passive experiment that used neither a power source nor communication. Therefore, in-situ information was not telemetered from space. Samples for monitoring the total dose of AO, UV, space radiation, and temperature were situated on board. This paper presents experimental methods along with results of analyses of the space environment derived from space environment monitoring samples.

### 2. Space Environment Monitoring Samples

#### 2.1 System description

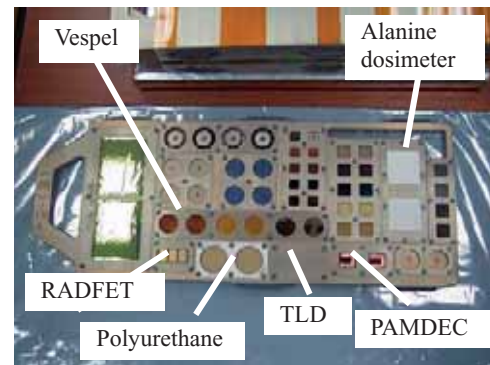
Figure 1 presents a photograph of two trays of an MPAC&SEED unit. Each unit had four trays. The temperature-monitoring sample was mounted on the back of all four trays; the remaining monitoring samples were mounted on two trays. The front face of the MPAC&SEED was designated as “ram”; the back face was termed “wake.” However, this orientation meant little because the ISS flight attitude often changed to maximize power and minimize negative thermal effects. The result of this directional analysis is described in a later section. This section explains detailed specifications for each monitoring sample.

For temperature monitoring, a thermolabel in a tray measured only the maximum temperature.

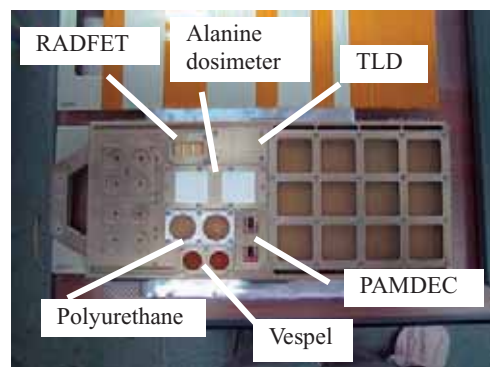
#### 2.2 Monitoring sample

##### 2.1 Atomic Oxygen (AO) monitoring

Carbon films and Vespel (SP-1) were selected for AO monitoring. Vespel is made from aromatic polyimide powder. Kapton-100H was selected for use as the AO monitoring sample on the ESEM mission [1]. Vespel ( $t=500\ \mu\text{m}$ ) is thicker than Kapton-100H ( $t=25\ \mu\text{m}$ ). If we were to extend the exposure period of MPAC&SEED on the SM mission, the AO would cause the Kapton-100H to disappear. Therefore, we selected



(a) Tray No.2 (Ram face)



(b) Tray No.2 (Wake face)

**Fig.1 Photographs of the monitoring samples on an MPAC&SEED unit.**

Vespel for its greater thickness. Ground AO irradiation testing was conducted to calibrate the atomic oxygen fluence. We conducted irradiation tests at JAXA’s Combined Space Effects Test Facility, which is equipped with a PSI FAST AO source, a deuterium UV-ray source, and an electron-beam source.

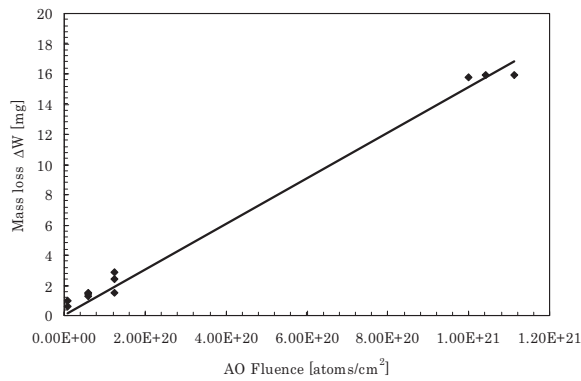
Figure 2 portrays the dependence of Vespel mass loss on



the AO fluence. The efficiency of mass loss on the linear part is equal to  $Re=3.33 \times 10^{-24}$  [ $\text{cm}^3/\text{atoms}$ ]. Using this relationship between AO fluence and mass loss, the AO fluence acting on the test specimen in orbit is derived as follows.

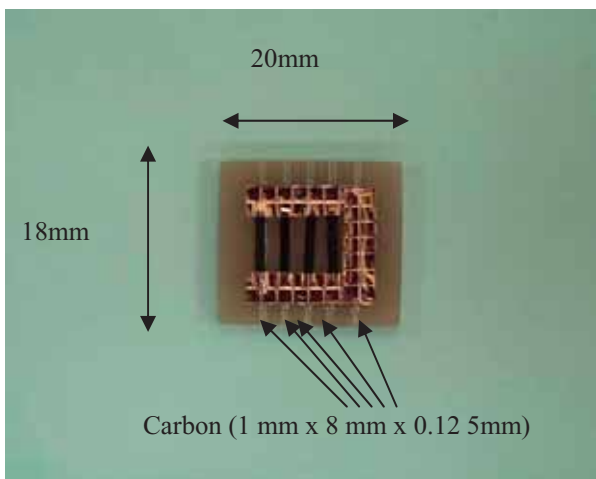
$$(1) \text{AOFluence}[\text{atoms} / \text{cm}^2] = \frac{\Delta W}{Re \cdot \rho \cdot A}$$

In that equation,  $\rho$  [= 1.45  $\text{g}/\text{cm}^3$ ] and  $A$  [= 3.14  $\text{cm}^2$ ].



**Fig. 2** Vespel mass loss attributable to AO exposure. The X-axis represents AO fluence; the Y-axis shows the mass difference from the initial value, which is divided by the density and exposed surface area.

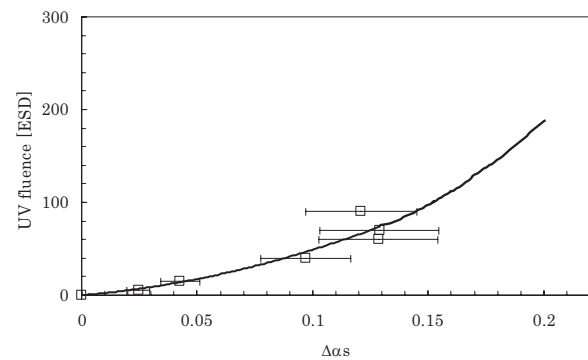
We cut a 125- $\mu\text{m}$ -thick carbon film into 1 mm  $\times$  8 mm strips and integrated the film into a small device called a Passive Atomic-Oxygen Monitoring Device Equipped with Carbon Film (PAMDEC), which consists of five strips, with one strip masked using copper tape. We arranged these strips on 20 mm  $\times$  18 mm FR-4 (glass, epoxy, copper-clad laminates). Figure 3 presents a photograph of the PAMDEC. This carbon film was used as an Atomic Oxygen Monitor (AOM) sensor aboard the Japanese Experiment Module Exposed Facility (JEM-EF) on the ISS [2]. Other carbon-based atomic oxygen actinometer sensors were developed [3]. The AO eroded the carbon film while increasing its resistance. We calibrated the AO fluence, comparing it to the resistance of the PAMDEC and the ground AO-irradiation test data.



**Fig. 3** Photograph of the PAMDEC

## 2.2 Ultraviolet (UV) monitoring

For our UV monitoring, we used a polyurethane sheet covered with glass to protect against AO erosion. The same type of sample was used in the ESEM [1] and EFFU missions [4]. For the Passive Optical Sample Assembly (POSA)-1 experiment mounted on the Mir space station from March 1996 to October 1997, VUV diodes were used for monitoring VUV radiation [5]. Solar-absorption ( $\alpha s$ ) data, along with calibration data acquired from the Xe-resonance lamp-irradiation test, helped us to evaluate the UV fluence. We arranged the samples on gel sheets in a vacuum chamber to prevent increased temperatures caused by the Xe lamp, which contains an infrared wavelength region. Figure 4 depicts the calibration curve for this sample.



**Fig. 4** Calibration curve for UV monitoring sample. The X-axis represents the difference of solar-absorption ( $\alpha s$ ) from the initial value ( $\Delta\alpha s$ ); the Y-axis shows the UV fluence.

## 2.3 SPACE-RADIATION EFFECT: TOTAL IONIZING DOSE (TID)

We used dosimeters of three types to evaluate the effect of space radiation: a thermo-luminescent dosimeter (TLD), an alanine dosimeter, and a radiation-sensitive field-effect transistor (RADFET). The TLD was also used on the ESEM mission [1]. A TLD is a small device that is used to evaluate radiation exposure by measuring the amount of visible light emitted by a crystal when heated in the detector. The amount of emitted light depends on the ionizing irradiation exposure. We arranged six TLDs behind a 4.5-mm-thick aluminum shield on both the ram and wake sides of a sample tray.

An alanine dosimeter is a solid device consisting mainly of alanine and polystyrene. The radical density increases in proportion to the dose of radiation received. The relative density of the radical is measured using Electron Spin Resonance (ESR). Four alanine dosimeters were arranged behind a 0.15-mm aluminum shield with white paint on both the ram and wake sides of a sample tray.

A RADFET is a specially designed P-channel metal oxide semiconductor (PMOS) transistor with a thick gate oxide, which is optimized for increased radiation sensitivity. The RADFET is suitable for real-time space dosimetry missions in terms of its cost, weight, and low power consumption specifications [6, 7]. The RADFETs used in MPAC&SEED were 400-nm implanted gate-oxide devices manufactured by the Tyndall National Institute of Ireland. We arranged three RADFETs on both the ram and wake sides of a tray. This RADFET had a 0.8-mm-thick equivalent aluminum lid.

**Table 1 Derivation results from the monitoring samples**

		Ram Face			Wake Face		
		#1	#2	#3	#1	#2	#3
Maximum Temperature [°C]		50 <sup>a</sup> 60 <sup>b</sup>	50 <sup>a</sup> 90 <sup>b</sup>	60 <sup>a</sup> 90 <sup>b</sup>	—	—	—
AO [atoms/cm <sup>2</sup> ]	Vespel	2.04 × 10 <sup>20</sup>	2.57 × 10 <sup>20</sup>	2.70 × 10 <sup>20</sup>	1.61 × 10 <sup>20</sup>	2.05 × 10 <sup>20</sup>	3.09 × 10 <sup>20</sup>
	PAMDEC	2.41 × 10 <sup>21</sup>	1.36 × 10 <sup>21</sup>	1.37 × 10 <sup>21</sup>	1.93 × 10 <sup>21</sup>	1.22 × 10 <sup>21</sup>	4.82 × 10 <sup>21</sup>
UV [ESD]		18.1	15.8	13.4	122.2	201.0	205.5
TID [Gy]	Alanine dosimeter <sup>c</sup>	1.95	15.3	32.0	3.5	21.9	58.3
	RADFET <sup>d</sup>	0.44	5.99	8.59	0.27	4.92	14.9
	TLD <sup>e</sup>	1.46 × 10 <sup>-3</sup>	0.12	0.29	3.41 × 10 <sup>-3</sup>	0.09	0.04

<sup>a</sup> At approximately 5 mm depth in Tray No. 1 and 2.

<sup>b</sup> At approximately 1 mm depth in Tray No. 3 and 4.

Shield thickness; <sup>c</sup> 0.04 [g/cm<sup>2</sup>], <sup>d</sup> 0.2 [g/cm<sup>2</sup>], <sup>e</sup> 1.2 [g/cm<sup>2</sup>]

### 3. Derivation results from the monitoring samples

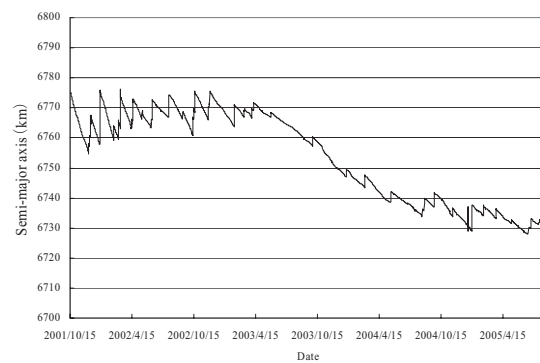
Table 1 presents results derived from sample monitoring. The first-retrieved monitoring sample data are labeled as #1; the second-retrieved are labeled as #2; the third-retrieved are labeled as #3.

The maximum temperatures in the three trays were 50–90°C. The AO fluence was 10<sup>20</sup> atoms/cm<sup>2</sup> from Vespel and 10<sup>21</sup> atoms/cm<sup>2</sup> from PAMDECs. The MPAC&SEED #1 data showed higher values than those of MPAC&SEED #2, although MPAC&SEED #2 had longer exposure than #1 in the AO fluence. A similarly unexpected result also occurred in the UV monitoring samples. The measured intensity of UV in the wake face was greater than that from the ram face. The TID data were dependent on the shield thickness.

### 4. Discussion

Orbital and attitude flight information of the ISS during this experiment period, provided by RSC Energia, was analyzed. The average flight altitude was 371 km, the inclination was 51.64 deg. Figure 5 shows ISS post-flight orbital and attitude changes. Table 2 shows the average orbital and attitude. The ISS has different attitude modes until the main solar arrays are in position. The main attitudes are the X-axis in the Velocity Vector (XV), the X-Axis Perpendicular to the Orbit Plane (XPOP), and the Y-axis in the Velocity Vector (YV). The ram and wake faces are oriented along the ram and wake directions of the ISS when the ISS flies in XV mode. However, during XPOP mode and during YV mode, the MPAC&SEED faces a direction that is perpendicular to the flight direction. During the first year of MPAC&SEED #1, the ISS spent 59% of its time in XV mode and 41% in XPOP mode. During MPAC&SEED #2, the ISS spent 54% of its time in XV mode and 46% in XPOP and YV mode. Therefore, both the ram and wake faces were pointed in the flight direction.

We compared flight data and data from the space-environment model for the atomic-oxygen fluence and calculated the AO fluence using the MSIS-86 model in the Space Environment & Effects System (SEES) [8] during 15 October 2001 – 26 February 2004. We used the F10.7 and Ap index data available from NOAA Space Weather Data and Products [9] and considered the flight-direction change in our calculation.

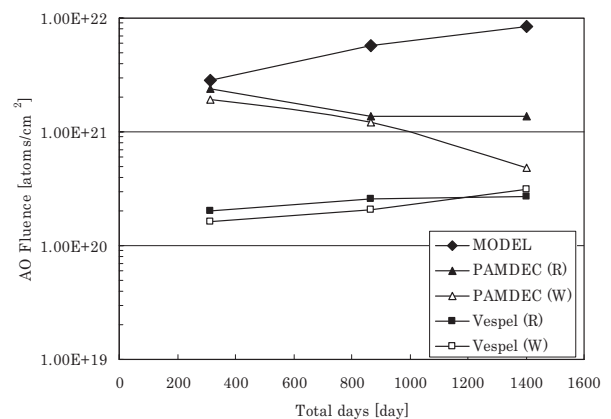


**Fig. 5 ISS post-flight orbital and attitude change.**

**Table 2 Average orbital information**

Orbital radius [km]	6748.904 (370.77 <sup>a</sup> )
Eccentricity [°]	0.00071
Inclination [°]	51.64

<sup>a</sup> Re=6378.134 km



**Fig. 6 AO fluence data compared to PAMDEC and Vespel monitoring sample data and model calculations.**

Figure 6 depicts the flight data. Although the results in Fig. 6 include consideration of the flight direction, the values of the flight data taken from the monitoring samples for the ram and wake faces were less than the values of the SEES-model calculation, which suggests that a contamination effect is responsible for the monitoring environment.

We also compared flight data and data from the space-environment model for the UV fluence and calculated the UV fluence using SEES [8]. In this analysis, a cube was used in place of the real ISS shape. We also considered the flight-direction change in our calculation. In Fig. 7, the UV fluence from the polyurethane sheet on the wake side was 1.3 times the data from the space-environmental model. However, the value from the ram side reached almost one-tenth of the data from the space-environment model. Moreover, the second-retrieved data were less than the first-retrieved data, which suggests that the ram side was not exposed to UV because the ISS itself or some components in the field view of the MPAC&SEED trays shaded the UV irradiation. Figure 8 shows fish-eye images from ram and wake sides of the MPAC/SEED. Actually, the Russian segment elements had the largest view factors to the MPAC&SEED trays in the ram side. The Russian segment elements of concern include the Functional Cargo Block (FCB), Service Module (SM), and Docking Compartment 1 (DC1). In addition, visiting vehicles (Orbiter, Soyuz, and Progress) had considerable view factors when mated to the ISS [10]. The field of view from the wake side is clear during the MPAC&SEED mission period. Furthermore, XPOP is the attitude at which the X-axis is perpendicular to the orbital plane; therefore, the +X direction is facing anti-sun. These reasons suggest that the ram side was not exposed to UV.

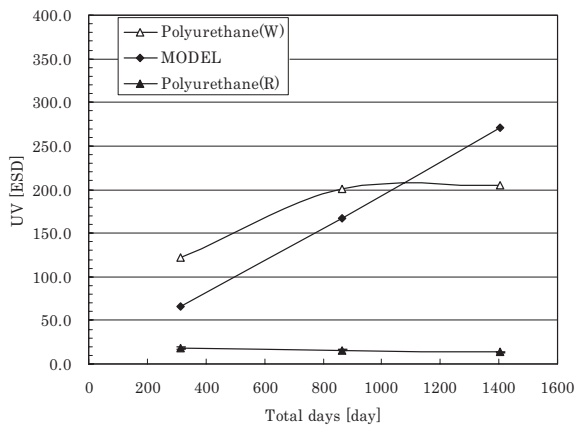
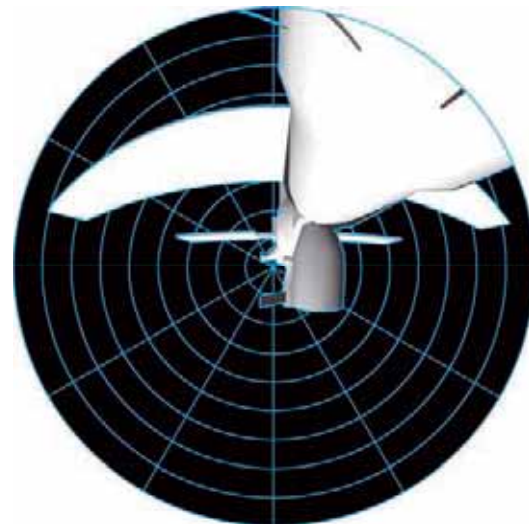
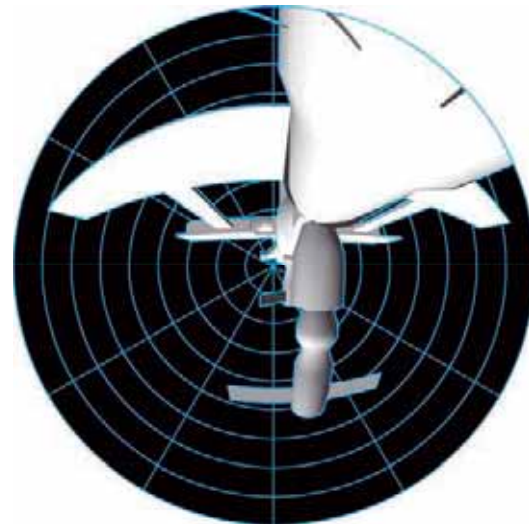


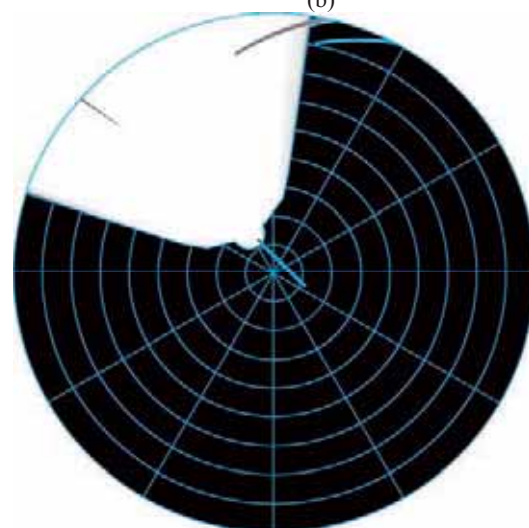
Fig. 7 UV fluence compared to data from polyurethane UV monitoring samples and model calculations.



(a)



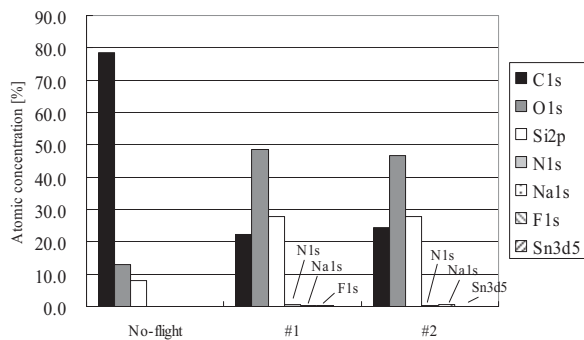
(b)



(c)

Fig. 8 Field view analysis from the MPAC&SEED (a: From ram side in 15 October 2001 (exposure just started), b: From the ram side in June 2003, c: From the wake side in 15 October 2001)

We used X-ray photoelectron spectroscopy (XPS) to analyze the surface chemical condition of the carbon film in the PAMDEC for AO monitoring samples. The XPS analyses were performed (ESCALab 220i-XL; Thermo VG Scientific) using Al K $\alpha$  radiation. The analysis area is a 700- $\mu$ m-diameter spot. The depth resolution performance is a few nanometers. For carbon on the ram face, XPS analysis was conducted. Figure 9 shows the atomic concentration of the external surface of the carbon film on the ram side and that of an unflown sample. The atomic concentration is the ratio of the element to all elements constituting the surface material. For the unflown sample, carbon itself was the dominant element. For the flight samples, however, more oxygen and silicon existed than carbon, suggesting that oxides of silicon were present on the very top surface. In addition, nitrogen, sodium, fluorine, and tin were detected, but not at concentrations greater than 1%.



**Fig. 9** External surface conditions of PAMDEC using XPS analysis

Figure 10 depicts a depth profile of the PAMDEC for an unflown sample and flight samples. For depth profiling, Ar-ion etching was used. The unflown sample did not have a dependent profile of elements. However, the flight samples had a dependent profile. The distribution of silicon and oxygen in the depth direction suggested that the oxides of the silicon layer existed below the surface. The layer thickness is defined as the point where the concentration of Si becomes greater than that of carbon. The layer thickness of the first-retrieved sample (#1) was estimated as 10 nm; that of the second-retrieved sample (#2) was estimated as 90 nm. This layer, produced by contamination, was grown in flight; it protected the surface of the monitoring sample from erosion.

Figure 11 depicts the total dose data vs. the aluminum-shield thickness (i.e., a dose-depth curve) of the flight data and model calculation. Contamination did not affect TID monitoring because it was of the several-hundred-nanometer level. The dose-depth curve was calculated from the Alanine dosimeter, RADFET, and TLD in MPAC&SEED samples #1, #2 and #3. Flight data were plotted by following their own shield thickness. In addition, AP8, AE8, JPL1991, and SHIELDOSE-2 models in the SEES model [8] were used for model calculation.

The results revealed that the flight data were less than, but approximately equal to, the model data.

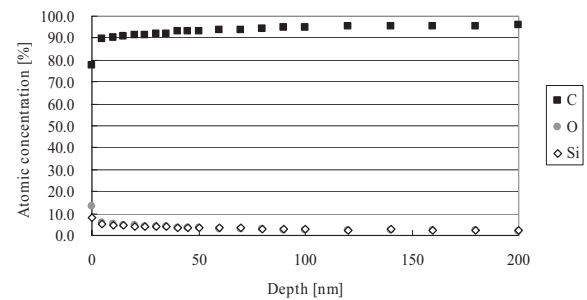
## 5. Conclusion

We analyzed monitoring samples from three MPAC&SEED trays that were retrieved after 315, 865 and 1403 days exposure. We derived space-environment data, AO, UV, and space-radiation effect data from monitoring samples. Values of AO fluence data and UV fluence in the ram data from the monitoring samples were smaller than those of the model

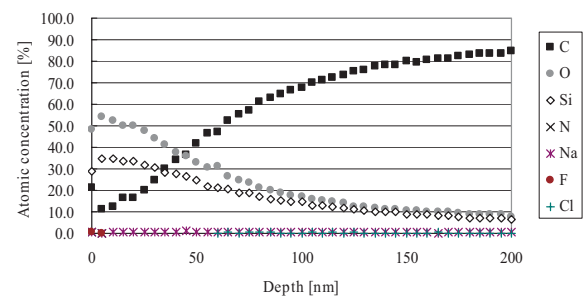
calculations. One reason for the discrepancies between the flight data and the model calculation was considered that both ram and wake faces were pointed in the flight direction for AO fluence. For UV fluence, the ISS itself or some components in the field view of the MPAC&SEED trays suggested shading of the UV irradiation in the ram direction. The flight total-dose data were estimated as lower than the model result.

## Acknowledgments

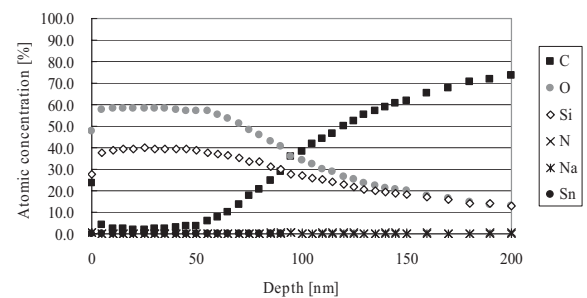
We wish to thank Mr. Susumu Baba of Advanced Engineering Services Co., Ltd. (AES) for his assistance in XPS analysis. We appreciate the work of all people involved in the development and operation of the SM/MPAC&SEED experiment.



(a)



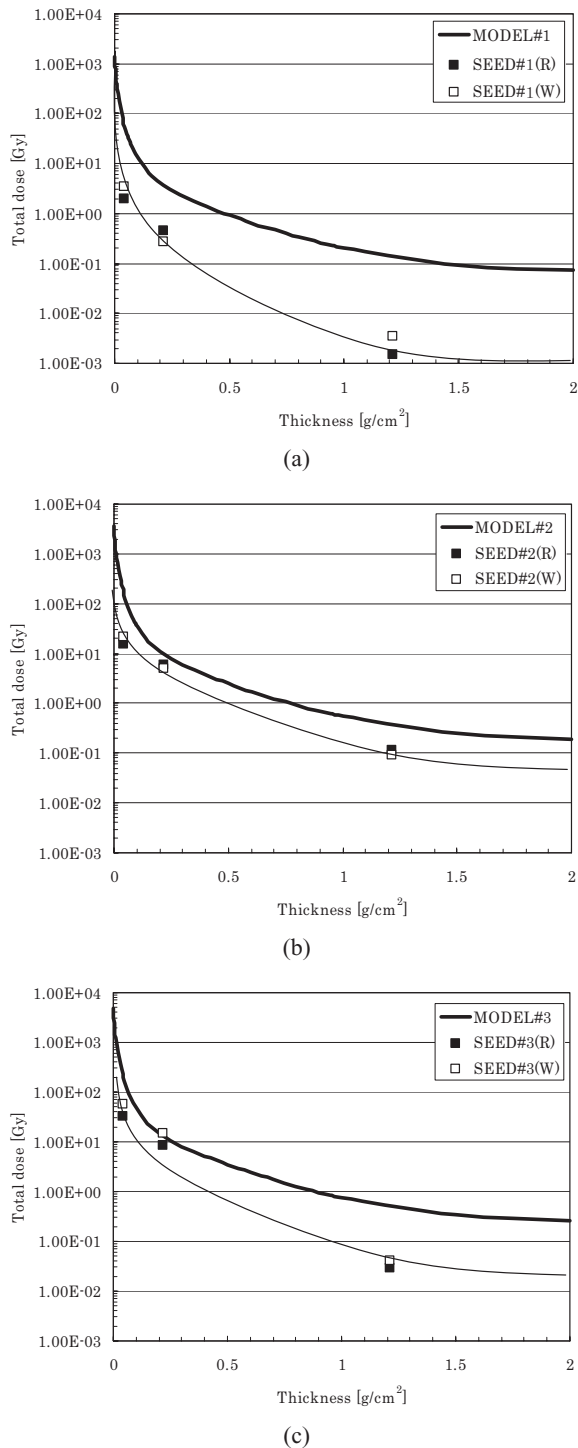
(b)



(c)

**Fig. 10** Depth profile from XPS analysis of the PAMDEC: a) Unflown sample, b) First retrieved sample (#1), and c) Second retrieved sample (#2).





**Fig. 11 Dose-depth curves from MPAC&SEED #1, MPAC&SEED #2, MPAC&SEED #3 and models**

## References

- [1] Imagawa, K., "Evaluation and Analysis of Parts and Materials installed on MFD-ESEM," NASDA-TMR-000011, Nov. 2002, URL: <http://matdb.jaxa.jp/SpaceExperiment/Image/MFD-ESEM-E.pdf>.
- [2] Koga K. et al., "Space environment data acquisition equipment – attached payload on the international space station," COSPAR Colloquia Series Vol. 14, "Solar-Terrestrial Magnetic Activity and Space Environment," Edited by Wang H., Xu R., 2002, pp. 365–366.
- [3] Galica, G. E., "Atomic Oxygen Monitor Based On Carbon Actinometers," Proceedings of the 10th International Symposium on "Materials in a Space Environment" (ISMSE) and 8th International Space Conference on "Protection of Materials and Structures from the Space Environment" (ICPMSE), June 2006 (SP-616, September 2006).
- [4] Fukatsu, T., "Post-flight Analysis of the exposed materials on the EFFU," Proceedings of the 7th Symposium of Materials in a Space Environment, 1997, pp. 287–292.
- [5] Zwiener, J.M., "Contamination observed on the Passive Optical Sample Assembly (POSA)-I experiment," SPIE Proceedings Vol. 3427, Oct. 1998
- [6] Kimoto, Y., "Space Radiation Environment and Its Effects on Satellites: Analysis of the First Data from TEDA on Board ADEOS-II," IEEE Trans. Nucl. Sci., Vol. 52, No. 5, Oct. 2005, pp. 1574–1578.
- [7] Kimoto, Y., "Total Dose Orbital Data by Dosimeter Onboard Tsubasa (MDS-1) Satellite," IEEE Trans. Nucl. Sci. Vol. 50, No. 6, Dec. 2003, pp.2301-2306.
- [8] <http://sees.tksc.jaxa.jp/>
- [9] <http://www.sec.noaa.gov/Data/index.html>
- [10] Pankop, C., "Induced Contamination onto JAXA'S Micro-Particles Capturer And Space Environment Exposure Device – Comparison of Predictions and Measurements," Proceedings of the 10th International Symposium on "Materials in a Space Environment" (ISMSE) and 8th International Space Conference on "Protection of Materials and Structures from the Space Environment" (ICPMSE), June 2006 (SP-616, September 2006)

**Publication list related to SM/MPAC&SEED**

Yugo Kimoto, Keiichi Yano, Junichiro Ishizawa, Eiji Miyazaki, and Ichiro Yamagata, “Passive measurement of atomic oxygen, UV fluence, and radiation effect on the ISS using the SEED experiment,” Proc. of the 10th International Symposium on “Materials in a Space Environment” (ISMSE) and 8th International Space Conference on “Protection of Materials and Structures from the Space Environment” (ICPMSE), June 2006.

Yugo Kimoto, Keiichi Yano, Junichiro Ishizawa, Eiji Miyazaki, and Ichiro Yamagata, “Space Environment Effects of on MPAC & SEED Missions in ISS,” Proc. of the 25th International Symposium on Space Technology and Space, Selected Papers, 2006.

Yugo Kimoto, Ichiro Yamagata, Eiji Miyazaki, Junichiro Ishizawa, Naoko Baba, and Mineo Suzuki, “Post Retrieval Analyses of Space Environment Monitoring Samples” (in Japanese), Proc. of International Space Station Russian Service Module (SM) / MPAC & SEED 2nd Post – Retrieval conference, JAXA-SP-06-021 2007.

Yugo Kimoto, Keiichi Yano, Junichiro Ishizawa, and Eiji Miyazaki, “Post Retrieval analysis of space environment monitor materials on the International Space Station Russian Service Module / Space Environment Exposure Device” (in Japanese), Proc. of the 51st Space Sciences and Technology Conference, 2007 (CD-ROM).

Yugo Kimoto, Keiichi Yano, Junichiro Ishizawa, Eiji Miyazaki, and Ichiro Yamagata, “Passive Space Environment Effect Measurement on the International Space Station,” Journal of Spacecraft and Rockets, Accepted in June 2008.

Yugo Kimoto, Shoichi Ichikawa, Eiji Miyazaki, Koji Matsumoto, Junichiro Ishizawa, Hiroyuki Shimamura, Riyo Yamanaka, and Mineo Suzuki, “Space Environment Effects on Materials at Different Positions and Operational Periods of ISS,” Proc. of the 9th International Space Conference Protection of Materials and Structures from the Space Environment (ICPMSE), 2008.

## INDUCED CONTAMINATION PREDICTIONS FOR JAXA'S MICRO-PARTICLES CAPTURER AND SPACE ENVIRONMENT EXPOSURE DEVICES

Courtney STEAGALL, Kendall SMITH, Alvin HUANG, Carlos SOARES, and Ronald MIKATARIAN

*The Boeing Company, Space Environments Team,  
13100 Space Center Blvd., M/C HB3-20, Houston, Texas, 77059, U.S.A*

A comparison of induced contamination predictions and measurements is presented for JAXA's Micro-Particles Capturer and Space Environment Exposure Device (MPAC&SEED), which was attached to the exterior of the Russian Service Module on the International Space Station (ISS). Material outgassing and thruster plume induced contamination was calculated using analytical and semi-empirical models developed by the Boeing Space Environments Team in Houston. Contamination depth predictions show good agreement (within a factor of 3) compared to measured contamination levels on the flight hardware. Induced contamination predictions are also presented for the next MPAC&SEED experiment to be deployed on the Japanese Experiment Module.

**Keywords:** MPAC&SEED, International Space Station, External Payloads, Induced Environment, Contamination

### 1. Introduction

The International Space Station (ISS) induced environment includes contributions from ISS elements and visiting vehicles (i.e., Space Shuttle Orbiter, Soyuz, and Progress). This induced environment is characterized by the Boeing Space Environments Team in Houston. Of key interest are induced contamination sources such as materials outgassing and thruster plumes.

The induced contamination environment is of great interest for externally mounted ISS payloads, such as JAXA's Micro-Particles Capturer and Space Environment Exposure Device (MPAC&SEED). The contribution of the induced environment must be understood to ensure successful on-orbit performance. In addition, the return of ISS external experiments provides a rare opportunity to compare induced contamination predictions with measurements from flight hardware.

The first MPAC&SEED experiment was mounted outside the Russian Service Module (SM) on October 15, 2001. The SM/MPAC&SEED consisted of 3 identical units which were exposed for periods ranging from 10 months to almost 4 years. Fig. 1 shows a view of the fully deployed experiment. This is a view of the ram-facing side (i.e., the side which pointed into the ISS velocity vector for the majority of the experiment). Fig. 2 shows a view of the experiment from the wake-facing side.[1]

All of the SM/MPAC&SEED units have been returned from ISS for ground-based testing. In addition to characterizing captured particles and materials degradation, JAXA conducted a thorough investigation of contamination deposited on the units.[2]

JAXA is currently preparing another MPAC&SEED experiment to be deployed on the Japanese Experiment Module (or JEM/MPAC&SEED). JEM/MPAC&SEED is expected to launch on ISS Flight 2J/A (tentatively scheduled for March 2009) and has a planned exposure duration of 3 years. Unlike SM/MPAC&SEED, this experiment will have samples on the ram-facing surface only.[3] Fig. 3 shows the approximate JEM/MPAC&SEED location on ISS.

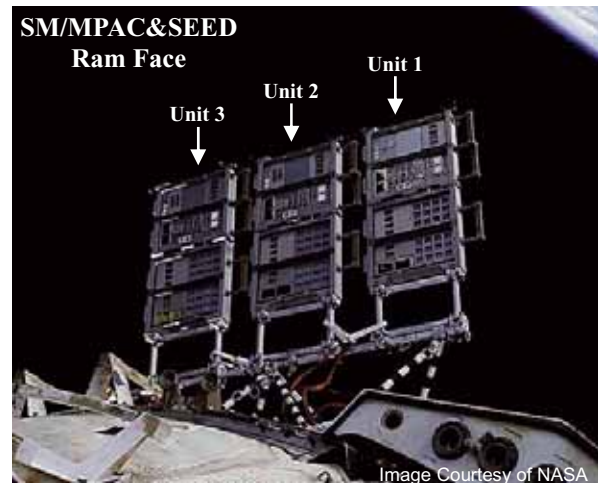
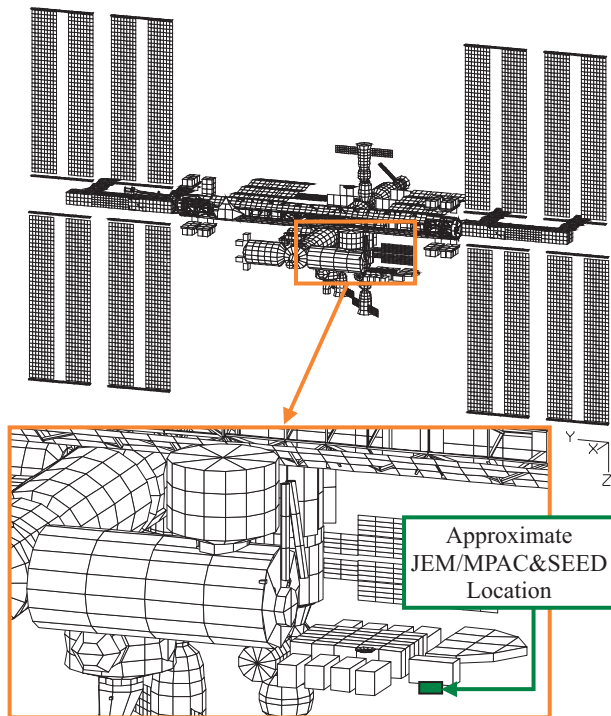


Fig. 1 SM/MPAC&SEED On-Orbit, Ram-Facing Side



Fig. 2 SM/MPAC&SEED On-Orbit, Wake-Facing Side



**Fig. 3 Approximate JEM/MPAC&SEED Location in ISS Geometric Model**

The Boeing Space Environments Team performed induced contamination analyses for SM/MPAC&SEED to compare predictions with measured contamination levels on the flight hardware. Induced contamination was also analyzed for JEM/MPAC&SEED.

## 2. ISS Contamination Sources

There are several ISS contamination sources which could affect the MPAC&SEED experiments. Given the significant size of ISS and number of elements, the MPAC&SEED experiment location and orientation must be considered when evaluating contamination sources. To identify these sources, views to and from MPAC&SEED were created using an ISS geometric model. These views were inspected to identify potential ISS contamination sources with a line-of-sight to the experiment. The primary contamination sources of concern include material outgassing from ISS hardware elements and thruster plume contamination.

Beyond material outgassing and thruster plume impingement, other potential contamination sources are present on ISS. For instance, there are several propellant purge ports on the Russian Segment which periodically vent fuel or oxidizer. The highest flux region for propellant purges is near the centerline. The MPAC&SEED experiment locations are both far from the centerlines of the purge ports, so this contamination source was neglected. There are also water vents on the Orbiter and US Segment, but these did not have a line-of-sight to either experiment location. Self-contamination from direct or return flux may also contribute to deposition. For the MPAC&SEED experiments, direct flux was not considered since there is no line-of-sight between the exposed surfaces. Return flux was neglected as a second order effect.

## 3. SM/MPAC&SEED Induced Contamination Predictions and Measurements

### 3.1 SM/MPAC&SEED Contamination Observations

Visual inspection of SM/MPAC&SEED revealed color changes on the wake face, which was covered in a uniform brownish contamination layer (see Fig. 4). Beyond the uniform contamination, many spots were also observed which are indicative of low-velocity droplet impacts. The spots varied in shape and color, with diameters ranging from approximately 1 to 1000  $\mu\text{m}$ . These features were more numerous on the wake face than the ram.[1,2,4,5]



**Fig. 4 Comparison of Unit 1 Ram & Wake Faces [1]**

JAXA used X-ray Photoelectron Spectroscopy (XPS) to measure element composition and depth profiles of the contamination layers. Four measurements were taken for each unit – two on the ram side and two on the wake side. Results show silicon to be a significant constituent on the ram side of all 3 units. Silicon was also present on the wake side but generally in lesser quantities. The presence of silicon is highly indicative of material outgassing induced contamination. Oxygen, carbon, nitrogen, sodium, iron, and nickel were also detected. Nitrogen was consistently more prominent on the wake side compared to the ram.[2,4]

Nitrogen is an important signature for thruster plume induced contamination, considering the propellants used for ISS thrusters. Nitrogen appeared in small quantities on the wake side (around 4% of the atomic concentration). Similarly, ground-based measurements have shown nitrogen concentrations on the order of 11-16% of the total residue remaining from the fuel-oxidizer reaction. The other constituents expected in fuel-oxidizer reaction products include carbon, hydrogen, and oxygen.[6] Although carbon and oxygen were present on SM/MPAC&SEED, these could be attributed to other sources.

Flight experiment data has shown that droplets are the primary mechanism for thruster plume contamination transport at operating temperatures expected on ISS (i.e., non-cryogenic).[7] The presence of nitrogen and droplet features strongly indicates thruster plume induced contamination.

A summary of contamination depths estimated from XPS results are provided in Table 1. The ram side of the trays



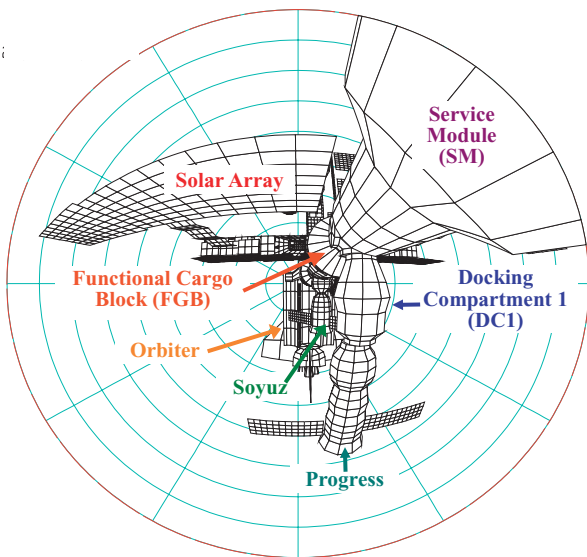
showed consistent depth measurements; the measurements on the wake side were more varied. It should be noted that XPS does not always render a clear and precise depth measurement, and results may be subject to interpretation.

**Table 1 Approximate SM/MPAC&SEED contamination depth based on XPS measurements.**

Measured Contamination Depth - Angstroms (Å)			
Side	Unit 1	Unit 2	Unit 3
Ram (1)	300	750	930
Ram (2)	300	750	940
Wake (1)	55	100	110
Wake (2)	500	70	85

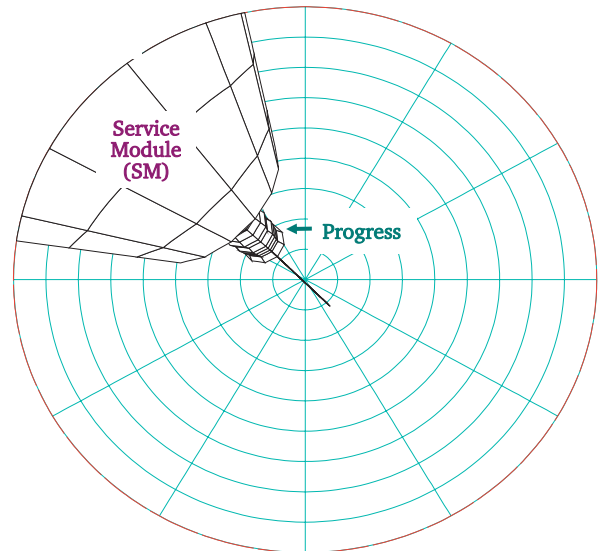
### 3.2 SM/MPAC&SEED Contamination Sources

Hemispherical views from the ram- and wake-facing sides of SM/MPAC&SEED were used to identify the major ISS outgassing sources (see Fig. 5 and Fig. 6). These views are centered along the surface normal vector and expanded out 90°. From this type of view, it is straightforward to determine which ISS elements had a line-of-sight to the experiment. The Functional Cargo Block (FGB), Service Module (SM), and Docking Compartment 1 (DC1) on the Russian Segment had the largest view factors to the SM/MPAC&SEED trays. In addition, visiting vehicles (i.e., Orbiter, Soyuz, and Progress) had significant view factors when mated to ISS.



**Fig. 5 Hemispherical View from SM/MPAC&SEED (Ram Direction)**

For each of these elements, a materials list was compiled and matched to available outgassing rate test data (i.e., ASTM-E 1559 testing or equivalent). On-orbit temperature estimates for ISS elements and SM/MPAC&SEED were taken into account where possible; however, appropriate outgassing rate test data did not always exist for the temperatures of interest. In these cases, best available outgassing data was used. An effective outgassing rate source term was then calculated based on quantity of material.



**Fig. 6 Hemispherical View from SM/MPAC&SEED (Wake Direction)**

The outgassing source terms account for the duration of exposure to the vacuum environment. The time decay rate of sources terms is determined from experimental data and diffusion theory. Visiting vehicles were of key interest as these had comparatively little reduction in outgassing rates due to time decay. For example, the aft-docked Progress cargo vehicles rotated every 3 to 4 months (i.e., a Progress vehicle departed and was replaced with a new one). As a result, the initial outgassing source term decayed very little between Progress vehicle rotations. In contrast, the sources terms for the permanent outgassing sources (e.g., FGB, SM, and DC1) continued to decay with time. The FGB, for instance, had been on-orbit several years by the time SM/MPAC&SEED was deployed. Consequently, it had a relatively low outgassing source term (due to time decay) compared to the Progress vehicles.

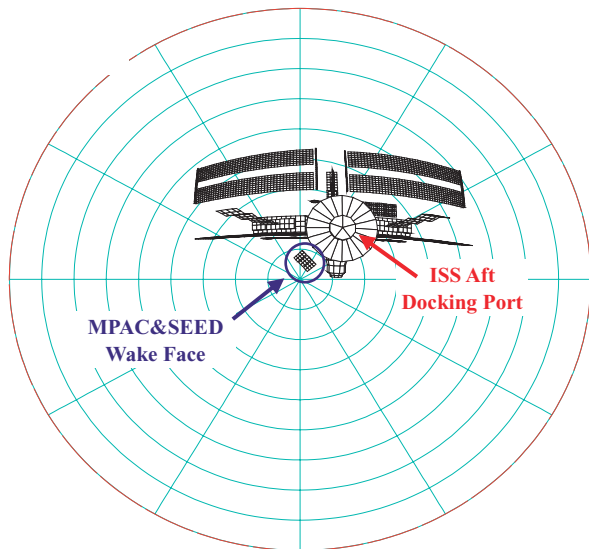
Material outgassing induced contamination was calculated using an analytical model developed by the Boeing Space Environments Team. This model is based on physical models of molecular transport and is coded into Boeing's NASAN-3 contamination computer model. NASAN-3 is an integrated computer model, utilizing NASTRAN geometric models, view factor calculations, and transport routines to analyze induced contamination on an ISS configuration, with results available in tabular or graphic formats.

To identify ISS thrusters of concern for plume impingement to SM/MPAC&SEED, views from all ISS thrusters were reviewed. This included ISS thrusters used for reboost/attitude control as well as thrusters on visiting vehicles (i.e., Orbiter, Soyuz, and Progress). Of key interest were thrusters with a centerline view to the experiment, since this is where the highest contamination flux is expected.[8]

On the ram-facing side of SM/MPAC&SEED, only visiting vehicles had thrusters with a line-of-sight to the tray. It is probable that these thrusters contributed to some of the spot features on the ram side. In general, however, SM/MPAC&SEED was at a very high angle off the thruster

centerlines, and it was decided to neglect these from the analysis. No ISS reboost/attitude control thrusters had a view to the ram side of the experiment.

On the SM/MPAC&SEED wake face, the only significant thruster contamination source was a Progress braking engine. The braking engines are fired during approach and separation to the docking port on the aft end of ISS. (See Fig. 2 for an on-orbit image of an aft-docked Progress). One of the Progress braking engines had a near-centerline view to the SM/MPAC&SEED wake side. Fig. 7 provides a hemispherical view from this thruster when 20 ft from the aft docking port.



**Fig. 7 Hemispherical View from Progress Braking Thruster, 20 ft to Docking**

The thruster plume induced contamination was analyzed using a semi-empirical model developed by the Space Environments Team. This model uses flight experiment and chamber test data for contamination characterization.[8] The plume contamination model is also coded into the NASAN-3 contamination computer tool to analyze a given thruster's effect on an ISS configuration. Available flight jet firing data for Progress proximity operations was used to simulate thruster firings and calculate thruster induced contamination to MPAC&SEED.

### 3.3 SM/MPAC&SEED Contamination Analysis Results

Analysis for SM/MPAC&SEED was performed for 3 time periods to correlate with measurements from each unit as they were retrieved. This timeline is summarized in Table 2. For each analysis period, total exposure time was taken into account as well as visiting vehicle traffic records to most accurately duplicate on-orbit conditions for SM/MPAC&SEED. Results for the ram side of the units showed measurable levels of outgassing-induced contamination while results for the wake side indicated a combination of outgassing and thruster plume contamination.

**Table 2 SM/MPAC&SEED Timeline used for Analysis**

Unit	Deployed	Retrieved	Total Time Days (Years)
1	10/15/2001	8/26/2002	315 (0.9)
2	10/15/2001	2/26/2004	865 (2.4)
3	10/15/2001	8/18/2005	1403 (3.8)

In addition to the permanent ISS elements, the ram side of SM/MPAC&SEED was exposed to outgassing from Orbiter, Soyuz, and Progress vehicles. Exposure time durations were taken into account for each element in computing outgassing to the ram side. Since no thrusters were identified as significant contamination sources to the ram face, the outgassing analysis results represent the total contamination prediction.

It was expected that SM/MPAC&SEED would have less outgassing induced contamination on the wake side since there are fewer sources compared to the ram side (see Figs. 5 and 6). Only one permanent ISS element had a view to the wake side of the tray (the Service Module); however, the Progress vehicles docked to the aft end of ISS caused induced contamination from materials outgassing as well as thruster firings.

A summary of the SM/MPAC&SEED contamination analysis results is provided in Table 3. Detailed analysis results for SM/MPAC&SEED have been previously reported.[9,10]

**Table 3 Summary of SM/MPAC&SEED Analysis Results**

Side	Predicted Contamination Depth (Å)		
	Unit 1	Unit 2	Unit 3
Ram	106 - 135	303 - 354	459 - 533
Wake	86 - 103	186 - 237	317 - 414

### 3.4 SM/MPAC&SEED Contamination Predictions vs. Measurements

Analysis results consistently showed measurable levels of material outgassing induced contamination on the SM/MPAC&SEED ram-facing surfaces. The wake-facing surfaces were predicted to incur contamination due to a combination of material outgassing and thruster plume impingement. These results are qualitatively consistent with visual inspection and XPS measurements of SM/MPAC&SEED. On the ram side, XPS results were dominated by a silicon-based contaminant. On the wake side, the presence of nitrogen in XPS measurements and droplet features is highly indicative of thruster plume induced contamination. XPS measurements on the wake side also showed the presence of silicon but to a lesser degree than on the ram side, which agrees with predictions that less than half of contamination on the wake side was due to outgassing. Qualitatively, therefore, the predictions have good agreement with measured and observed contamination.

Quantitative comparisons of the measured and predicted levels of contamination are provided in Table 4. The calculated depth of contamination on the ram side surfaces is within a factor of 3 of measured contamination. Predictions may

improve with better characterization of outgassing sources. For instance, available data for the Russian Segment elements only included characterization of materials with a relatively large surface area. As a result, it is likely that there are significant outgassing sources that have not been identified. In addition, the on-orbit thermal environment has a considerable effect on outgassing but only limited thermal data was available. Considering, however, the number of outgassing sources on ISS and long duration of the experiment, the predicted results for the ram side represent excellent agreement with the measured depth of contamination.

**Table 4 Comparison of SM/MPAC&SEED Measured and Predicted Contamination**

Measured Vs. Predicted Contamination Depth (Å)

Side	Unit 1		Unit 2		Unit 3	
	Measured	Predicted	Measured	Predicted	Measured	Predicted
Ram	300	106 - 135	750	303 - 354	930	459 - 533
Ram	300		750		940	
Wake	55	86 - 103	70	186 - 237	110	317 - 414
Wake	500		100		85	

Plume contamination can be more difficult to quantify with XPS measurements than outgassing induced contamination. Whereas the outgassing contamination was dominated by silicon-based outgassing sources, thruster plumes have multiple byproducts (as described in Section 2). Whereas outgassing yields a fairly uniform molecular contamination layer, thruster plume induced contamination is dominated by the liquid phase, producing droplet features and a non-uniform distribution of contaminants. Hence, XPS measurements for the ram side of SM/MPAC&SEED are a good gauge for qualitative and quantitative comparison with predicted contamination; XPS measurements for the wake side are a good gauge for qualitative comparison but have limitations in regard to quantitative comparison. Nevertheless, consistent XPS results showing the most prominent presence of nitrogen on the wake face from all 3 units give much confidence in predictions for plume contamination on the wake side.

The XPS results on the Unit 1 wake side gave somewhat inconsistent measurements between the two locations, with depths of 55Å and 500Å, respectively. Some variation could be attributed to the nature of thruster plume induced contamination; however, it is likely that the 500Å measurement is a local anomaly. The 55Å measurement is much more consistent with measurements from the Unit 2 and 3 wake sides. Excluding the 500Å data point, the measured and predicted results for the wake side are of similar scale and represent good agreement considering the limitations of XPS in characterizing depth of plume contamination.

#### 4. JEM/MPAC&SEED Induced Contamination Predictions

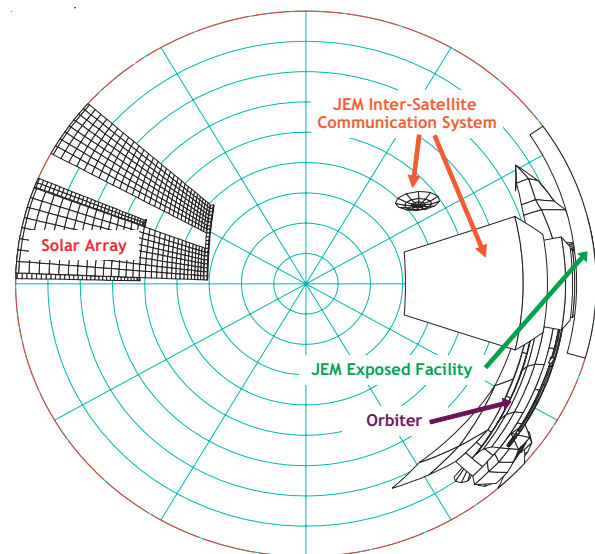
SM/MPAC&SEED provided a unique opportunity to measure the ISS induced contamination environment; however, the primary purpose of the experiment was related to microparticle capture and materials exposure. For this purpose, contamination is an undesirable effect.

The upcoming JEM/MPAC&SEED experiment will be

installed at a different location on ISS than SM/MPAC&SEED. As a result, it will be exposed to different contamination sources. The induced contamination environment is of high interest to JEM/MPAC&SEED developers and investigators to ensure good experimental data can be obtained.

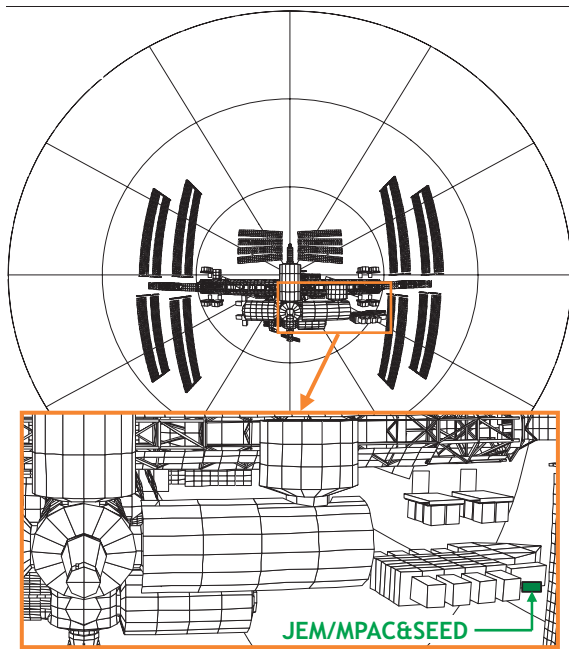
#### 4.1 JEM/MPAC&SEED Contamination Sources

Unlike SM/MPAC&SEED, JEM/MPAC&SEED will have samples on the ram surface only. A hemispherical view from the ram-facing side of JEM/MPAC&SEED was used to identify the major ISS outgassing sources (see Fig. 8). The JEM Inter-Satellite Communication System (ICS) and the ISS Solar Array have the largest view factors. The JEM Exposed Facility (EF) has a slight view. In addition, Orbiter will contribute to contamination when mated to ISS. The Solar Array will have been on orbit for nearly 3 years when JEM/MPAC&SEED is deployed. On the other hand, JEM ICS and EF will deploy at the same time as JEM/MPAC&SEED, so there will be no initial reduction in their outgassing rates due to time decay. It should be noted that the outgassing sources affecting JEM/MPAC&SEED are better characterized (in terms of material identification and outgassing rate data) than the SM/MPAC&SEED outgassing sources.



**Fig. 8 Hemispherical View from JEM/MPAC&SEED (Ram Direction)**

Orbiter thrusters are the only thruster contamination sources for JEM/MPAC&SEED. These thrusters may fire during docking/undocking operations as well during mated operations with ISS. Fig. 9 provides a hemispherical view from an Orbiter braking thruster (fired during docking/undocking operations). As shown in the figure, the JEM/MPAC&SEED experiment is approximately 30 degrees outside the thruster centerline. In fact, none of the Orbiter thrusters fired during docking/undocking operations or mated operations have a near-centerline view to JEM/MPAC&SEED. Therefore, the contamination contribution from Orbiter thrusters was expected to be insignificant.



**Fig. 9 Hemispherical View from Orbiter Braking Thruster, 100 ft to Docking**

#### 4.2 JEM/MPAC&SEED Contamination Analysis Results

Analysis for JEM/MPAC&SEED was performed for the expected experiment duration of 3 years. The current Orbiter launch schedule was used to predict the contribution of Orbiter outgassing and thruster plumes to JEM/MPAC&SEED induced contamination. Results show measurable levels of outgassing-induced contamination and negligible levels of thruster plume contamination.

A summary of the JEM/MPAC&SEED contamination analysis results is provided in Table 5. The table gives the total predicted outgassing-induced contamination as well as the individual contributions from the JEM elements (the EF and the ICS) and the ISS elements (Solar Array and Orbiter). As shown, the depth of the contamination layer depends on the surface temperature of JEM/MPAC&SEED. The JEM elements dominate the induced contamination prediction since they are fresh outgassing sources (deploying on the same flight as JEM/MPAC&SEED) and have a significant view factor. Based on these analysis results, the JEM/MPAC&SEED location will have a less severe contamination environment compared to SM/MPAC&SEED. This is true even for the predicted contamination at the coldest temperature ( $-40^{\circ}\text{C}$ ), though this is lower than expected for nominal JEM/MPAC&SEED operation.

**Table 5 Summary of JEM/MPAC&SEED Analysis Results**

JEM/MPAC&SEED Temperature	Predicted Contamination Depth (Å)		
	JEM (EF and ICS)	ISS (Solar Array & Orbiter)	Total
$-40^{\circ}\text{C}$	448.2 Å	4.4 Å	453 Å
$-10^{\circ}\text{C}$	151.2 Å	4.3 Å	156 Å
$25^{\circ}\text{C}$	72.0 Å	3.4 Å	75 Å

#### 5. Conclusion

The contribution of the induced environment for externally mounted payloads must be understood to ensure successful on-orbit performance. On ISS, the induced contamination environment varies by location and time, as evidenced by the many different contamination sources for SM/MPAC&SEED and JEM/MPAC&SEED. The Boeing Space Environments Team performed analyses to calculate material outgassing and thruster plume induced contamination to both experiments.

Analysis results for SM/MPAC&SEED consistently showed high levels of material outgassing induced contamination on the ram-facing surfaces. The wake-facing surfaces were predicted to accrue contamination due to a combination of material outgassing and thruster plume impingement. These results are qualitatively consistent with visual inspection and XPS measurements of the flight hardware. The calculated depth of contamination on the ram side surfaces is within a factor of 3 of measurements. Although XPS is limited in characterizing depth of plume contamination, the measured and predicted results are of similar scale for the wake-facing surfaces.

Analysis results for JEM/MPAC&SEED showed measurable levels of material outgassing induced contamination. No significant thruster plume induced contamination is expected. The JEM/MPAC&SEED location appears to have a less severe contamination environment compared to SM/MPAC&SEED. However, the extent of induced contamination will depend on the JEM/MPAC&SEED thermal environment.

The return of JAXA's MPAC&SEED external experiments provided a unique opportunity to compare induced contamination predictions with measurements from flight hardware. The Boeing Space Environments Team will continue to work with JAXA to characterize contamination of the MPAC&SEED experiments. These activities are pursued to ensure a known induced contamination environment around the ISS.

#### References

- [1] M. Neish, K. Imagawa, T. Inoue, J. Ishizawa, Y. Kitazawa, Y. Yamaura, A. Murakami, and Y. Ochi: Microparticle Capture on the International Space Station Using Aerogel and Polyimide Foam, *Proceedings of the 9th International Symposium on Materials in a Space Environment*, ESA SP-540, Noordwijk, The Netherlands, 16-20 June 2003, pp. 431 – 435.
- [2] N. Baba, M. Suzuki, I. Yamagata, Y. Kimoto, and J. Ishizawa: External Contamination Observed on the Micro-Particles Capturer and Space Environment Exposure Device, *Proceedings of the 10th International Symposium on Materials in a Space Environment*, Collioure, France, 19-23 June 2006.
- [3] JAXA: Space Environment Data Acquisition equipment-Attached Payload (Website), [http://kibo.jaxa.jp/en/experiment/ef/seda\\_ap/](http://kibo.jaxa.jp/en/experiment/ef/seda_ap/), 15 Feb. 08.
- [4] N. Baba, K. Imagawa, M. Neish, and T. Inoue: External Contamination Control for JAXA Spacecraft, *Proceedings*



*of the 24th International Symposium on Space Technology and Science, ISTS 2004-h-06, Miyazaki, Japan, 30 May-6 June 2004, pp. 760-764.*

- [5] M. Neish, Y. Kitazawa, T. Noguchi, T. Inoue, K. Imagawa, T. Goka, and Y. Ochi: Passive Measurement of Dust Particles on the ISS Using MPAC: Experiment Summary, Particle Fluxes and Chemical Analysis, *Proceedings of the 4th European Conference on Space Debris*, ESA SP-587, Darmstadt, Germany, 18-20 April 2005.
- [6] Evaporation Rate Study and NDMA Formation from UDMH/NO<sub>2</sub> Reaction Product, Part 2, *White Sands Test Facility Investigative Report WSTF-IR-0188-002-04*, 17 Sept. 2004.
- [7] C. Soares and R. Mikatarijan: Thruster Plume Induced Contamination Measurements from the PIC and SPIFEX Flight Experiments, *Proceedings of the International Symposium on Optical Science and Technology 47th Annual Meeting*, SPIE 4774-20, Seattle, Washington, 7-11 July 2002.
- [8] C. Soares, R. Mikatarijan, and H. Barsamian: International Space Station Bipropellant Plume Contamination Model, *Proceedings of the 8th AIAA/ASMT Joint Thermophysics and Heat Transfer Conference*, AIAA 2002-3016, St. Louis, Missouri, 24-27 June 2002.
- [9] C. Pankop, K. Smith, C. Soares, R. Mikatarijan, and N. Baba: Induced Contamination onto JAXA's Micro-Particles Capturer and Space Environment Exposure Device – Comparison of Predictions and Measurements, *Proceedings of the 10th International Symposium on Materials in a Space Environment*, Collioure, France, 19-23 June 2006.
- [10] C. Steagall, K. Smith, C. Soares, R. Mikatarijan, and N. Baba: Induced Contamination Measurements and Predictions for JAXA'S Micro-Particles Capturer and Space Environment Exposure Device, *AIAA Journal of Spacecraft and Rockets*, Publication Pending.

#### **Acknowledgements**

The assistance of Naoko Baba and Kichiro Imagawa (JAXA) in obtaining SM/MPAC&SEED contamination measurements is gratefully acknowledged.

## Contamination Effect on SM/MPAC&SEED Experiment

Naoko BABA<sup>1</sup> and Yugo KIMOTO<sup>2</sup>

<sup>1</sup> *Manned Space Systems Department, Japan Manned Space Systems Corporation,  
Tsuchiura, Ibaraki 300-0033, Japan*

<sup>2</sup> *Institute of Aerospace Technology, Japan Aerospace Exploration Agency, Tsukuba, Ibaraki 305-8505, Japan*

Material exposure experiments are expected to present the material degradation under space environment. However, the exposure experiments can not be free from induced environments. Contamination from the International Space Station (ISS) produced the most readily change to the SM/MPAC&SEED samples, other than natural environments. Since measured characteristics of retrieved materials are affected by both natural and induced environments, it is difficult to investigate the net effect of natural environments. Energetic particles easily penetrate the contamination layer and their effects are maintained. In contrast, contaminant deposition masks the mass loss by atomic oxygen (AO), and contamination discoloration decorates the net change in sample optical characteristics induced by ultraviolet (UV) radiation. This paper was prepared to suggest when, what materials deposited on the samples how much.

**Keywords:** MPAC&SEED, Contamination, Material exposure experiment, ISS

### 1. Introduction

The Japan Aerospace Exploration Agency (JAXA) deployed three identical MPAC&SEED units for two passive experiments on the exterior of the Russian Service Module (SM) on the International Space Station (ISS) [1]. The three units were retrieved individually, after 315, 865, and 1403 days of exposure. To capture micrometeoroids or debris, very light-weight materials such as silica aerogel and polyimide foam were mounted on the both faces of the MPAC units. The SEED exposed 28 organic and inorganic samples to investigate their performances on low Earth orbit. The overall dimensions of one MPAC&SEED unit are W570 mm, H875 mm, and D158 mm. Each unit consists of four sample holders which are compact enough to be retrieved via extra vehicular activity (EVA).

### 2. Contamination Environment of SM/MPAC&SEED

The Service Module (SM) of the International Space Station (ISS) is located on the aft end, where visiting Russian vehicles dock. External contamination from vehicle thruster plumes and propellant purges had been predicted, in addition to outgassing from organic materials on the Service Module Micro-Particles Capturer and Space Environment Exposure Device (SM/MPAC&SEED) [2]. The ram faces of SM/MPAC&SEED units point toward the ISS velocity vector when the ISS flies in the X-axis in the Velocity Vector (XVV). The ISS spent more than 40% of its time in other attitudes while SM/MPAC&SEED was on board; the ram and wake face orientations also changed [3].

Pankop et al. performed induced contamination analyses of the ISS, including MPAC&SEED [4]. The field of view from and to MPAC&SEED was analyzed using an ISS geometric model, indicating that a large fraction of the view from the ram face was occupied by the SM, the SM solar array, the Functional Cargo Block, and docked vehicles such as Soyuz and Progress. Only the SM and Progress docking on the SM aft

port entered into the view from the wake face. They estimated that more contamination on the wake face was induced by the thruster rather than by outgassing. In contrast, the predicted thruster-induced contamination on the ram face was negligible [4].

Contamination of external surfaces is a complicated process that is generated by molecular deposition, crosslinking induced by ultraviolet (UV) radiation, and reaction with and erosion by atomic oxygen (AO). Passive space environment monitors were mounted on the MPAC&SEED to measure the total dose of AO, UV, space radiation, and the temperature.

Thermal analysis predicted the maximum temperature as 102°C, and minimum as -105°C at the ram surface. Only the maximum experienced temperatures were recorded using passive thermal labels on orbit. Temperature indicator 8E-50 (Nichiyu Giken Kogyo Co., Japan) mounted 1 mm under the ram surface recorded 90°C. The maximum temperatures were 50-60°C at other measurement points, 5 mm under the ram surface. The observed temperatures suggest that the thermal analysis estimated the on orbit temperature almost precisely.

### 3. Contamination Observations

#### 3.1. Optical Observation

All retrieved trays had brownish surfaces. The different coloration among units with three different exposure durations was not significant (Fig. 1).

On each unit, the wake face was a much darker color than the ram face (Fig. 2). The white donut around the fastener hole was covered by a fastener head on orbit. The brown color of the contaminated areas was deeper at the rim of the white donut.

The aerogel tile surfaces were darkened, with a roughened texture [5]. Originally it was expected that the flat and semi-transparent texture of the aerogel surface make the visual investigation easy. At the post-retrieval observation, we found that the aerogel on the wake face suffered much greater damage

than that on the ram face. The cracks on the crispy altered surfaces were increased by exposure duration. Even the aerogel on the ram face had a rough surface after extended exposure.



Fig. 1 Retrieved SM/MPAC&SEED units

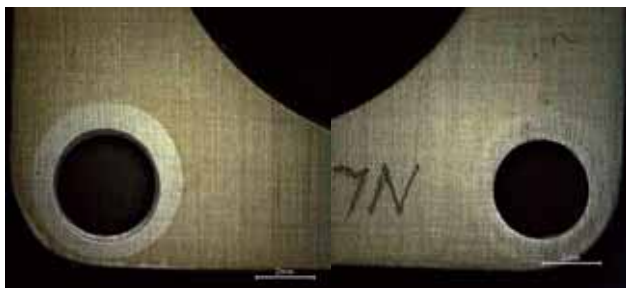


Fig. 2 Aluminum plates removed from the 3<sup>rd</sup> retrieved unit

The numerous colored spots found on the samples were roughly categorizable into 1) White clouds, 2) Brown clouds, 3) Brown spots, 4) Gray spots, 5) Black flakes, and 6) Others.

### 3.2. XPS and TOF-SIMS Analysis

Contamination of the aluminum plates that had been mounted on both the ram and wake faces of the three units was analyzed using X-ray photoelectron spectroscopy (XPS) and time-of-flight secondary ion mass spectroscopy (TOF-SIMS). The plates, which were used to fix the SEED samples, were made of A6061-T6 alloy with MIL-A-8625 type I anodic coating. The coating must be completely sealed because it has porous structure. Cobalt or nickel acetate are often used in a sealing agent.

First, XPS analyses were performed to obtain the atomic composition of the top surfaces using Quantera SXM (PHI, USA). The analysis points were selected from uniformly contaminated areas and colored spots on each plate. Moreover, XPS depth profiling using Ar-ion etching was performed on the uniformly contaminated parts, thereby revealing the internal structure of the contamination. The sputtering rate was calculated using measurement data obtained by etching with a

standard sample of SiO<sub>2</sub> film.

TOF-SIMS analyses were also performed using TFS-2000 (Physical Electronics Co., USA) on the uniform contamination to facilitate identification of the contaminant molecules: 15 kV Ga<sup>+</sup> was used as the primary ion; the raster size was 80 μm × 80 μm.

## 4. Analysis Results

### 4.1. Contamination materials identification

The XPS analysis results are presented in Fig. 3. The analyzed area was 200 μm in diameter and less than 10 nm deep. Therefore, the detected elements are inferred to include both terrestrial and on-orbit contamination.

At all analysis points on the ram and wake faces, O, C, Si, N, Al, and Ni were commonly detected. About 70% of the carbon appeared as CH<sub>x</sub>. Others were C-O, C=O, and COO. In addition, Zn, F, Na, S, Ca, Sn, P, K, and Pb were found on some analysis points.

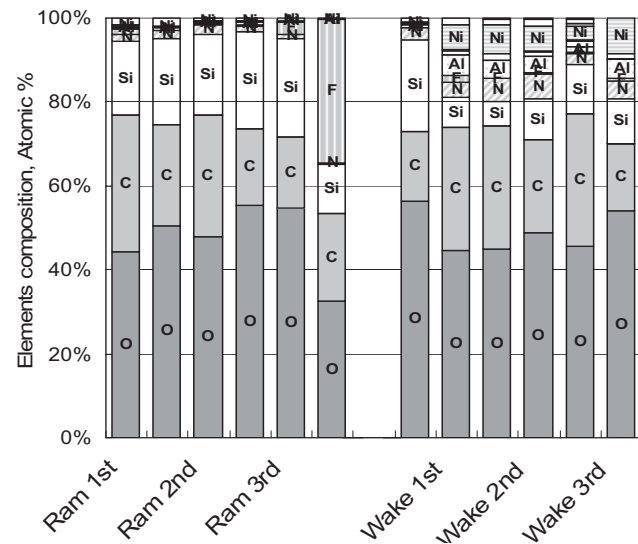


Fig. 3 Elements composition of uniform contamination analyzed by XPS [Atomic %]

In general, more Si was detected from the ram face; the wake face had more Al and Ni. Depth profile charts revealed the balance of Si, Al, and Ni. A thick SiO<sub>x</sub> layer covered the original surface on the ram face, whereas the SiO<sub>x</sub> layer on the wake face was very thin (Fig. 4). Therefore, components of an aluminum anodic coating and Ni from the sealing agent appeared immediately below the very top surface, even after 1403 days' exposure.

Nitrogen concentrations on the wake faces were considerably higher than on the ram faces (Fig. 3). Whereas N does not often appear in outgassed molecules, thruster plume contains a certain amount of nitrogen-bearing substances produced from the propellants. This supports the prediction of thruster plume-induced contamination [4]. Sulfur concentrations were 1.1–1.6% on the wake faces, but S was scarcely detectable on the ram faces; for unknown reasons.

One sample from the ram face of the third retrieved unit had significantly more fluorine than the other samples (Fig. 3). In the analyzed area, 75% of the carbon was combined with F. The depth profile indicated that an F- and C-rich top layer, 6–7

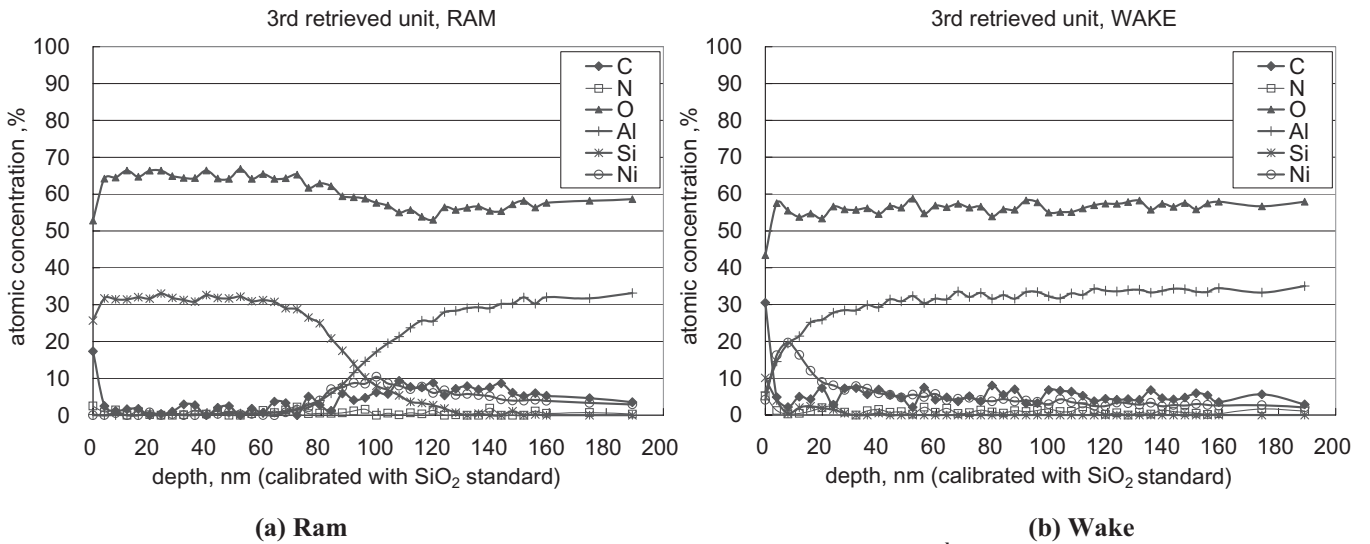


Fig. 4 Depth profiles from XPS analyses of the 3<sup>rd</sup> unit

nm thick, covered the next SiO<sub>2</sub> layer. TOF-SIMS analysis depicted the fluorine distribution.

Figure 5 presents a comparison of the major fluoride ion intensities that were analyzed using TOF-SIMS. The measured ion counts were normalized by the total count. Intensities of the CF<sup>+</sup>, CF<sub>3</sub><sup>+</sup>, C<sub>2</sub>F<sub>4</sub><sup>+</sup>, and C<sub>2</sub>F<sub>5</sub><sup>+</sup> peaks were remarkably strong on the third retrieved unit compared to the first and second units. Negative ions of fluorides, such as CFO<sup>-</sup>, C<sub>2</sub>F<sub>5</sub>O<sup>-</sup>, and C<sub>3</sub>F<sub>5</sub>O<sub>2</sub><sup>-</sup>, also had strong intensities on the third unit. They might be fragments of perfluoropolyether or polytetrafluoroethylene (PTFE) [6], etc. The intensities of the fluoride ions varied widely among the four analyzed areas on the third unit. This diversity suggests that fluorine was distributed unevenly within the same face of the third unit.

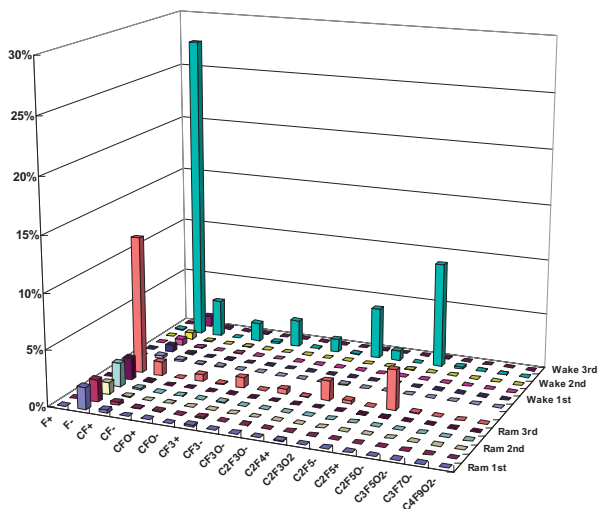


Fig.5 Normalized fluoride ion spectra analyzed by TOF-SIMS.

Five points were chosen from an aluminum plate on the wake face for XPS analysis to determine the contamination distribution in a smaller scale (Fig. 6). Contamination observed on the three sides was almost identical to that on the top, in spite of their different lines-of-sight. One side, closely faced to the frame that held the tray on orbit, presented a unique

composition. This side had much more C and F, instead of O and Si. The XPS results depict the centimeter-scale unevenness in fluorine distribution within a small area, as observed on the ram face using TOF-SIMS.

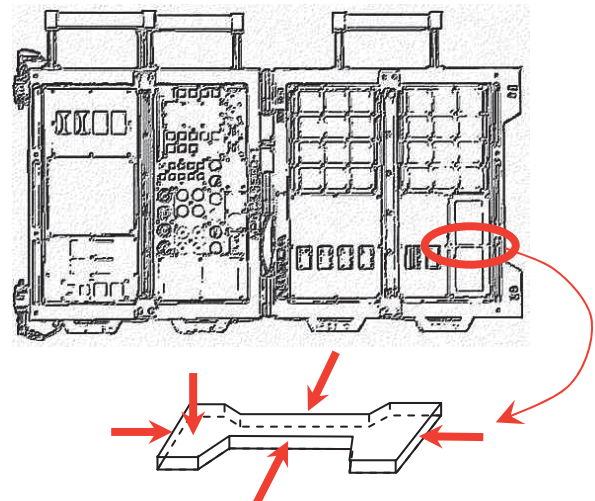


Fig. 6 XPS analysis points on an aluminum plate

The ESA Matroshka experiment facility is one possible source of outgassing fluorocarbon. Matroshka was covered by Teflon and was deployed in front of MPAC&SEED 18 days after the second unit retrieval. However, Matroshka's effects cannot fully explain the local unevenness within the third retrieved unit.

**Layered Structure of Contamination**

A C-rich layer, which was less than 2-nm thick, covered the uppermost surfaces of all specimens. The discontinuation of the depth profile suggests that the layer was the result of terrestrial contamination (Fig. 4). Next layer, which was rich in Si- and O-, was considered to be a SiOx contaminant layer that was produced by AO reaction with siloxane. Within the SiOx layer, the ratio of Si to O was 2.01–2.30. Binding energy of

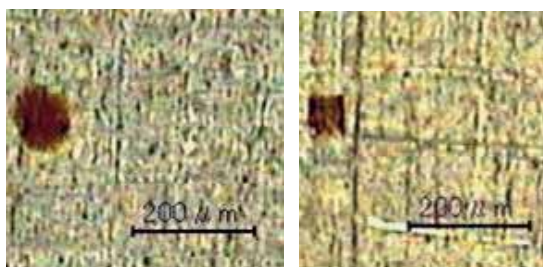


-Si2p and -O1s corroborate the identification of the layer as SiO<sub>2</sub>. The layered structure closely resembled the contamination noted at the Passive Optical Sample Assembly-I (POSA-I), one of the Mir Environmental Effect Payloads, post retrieval analysis [7]. Subsequent TOF-SIMS analysis detected fragmentary ions of polydimethylsiloxane (PDMS) on both ram and wake faces of all three units. This result suggests that the SiO<sub>2</sub> layer was formed with Si originating from PDMS contamination effused from silicone products.

### Spots Contamination

Numerous colored spots were detected on the retrieved units. They were of various shapes and colors; their diameters were of 1–1,000 μm. Though full attribution is not achievable, XPS analyses provided information to assume their origins. Some irregular shaped spots had unique elements, such as Fe or Pb. Spots that contain much more C binding F were assumed to be organic fluorides. Zinc Oxide is a typical white pigment and widely used for thermal control paint. Paint chips were possible origin of the spots containing more Zn than normal surfaces. PO<sub>4</sub><sup>2-</sup> and K<sup>+</sup> were found in a spot. Since these ions were considered to be human origin, the water dumped from the transport vehicles was a possible source.

Among the spots, roughly circular spots were considered to be formed by the impact of low-velocity droplets. There was a known source of the droplets; thruster plume. Some of the spot contaminations would be produced by the thruster plume impingement. It is possible that the thick molecular contamination layer had covered up the particles and/or liquid droplet substances on the ram faces. Accordingly, we selected two similar brown, rounded spots from various shaped/colored spots on the wake face of the third unit (Fig. 7) and analyzed their element compositions using XPS. Table 1 presents the elemental compositions of the spots.



Spot A

Spot B

Fig. 7 Brown round spots on the wake face of the 3rd retrieved unit

Table 1 Element composition of the brown spots analyzed by XPS [Unit; Atomic %]

	C	N	O	F	Al	Si	Ni	Zn	S
Spot A	45.2	23.1	22.6	2.4	1.1	2.9	2	0.3	0.4
Spot B	45.4	10.2	24.8	11.1	1.3	4.2	1.6	0.7	0.7
Normal <sup>a</sup>	24.2	4.1	49.1	0.6	3.3	11.1	5.2	0.4	1.1

<sup>a</sup>The element composition of the normal surface shows the average of the wake surfaces from the three units.

The nitrogen concentration was remarkably greater than on normal surfaces. The two compositions of the spots were very similar, except for the F and N concentrations. The time of the droplet impingement is unknown. The F concentration would vary according to the thickness of the molecular contamination layer covering the droplet. There would be sufficient time for a droplet deposited long before retrieval to develop an F-rich molecular contamination layer that covers it.

### 4.2. Contamination Layer thickness

Figure 8 indicates the contamination layer thicknesses of the three units observed by XPS depth profiling. The boundary surface between the contamination layer and the aluminum plates was not sharply defined because of the porous structure of the anodic coatings on the aluminum plates. We considered the depth at which the Si concentration exceeded Al to be the contamination layer thickness. The existence of Ni also indicates the position of the original surface. The Ni that appeared between the SiO<sub>2</sub> layer and Al-O layer is attributable to nickel acetate in the sealing agent for the anodic coating. The maximum Ni concentration appeared at almost the same depth with the crossing of Si and Al concentration curves (Fig. 4).

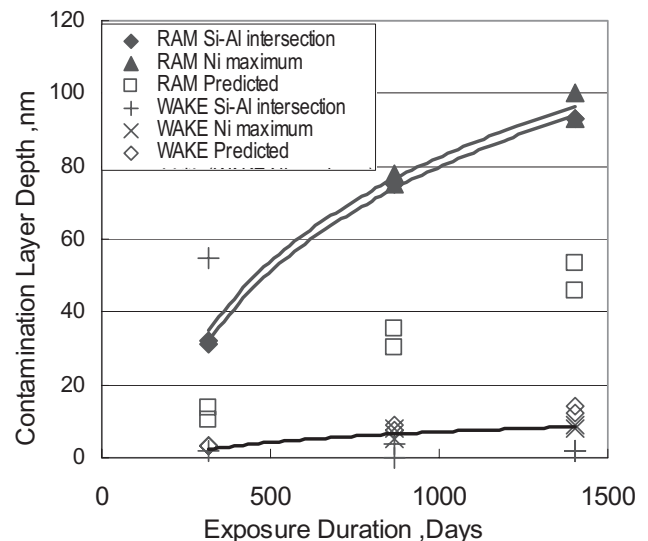
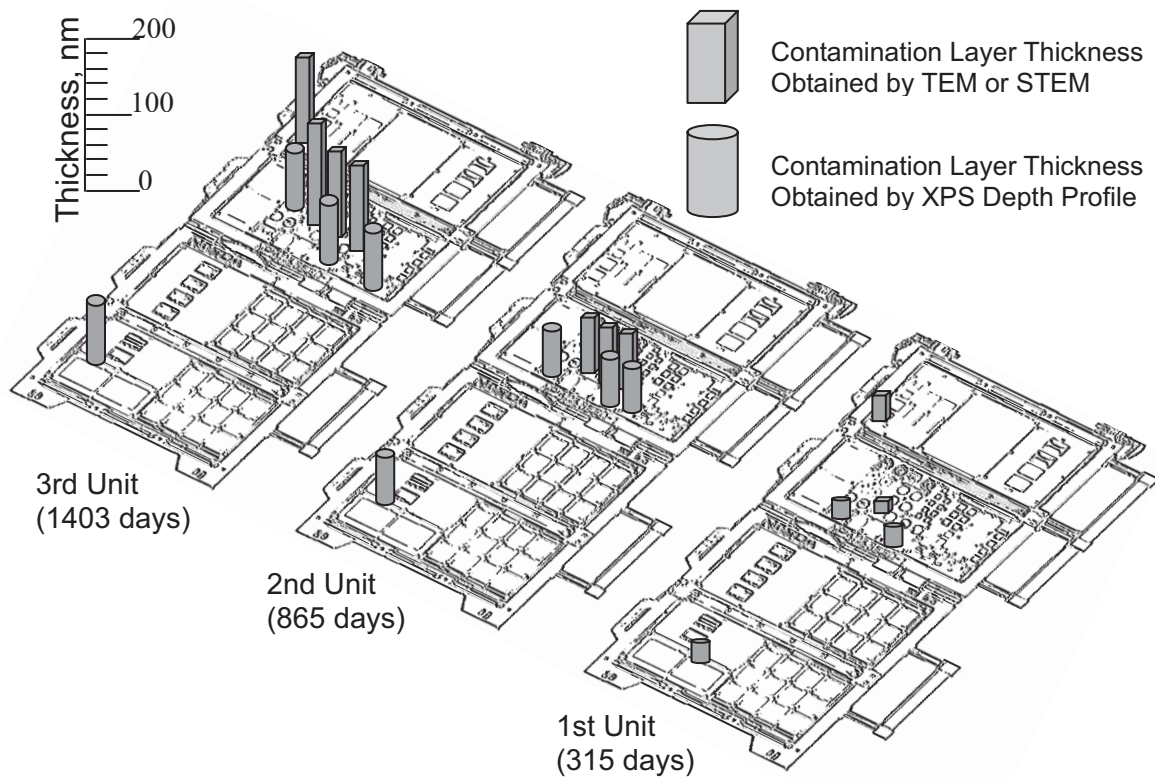


Fig. 8 Contamination Layer growth with the exposure duration

Formation and growth of the SiO<sub>2</sub> layer was also observed on several SEED samples and monitoring samples [3],[8],[9]. These SiO<sub>2</sub> layer thicknesses were measured using transmission-electron microscope (TEM) or scanning TEM – electron energy loss spectroscopy (STEM-EELS). TEM analyses were performed using H-7100FA (Hitachi, Japan), with an acceleration voltage of 100kV. The samples were prepared by ultramicrotome and RuO<sub>4</sub> stained. Figure 9 summarizes the contamination layer thicknesses observed on the three units. The SiO<sub>2</sub> layer thicknesses obtained by the TEM cross-sectional observation were 120–140 nm on the third retrieved samples. Though the TEM reported more thicknesses than XPS, the difference in analytical methods prevents equal comparison among the data. XPS depth resolution decrease related with the ion sputter time, because ion etching increase

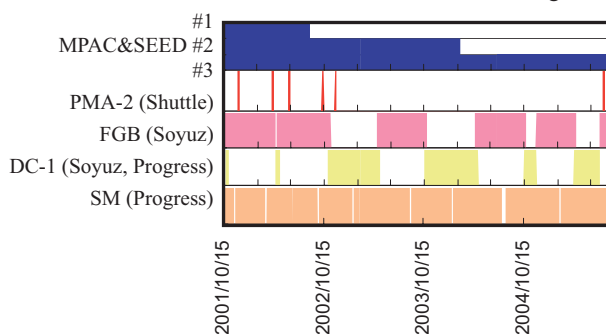


**Fig. 9 Contamination Thickness observed on the ram face**

the surface roughness, and the etching rate must be affected by the sputtering angle. On account of the surface roughness of the samples, XPS depth resolution is supposed to be not as good as TEM for thicker contamination layer analysis. One data set obtained by a method indicates that the  $\text{SiO}_2$  layer on a unit has almost even thickness for different positions. Boeing also predicted that the contamination thickness distributes within 8-nm difference on a unit [4].

#### 4.3. Term of deposition

The  $\text{SiO}_2$  layer was observed more clearly on the ram face; its thickness increased in relation to the exposure duration (Fig. 8). This observation indicates a continuous supply of siloxane, even after a long duration of exposure. About thirty vehicles visited and docked to the ISS while MPAC&SEED was on board (Fig. 10). The vehicles were constructed by flesh materials and considered to have effused more outgassing.



**Fig. 10 Visiting Vehicles Docking Durations**

From February 2003 to July 2005, the later half of MPAC&SEED exposure, no module nor truss segment was attached to the ISS owing to suspension of the space shuttle flight. The formation of the  $\text{SiO}_2$  layer on the ram faces slowed as time progressed, perhaps because of a reduction of the outgassing rates of the source materials on orbit. One analyzed area on the wake face of the first unit had much thicker contamination than other areas on the wake face. This local characteristic was inconsistent with the others; the reason is unclear.

## 5. Discussion

### 5.1. Contamination Thickness Versus Color Change

Although the contamination layers on the ram faces were much thicker than those on the wake faces, the brown color on the wake faces was deeper than that on the ram. One reason for this might be the magnitude of UV irradiation. Two passive UV monitors were mounted on both the ram and wake faces of each unit. Unexpected results were obtained from the calibration results of the monitoring samples. Data from the second unit suggest that the wake face was irradiated by 13 times more UV than the ram face [3]. The UV fluence on the MPAC&SEED is also calculated using the ISS geometric model and attitudes. Predicted UV fluence on the wake face was six times more than on the ram face. These results differ in their magnitudes. However, they are consistent with the optical appearances of the contaminated surfaces.

Thruster-induced contamination is another possible cause of the color difference. Brown coloration, which is inferred to be the result of thruster plume impingements, has been

observed commonly on the Mir space station, the space shuttle, and the ISS. Boeing predicted that the wake face would have more thruster-induced contamination than the ram face [4]. The higher nitrogen concentration observed on the wake face confirmed the prediction (Fig. 3). The darker color on the wake face is attributable to the thruster plume.

## 5.2. Contamination Layer Growth

The observed contamination layer thicknesses on the wake faces were much less than the predicted values. The cause of this difference is explainable by the process of contamination layer formation.

Although C had greater concentrations at the top surfaces, the contamination layers observed on the ram faces were formed mostly from only Si and O. The most likely scenario is selective reaction of Si with AO. In fact, SiO<sub>2</sub> formation under vacuum-UV (VUV) irradiation is reported often [10]. Because VUV electromagnetic radiation has more energy than the binding energy of C-H or Si-C, VUV separates methyl-group from PDMS [11]. Remaining Si-sites bind to AO and form rigid SiO<sub>2</sub>. Other atoms, such as C, were rejected or formed volatile molecules, and did not remain on the surface. Although the molecular deposition rate on a cryogenic surface depends strongly on the surface temperature, the maximum temperature recorded on the SM/MPAC&SEED was 60–90°C; sufficiently high to be free from light-molecule deposition.

This scenario indicates that the permanent contamination layer thickness depends on the mass of Si in the contaminants, not on the total mass of contaminants. Table 2 summarizes levels of the outgassing induced contamination predicted by Boeing [4]. The figures do not include thruster plume impingement, which does not contribute to SiO<sub>2</sub> formation. The predicted value agrees with the measured SiO<sub>2</sub> layer thickness of the order.

However, no significant difference is visible in fragmentary ion counts of PDMS between the ram and wake

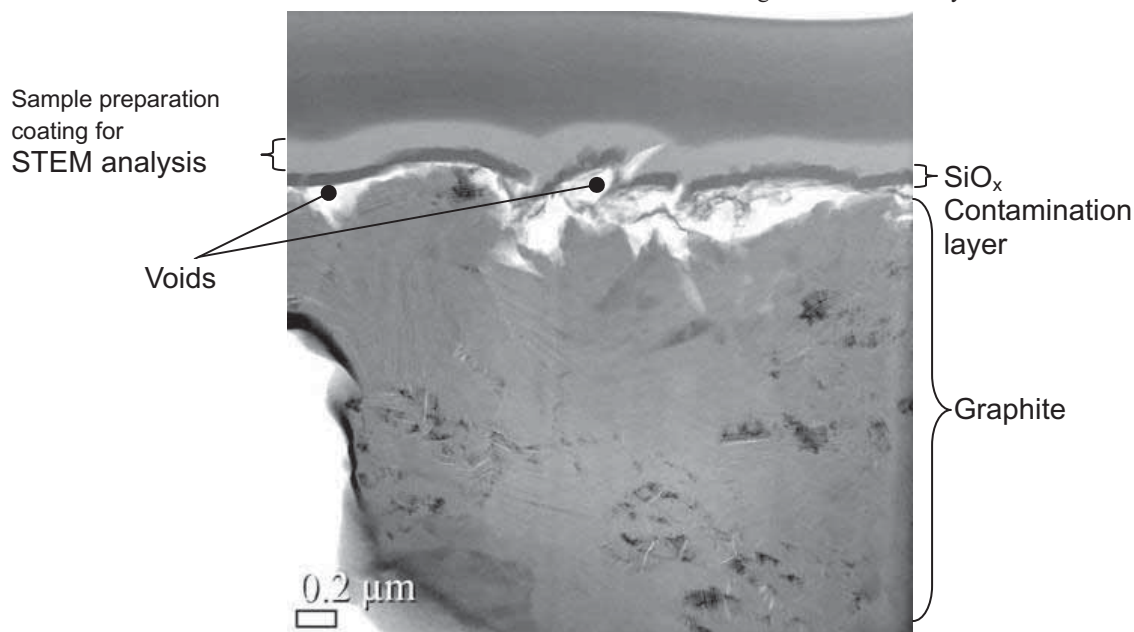
faces. It suggests that the wake face also had the siloxane supply.

**Table 2 Contamination depth, predicted<sup>[4]</sup> and measured [Unit; nm]**

		Unit 1	Unit 2	Unit 3
Ram	Predicted	10.6 – 13.5	30.3 – 35.4	45.9 – 53.3
	Measured	31, 32	75, 75	93, 93
Wake	Predicted	3.5	7.7 – 9.1	12.1 – 14.3
	Measured	2, 55	0, 4	2, 2

The difference in AO radiation still poses an eminently plausible hypothesis, although it has not been confirmed by the AO flux measurement on MPAC&SEED. Two passive AO monitors of different types were mounted on both the ram and wake faces [3]. They indicated that AO irradiation on the ram face was 1.3–1.8 times greater than on the wake face. This difference seems to be too small when compared with the observed contamination thicknesses. The AO monitors measure mass loss and the change in electric resistance by AO erosion. However, thick SiO<sub>2</sub> layer was also noted on the AO monitors on the ram face. The AO fluence on the imaginary plane on the ISS ram end was calculated using the MSIS-86 model in JAXA developed Space Environment and Effects System (SEES <http://sees.tks.jaxa.jp>). The ISS attitude changes were considered in the analysis. SEES predicted 10 times or more higher fluence than measured values. Even though the analysis did not take into account the screening by the ISS elements, the net AO fluence on the ram face could be much more than the measured value, and explainable the difference in SiO<sub>2</sub> layer thicknesses.

The observed SiO<sub>2</sub> layer thicknesses did not depend on the contaminated surface material. In fact, STEM analysis presented a crosscut image of a graphite sample that shows that the SiO<sub>2</sub> layer did not conformally trace the original surface. Figure 11 was obtained using HF-2210 (Hitachi, Japan) with an acceleration voltage of 200kV. Many voids were found under



**Fig. 11 Voids observed between SiO<sub>2</sub> layer and the original graphite surface**



the SiO<sub>2</sub> layer covering coarse surfaces, such as the graphite AO monitor or the AO eroded polyimide. This observation suggests that the SiO<sub>2</sub> formation process does not require absorption of silicone contaminants on a surface. Under such a SiO<sub>2</sub> forming environment, contamination proof surface modifications may not be effective to prevent the contamination layer growth.

### 5.3. Thruster Plume Impingement

Bipropellant thrusters on the ISS and visiting vehicles are used for reboost and attitude control. Fuel/oxidizer reaction products (FORP) are produced by an unsymmetrical dimethylhydrazine (UDMH) and nitrogen tetroxide (NTO) reaction [12]. The Energia and the Keldysh Center investigated contamination of FORP by ground experiments and sample collection from the Mir space station [13]. They obtained very close figures for the final gross-formula of an organic part of FORP, i.e. C<sub>1</sub>H<sub>3.1</sub>N<sub>0.8</sub>O<sub>0.1</sub> by a ground test and C<sub>1</sub>H<sub>2.3</sub>N<sub>0.8</sub>O<sub>0.1</sub> by analysis of samples collected on-orbit. Comparing the analyzed data, the elemental composition of the brown circular spots had sufficient compatibility to be attributable to FORP.

### 6. Conclusion

We retrieved three identical SM/MPAC&SEED units after different exposure durations. The units were covered uniformly with molecular contamination and had numerous colored spots. Contamination was much thicker on the ram faces than on the wake faces, and increased continuously with the exposure duration. XPS depth profiling revealed that the uniform contamination had a layered structure. Under the thin uppermost layer, which is considered to be terrestrial contamination, a Si- and O-rich layer followed. Within this SiO<sub>2</sub> layer, other atoms were barely detected. XPS and TOF-SIMS analysis identified the elements contained in both uniform and spot contamination. Siloxane, which forms rigid SiO<sub>2</sub> under AO radiation, was considered to be the dominant contaminant. The SiO<sub>2</sub> layer was formed without surface deposition, even on the voids of coarse surfaces. Severe UV irradiation and the repeated thruster plume impingement could cause the deep brown color specifically noted on the wake face. Brown spots found on the wake faces were presumed to have been formed by FORP impact.

### Acknowledgments

The MPAC&SEED project was carried out with the help of Roscosmos and S.P. Korolev Rocket and Space Corporation Energia (RSC Energia). The author would like to express particular gratitude to the following for their help and assistance during the course of this work: Courtney A. Pankop, Kendall Smith, Carlos Soares, and Ronald Mikatariyan of the Boeing Company, for performing induced contamination analyses; Igor V. Sorokin and co-workers of RSC Energia for the space environment exposure opportunity. Without their kind assistance, this study would not have been possible.

### References

- [1] Yamagata, I., Kimoto, Y., Miyazaki, E., Ishizawa, J., Shimamura, H., Baba, N., Imagawa, K., Suzuki, M.,

"Overview of the Micro-Particles Capturer and Space Environment Exposure Device (MPAC&SEED) Experiment," Proc. of the 10th ISMSE, ESA SP-616, September 2006

- [2] Soares, C., Mikatariyan, R., Schmidl, D., Smith, K., Pankop, C., Alred, J.W., Boeder, P.A., Pilkinton, G.D., Koontz, S., Engle, M., "Natural and Induced Space Environments Effects on the International Space Station," IAC-05-B4.2.07., 2005
- [3] Kimoto, Y., Yano, K., Ishizawa, J., Miyazaki, E., Yamagata, I., "Passive Measurement of Atomic Oxygen, UV Fluence and Radiation Effect on the ISS Using SEED Experiment," Proc. of the 10th ISMSE, ESA SP-616, September 2006
- [4] Pankop, C., Smith, K., Soares, C., Mikatariyan, R., Baba, N., "Induced contamination onto JAXA's Micro-Particles Capturer and Space Environment Exposure Device – Comparison of Predictions and Measurements," Proc. of the 10th ISMSE, ESA SP-616, September 2006
- [5] Neish, M.J. Imagawa, K., Inoue, T., Ishizawa, J., Kitazawa, Y., Yamaura, Y., Murakami, A., Ochi, Y., "Microparticle capture on the International Space Station using Aerogel and Polyimide foam," Proc. of the 9th ISMSE, ESA SP-540, pp.431-435. June 2003
- [6] Tozu-Sekiya, M., Takahashi, M., Hirokawa, K., "An Inference of the Fragmentation of Some Organic Compounds in Ga+ Primary Ion TOF-SIMS," Hyomen-Kagaku (Surface Science), Vol. 23, No. 11, pp.708-719, 2002
- [7] Zwiener, J.M., Kamenetzky, R.R., Vaughn, J.A., Finckenor, M.M., "Contamination observed on the Passive Optical Sample Assembly (POSA)-I experiment," SPIE Vol. 3427
- [8] Ishizawa, J., Mori, K., Imai, F., Yamagata, I., Suzuki, M., "Results of the Space-Environment Exposure Experiment "SM/MPAC&SEED" on the International Space Station (2): Siloxane Coated Polyimide Films, and Silicone Based Paints and Adhesives," Proc. of the 10th ISMSE, ESA SP-616, September 2006
- [9] Miyazaki, E., Yamagata, I., "Results of the Space-Environment Exposure Experiment "SM/MPAC&SEED" on the International Space Station: Flexible Optical Solar Reflector," Proc. of the 10th ISMSE, ESA SP-616, September 2006
- [10] Pippin, G., Crutcher, R., "Contamination on LDEF: Sources, Distribution, and History," NASA-CP-3194-PT-3, 1993
- [11] Murahara, M., Ogawa, Y., Yoshida, K., Okamoto, Y., "Photochemical laminating of low-refractive-index transparent antireflective SiO<sub>2</sub> film," Proc. of SPIE Volume 4932, 2002
- [12] Naumov, S.F., Gerasimov, Y.I., Sokolova, S.P., Rebrov, S.G., Gerasimova, T.I., Kalistratova, M.A., Prokofyev, A.V., Grigorevsky, A.V., Prosvirnikov, V.M., Buryak, A.K., Chernik, V.N., "Influence Orientation Thrusters Fuel/Oxidizer Reaction Products on Thermo-Optic Properties of Spacecraft Thermal Control Coatings," Proc. of the 9th ISMSE, ESA SP-540, September 2003
- [13] Rebrov, S.G. and Gerasimov, Y.I., "Investigation of the



Contamination Properties of Bipropellant Thrusters,” AIAA  
2001-2818, 35th AIAA Thermophysics Conference

**Publication list related SM/MPAC&SEED**

- [1] Baba, N., Imagawa, K., Neish, M.J., Inoue, T., “External contamination control for JAXA Spacecraft” Proc. of the 24th ISTS, June 2004
- [2] Baba, N., Suzuki, M., Yamagata, I., Kimoto, Y., Ishizawa, J., “External contamination observed on the Micro-Particles Capturer and Space Environment Exposure Device” Proc. of the 10th ISMSE, ESA SP-616, September 2006

**Thermal and Environmental Stability of Polymeric Materials**  
**-New Generation, Novel Asymmetric Polyimides for Aerospace Materials-**

Rikio YOKOTA

Institute of Space and Astronautical Science, ISAS/JAXA, 3-3-1 Yoshinodai, Sagami-hara-shi,  
Kanagawa 229-8510, Japan

For developing heat resistant and high performance polyimides, the relationships between the stereochemical imide structures and thermo-mechanical properties have been discussed. Addition type imide oligomers (TriA-PI) such as 2, 3, 3', 4'-biphenyltetracarboxylic dianhydride (a-BPDA), /oxydianiline (ODA)/4-phenylethynyl phthalic anhydride (PEPA) and/or other asymmetric monomers (fluorenylidene groups: BAFL, BAOFL) were synthesized and characterized. The cured oligoimides exhibited high thermal, mechanical properties in addition to the excellent melt fluidity and solubility, TriA-PI/carbon fiber composites were well consolidated for high temperature structural components. The heat sealable, thermoplastic thin films having high durability in space has been successfully developed by using asymmetric 2,3,3',4'-oxydiphthalic anhydride (a-ODPA) as well. Thin film of a-ODPA polyimide exhibited excellent high thermo-mechanical properties ( $T_g = 270^\circ\text{C}$ ) and heat sealing property with durability for irradiation of proton. It is shown that asymmetric aromatic imide structures without any weak linkages such as alkyl and methylene groups are powerful tools for a molecular design of high performance polymeric materials for solar sail membrane.

**Keywords:** Thermo plasticity, Asymmetric polyimide, Heat resistance, Solar sail, Primary structure

### 1, Introduction

Aromatic polyimides such as PMDA/ODA and BPDA/PDA have been widely used for aerospace applications due to their outstanding combinations of thermo-mechanical and space environmental stability [1-5]. However, these rigid and symmetric polyimides prefer to form order-structure because of geometrically planar, rod-like structures resulting in poor solubility and melt fluidity. Therefore, it is normally difficult to have thermo plasticity and to use as a molding or a matrix resin for carbon fiber reinforced composites [6]. Recently, the polyimides derived from asymmetric aromatic dianhydride such as BPDA and ODPA have been reported as novel high performance polymeric materials with unusual and attractive properties [7].

We have successfully reported at the Polycondensation 2004 in V.A. that the polyimides consisting of asymmetric BPDA dianhydrides (a-BPDA or I-BPDA) indicated not only high  $T_g$  but also amorphous processable polyimide resins due to bent and rotationally hindered structure of a,i-BPDA, resulting in high solubility in organic solvent and high melt fluidity [8]. A strong demand of improving high performance polymeric materials for spacecrafts is increases year after year [9-13]. So, this paper will describe a way of improving thermal, mechanical and space environmental properties by using asymmetric imide structures as follows: 1) Isomeric biphenyl (BPDA) polyimides. -Attractive characteristics of asymmetric aromatic polyimides-, 2) Novel heat resistant thermoset-polyimide resins (TriA-PI) and their graphite fiber composites, 3) Newly developed asymmetric thermoplastic polyimide films for solar sail membrane [14]

3/10/2008 Tsukuba

## Thermal and Environmental Stability of Polymeric Materials -New Generation, Novel Asymmetric Polyimides

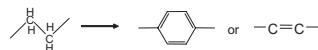
Rikio YOKOTA

Institute of Space and Astronautical Science, ISAS/JAXA, 3-3-1 Yoshinodai, Sagami-hara-shi, Kanagawa Japan 229-8510, tel: +81-42759-8056, fax: +81-42759-4251, E-mail: riki@isas.jaxa.jp.

### 1, Thermal Stability of Polymeric Materials

1) Physical view point: Max. service temperature :  $T_g$  ( $T_m$ )

Chemical structure : flexible to rigid



Disadvantages : Insoluble, difficultly on molding

2) Chemical view point: Polymer degradation : Bond dissociation (D)

C-C (83kcal/mol)  $\rightarrow$  C=C (145 kcal/mol)

C-H (99kcal/mol)  $\rightarrow$  C=C (123 kcal/mol)

3) Ablation and thermal insulation; evaporation of low molecules and carbonization---hetero-aromatic rings with ??

[5]Yokota R 1995 *Photosensitive Polyimides: Fundamentals and Applications* eds (Lancaster, PA: Technomic)

### Evaluation of thermal stability of polymers by TG

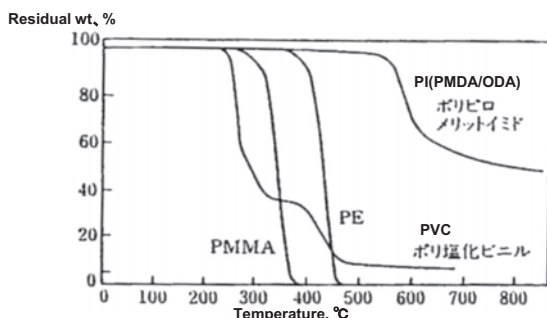


Figure 1. Thermal stabilities of various polymers in  $N_2$  flow by thermo-gravimetric measurement

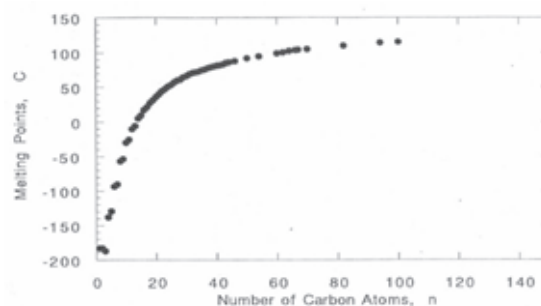


Figure 2 Melting temperature of normal alkanes vs  $-(CH_2)_n-$

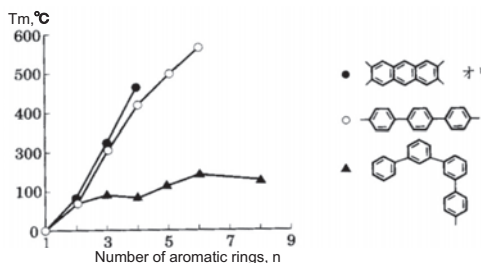


Figure 3 Melting temperature, vs number of aromatic rings, n

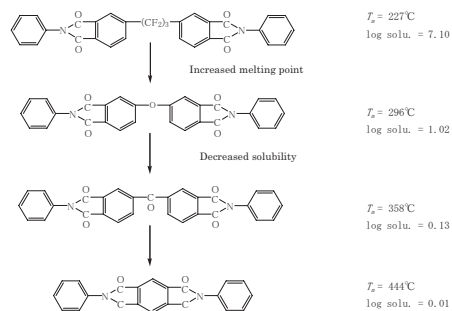


Figure 4. Relationships between chemical structure and  $T_m$ , solubility of aromatic imide model compounds (Dine hart et al)

Table 1 Commercially available polyimide and heteroaromatic polymers

Name	Structure	Film (μm)	Tg (°C)	Modulus (GPa)	Elong. (%)	Stability UV	Stability Red	Plasticity
APIOL AH (KAPTON)		~7.5	420	3.0	~50	○	○	X
UPILEX-S		~7.5	380	9.0	30	○	○	X
UPILEX-R		12.5	300	3.0	100	○	○	Δ
AURAM		25	250 (Tm: 380)	3.0	90	○	○	○
ULTEM		12.5	218	3.0	80			Δ ○
ZYLON (PBO)		Δ	?	(10.0)		Δ	○	X
ARAMIDA (ARAMID)		2.5	?	15.0	20	Δ	Δ	X

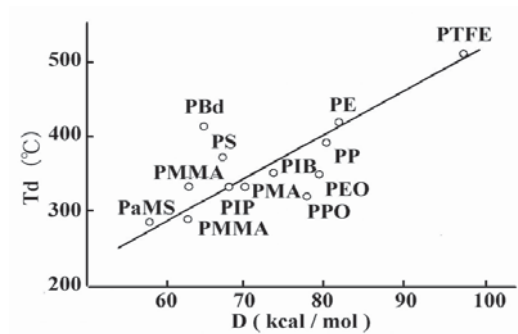


Figure 5. Thermal stability at 50% wt loss temperature vs the lowest bond dissociation energy, D in the polymers

Table 2. Important bond strength

Bond	Bond Strength (eV)
C-N	3.16
C-C	3.58 (82.7kcal mol <sup>-1</sup> )
C-O	3.70
C-H	4.24
C-F	5.02 (132.3kcal mol <sup>-1</sup> )
Al-O	5.30
P=O	5.63
C=C	6.24 (144.1kcal mol <sup>-1</sup> )
N=O	6.28
Zr-O	8.10
C=O	8.27
Si-O	8.30

Photon of λ = 200 nm corresponds to 143 kcal mol<sup>-1</sup> (λ = 500 nm : 57 kcal mol<sup>-1</sup> (1 eV = 23.1kcal))

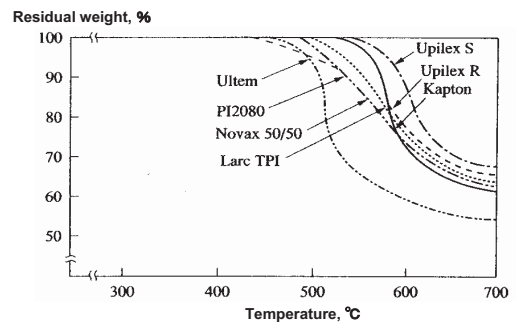


Figure 6. Thermal stability for commercially available aromatic polyimides in N<sub>2</sub> flow, ΔT = 5°C/min

Table 3. Chemical structures and Tgs of polyimides

Kapton		428
Novax		407
Upilex R		303
Upilex S		359
Larc TPI		256
PI2080		310
Aurum		250
Ultem		215

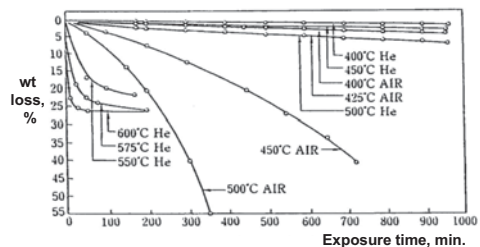


Figure 7. Isothermal thermal stability of KAPTON H  
C.E.Sroog et al, J.Polym.Part A,vol3. 1373(1965).Sci.,



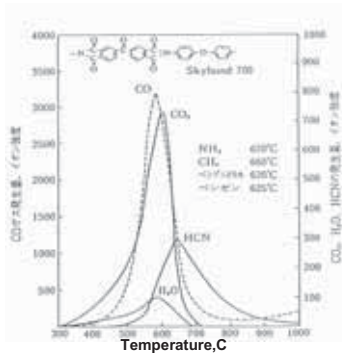
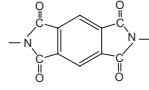


Figure 8. Temperature dependence of volatile gases for Skybond 700 polyimide

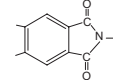
### Symmetric type Aromatic Polyimide

pyromellitimide



rigid and planar structure  
strong intermolecular interaction  
charge transfer complex,  
high-order structure

phthalimide



excellent thermal stability,  
low C.T.E  
Outstanding Environmental Stability  
Difficulty on Molding: need a flexible structure into diamine part  
Decrease Max. Service Temperature

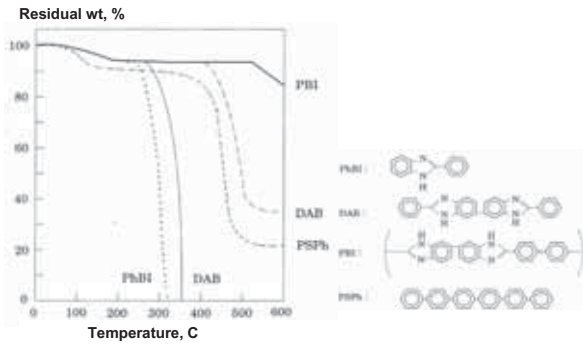
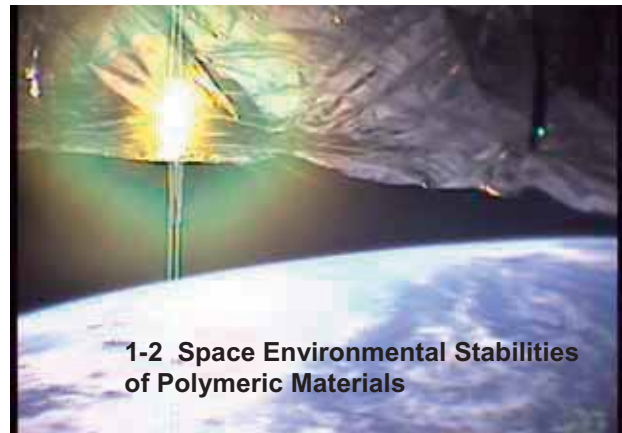


Figure 9. Tg curves of aromatic polybenzimidazole and their model compounds: — in vac, ---- in N<sub>2</sub> flow



1-2 Space Environmental Stabilities of Polymeric Materials

Table 4. Space environments-pressure, gases and radiation

Altitude (km)	Pressure (torr)	Thermo-dynamic temperature (K)	Gas concentration (No. of particle)	Composition	Ultraviolet radiation	Particle radiation (particles cm <sup>-2</sup> s <sup>-1</sup> )
Sea level	760	~300	2.6 × 10 <sup>19</sup>	78%N <sub>2</sub> , 21%O <sub>2</sub> , 1%Ar	Section of solar spectrum λ	—
80	10 <sup>-6</sup>	—	4 × 10 <sup>17</sup>	N <sub>2</sub> , O <sub>2</sub> , Ar	—	—
200	10 <sup>-8</sup>	~1200	10 <sup>16</sup>	N <sub>2</sub> , O <sub>2</sub> , O*	—	—
800	10 <sup>-9</sup>	~1300	10 <sup>8</sup>	O, He, O*, H	>0.3	10 <sup>10</sup> protons>85MeV
6,500	10 <sup>-12</sup>	—	10 <sup>5</sup>	H*, H, He*	Absorption zone	10 <sup>10</sup> electrons>40KeV
23,000	<10 <sup>-14</sup>	—	10 <sup>-10</sup>	86%H <sup>+</sup> , 14%He <sup>2+</sup>	Full solar spectrum	10 <sup>10</sup> protons>5MeV
					Full solar spectrum	10 <sup>10</sup> electrons>40KeV
						10 <sup>10</sup> electrons>1.6MeV

Table 5. Variation of space environment with altitude Categories

Categories	Distance from earth	Constituents
Low Earth Orbit (LEO)	up to 1,000 km	Atomic Oxygen, Meteoroids, Debris, Ultraviolet, Thermal Cycling
Mid Earth Orbit (MEO)	1,000-35,000 km	Van Allen Radiation, Meteoroids, Debris, Ultraviolet, Thermal Cycling
Geosynchronous Orbit (GEO)	> 35,000 km	Solar Flare Protons, Spacecraft Charging, Ultraviolet Thermal Cycling

Table 6. Space environments and the durability of polymeric materials

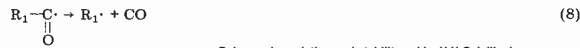
Space environment	Effects and factors	Changes of materials	Items
High vacuum	Vaporization of the additives and degradation volatiles	Contamination to the surfaces, decreasing transparency	Rubber and lubricant, grease
Micro-gravity	Diffusion and condensation	Contamination to the surfaces	
Thermal cycle	Thermal stress and C.T.E mismatching	Delamination and crack	Composites, adhesives
High and low temperatures	Thermal degradation	Brittleness	Films, adhesives and composites
Visible. & UV exposure	Absorption and degradation	Decreasing Mw and increasing coloration, Brittleness	Films, TML
Space radiations	Degradation	Decreasing Mw, crosslink and coloration, Brittleness	Films, TML, Solar cell
Atomic Oxygen	Oxidation and erosion	Decreasing thickness and coloration	All organic materials
Electrification	Static electricity	Electric discharge	Solar array, cables and spacecrafts

1.3 Photochemical reactions

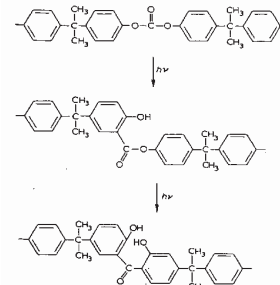
Most photochemical processes studied so far in polymers involve excited singlet or triplet states. In general, the distinction must be made between primary and secondary photochemical processes. In a primary process, the excited molecule dissociates into free radical fragments.



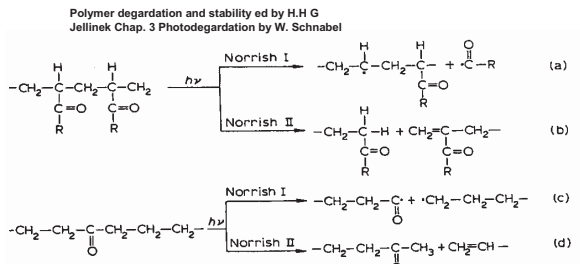
This will always happen if the excitation level reached is greater than the bond dissociation energy corresponding to this level or if the excited state is a repulsive one. Reaction (6) is supposed to occur very rapidly. A primary process according to reaction (6) was suggested to be responsible for the fragmentation of ketones during the Norrish type I process



Polymer degradation and stability, ed by H.H G Jellinek  
Chap. 3 Photodegradation by W. Schnabel

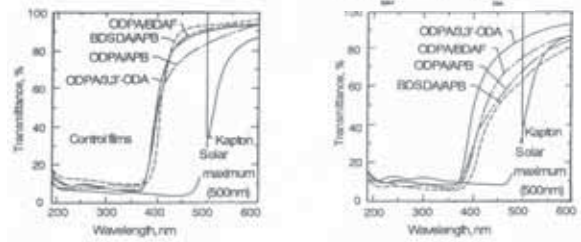


Scheme 4. Photo-Fries rearrangement of polycarbonate. Polymer degradation and stability ed by H.H G Jellinek Chap. 3 Photodegradation by W. Schnabel



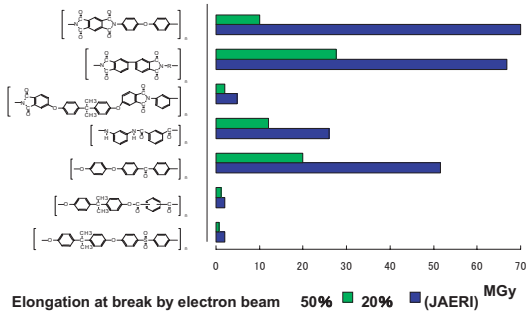
Scheme 2. Chemical reactions induced by light absorption of ketochron

Figure 10. UV - Vis spectra of polyimides :controlled and exposed (300 esh)



T.StClair et al, Sampe J, July/Aug, p28 1985

Figure 11. Space environmental stability of aromatic polymers



A STUDY ON POLYIMIDE MLJ OF THE TEN MONTHS FLOW SPACE FLYER UNIT

Riho Yokota, Akira Ohnishi, Yuzuru Hoshizono, Kyo-ichiro Taki  
Institute of Space and Astronautical Science, Ministry of Education, 3-1-1 Yoshinodai, Sagami-ku, Kanagawa, Japan  
phone: 0581-427-5139(1), fax: 51-1183  
Shin-ichi Kumada  
Department of Chemistry, Gosei University  
Kiryu-shi, Gunma, Japan, phone:0361-271-5312, fax: 35-1311  
Kiyokazu Akahori, Hirotsugu Nagano  
Electronic Materials R&D Div  
Chubu-oku, Shiga, Japan 521

Figure 12 Illustrated SFU





Figure 13 Discolored polyimide MLI surface of EPEX on SFU [5]

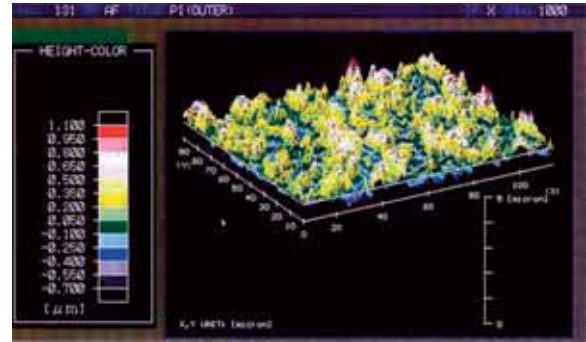


Figure 14. 3D SEM of retrieved polyimide MLI surface of EPEX on SFU

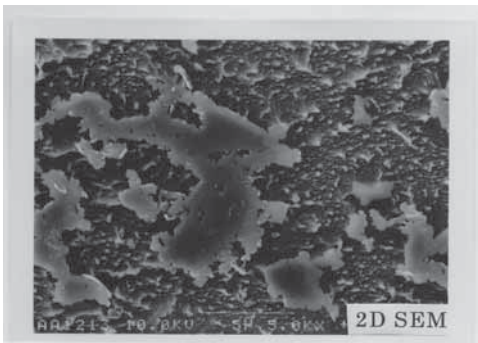
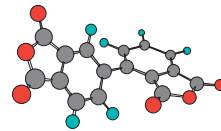
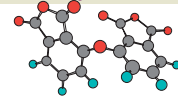


Figure 15. 2D SEM for the contaminated EPEX MLI surface retrieved



**2-1) Asymmetric aromatic polyimides**

We have reported at the Polycondensation 2004 in V.A. that the polyimides using asymmetric BPDA dianhydrides (a-BPDA or i-BPDA) are very attractive monomers for heat resistant polymeric materials. This is because asymmetric BPDA gives not only high T<sub>g</sub> but also amorphous PIs due to bent and rotationally hindered structure of a,i-BPDA, resulting in high melt fluidity.



**Why is polyimide almost the only heat resistant polymer films in industry ?**

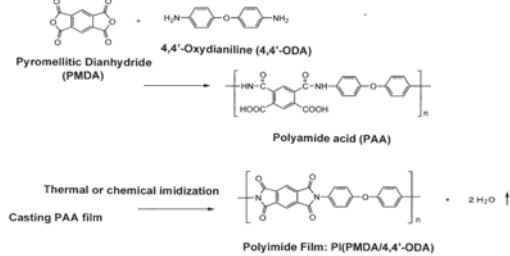
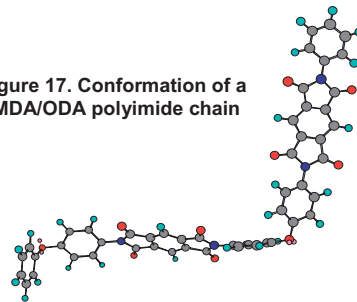


Figure 16 Process of Polyimide Film

PMDA/4,4'-ODA polyimide has been prepared by two step method through thermal imidization process of precursor PAA film

Figure 17. Conformation of a PMDA/ODA polyimide chain



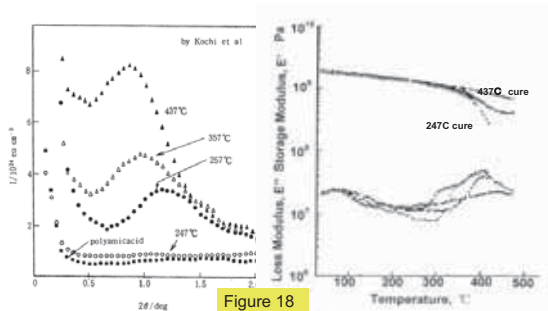
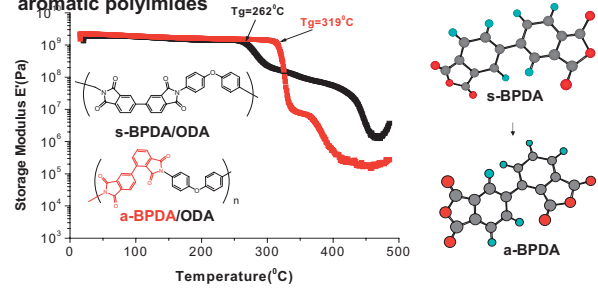


Figure 18

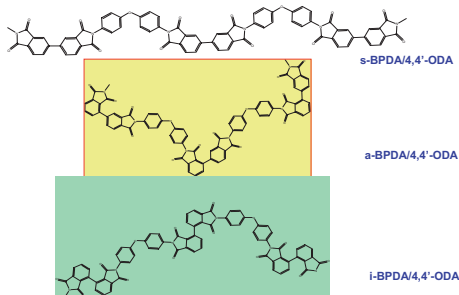
Ordered structures of PMDA/ODA are developed and thermal, mechanical properties of the films are extremely improved. [6]

Figure 19. Attractive characteristics of asymmetric aromatic polyimides



Highly bend a-BPDA/ODA, the Tg shifts to high temperature, and a large drop in E' at Tg indicates the possibility of processable polyimide with high Tg [8].

Figure 20. Conformation of Isomeric BPDA/4,4'-ODA polyimides



i-BPDA/4,4'-ODA needs the largest space for the segmental motion to a relaxation process, while s-BPDA needs the smallest space

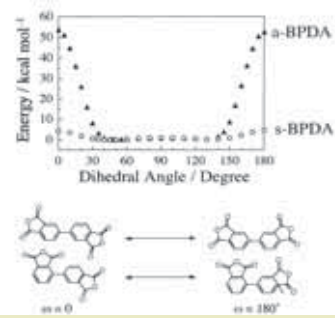


Figure 21. Rotational barrier estimated by semi-empirical M.O of s- & a-BPDA s-BPDA is very low rotational barrier, while free rotation in a-BPDA practically is inhibited due to steric hindrance between ortho-H & carbonyl group

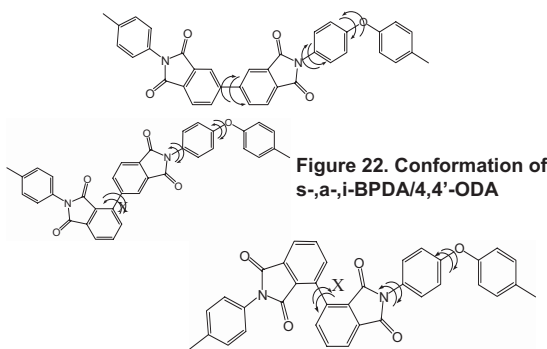


Figure 22. Conformation of s-, a-, i-BPDA/4,4'-ODA

The local rotation of the rigid segment composed of BPDA group and an adjacent diamine group were hindered

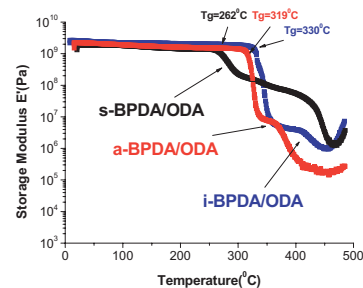


Figure 23. DMA curves of isomeric BPDA polyimides with 4,4'-ODA Tg moves towards high temperature with highly bend BPDA, suggesting the largest space for the segmental motion. The large drop in E' at Tg for a-, i-BPDA PIs provides much larger space in comparison with that of s-BPDA PI



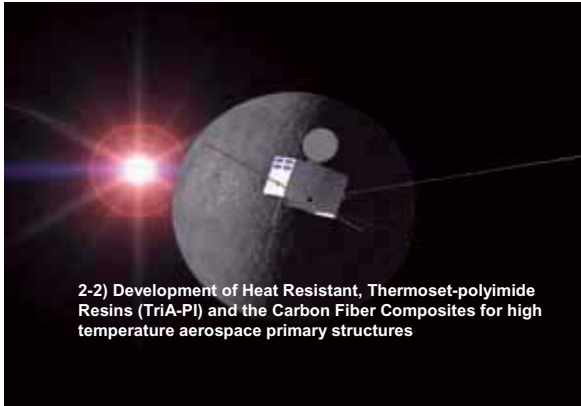
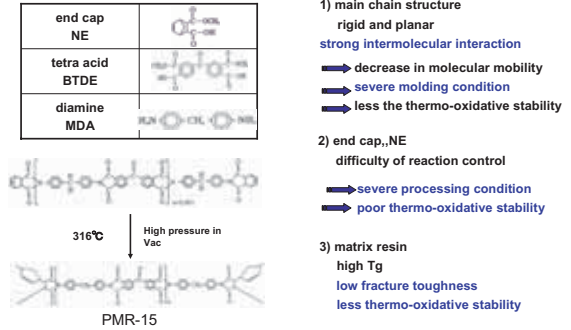


Figure 24. 1<sup>st</sup> Generation addition type polyimide resin:PMR-15 for heat resistant composites [9]



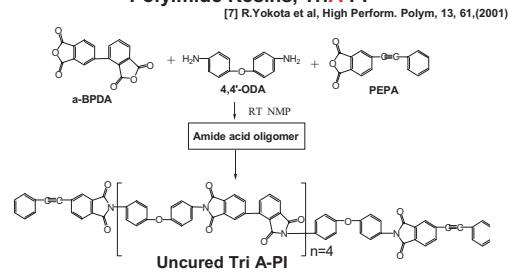
**Figure 25. 2<sup>nd</sup> Generation Polyimide Resin: PETI-5**  
NASA Langley Research Center  
P.M.Hergenrother et al. Polymer, 34, 630(1993)

Molecular weight (calc.), Mn	5000
Monomers	s-BPDA (3,3',4,4'- Biphenyl tetracarboxylic dianhydride) 3,4'- ODA (oxydiamiline) 1,3- APB (bis 3-aminophenoxy benzene) 4- PEPA (Phenylethynylphthalic anhydride)

PEPA s-BPDA/Ar PETI-5 85%:15%

Medium high temperature addition polyimide: Tg=270C(cured),  
Good processability, High fracture toughness,  
High oxidative stability(PEPA)

Figure 26. Asymmetric Aromatic Addition-type Polyimide Resins, TriA-PI



Cured TriA has high fracture toughness and good processability in addition to high Tg and high oxidation stability. We are developing the heat resistant fiber reinforced composites.

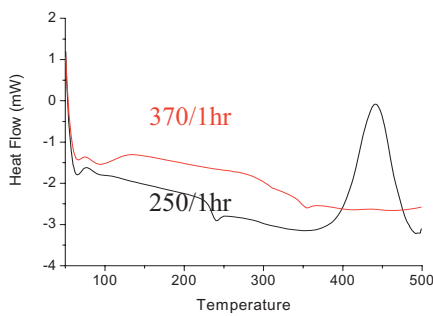
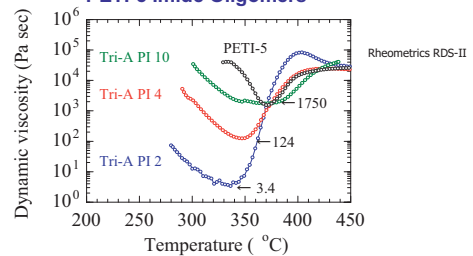


Figure 27. DSC curves of TriA-PI(n=4) resins with and without cured

Figure 28. Dynamic Melt Viscosities of the Tri-A PI and PETI-5 Imide Oligomers



- The minimum viscosities were 3.4, 124, and 1750 Pa sec for Tri-A PI 2 (Mw~1600), Tri-A PI 4 (Mw~2500), and Tri-A PI 10 (Mw~5250), respectively
- This corresponded to the viscosities reported for PETI-5 (5.0, 90, and 1000 Pa sec for Mw~1250, ~2500, and ~5000).

Figure 29. Physical and mechanical properties of TriA-PI, PETI-5 and PMR-5 cured and the carbon fiber composite

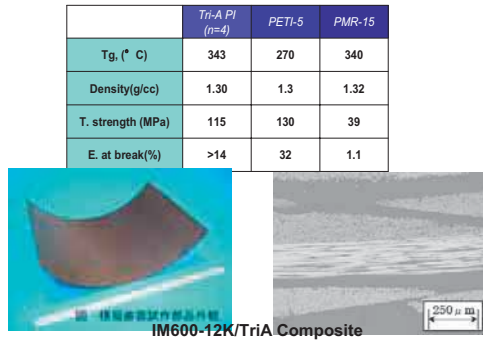


Figure 30. Fabrication of TriA-PI/CF composites by routing from amide acid solution prepreg

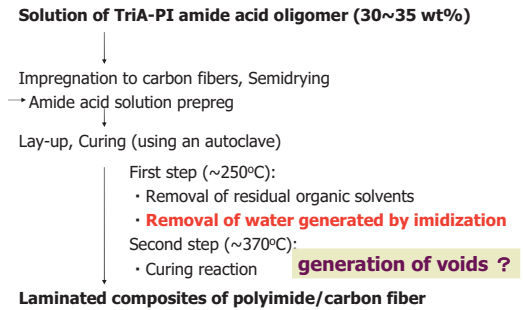


Figure 31. Incorporation of additive fluorenylidene groups into TriA for improving solubility of the oligomers (Y.Ishida, R.Yokota, T.Ogasawara, 7<sup>th</sup> China-Japan seminar on polyimides 2006, 9 in Tokyo)

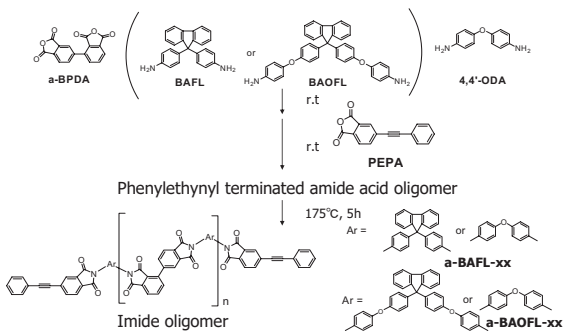


Figure 32. Synthesis of an additive imide oligomer with fluorenylidene groups: s-BPDA/BAOFL/PEPA

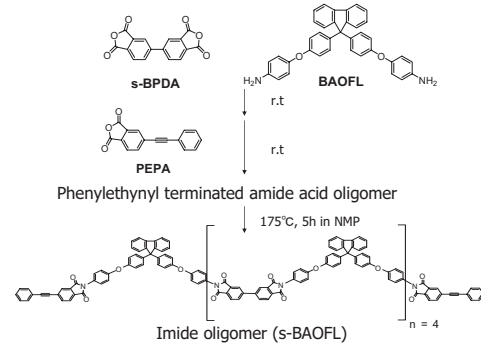


Figure 33. Properties of the imide oligomer and cured resins

	Monomer			Solubility in NMP (wt %)	Processability	Min. melt viscosity <sup>a)</sup> (Pa s)
	s-BPDA (mmol)	BAOFL (mmol)	PEPA (mmol)			
s-BAOFL	4	5	2	33	good	326

a) Measured by a rheometer.

- Imide solution prepregs can be prepared
- Low minimum melt viscosity, good processability

Properties of the cured resin film based on s-BPDA and BAOFL<sup>a)</sup>

	T <sub>g</sub> (°C) <sup>b)</sup>	T <sub>5%</sub> (°C) <sup>c)</sup>	E (GPa) <sup>d)</sup>	σ <sub>b</sub> (MPa) <sup>e)</sup>	ε <sub>b</sub> (%) <sup>f)</sup>
s-BAOFL	321	551	2.79	110	10.2

a) Cured at 370°C for 1h. b) Determined by DSC at a heating rate of 10°C/min under argon. c) Determined by TGA at a heating rate of 10°C/min under argon. d) E: tensile modulus e) σ<sub>b</sub>: tensile strength f) ε<sub>b</sub>: elongation at break

**High thermal resistance, good mechanical properties**

**T<sub>g</sub> was 50 °C higher than that of PETI-5 (based on s-BPDA, T<sub>g</sub>=270 °C)**

Figure 34. Comparison between dianhydride isomers : properties of imide oligomers

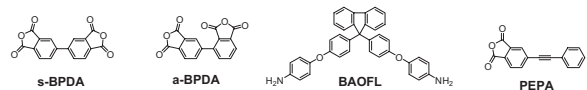
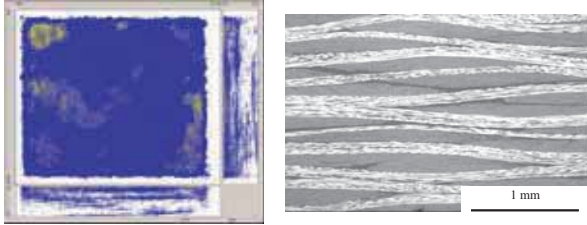


Table. Properties of the imide oligomers containing fluorenylidene groups

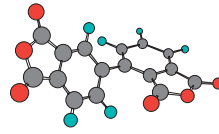
	Dianhydrides	Diamines BAOFL/4,4'-ODA	Solubility in NMP (wt %)	Processability	Min. melt viscosity <sup>a)</sup> (Pa s)
s-BAOFL-50	s-BPDA	50 / 50	partially soluble	good	1084
s-BAOFL-100	s-BPDA	100 / 0	33	good	326
a-BAOFL-50	a-BPDA	50 / 50	40	good	120
a-BAOFL-100	a-BPDA	100 / 0	40	good	167

a) Measured by a rheometer.

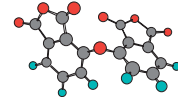
Figure 35. Evaluation of the polyimide/CF composite by ultrasonic inspection and optical micrograph



Good quality  
No voids and no clacks  
100 mm x 100 mm, plain woven fabric 12 ply



**Conclusions**  
Monomers of highly bent, asymmetric structures such as BPDAs, ODPAs, BOAFL etc are demonstrated as the key materials for new generation, high temperature composites with good processability and high temperature mechanical properties

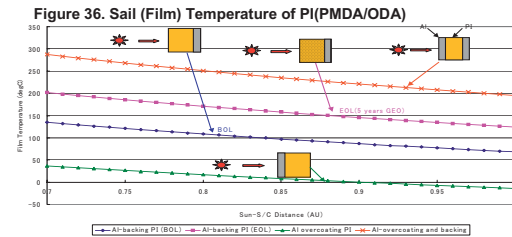


**What is a solar sail spacecraft ?**

Fridrikh Tsander proposed the concept of solar sail spacecraft obtained by reflecting sunlight off of a large, a very thin, metalized polymer film.

**What kinds of polymeric films can be used ?**

The key technologies for solar sail spacecraft are the sealing, fabricating, packaging, and deployment in addition to the development of thermally and space environmentally stable polymer film



**How can you fabricate a large solar sail**

Figure 37. Feasibility on various sealing methods of thin films for solar sail

Case 1. A high Tg polyimide film with a low Tg polymer on the surface layer for heat sealing  
Requirement : 1) Development of the coating technology and of the sealing machine for polyimide film. 2) Environmental stability (heat, radiation and UV)

Case 2. Thermo-plastic polyimide with relatively low Tg  
Requirement : 1) Evaluation of space environmental stability. 2) Sealing conditions such as temperature, pressure, time, etc.

Case 3. Sealing by using an adhesive tape  
Requirement : 1) Creep deformation of the adhesive layer, out gases, 2) Evaluation of space environmental stability



Polyimide Solar Sail Deployment in Space by S-310-34 rocket 2004.8  
Sail material and fabrication

1. Sail film: Aluminized Apical AH polyimide 7.5 μ m, width 109cm
2. Fabrication: PET based acrylic adhesive tape



Figure 38. S-310-34 sounding rocket at 2004.8

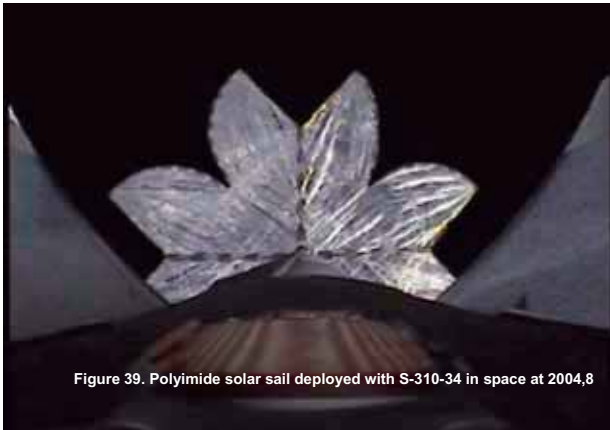
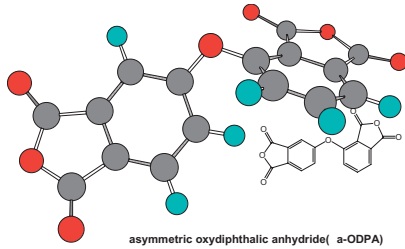


Figure 39. Polyimide solar sail deployed with S-310-34 in space at 2004,8

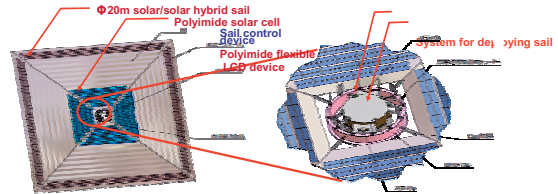


Figure 40. Polyimide solar sail deployed in space by S-310-34

**2-3) Newly developed asymmetric aromatic thermoplastic polyimide films for solar/solar cell hybrid sail spacecraft**



**Figure 41. Configuration of Solar/solar cell hybrid sail**



**Sail membrane and devices of hybrid sail**

- 1, Solar sail : ISAS/JAXA developed a-ODPA/ODA film (7 μ m) or Kaneka APICAL- AH 7.5 μ m
- 2, Polyimide thin solar cell film : Fuji FWAVE polyimide solar cell or ITFT(U.S.A) 25 μ m, 30cm(w)
- 3, Sail control device Polyimide flexible LCD device (Nihon Itagarasu )
- 4, Space debris counter PVDF film (Kureha)
- 5, Silicon adhesives : Toray/Dow (Silicone RTV4086)

**Developments of thermoplastic polyimide sail membrane**

- Goal
1. Heat sealing: 320 - 350 °C, 1min
  2. Solubility in DMAc or NMP 30 % <
  3. Space environment; proton 10kGy (1 year) radiation: 10~20MGy
  4. Thermal stability: Tg = 280 °C
  5. Film ( t ) 5~7 μ m, ( w ) 100cm width
  6. Mechanical properties σ b 100~200MPa modulus (E) 1~3GPa elongation at break, 50-80%

**Figure 42, Chemical structure of X linkage vs Tg for PMDA and BPDA**

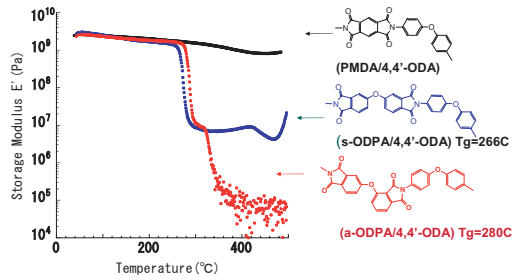
略号	ポリイミド単位構造	Xの化学構造とTg (°C)				
		-C-	-CF-	-CH-	-C-	-S-
PMDA		271	248	247	233	217
BPDA		242	230	220	210	206

**Figure 43, Commercially available thermoplastic polyimides**

Larc TPI		256
PI2080		310
Aurum		250
Ultem		215



Figure 44, Chemical structure/molecular mobility relationship



Asymmetric PI(a-ODPA/4,4'-ODA) polyimide exhibits an high Tg and very large drop in E' at Tg, indicating amorphous and low melt viscosity (thermo-plasticity).

Figure 45, Space environmental stability of aromatic polymers

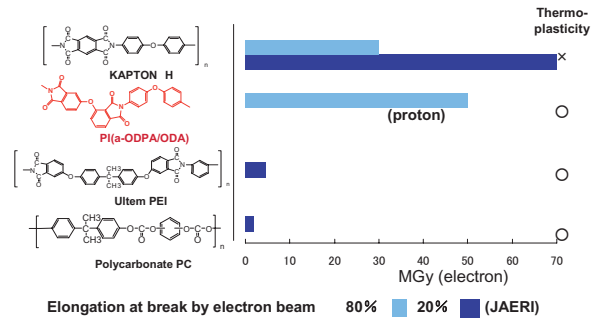


Figure 46, Summary of physical properties of ISAS Polyimides

Polyimide	[η]	Tg	Elongation at break	Solubility in NMP	Heat sealing
	(dl/g)	(°C)	(%)	(%)	
PI(a-ODPA/1,3,4-APB)	1.0	214	60	>20	Good
PI(a-ODPA/4,4'-ODA) (ISAS laboratory)	0.84	264	28	>20	Good
PI(a-ODPA/4,4'-ODA) (Fujimori Co.)	0.62	265	75	>20	Good

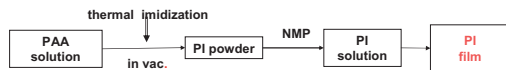


Figure 47, Development of Asymmetric ODPA thermoplastic polyimide sail membrane in ISAS

- Results (March 10, 2008)
- Heat sealing: 320 - 350 °C, 1min
  - Solubility in DMAc or NMP 30 % <
  - Space environment; proton 50MGy
  - Thermal stability: Tg = 280 °C
  - Film fabrication (t) 5~7 μm, (w) 100cm width
  - Mechanical properties σ b 100~200MPa  
modulus (E) 1~3GPa  
elongation at break, 50-80%

## Conclusion

Monomers of the highly bent, asymmetric structures such as BPDAs, ODPAs, BOAFL etc were demonstrated as the powerful tools for improving new generation, high temperature composites with good processability, thermo-mechanical properties, and high aerospace environmental durability. The heat sealable, thermoplastic thin films having high durability in space has been successfully developed by using asymmetric aromatic a-ODPA imide structures as a solar sail membrane. It is concluded that asymmetric aromatic imide structures without any weak linkages such as alkyl and methylene groups are very powerful tools for molecular design of high performance polyimides. The excellent properties exhibited of the asymmetric polyimides demonstrated a high potential for future aerospace applications.

## References

- 1, K.L.Mittal and M.K.Ghosh: Polyimides Fundamentals and Applications, Marcel Decker, New York (1995)
- 2, Dexter B: NASA CP2321 (1984)
- 3, Levine A.S: NASA CP3134 Part1-3 (1992) , NASA CP3164 Part1-2 (1992)、 NASA CP3194 Part1-3 (1993), Silverman E.M: NASA CR 4661 (1995)
- 4, Bessonov MI, Koton MM, Kudryavtsev VV and Laius LA 1987 *Polyimides : Thermally Stable Polymers* ( New York : Consultants Bureau)
- 5, Yokota R 1995 *Photosensitive Polyimides: Fundamentals and Applications* eds K Horie and T Yamashita (Lancaster, PA: Technomic) p 49
- 6, Kochi M, Shimada H and Kambe H, *J. Polymer. Sci.: Polym. Phys. Edn.* **22** 1979
- 7, Yokota R, Yamamoto S, Yano S, Sawaguchi T, Hasegawa M, Yamaguchi H, Ozawa H and Sato R 2001 *High Perform. Polym.* **13** 61
- 8, Chunhai Chen, Masatoshi Hasegawa, Masakatsu Kochi, Kazuyuki Horie, Paul M. Hergenrother and Rikio Yokota, High Performance Polymer,
- 9, T.T.Serafini: Polyimides; Synthesis, Characterization, and Applications, K.L.Mittal, Ed., vol.2, Plenum Press, New York, p.957 (1984)
- 10, A.K.St.Clair et.al, SAMPE J, July/Aug. p28 1985
- 11, T.H.Hou, B.J.Jensen and P.M.Hergenrother: J. Composite Materials, **30**, 109 (1996)
- 12, Yokota R, Proceedings of 7<sup>th</sup> Int. Symposium. on Materials in a Space Environment, ESA/ONERA p293 (1997)
- 13, Special Issue: High performance polymeric materials for space applications, High performance Polymer, vol.12 No.1 March 2000
- 14, Yokota R. Solar Sail WG Heisei 16 Nendo Seika Houkokusyo, JAXA/ISAS (2005)

## OVERVIEW OF THE MPAC EXPERIMENT - DEVELOPMENT OF DUST COLLECTORS, HYPERVELOCITY IMPACT EXPERIMENTS, AND POST FLIGHT ANALYSIS -

Yukihito KITAZAWA<sup>1,2,3</sup>, Akira FUJIWARA<sup>2,4</sup>, Toshihiko KADONO<sup>5</sup>, Takaaki NOGUCHI<sup>6</sup>,  
Riyo YAMANAKA<sup>3</sup>, Yugo KIMOTO<sup>3</sup>, and Mineo SUZUKI<sup>3</sup>

<sup>1</sup> Aero-Engine & Space Operations, IHI Corporation, Koto, Tokyo 135-8710, JAPAN

<sup>2</sup> Institute of Space and Astronautical Science, Japan Aerospace Exploration Agency, Sagami-hara, Kanagawa 229-8510, Japan

<sup>3</sup> Institute of Aerospace Technology, Japan Aerospace Exploration Agency, Tsukuba, Ibaraki 305-8505, Japan

<sup>4</sup> Kansai University, Suita, Osaka 564-8680, Japan

<sup>5</sup> Institute of Laser Engineering, Osaka University, Suita, Osaka 566-0871, Japan

<sup>6</sup> Department of Materials and Biological Sciences, Ibaraki University, Mito, Ibaraki 310-8512, Japan

The Micro-Particles Capturer (MPAC) is a passive experiment designed to evaluate the micrometeoroid and space debris environment, and to capture particle residues for later chemical analysis. Three MPAC units were aboard the Russian SM (Service Module) of the ISS (International Space Station), performs experiments regarding capturing dust particles in orbit. Silica aerogels and polyimide foams are used as the dust (or the dust's fragments) capturing materials, and metal plates are used as measuring materials of dust fluxes. The MPAC unit is complete passive equipment and does need no electrical power or communication. The exposure duration of each unit is about 1, 2 and 4 years respectively. After the exposure duration, MPAC units were brought back to the earth and retrieved. One more unit is installed on the front surface of "KIBO" (JEM : Japanese Experiment Module). In this paper we describe on the overview of MPAC experiment, which includes (1) Development of the MPAC unit, (2) Hypervelocity impact experiments, and (3) Post flight analysis (PFA).

**Keywords:** MPAC, ISS Service Module, JEM, Space Debris, Meteoroid, Dust, Aerogel, ESEM, SOCCOR, Comet, Asteroid, Ejecta, Micro Particle, Space Environment

### 1. Introduction

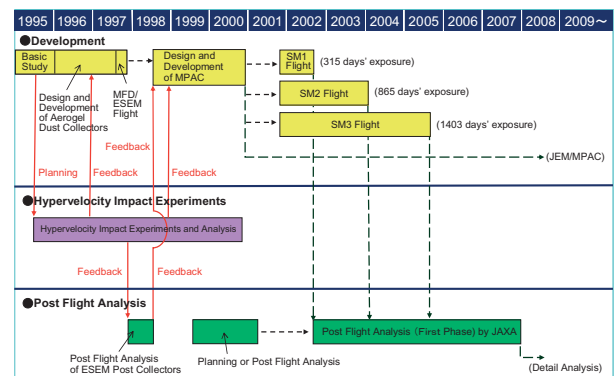
The Micro Particle Capturer (MPAC) is a passive experiment designed to evaluate the micrometeoroid and space debris environment and to capture particle residues for getting material information by chemical analysis. The MPAC experimental equipment is consisting of three identical units (numbered SM1 to SM3) deployed on the exterior of the Russian Service Module (SM) of the International Space Station (ISS). MPAC is mounted on a frame about 1 m long, which it shares with the Space Environment Exposure Device (SEED), a materials exposure experiment. MPAC experiment is not only useful for evaluation of the dust environment in the orbit of ISS, but also useful in estimating the effects of dust collisions on the ISS, and getting material information of dust particles to identify dust origin.

MPAC experiments on SM (hereafter, SM/MPAC) are the first systematic debris capturing experiments in the world. Since three units are complete same structures, it is able to purely evaluate space environment effects (ex. Impact flux, varieties of chemical data for impact residues) only by difference of exposure duration. And since aerogels are used as dust capturing material, material information of the captured dust particle, and impact parameters (incident direction, particle diameter, and impact velocity) are estimated. As the results, SM/MPAC(&SEED) mission is important not only as a precursor mission of ISS's exposed experiments, but also as a great opportunity of research of dust origin through the material information of captured dust particles.

Each MPAC equipment contains aerogels, polyimide foams with polyimide films and an aluminum witness plate. The most important material is Silica-aerogel [hereafter aerogel]. It is used for intact capturing of dust particles and also used for estimations of impact parameters (incident direction, particle diameter, and impact velocity) based on the impact track morphology.

### 2. Overview of the MPAC experiment

Fig.1 shows the project scenario (mission outline) of SM/MPAC. The project consists of major three tasks; 1) Development of dust collectors, 2) Hypervelocity impact experiments (calibrations of dust collectors), 3) Post flight analysis (PFA). In following sections, details of the tasks are described.



**Fig.1 Project Scenario (Mission Outline) of SM/MPAC**

## 2.1 Development of Dust Collectors for the SM/MPAC

The mission plan of “SOCCER” (Comet Coma Sample Return Mission) was propped in 1988. Hypervelocity impact experiments and simulations on many kinds of low density materials were performed for basic study for the SOCCER [1]. But the mission was not accepted, because no comets which have encounter velocity less than 6 km/sec were found in that time. In addition, the mission plan of the SOCCER was succeeded by “STARDUST”.

Based on the SOCCER heritage, the developments for aerogel dust collectors were started in 1995 for focus on measurement of micro debris. Characteristics of the aerogel are followings. 1) Since the aerogel is very low density ( $\sim 0.03 \text{ g/cm}^3$ ) material, it is effective for intact capturing of dust particles. 2) The aerogel is transparent and it is easy to locate dust captured in the aerogel. 3) The aerogel consists mainly pure silicate ( $\text{SiO}_2$ ) and it is robust material against space environment. In 1997, the aerogel dust collectors were aboard the space shuttle (Fig.2). Details of the flight experiment are reported by Kitazawa *et al.*, [2], and NASDA and NASA [3].

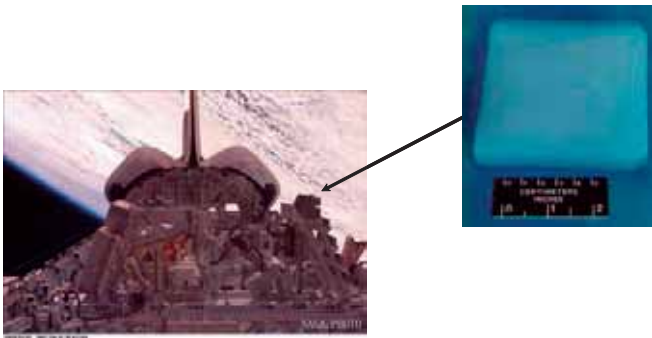


Fig.2 Aerogel Dust Collectors on the Space Shuttle (STS-85), 1997 (Kitazawa *et al.*, [2]).

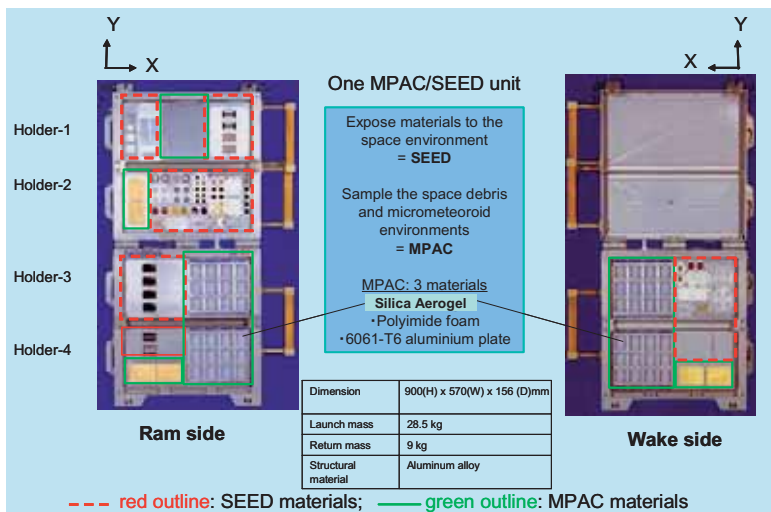


Fig.3 Locations of MPAC Equipments

For the SM/MPAC, another low density material is also used. The material is the polyimide foam with polyimide film. Objectives of the material are 1) Estimation of impact flux, and 2) Capturing dust particles fragments. Bulk density of the polyimide foam is  $0.011 \text{ g/cm}^3$  and the density is lower than the

aerogel. But the pore size of the foam is several ten micrometers and is very larger than the aerogel pore size which is a few to several nanometers. Although the large pore size is not suitable for intact capturing of dust particles, but the low density portion is enough to capture fragments of dust particles. And the cost of the foam is very lower than that of aerogel and the handling of the foam is very easy. In addition, the polyimide film (thickness:  $12.5 \mu\text{m}$ ), which is covered on the exposed surface of the polyimide foam, is sensitive to dust impact and it is useful for the estimation of the impact flux of dust particles. The polished metal plates (6061-T6 Aluminum plate) are used for detail estimation of impact flux, estimation of impact energy, and analysis of residual material (if possible). AU (gold) plates will be used for JEM (Japanese Experiment Module “KIBO”)/MPAC. Fig.3 and Table 1 show dimensions and locations of SM/MPAC equipments.

Table 1 Dimensions of MPAC Equipments

Material	Ram side		Wake side	
	Tiles	Exposed Area of One Tile/Plate	Tiles	Exposed Area of One Tile/Plate
Aerogel	24	37 x 37 mm (thickness 15 mm)	24	37 x 37 mm (thickness 15 mm)
Polyimide Foam	4	two tiles: 50 x 78.5 mm* (thickness 30 mm) two tiles: 50 x 63 mm (thickness 7 mm)	2	two tiles: 50 x 78.5 mm*
6061-T6 Aluminium Plate	1	13.6 x 15.25 mm (thickness 2 mm)	-	-

\*the same tiles have both ram- and wake-exposed surfaces.

## 2.2 Hypervelocity Impact Experiments

Detailed understanding of hypervelocity impact-induced features on MPAC dust collectors is help to get information of characterization of the dust particles environment (ex. mass, velocity, material of dust particles). We performed hypervelocity impact experiments on MPAC equipment materials, mainly aerogels and metal plates. In following sections, we mention the experiments

### 2.2.1 Hypervelocity Impact Experiments on Aerogel

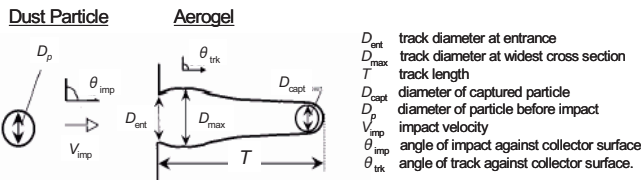
Laboratory hypervelocity impact experiments were conducted to verify the performance of aerogel dust collectors to derive the relationships of various parameters characterizing the projectile with morphology of tracks left by the penetrating projectile in the aerogel pad. Aerogel collectors were impacted at velocities ranging from 1 to 14 km/s with projectiles of aluminum oxide, olivine, or sodalime glass, with diameters ranging from 10 to  $400 \mu\text{m}$ . Table 2 shows the summary of the experimental condition, and Fig.4 shows measurement parameters. Data from laboratory experiments used in the MPAC study comprised 149 hypervelocity impact data points, among which 141 were from the plasma-gun of the Hypervelocity Impact Facilities (HIF) of the Space Power Institute, Auburn University, 4 from the two-stage light-gas gun of the Institute of Space and Astronautical Science (ISAS/JAXA), JAPAN, and the remaining 4 from the electro-thermal gun of IHI Corporation., JAPAN. The ranges of impact velocity covered by the three data sets were 3 - 14 km/s with the plasma-gun, 1 - 5 km/s with the light-gas gun, and 1 - 2 km/s with the electro-thermal gun. As the results of the hypervelocity



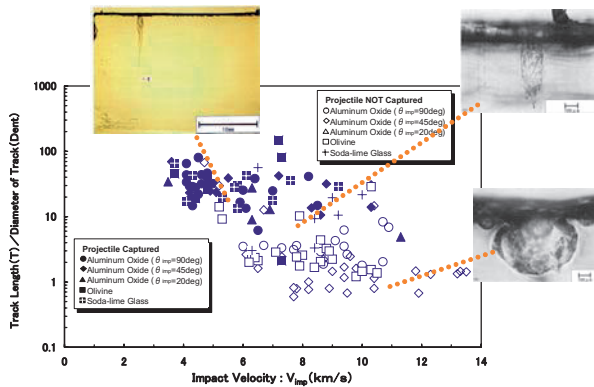
impact experiments, shapes and dimensions of the penetration tracks left in the aerogel collector were correlated with the impact parameters, and the results permitted derivation of a series of equations relating the track dimensions incoming projectile size, impact energy, and other projectile parameters. In addition, a simplified model, similar to meteor-entry phenomena, was used to predict the trends in experimental penetration track lengths and the diameters of captured projectiles. Details of experiments are described in Kitazawa *et al.*[4]. In here, we introduce typical experimental results, which bring useful information for the design of dust collectors and for the PFA.

**Table 2 Summary of the Experimental Condition**

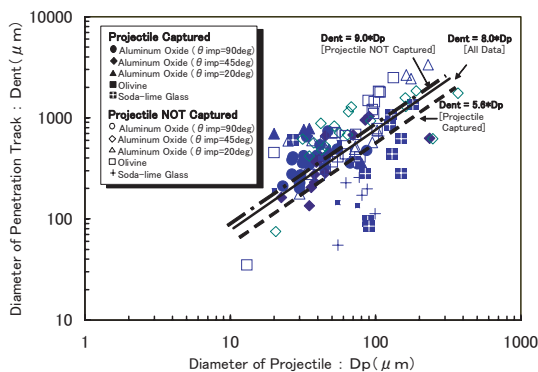
Category	Item	Value	Unit
Environment Projectile	vacuum level	$10^{-5}$ or $10^{-1}$	torr
	temperature	room temperature	
	diameter	10-400	$\mu\text{m}$
Impact condition	material	$\text{Al}_2\text{O}_3$ , olivine, glass	
	velocity	1-14	km/s
	angle	90, 45, 20	degree



**Fig.4 Measurement Parameters of the Hypervelocity Experiments on Aerogel Dust Collectors (Kitazawa *et al.*,[4])**



**Fig.5 Relation of aspect ratio of the tracks ( $T/D_{ent}$ ) with impact velocity (Kitazawa *et al.*,[4])**



**Fig.6 Relation between track diameter at the aerogel surface,  $D_{ent}$ , and projectile diameter,  $D_p$ . (Kitazawa *et al.*,[4])**

Fig.5 shows relation of aspect ratio of the tracks ( $T/D_{ent}$ ) with impact velocity. At impact velocities below 6 km/s the projectiles were captured without fragmentation by the aerogel collector and, in many instances, without complete ablation even at 12 km/s. Fig.6 Relation between track diameter at the aerogel surface,  $D_{ent}$ , and projectile diameter,  $D_p$ .

The main results obtained are summarized as follows:

1) The silica-aerogel collector (density:  $0.03 \text{ g/cm}^3$ ) is feasible for the intact capturing of dust particles. It can capture projectiles without appreciable damage at impact velocities less than 6 km/s, and even has the capability to capture some part of projectiles at velocities as great as 12 km/s.

Projectiles can be captured under the following condition,

$$D_p \leq 1.2 \cdot 10^7 / \delta v_{imp}^2, \quad \dots (1)$$

where  $D_p$  is the projectile diameter,  $\delta$  is the projectile density and  $v_{imp}$  is the impact velocity of the projectile.

2) Dimensions and features of penetration tracks caused by projectiles impacts are correlated with projectile size and impact velocity. The aspect ratio ( $T/D_{ent}$ ) and track features correspond to the impact velocity of the projectile, where  $T$  is the track length, and  $D_{ent}$  is the track diameter. At velocities lower than about 5 km/s,  $T/D_{ent}$  is greater than 10, and the tracks are "carrot-shaped". The characteristics of the track change, depending on the impact velocity range. At impact velocities less than about 3-4 km/s, many branches around the track and the bottom of the track are observed, and are similar in shape to the appearance of aerogel pricked by a needle. At impact velocities greater than 3-4 km/s, there are few main branches around the "trunk" of the track between the surface of the aerogel and the bottom of the track, but there are small branches or cracks surrounding the bottom of the track and just before the bottom, and the shape of the end of the track often fits the captured projectile shape. Above about 5 km/s, the aspect ratio  $T/D_{ent}$  decrease with increasing velocity. Particularly at 12 - 13 km/s these quantities assume very small values, and the spindle-shaped or crater-shaped track becomes dominant. When  $T/D_{ent} \geq 10$ , the track is spindle-shaped and sometimes has several branches at the bottom of the track. In some cases, fragmented projectiles are found in each branch. When  $T/D_{ent} < 10$ , the track is crater-shaped and the tracks have few projectile fragments.

Figure 11 shows  $D_{ent}$ , which increases with projectile size. The relation between  $D_{ent}$  and  $D_p$  obtained by the least squares fit is represented by

$$D_{ent} = 8.0 D_p, \quad \dots (2)$$

and the correlation coefficient ( $r$ ) of the equation is 0.6.

Also indicated are the best-fit lines for data from tracks both with and without residue. Dent for tracks which have projectile residues are the following;

$$D_{ent} = 5.6 D_p, \quad \dots (3)$$

while, Dent of tracks which have no projectile residues are the following;

$$D_{ent} = 9.0D_p \quad \dots (4)$$

The track angle measured from the surface of the aerogel ( $\theta_{trk}$ ) gives information on impact angle ( $\theta_{imp}$ ) for  $T/D_{ent} \leq 10$ .

3) Projectiles captures in aerogel and those before impact are almost the same in chemical content, although captured projectiles have a partial 'cover' of molten aerogel. Even when no captured projectile can be found in aerogel with an optical microscope, chemical components of the projectile are sometimes detected on the inner wall of the penetration track.

Those correlations suggest that it is possible to estimate projectile impact parameters from penetration track observations when post-flight analysis of the dust collectors is performed.

4) A simplified model can predict penetration track lengths and diameters of captured projectiles. This model assumes that a projectile penetrating into an aerogel suffers dynamic drag and ablation from the aerogel in a similar way to that of a meteoroid penetrating the atmosphere.

The velocity  $v(t)$  and mass  $m(t)$  of a projectile are represented by the following equations,

$$m(t) \frac{dv(t)}{dt} = -\Gamma S(t) \rho v(t)^2 - T_s S(t) \quad \dots (5)$$

$$\frac{dm(t)}{dt} = -A \frac{S(t) \rho v(t)^3}{2Q} \quad \dots (6)$$

where  $t$  is time,  $\Gamma$  is drag coefficient,  $S(t)$  is midsectional area of the projectile,  $\rho$  is density of the aerogel,  $T_s$  is tensile strength of the aerogel,  $A$  is heat-transfer coefficient (equal to or less than unity) and  $Q$  is latent heat of vaporization or fusion of the projectile. The second term on the right-hand side of equation (16) represents the effects of tensile strength of the aerogel. The length of the penetration track ( $T$ ) is given by the following equation.

$$T = \int_0^{t_e} v(t) dt \quad \dots (7)$$

where  $t_e$  is time at which  $v(t) = 0$ , and  $t_e$  is estimated by

$$\frac{1}{2} m(t_e) v(t_e)^2 / S \leq K_c^2 (1 - \nu^2) / E \quad \dots (8)$$

where  $K_c$  is fracture toughness of the aerogel,  $\nu$  is Poisson's ratio of the aerogel and  $E$  is Young's modulus of the aerogel.

The method is an appropriate analytical treatment of hypervelocity impacts of projectiles on aerogel.

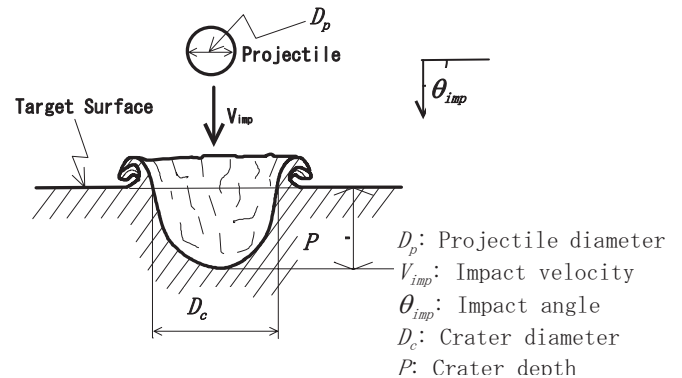
## 2.2.2 Hypervelocity Impact Experiments on Metal Plates

Details of experiments are reported in Kitazawa *et al.*[5]. All hypervelocity impact experiments were carried out using the plasma gun at Auburn University - A square shaped target was used for this study (Al: 10cm x 10 cm x 2mm, Au: 10cm x 10cm x 1mm). Table 3 shows the experimental condition and Fig.7 shows measurement parameters. Crater diameter ( $D_c$ ) and crater depth ( $P$ ) were measured using a laser microscope (Lasertec 1LM21) with accuracy of  $\pm 0.1 \mu\text{m}$ .  $D_c$  and  $P$  measurements refer to the initial target surface as reference datum (Fig. 7). Detail morphological fixtures of craters were observed with a Scanning Electron Microscope (SEM), and identification of projectile specific elements of residual materials in craters was performed using an SEM Energy Dispersive X-ray (SEM-EDX) analyzer (Elinox ERA-8000 with EDAX DX-4).

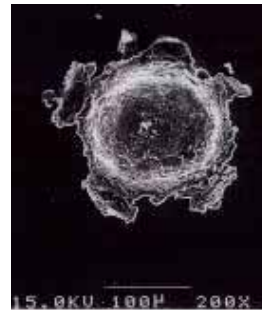
**Table 3 Experimental Condition**

Category of Conditions	Item	Value	Unit
Environment	Vacuum Level	$10^{-3}$	Pa
	Temperature	Room Temp.	
Projectile	Diameter	5 - 135	$\mu\text{m}$
	Material	$\text{Al}_2\text{O}_3$ ,	
Impact Condition	Velocity	3 - 10	km/s
	Angle	90	Deg.

(vertical to the target surface)



**Fig. 7 Measurement parameters of projectiles and craters**



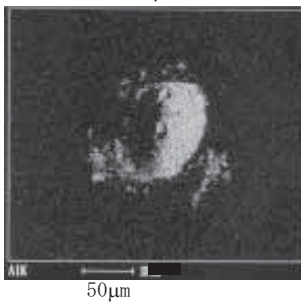
**Fig. 8 SEM image of the crater on the Al plate. Projectile material is  $\text{Al}_2\text{O}_3$ , projectile diameter ( $D_p$ ) is 34 x 48  $\mu\text{m}$ , impact velocity ( $V_{imp}$ ) is 6.3 km/s, crater diameter ( $D_c$ ) is 135  $\mu\text{m}$ , crater depth ( $P$ ) is 48  $\mu\text{m}$ .**

Fig. 8 and Fig. 9 show examples of craters on Al plate and Au plate respectively. Most craters were round in shape and possessed raised rims. The greater part of the impacting projectile can still be found. In Fig.10 and Fig. 11, the projectile material can be found at the wall

and on the bottom of the crater, and it also can be found as ejecta around the crater. Especially, in case of the Au plate, a large amount of the projectile residual can be seen on the bottom of the craters. It seems that the amount of residual in craters on the Au plate is relatively greater than that on the Al plate.



(a) SEM image of the crater on the Au plate.



(b) EDX mapping image. Light dots show Al components of the same area of the SEM image.

**Fig. 9 SEM image and EDX element mapping image of the crater on the Au plate. Projectile material is  $Al_2O_3$ , projectile diameter ( $D_p$ ) is 45  $\mu m$ , impact velocity ( $V_{imp}$ ) is 4.2 km/s, crater diameter ( $D_c$ ) is 66  $\mu m$ , crater depth ( $P$ ) is 25  $\mu m$ .**

Mizutani [6] reviewed the previous semi-empirical equations for various material combination of targets and projectiles, and he suggests a relationship of projectile kinetic energy ( $E$ ) and crater diameter ( $D_c$ ) as follows;

$$D_c \propto E^{1/3} \quad \dots (9)$$

Fig. 10 shows the crater diameter ( $D_c$ ), as a function of the 1/3 power of projectile kinetic energy. The best-fit relationship between  $D_c$  ( $\mu m$ ) and  $E(J)$  are described as the following equations.

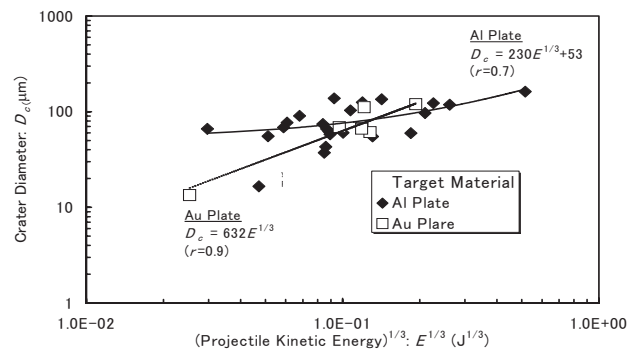
$$Al: D_c = 230E^{1/3} + 53 \quad \dots (10)$$

with a correlation coefficient of 0.7.

$$Au: D_c = 623E^{1/3} \quad \dots (11)$$

with a correlation coefficient of 0.9.

The diameter of a crater ( $D_c$ ) is correlated with projectile kinetic energy ( $E$ ) as shown in Fig. 10. Therefore, it is thought possible to presume the kinetic energy of a projectile from the diameter of a crater.

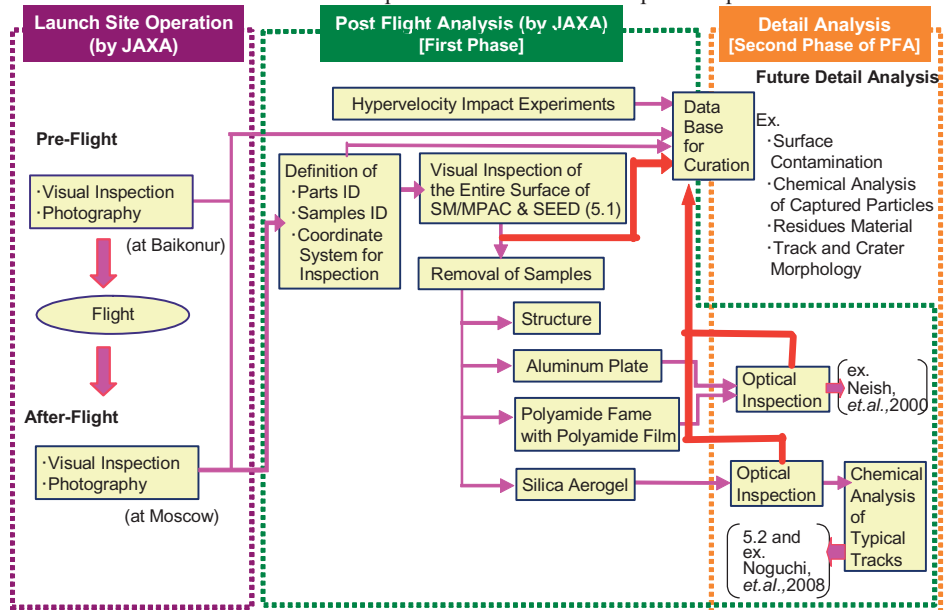


**Fig. 10 Relationship between crater diameter ( $D_c$ ) and the 1/3 power of projectile kinetic energy.**

### 2.3 Post Flight Analysis (PFA)

The procedure of the pre-flight inspection, the post flight analysis, and detail analysis of SM/MPAC(&SEED) is described in Fig.11. Before the flight, the preflight inspection was performed on whole SM/MPAC&SEED structures and on each samples at the Baikonur Cosmodrome, and the inspection was consists of the visual inspection and the photographic survey using a camera (PENTAX 67II) with lenses (9 0mm F2.8 and Macro 100 mm F4). After the flight, the same inspection was performed at the S.P.Korolev Rocket and Space Corporation (RSC) “Energia” in Moscow. We did after-flight inspection SM1, SM2, and SM3 individually, just after retrieves of the sample holders. Objectives of those inspections were recording of the surface condition at just before the launch and at the just after the flight. The inspection results were used for quick comparison between the pre-flight and the post flight and are used for the baseline data of surface conditions of each SM/MPAC&SEED. Those data will be included for the data base for the curation.

The PFA is divided in two phases. Main purpose of the first phase is making data base for curation and detail analysis of several typical impact features. The data base includes visual inspection results on the entire surface of SM/MPAC&SEED and MPAC samplers. Details of the inspection procedures



**Fig. 11 Procedure of PFA (Post Flight Analysis)**

described in the section 2.3.1. In addition, inspection data and discussion of dust impacts on the 6061-T6 Al plate and polyimide foams are reviewed in Neish, *et al.*[7] and Neish, *et al.*[8]. In here, we mentioned the visual inspection of the entire surface of SM/MPAC&SEED and the inspection and analysis on aerogels.

**2.3.1 Inspection Procedures**

**(1) Visual inspection of the entire surface of SM/MPAC&SEED**

Visual inspection of the entire surface and creation of basic data sets for curation were carried out according to the following procedures. 1) Each surface of the SM/MPAC&SEED structure (includes MPAC's samples and SEED's environment monitor samples) was scanned with the aid of an 8x optical microscope. 2) When an impact-like feature was detected, the ID of the impacted part and the X and Y coordinates of the impact were recorded with accuracy of 0.1mm. 3) Dimensions of the feature were measured, and photographs and/or sketches were made of the feature with the aid of a 50-175x CCD (Charge-Coupled Device) optical scope ((KEYENCE VH-Z25 (CCD fiber scope lens) and VH-6300 (Image recorder and device controller)). 4) A morphological assessment of the feature was made (impact-induced or not).

**(2) Silica Aerogel Inspection**

After removal of all aerogel tiles from the frame, silica aerogel tiles (exposed area: 37mm x 37mm per tile) were inspected as follows: 1) Each tile was scanned individually with the aid of a 150x CCD optical scope. 2) When an impact feature was located, its X and Y coordinates were recorded and photographs and/or sketches of the feature were made. 3) Morphological parameters of the track were measured, and particle remnants were searched for. When typical tracks were found, aerogels were sliced with a microtome into thin, small pieces of between 1 and 3 mm thickness. After the slicing of aerogels, the following procedures were performed. 4) Optical microscope images and SEM images of selected typical tracks were obtained. 5) EDS, X-ray diffraction and Raman spectroscopic analyses were carried out to determine the chemical composition of residues left in the tracks. [Details of 4) and 5) are described in Noguchi, *et al.*[9].]

**2.3.2 Inspection results**

**(1) Visual inspection of the entire surface of SM/MPAC&SEED**

Visual inspection of SM/MPAC&SEED was conducted on all sample holders. Data sets of impact features were compiled for curation (Fig. 12). Morphological judgment placed the feature in one of three categories. Class I (the first quality level): hypervelocity impact-induced features which meet all of three criteria (<1> the feature has a crater-like rim and/or central peak, <2> the feature has radial cracks and/or ejecta, <3> the feature has a shape similar to those induced by hypervelocity impact experiments.). Class II (the second quality level): probably hypervelocity impact-induced features

which meet one or two of the criteria. Class III: not hypervelocity impact-induced features. The number of impact-induced features was almost directly related to the exposure period (Fig. 13). The impact rate was almost constant, with the sum of Class I and Class II events about 15 impacts per year.

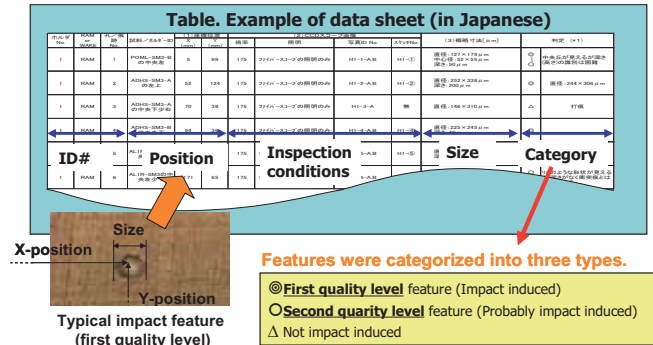
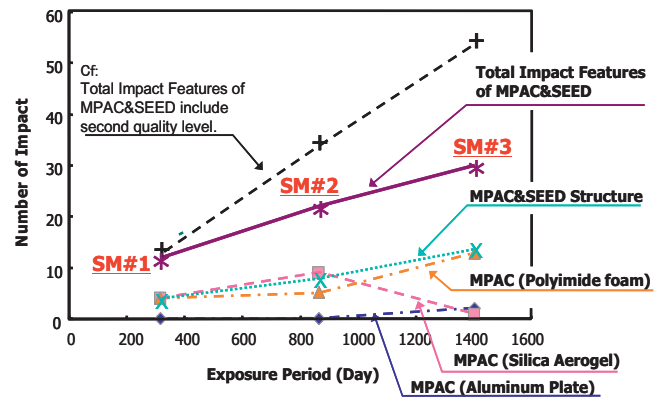


Fig.12 An example of data record format.



**(2) Silica Aerogel Inspection**

**1) Surface alterations of silica aerogel**

Fig. 14 shows surfaces of retrieved aerogels. The aerogel surfaces on the WAKE side are yellowish and have countless fine cracks. SM3/MPAC and SM2/MPAC display more pronounced yellow discoloration and more fine cracks than SM1/MPAC. The appearance of the surface of the aerogel near the cracks is similar to that produced by the deposition of metal vapor with a thickness on the order of one μm. In contrast, the RAM sides became whitened and a maximum of about seventy very minute tracks ( $D_{ent} < 20\mu\text{m}$ , and  $T < 300\mu\text{m}$ ) per aerogel were detected in SM1/MPAC. Moreover, in SM2 and SM3, about a thousand foreign bodies were found in each aerogel (milk-white ellipses, average diameter about 100 μm) instead of minute tracks. Similar shapes are produced when atomized organic solvent hits the aerogel. EDS detected carbon in addition to the Si and O that are the main ingredients of the aerogel. Details of the surface alterations are discussed by Noguchi, *et al.*[9].



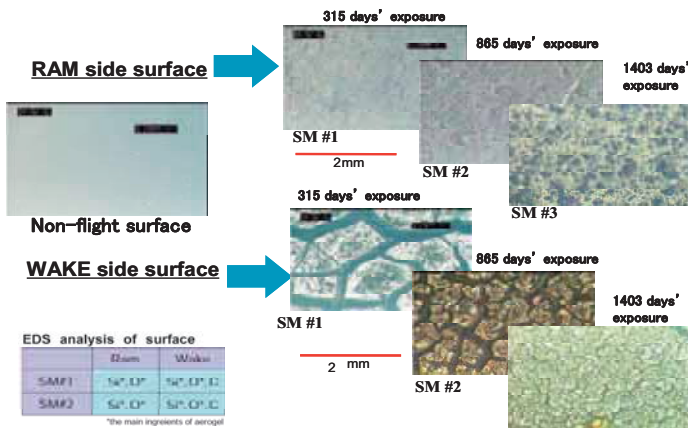


Fig. 14 Surface alterations of exposed aerogel.

2) Typical tracks in silica aerogels

Fig. 15 shows comparisons of two impacts with hypervelocity impact experiment results (Kitazawa, *et al.*, [5]). Regardless of surface alterations of the aerogel, tracks from experimental hypervelocity impacts are quite similar to those seen in flight experiments.

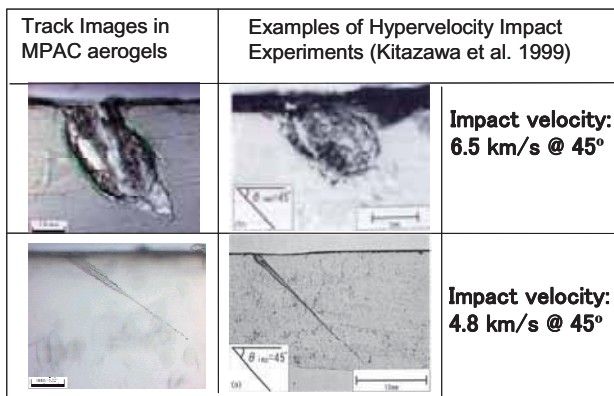


Fig.15 Comparison of tracks in MPAC aerogels with experimental hypervelocity impact tracks.

3) Captured particles

Combined SEM, transmission electron microscope (TEM), micro Raman spectroscopy, and synchrotron radiation X-ray diffraction analyses revealed that captured particles are space debris, secondary debris, and a micrometeoroid, respectively. Details are discussed in Noguchi, *et al.* [9].

4) Estimated impact flux on silica aerogel

We compared calculated impact fluxes of the three environment models with the impact fluxes on aerogels. Fig. 16 shows a comparison of the impact flux estimated from inspection of the aerogel and calculated results from MASTER-2001, MASTER-2005 and ORDEM 2000 (Fukushige *et al.* [10]). Particle diameter *d* was estimated using a linear relationship between *d* and *Dent*, which shown in Fig.6 and equations (2) – (4). By the surface alteration of aerogels, it is difficult to inspect small tracks and it was not able to estimate the fluxes of diameter >10 μm of SM2 aerogels and SM3 aerogels.

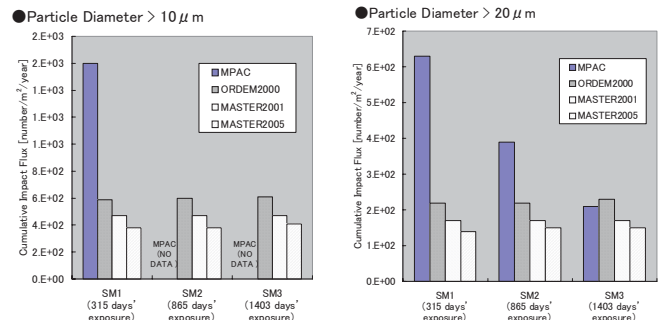


Fig.16 Comparison with impact flux of MPAC aerogels and calculated results of three models (Left: Particle diameter >10 μm, Right Particle diameter >20 μm )

In Fig.16, impact fluxes of aerogels are seemed to be in inversion portion to the exposure period and the fluxes are greater than model results.

3. Discussion

3.1 Entire Surface of MPAC&SEED

A database of impact-like features and part IDs of all MPAC&SEEDs are available for curation. The database also includes detailed inspection results for MPAC samples. The sample curation system and sample distribution plan will be discussed in the next step. In Fig. 4, the number of impact-induced features was almost directly related to exposure period and the impact rate was almost constant. These data show that during the exposure period of MPAC&SEED (October 15, 2001 - August 19, 2005), there was no noteworthy change in the dust flux environment.

3.2 Silica Aerogel Inspection

3.2.1 Surface alterations of silica aerogel

In a previous aerogel experiment in space (Kitazawa, *et al.*, 1998), no noteworthy surface alterations were reported. In contrast, the surface alterations of MPAC’s aerogels are quite remarkable, and seem to be the result of the deposition of carbon-containing particles (whether gas, liquid or solid) over the entire aerogel surface. Problems in the operation of space stations such as MIR and ISS are strongly related to the gas-particle environment that forms around the station, which can contaminate external surfaces. The attitude control thrusters widely used on space stations contribute significantly to the formation of a gas-particle environment [11]. The effects of contaminants emitted from the thrusters of the ISS, Soyuz and Progress are under discussion. Detail analysis results on the surfaces of aerogels are reported by Noguchi, *et al.* [9].

3.2.2 Typical tracks in silica aerogels

Regardless of any surface alterations of the aerogels, the shape of penetration tracks, which are presumed to have been formed by hypervelocity collisions with dust particles, are in good agreement with track shapes observed in hypervelocity impact experiments (Kitazawa, *et al.* [4]). Therefore, it is possible to estimate the impact parameters of the dust particles, such as their diameter, impact velocity, impact direction, etc., from the results of the hypervelocity impact experiment. The

typical carrot-shape tracks captured dust particles and the chemical analysis on the particles were performed by Noguchi, *et al.* [9].

### 3.2.3 Estimated impact flux on silica aerogel

Flux values estimated from inspection of the aerogels shown in Fig.16 are contradictory to the inspection results on the entire surface of MPAC&SEED (See, 3.2.1). Surface alterations of aerogels induce the difficulties of surface inspection of aerogels. As the results, it is thought that it seems seemingly that flux is decreasing by the alterations. It assumes that there is no remarkable change, the inspection result of SM1 should be trusted and the flux value is five to 100 times higher than calculated fluxes by the models. The causes of elevated flux levels may be; 1) model uncertainties, 2) elevated flux values from dust swarms (dust clouds), 3) contaminants emitted from the ISS, Soyuz, Progress or the Shuttle, 4) secondary debris. It is thought that at least the flux of the smallest particles (less than 10  $\mu\text{m}$ ) is affected by contaminants.

## 4. Summary

### 4.1 Development of Dust collectors

Based on the SOCCER heritage, dust collectors were developed for focus on measurement of micro debris. Aerogel is selected for the dust capturing material, and as the auxiliary material, the polyimide foam with polyimide film is selected. The polished metal plates (6061-T6 Aluminum plate) are used for detail estimation of impact flux, estimation of impact energy, and analysis of residual material (if possible). In addition, AU (gold) plates will be used for JEM/MPAC.

### 4.2 Hypervelocity Impact experiments

Laboratory hypervelocity impact experiments were conducted to verify the performance of dust collectors. The shapes and dimensions of the penetration tracks left in the aerogel collector were correlated with the impact parameters, and the results permitted derivation of a series of equations relating the track dimensions to incoming projectile size, impact energy and other projectile parameters. A simplified model, similar to meteor entry-phenomena, was used to predict the trends in experimental penetration track lengths and the diameters of captured projectiles. The diameter of a crater is correlated with projectile kinetic energy. Experimental results helped the design of dust collectors and will give useful information for the PFA.

### 4.3 Post Flight Analysis

Main purpose of the first phase of the PFA is making data base for the curation for sample users and detail analysis of several typical impact features. The data base includes visual inspection results on the entire surface of SM/MPAC&SEED and MPAC samplers. Those data will be included for the data base for the curation. Detail analysis of several typical impact features suggest MPAC samples captured many space materials (meteoroids, space debris, secondary debris and contamination materials). Surface alteration of aerogels, which were caused by contamination probably, causes the difficulty for the surface inspection, and more sophisticated inspection

methods should be developed.

## References

- [1] A. Fujiwara: Comet coma sample return intact captures technology, SOCCER comet coma sample return, Proceedings of ISAS/NASA Joint Working Group Meeting, October 17 and 18, 1988, Institute of Space and Astronautical Science (1988).
- [2] Y. Kitazawa, K. Imagawa, Y. Okada, A. Fujiwara, T. Kadono, and R. Amagata: Hypervelocity impact tests and post-flight Analysis on MFD dust collectors, Proceedings of the 21<sup>st</sup> International Symposium on Space Technology and Science, 1842-1847 (1998).
- [3] NASDA: NASDA ESEM final report, Evaluation of Space Environment and Effects on Materials (ESEM), Archive System, NASA Langley Research Center, NASA Home Page, 1998, <http://setas-www.larc.nasa.gov/esem/AOE.html>, (1998).
- [4] Y. Kitazawa, A. Fujiwara, T. Kadono, K. Imagawa, Y. Okada and K. Uematsu; Hypervelocity impact experiments on aerogel dust-collector, Journal of Geophysical Research, Vol. 104 E9, 22035-22052, (1999).
- [5] Y. Kitazawa, K. Kawachi, K. Fukasawa, Y. Yamaura, T. Miyadera, R. Nakamura, K. Imagawa, C. Kamakura, Y. Nakayama, and Y. Tachi; MPAC; Passive measurement experiment of dust particles on ISS, Proceedings of the 22nd International Symposium on Space Technology and Science, 2077-2082, (2000).
- [6] H. Mizutani: Science of craters (Kure-ta no kagaku), UP Earth Science, Tokyo-daigaku syuppan-kai, Tokyo, 102-120, 1980, text in Japanese.
- [7] M. J. Neish, K. Imagawa, T. Inoue, J. Ishizawa, Y. Kitazawa, Y. Yamaura, A. Murakami and Y. Ochi; Microparticle capture on the international space station using aerogel and polyimide foam: Proceeding of 9th International Symposium on Materials in a Space Environment, Noordwijk, The Netherlands, 16-20 June 2003, ESA SP-540, pp.431-435,(2003).
- [8] M. J. Neish, Y. Kitazawa, T. Noguchi, T. Inoue, K. Imagawa, T. Goka, Y. Ochi; Passive measurement of dust particles on the ISS using MPAC: Experiment summary, particle fluxes and chemical analysis, Proceedings of the Fourth European Conference on Space Debris, Darmstadt, Germany, 18-20 April 2005, ESA SP-587, pp.221-226,(2005)
- [9] T. Noguchi, T. Nakamura, Y. Kitazawa, R. Yamanaka, Y. Kimoto, M. Suzuki: Internal investigation of silica aerogel equipped on SM/MPAC & SEED recovered from the ISS in 2003, 2004, AND 2005., Proceedings of the International Symposium on "SM/MPAC&SEED Experiment.", Tsukuba, Japan, March 10-11, 2008, JAXA-SP (in printing), (2008).
- [10] S. Fukushima, Y. Akahoshi, Y. Kitazawa, T. Goka: Comparison of debris environment models; ORDEM2000, MASTER2001 and MASTER2005, IHI Engineering Review Vol.40, No. 1, 31-41, (2008).
- [11] S. Rebrov and Y. Gerasimov: Investigation of the Contamination Properties of Bipropellant Thrusters, 35th AIAA Thermophysics Conference, 11-14 June 2001, Anaheim, CA, AIAA 2001-2818, (2001).

**Publication list**

- T. Noguchi, T. Nakamura, Y. Kitazawa, R. Yamanaka, Y. Kimoto, M. Suzuki: Internal investigation of silica aerogel equipped on SM/MPAC & SEED recovered from the ISS in 2003, 2004, AND 2005., Proceedings of the International Symposium on "SM/MPAC&SEED Experiment.", March 10-11, 2008, Tsukuba, Japan, JAXA-SP (in printing) (2008)
- Y. Kitazawa, S. Fukushige, M. Uchino, Y. Akahoshi, T. Goka, A. Sakurai, T. Yasaka, K. Funakoshi, T. Hanada, H. Matsumoto, T. Noguchi, R. Yamanaka, Y. Kimoto, and M. Suzuki: Current Problems of Debris Environment Models and Related Studies of JAXA, E European Geosciences Union, General Assembly 2007 Vienna, Austria, 13-18 April 2008, CD-ROM (EGU2008 EGU2008-A-01753) (Abstract) (2008).
- Y. Kitazawa, S. Fukushige, M. Uchino, Y. Akahoshi, T. Goka, A. Sakurai, T. Yasaka, K. Funakoshi, T. Hanada, H. Matsumoto, T. Noguchi, R. Yamanaka, Y. Kimoto, and M. Suzuki: Current Problems of Debris Environment Models and Related Studies of JAXA, Proceedings of the JAXA 3<sup>rd</sup> Space Debris Workshop, Tokyo, Japan, 21-22 January, 2008, JAXA-SP-TBD (in printing) (2008).
- S. Fukushige, Y. Akahoshi, Y. Kitazawa, and T. Goka; Comparison of Debris Environment Models; ORDEM2000, MASTER2001 and MASTER2005 - Status Report of the Candidate of an ISO's Standard Entitled 'Process-based Implementation of Meteoroid and Debris Environment Models' -, the 58th Meeting of the Aeroballistic Range Association, Aeroballistic Range Association, Las Cruces, New Mexico, U.S.A., 17-20 September, 2007, (CD-ROM) (2007).
- Y. Kitazawa, T. Noguchi, M.J. Neish, I. Yamagata, Y. Kimoto, J. Ishizawa, A. Fujiwara, M. Suzuki, Y. Yamaura, and S. Yamane; Passive Measurement of Dust Particles on the ISS (MPAC): Status report of the post flight analysis, European Geosciences Union, General Assembly 2007 Vienna, Austria, 15-20 April 2007, CD-ROM (EGU2007-A-01406) (Abstract) (2007)
- Y. Kitazawa, M. J. Neish, T. Noguchi, I. Yamagata, Y. Kimoto, J. Ishizawa, A. Fujiwara, M. Suzuki, Y. Yamaura, Y. Watanabe, and S. Yamane; Passive measurement of dust particles on the ISS (MPAC): Third report on aerogel dust collectors, the 57th Meeting of the Aeroballistic Range Association, Venice, Italy, 18-22 September, 2006 CD-ROM (2007)
- Y. Kitazawa, M. J. Neish, T. Noguchi, I. Yamagata, Y. Kimoto, J. Ishizawa, M. Suzuki, and A. Fujiwara: Preliminary analysis report on SM/MPAC, Proceedings of 2<sup>nd</sup> Symposium on "SM/MPAC&SEED EXPERIMENT", 21-24, February 21, 2006, Tsukuba, Japan, JAXA-SP-06-021, ISSN1349-113X (2007) (in Japanese)
- Y. Kitazawa, M. J. Neish, T. Noguchi, I. Yamagata, Y. Kimoto, J. Ishizawa, A. Fujiwara, and M. Suzuki: Dust capturing experiment on the international space station (MPAC), Proceedings of the 3<sup>rd</sup> Space Environment Symposium, December 14 - 15, 2006, Tsukuba, Japan (2006) (in Japanese)
- Y. Kitazawa, M. J. Neish, T. Noguchi, I. Yamagata, Y. Kimoto, J. Ishizawa, A. Fujiwara, and M. Suzuki: Dust capturing experiment on the international space station (MPAC), Proceedings of the 22<sup>nd</sup> Space Structure and Material Symposium, December 8 - 9, 2006, Sagami-hara, Japan (2006) (in Japanese)
- Y. Kitazawa, M. J. Neish, T. Inoue, J. Ishizawa, A. Fujiwara, K. Imagawa, Y. Yamaura, S. Yamane, and S. Nakazato; Passive measurement of dust particles on the ISS (MPAC): Second report on aerogel dust collectors, Preprints of the 25th International Symposium on Space Technology and Science, (CD-ROM), Kanazawa, Japan, 30 May - 6 June 2006, (2006)
- T. Noguchi, Y. Kitazawa, M. J. Neish, I. Yamagata, Y. Kimoto, J. Ishizawa, M. Suzuki, A. Fujiwara, Y. Yamaura, and S. Yamane; Passive measurement of dust particles on the ISS (MPAC): Third report on aerogel dust collectors, European Geosciences Union, General Assembly 2006 Vienna, Austria, 02 - 07 April 2006 (Abstract) (2006).
- Y. Kitazawa, M. J. Neish, T. Noguchi, I. Yamagata, Y. Kimoto, J. Ishizawa, A. Fujiwara, and M. Suzuki: The dust capturing Experiment on the international space station (MPAC), Proceedings of the annual meetings of the Japan Institute of Metals (JIM), 161, March 21- 23, 2006, Waseda University, Tokyo, Japan. (2006). (in Japanese)
- Y. Kitazawa, M. J. Neish, T. Noguchi, I. Yamagata, Y. Kimoto, J. Ishizawa, A. Fujiwara, and M. Suzuki: The dust capturing Experiment on the international space station (MPAC), Proceedings of the JAXA 2<sup>nd</sup> Space Debris Workshop, 78-90, December 8 - 9, 2005, Chofu, Tokyo, Japan. (2005). (in Japanese)
- M. J. Neish, Y. Kitazawa, T. Noguchi, T. Inoue, K. Imagawa, T. Goka, and Y. Ochi: Passive measurement of dust particles on the ISS using MPAC: Experiment summary, particle fluxes and chemical analysis, Proceedings of the Fourth European Conference on Space Debris, Darmstadt, Germany, 18-20 April 2005, ESA SP-587 (2005).
- Y. Kitazawa: Space development and space dust, Proceedings of the Rotary International District 2750 (Minato-ku Rotary Club) 2004-2005, 32-34, (2005)
- Y. Kitazawa, T. Noguchi, M. J. Neish, T. Inoue, J. Ishizawa, A. Fujiwara, K. Imagawa, Y. Yamaura, Y. Watanabe, and A. Murakami: First year mission results of passive measurement experiment of dust particles on ISS (MPAC), Preprints of the 24th International Symposium on Space Technology and Science, Miyazaki, Japan, 30 May to 6 June 2004 (CD-ROM), (2004).
- Y. Kitazawa, M. J. Neish, T. Inoue, K. Imagawa, A. Fujiwara: First year mission results of passive measurement experiment of dust particles on ISS (MPAC), the 35th COSPAR Assembly, Paris, France, 17-25 July 2004, (Abstract) (2004).
- M. J. Neish, K. Imagawa, T. Inoue, J. Ishizawa, Y. Kitazawa, Y. Yamaura, A. Murakami and Y. Ochi, Microparticle capture on the International Space Station using aerogel and polyimide foam; Proceeding of the 9th International Symposium on Materials in a Space Environment, Noordwijk, The Netherlands, 16-20 June 2003, ESA SP-540, 431-435 (2003).
- NASDA: MFD /ESEM final report, NASDA-TMR-000011, ISSN1345-7888 (2001). (in Japanese)
- Y. Kitazawa, K. Kawachi, K. Fukasawa, Y. Yamaura, T. Miyadera, R. Nakamura, K. Imagawa, C. Kamakura, Y. Nakayama, and Y. Tachi: MPAC: Passive measurement



- experiment of dust particles on ISS, Proceedings of the twenty-second international symposium on space technology and science, 2077-2082, (2000).
- Y. Kitazawa: Recent studies on dust particles in space – from a point of view of space experiment -, The Japan Society of Microgravity Application (JASMA) Journal, Vol.17, No.2, 104-113 (2000) (text in Japanese, abstract in English)
- Y. Kitazawa: Dust particles in space, NISSAN ARC Monthly, Vol.9, No.9 (2000) (in Japanese)
- Y. Kitazawa, A. Fujiwara, T. Kadono, K. Imagawa, C. Kamakura, Y. Okada and K. Uematsu; Hypervelocity impact experiments on aerogel dust-collector, Proceedings of the fall meeting of the Japanese Society for Planetary Sciences,305 (1999) (in Japanese)
- Y. Kitazawa, K. Kawachi, K. Ogiwara, T. Miyadera, R. Nakamura, K. Imagawa, C. Kamakura, Y. Nakayama, and Y. Tachi: Overview of dust capturing experiment (MPAC) on the international space station (ISS), Proceedings of the fall meeting of the Japanese Society for Planetary Sciences,306 (1999) (in Japanese)
- C. Kamakura, K. Imagawa, Y. Nakayama, Y. Tachi, K. Kawachi, Y. Kitazawa, K. Ogiwara, T. Miyadera and R. Nakamura: Overview of dust capturing experiment and space exposure experiment on the international space station (ISS), Proceedings of the 43<sup>rd</sup> Space Sciences and Technology Conference, October 20 -22, 1999, Kobe, Japan (1999) (in Japanese)
- Y. Kitazawa, A. Fujiwara, T. Kadono, K. Imagawa, Y. Okada and K. Uematsu; Hypervelocity impact experiments on aerogel dust-collector, Journal of Geophysical Research , Vol. 104 E9,22035-22052, (1999).
- Y. Kitazawa, R. Amagata, K. Kawachi, K. Fusegi, K. Imagawa and Y. Okada: Development of dust collector for the JEM exposed module, Proceedings of the 14<sup>th</sup> Space Station Conference, 105-106 (1998) (in Japanese)
- Y. Kitazawa, K. Imagawa, Y.Okada, A. Fujiwara, and T. Kadono: Hypervelocity impact Experiments on Aerogel Dust-Collector, Proceedings of Solar System Science Symposium, 53-56 (1998) (in Japanese)
- Y. Kitazawa, K. Imagawa, Y. Okada, A. Fujiwara, T. Kadono, and R. Amagata: Hypervelocity impact tests and post-flight analysis on MFD dust collectors, Proceedings of the 21st International Symposium on Space Technology and Science, 1842-1847 (1998)
- NASDA: NASDA ESEM Final Report, Evaluation of Space Environment and Effects on Materials (ESEM) Archive System, NASA Langley Research Center ,NASA Home Page,1998, <http://setas-www.larc.nasa.gov/esem/AOE.html>, (1998)
- H. Ohashi, Y. Kitazawa and H. Yano: In-situ measurement and capturing of meteoroid & space debris, of the Japanese Society for Planetary Sciences, Vol.6, No.7, 312-325 (1997) (in Japanese)
- H. Yano, Y. Kitazawa, S. Kibe, and K. Nogami: In-situ measurement and capturing of meteoroid & space debris using JEM exposed module, Proceedings of the 13<sup>th</sup> Space Station Conference, 1997 (in Japanese)
- M.J. Neish, S.P. Deshpande, S. Kibe, H. Yano, Y. Kitazawa, and S. Yamamoto: Micrometeoroid and space debris impacts on the Space Flyer Unit and hypervelocity impact calibration of its materials, Proc. Second European Conf. on Space Debris, ESA-SP-393, 177-182, (1997).
- M.J Neish, H. Yano, S. Kibe, S.P. Deshpande, Y. Kitazawa, and S. Yamamoto: Hypervelocity impact damage to Space Flyer Unit multi-layer insulation, Proceedings of the International Symposium. on Materials in Space Environment, Toulouse, France, (1997)
- M.J. Neish, S. Kibe, H. Yano and Y. Kitazawa: Impact calibration of SFU surfaces, Proceedings of the 17<sup>th</sup> Symposium on Shock Waves in Japan, 233-236, (1997)
- Y. Kitazawa, K. Imagawa, A. Fujiwara, and Y. Okada: Development of the MFD dust collector, Proceedings of the 17<sup>th</sup> Symposium on Shock Waves in Japan, 233-236, (1997) (in Japanese)
- H. Yoshida, H. Hoshi, K. Uematsu and Y. itazawa: A single, small particle launch system by electrothermal gun and microsabot, Review of Scientific Instruments Vol.68, No.1, Part 1, 178-183, (1997)
- Y. Kitazawa, K. Imagawa, A. Fujiwara, H. Yoshida, and K. Fusegi: Preliminary study on development of dust collector using low density material, the 20<sup>th</sup> International Symposium on Space Technology and Science (Abstract), (1996)
- Y. Kitazawa and K. Uemats: Micro-debris problems and its related studies, Proceedings of the 15<sup>th</sup> Symposium on Shock Waves in Japan, (1995) (in Japanese)
- Y. Kitazawa: Preliminary study of micro-debris measurement on the international space station, Proceedings of the 11<sup>th</sup> Space Station Conference, 73-74 (1995) (in Japanese)
- Y. Kitazawa, A. Fujiwara, H. Yoshida, and K. Uematsu: Preliminary study of dust impact onto low density material, International Astronomical Union (150th Colloquium) , (Abstract), (1995).
- Y. Kitazawa, K. Imagawa, A. Fujiwara, and Y. Okada: Development of dust collector using low density material, Proceedings of the fall meeting of the Japanese Society for Planetary Sciences (1995) (in Japanese)
- Y. Kitazawa and K. Uemats: Micro-debris problems and its related studies of IHI, Ishikawajima-Harima Engineering Review, Vol.35, No.2, 143-149, (1995) (text in Japanese, abstract in English)
- Y. Kitazawa: Preliminary study of the combined system of in-situ measurement with capturing of micro-debris, Proceedings of the 38<sup>th</sup> Space Sciences and Technology Conference (1994) (in Japanese)
- Y. Kitazawa, K. Uematsu, and H. Yoshida: Hypervelocity impact experiments on the multi-layer insulation (MLI), Proceedings of the 38<sup>th</sup> Space Sciences and Technology Conference (1994) (in Japanese)
- K. Uematsu, H. Yoshida and Y.Kitazawa: micro-debris impact experiments using ET-gun, Proceedings of the 37<sup>th</sup> Space Sciences and Technology Conference (1993) (in Japanese)
- The Japan Society for Aeronautical and Space Sciences (editor) : The report of the space debris study group (1993).
- K. Kimoto, H. Mori, K. Sato, Y. Kitazawa, and K. Miyoshi: Conceptual study of debris measurement/capturing experiment satellite, Proceedings of the future activity workshop/Lunar Base Workshop, Tsukuba, Japan (1992) (in Japanese)



## INITIAL INVESTIGATION OF SILICA AEROGEL EQUIPPED ON SM/MPAC & SEED RECOVERED FROM THE ISS IN 2002, 2004, AND 2005

Takaaki NOGUCHI<sup>1</sup>, Tomoki NAKAMURA<sup>2</sup>, Yukihito KITAZAWA<sup>3,\*</sup>, Riyo YAMANAKA<sup>4</sup>, Yugo KIMOTO<sup>4</sup>, and Mineo SUZUKI<sup>4</sup>

<sup>1</sup>College of Science, Ibaraki University, Mito, Ibaraki 310-8512, Japan

<sup>2</sup>Department of Earth and Planetary Science, Faculty of Science, Kyushu University, Hakozaki, Fukuoka 812-8582, Japan

<sup>3</sup>IHI Corporation, Toyosu IHI Building, Toyosu, Koto, Tokyo 135-8710, Japan

<sup>4</sup>Institute of Aerospace Technology, Japan Aerospace Exploration Agency, Tsukuba, Ibaraki 305-8505, Japan

\*Guest researcher of JAXA/IAT and NiCT, Visiting researcher of JAXA/IASA

Silica aerogel was equipped on the SM/MPAC (Service Module/Micro-Particle Capturer) to collect both artificial and natural fine-grained particles on the orbit of International Space Station (ISS). We performed initial investigation of the silica aerogel tiles retrieved in 2002, 2004, and 2005. Scanning electron microscope (SEM) observation of the surfaces of the RAM facing tiles revealed that those retrieved in 2004 and 2005 are covered by considerable craters. Each bottom of crater has a wrinkled area. Based on the comparison between them and the surface morphology of silica aerogel reacted with a droplet of ethanol, that these craters were probably formed by low speed impact of liquid droplets. On the surfaces of the WAKE facing tiles, number density of craters is lower than that the RAM facing aerogel. However, their depth/crater diameter ratios are larger than those facing to the RAM direction. We investigated three terminal particles found on the ends of tracks in silica aerogel, retrieved in 2002, 2004, and 2005. Combined SEM, transmission electron microscope (TEM), micro Raman spectroscopy, and synchrotron radiation X-ray diffraction analyses revealed that they are space debris, secondary debris, and a micrometeoroid, respectively.

**Keywords:** MPAC, Silica aerogel, Space debris, Micrometeoroid

### 1. Introduction

Silica aerogel is an ultra-low density SiO<sub>2</sub> gel (0.01 to 0.03 g/cm<sup>3</sup>). Due to its very low density, it is one of the best media to capture fine-grained particles that move in hypervelocities (ca. 1 to 10 km/s) in space. Because the material is almost colorless and transparent, it is easy to identify captured particles. It has been equipped on manmade satellites on low earth orbits (LEO) (e. g. EuReCa [1]; Orbital debris collector (ODC)-MIR [2]) to collect micrometeoroids and space debris, and on the Stardust spacecraft to collect cometary dust that emitted from 81P/Wild 2 comet (e. g. [3]). Hörz et al. [2] have successfully recovered some micrometeoroids from the aerogel mounted on the ODC on the Mir. Zolensky et al. [4] have also recovered cometary dust originated from 81P/Wild2.

SM/MPAC & SEED (Service Module/ Micro-Particles Capturer and Space Environment Exposure Device) equipped on the international space station (ISS) also contained silica aerogel. SM/MPAC & SEED is composed of three sets of units, each of which is formed by the same modules. Silica aerogels are set in the third and fourth modules in a unit. In each unit, 24 silica aerogel tiles faced the RAM side and the same number of silica aerogel tiles faced the WAKE side. Each of the tiles has a 37 x 37 mm exposure area. These three units of the SM/MPAC & SEED have been retrieved from the ISS in 2002, 2004, and 2005. Here we report the initial investigation of the silica aerogel tiles equipped on the ISS and three captured particles (terminal particles) in the silica aerogel

tiles. This is the second success of detailed analysis of individual terminal particles in silica aerogel from low earth orbit (LEO).

### 2. Experimental methods

Silica aerogel tiles are in the third and fourth trays of the SM/MPAC & SEED. The three pairs of RAM and WAKE facing silica aerogel tiles were used for detailed inspection of both their surfaces. Two silica aerogel tiles that set in the same positions in each third tray of the SM/MPAC were selected. One faced the RAM side and another faced the WAKE side. Their positions in each tray are shown in Fig. 1. They are set at the cross point between the D column and third row facing to both RAM and WAKE sides. Each unit has been retrieved in 2002, 2004, and 2005 after 315, 865, and 1403-day exposure to space, respectively [5]. We use the following abbreviations for each silica aerogel tile in this paper. For example, a silica aerogel tile retrieved in 2004, set in third unit of the MPAC, facing to the WAKE direction, and set in the cross point between the D column and third row is called as SM2\_3WD3.

These silica aerogel blocks were transferred to a clean room (class 1000) at Ibaraki University and they were placed on a special sample holder for scanning electron microscopy (SEM). Scanning electron microscope (SEM) with energy dispersive spectrometer (EDS) at Ibaraki University was used for the observation of these silica aerogel tiles. Low vacuum mode (ambient pressure in the sample chamber: 25 Pa) was

used to prevent the use of carbon coating for SEM/EDS analysis. Accelerating voltages used were 10 and 15 kV. In both cases, we could obtain good backscattered electron (BSE) images.

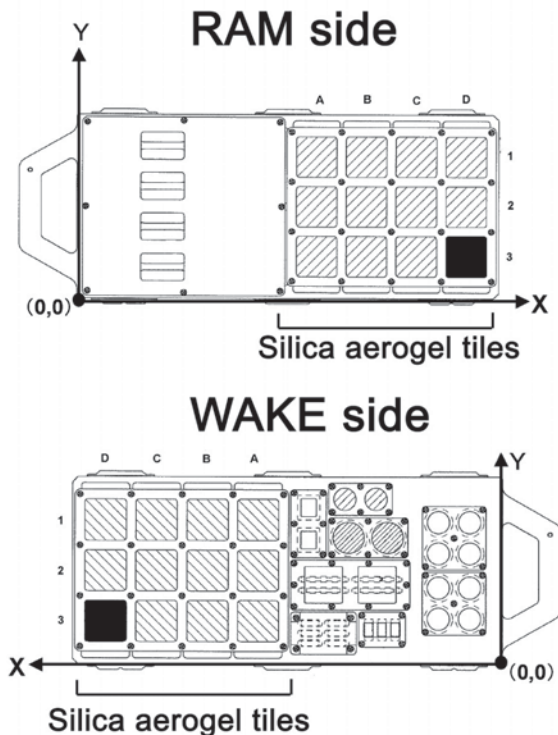


Fig. 1 Positions of silica aerogel tiles used for detailed inspection by using SEM/EDS are indicated by solid symbols. Silica aerogel tiles mounted on third module of each unit of the SM/MPAC & SEED was used for detailed inspection.

During the optical inspection of silica aerogel tiles, it was recognized that several tiles contain remarkable “tracks”. “Tracks” are recognized as white straight lines in silica aerogel tiles. Such tracks were formed during hypervelocity capture of fine-grained particles. We selected three tracks containing residual particles at the end of them. Such captured particles are called as “terminal particles” in studies of STARDUST (e. g. [3]). Slabs of silica aerogel that contained tracks were carved out from the tiles. The thickness of the slabs is from 3 to 10 mm thick and depends on the line thickness of the tracks. The slabs were cut out from the tiles at NISSAN ARC LTD. and Ibaraki University. The terminal particles were extracted from the slabs by hand or an electric micromanipulator under a stereomicroscope in a clean bench (class 100) in the clean room.

To characterize the individual terminal particles, synchrotron radiation X-ray diffraction (SR-XRD), micro Raman spectroscopy, transmission electron microscope (TEM), and SEM/EDS were used. Three different methods were applied for each particle. Nondestructive analyses (SR-XRD or micro Raman spectroscopy) were firstly applied and then destructive analysis (TEM and SEM/EDS) were applied. For the terminal particle retrieved in 2004, we utilized SR-XRD at beam line 3A of the Photon Factory Institute of Material Science, High Energy Accelerator Research Organization,

Tsukuba, Japan. We could obtain powder diffraction pattern by using Gandolfi camera within 30 minutes. For the other two terminal particles, we utilized micro Raman spectroscopy to characterize constituent material in the clean room. Excitation wavelength of laser is 785 nm. After these nondestructive analyses, terminal particles were embedded in epoxy resin and ultramicrotomed into 70-nm ultrathin sections by using ultramicrotomes at Ibaraki University. The ultrathin sections were investigated by a transmission electron microscope (TEM) equipped with EDS at Ibaraki University. Accelerating voltage of TEM was 200 kV. The remainders after ultramicrotomy (“potted butts”) of the terminal particles were used SEM/EDS to obtain petrographic data from their cross sections.

### 3. Results

#### 3.1 SEM/EDS analysis of the surface of silica aerogel tiles retrieved in 2002, 2004, and 2005

Silica aerogel tiles facing to the WAKE directions are browner than the RAM facing tiles in all the three units retrieved in 2002, 2004, and 2005. Figure 2 are mosaic photographs of silica aerogel tiles retrieved in 2005 taken under transmitted light. The brown coloring on the WAKE facing tiles retrieved in 2004 and 2005 are quite obvious. The color becomes darker as the exposure time to space increased. Many dark spots can be recognized on the WAKE facing tiles although their real color not always dark. In some cases, their real color is white under reflective light. Coloring shown on the surface of aerogel tiles has been reported in previous studies (e. g. [5], [6], [7]). Both tiles have deep cracks in their central areas. They are probably related to shrinkage of the tiles during return to one atmospheric pressure in the Russian service module because no coloring was observed in the deep interior of the cracks.

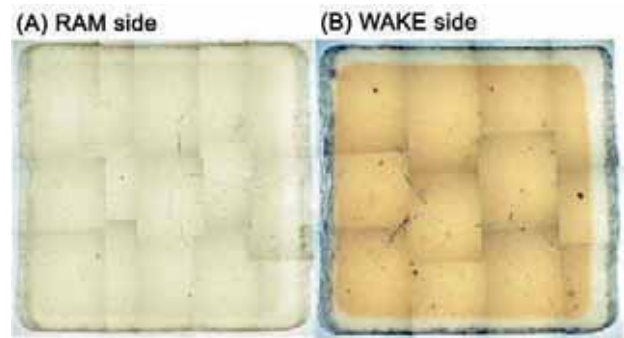


Fig. 2 Mosaic photographs of silica aerogel tiles retrieved in 2005. It is obvious that the WAKE facing tile is browner than the RAM facing one. Many dark spots can be recognized in the WAKE facing tile. The orthogonal lines in both tiles are artifacts due to limb darkening of each photograph.

After optical inspection, the surfaces of the silica aerogel tiles were investigated by SEM/EDS. Figure 3 shows change of surface morphology of the RAM facing silica aerogel tiles and their typical EDS spectra. It is obvious that number density of craters abruptly increased in the second retrieved sample. On the contrary, number densities of craters are not so different between samples retrieved in 2004 and 2005.

Elements except for O and Si derived from silica aerogel were hardly detected. Although a small peak of C K $\alpha$  was detected from the surface of SM2\_3RD3, we could not find C K $\alpha$  peak from SM3\_3RD3 (Figs. 3B, C).

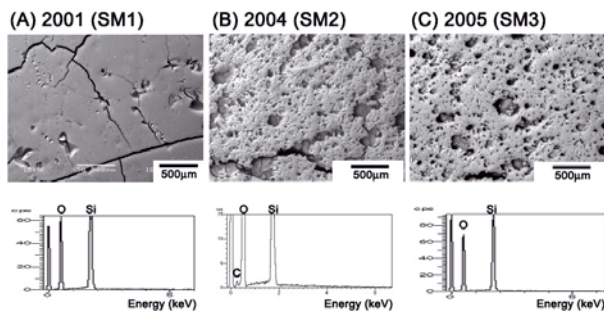


Fig. 3 BSE images of the surface of SM1, 2, and 3\_3RD3 tiles and their surface EDS spectra. Detected elements are O and Si derived from silica aerogel itself except for a small peak of C K $\alpha$  in SM2\_3RD3.

Abundant shallow craters observed in SM2 and 3\_3WD3 tiles have a common morphological feature. As shown in Fig. 4A, bottom of a crater has a wrinkled area. The wrinkled areas are usually off the center of each bottom. The directions from the center of the bottom to the wrinkled area are similar to each other. Relatively large (typically larger than 200  $\mu\text{m}$  in diameter) wrinkled areas are white under optical microscope when reflective illumination is used (Fig. 4B). We performed several simple experiments to reproduce these features. One of the results is shown in Figs. 4C and D. In this case, a droplet of ethanol was put on the surface of silica aerogel. The droplet was rapidly started to react with silica aerogel. The aerogel tile was promptly placed in a vacuum desiccator and evacuated for 30 minutes. It becomes white under optical microscope and the bottom of the “crater” has wrinkled areas. The morphological similarities between these figures suggest that the abundant shallow craters shown in the RAM facing craters were formed by low speed impacts of liquid droplets.

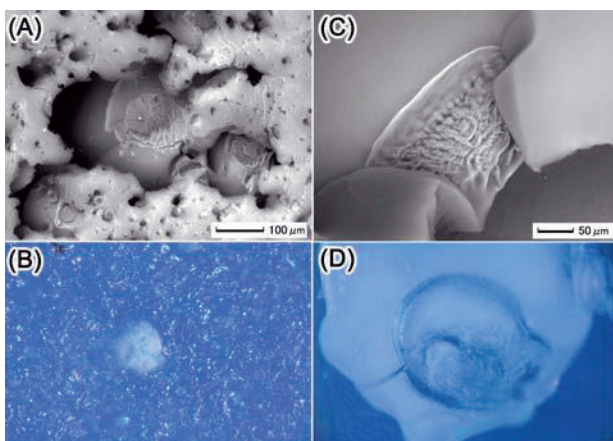


Fig. 4 BSE images and optical photomicrographs of a typical crater on the surface of the RAM facing silica aerogel and reproduction of “a crater” having similar morphology. (A) BSE image of a crater. Bottom of a crater has a wrinkled area and (B) it often corresponds to white stain under optical microscope. Reaction between silica aerogel and a droplet of ethanol formed a dent. (C) The reproduced “crater” (dent) has

several wrinkled areas in its bottom and (D) the dent is white under optical microscope.

Figure 5 shows the change in surface morphology of the WAKE facing tiles and their typical EDS spectra. A small amount of C was detected from this side. However, its relative abundances to O or Si were not increased with exposure duration to space. Carbon relative abundance on the tile retrieved in 2005 is the lowest among the three samples. Therefore it is clear that C content is not directly related to the brown coloring of the WAKE facing tiles. Although elements that constitute the brown color coating were not detected by EDS, the material that probably corresponds to the brown thin coating can be seen in BSE images (Fig. 6). Along the walls of the cracks, we can see at least three “layers” that cover the surface of the tile. Upper “layers” seem to be thicker than the lower “layers”.

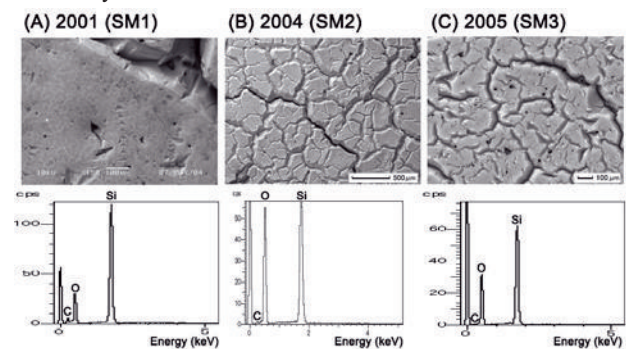


Fig. 5 BSE images of the surface of SM1, 2, and 3\_3WD3 tiles and their surface EDS spectra. Detected elements are O and Si derived from silica aerogel itself and a small peak of C.

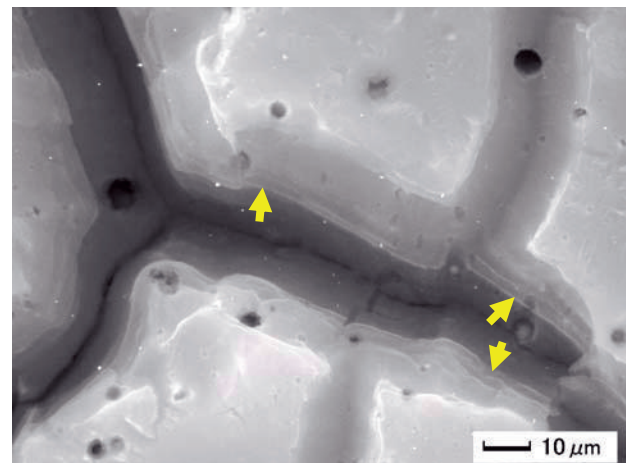


Fig. 6 An enlarged BSE image of cracks in SM3\_3WD3. As propagation of cracks into the interior of the silica aerogel tile, the thickness of the coated material seems to be different.

On the WAKE face tiles, we also observed abundant craters as well as cracks. Figures 7A and C are distribution of craters on the RAM and the WAKE facing tiles. Because the number density of craters in the RAM facing tiles is quite high, positions of craters larger than 250  $\mu\text{m}$  in diameter were plotted. On the other hand, craters larger than 100  $\mu\text{m}$  in diameter were plotted in the case of the WAKE side. Even though, the number density of craters in the RAM side is higher than that in



the WAKE side. In addition to the difference in number density of craters, there is an obvious difference in morphology of craters between the RAM facing and the WAKE facing tiles. As can be estimated from Figs. 7B and D, the ratios between depth and diameter of craters are obviously different. The craters on the WAKE side have higher depth/diameter ratios than those on the RAM side. In Fig. 7D, the deep crater also has a wrinkled area in its bottom. The similarity of the morphology of the bottom of craters facing both sides suggests that craters on the WAKE side were also formed by the impacts of liquid droplets. Different depth/diameter ratios between the both sides were probably related to the difference in impact speeds. Formation mechanism of the craters and brown layer will be discussed in chapter 4.

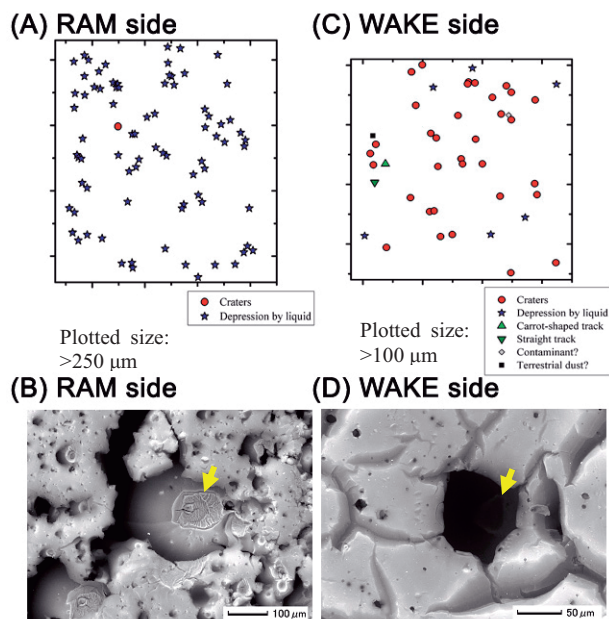


Fig. 7 Distribution of craters on the SM3\_3RD3 and SM3\_3WD3 tiles and typical morphology of craters in these tiles (BSE images). (A) and (C) Deep craters are plotted by red circles and shallow craters are plotted by blue stars. (B) and (D) Both craters have a wrinkled area in their bottom as indicated by yellow arrows.

### 3.2 Detailed analyses of terminal particles retrieved in 2002, 2004, and 2005

During optical inspection of silica aerogel tiles at IHI Aerospace LTD, we found many tracks that are easily identified by naked eyes. We identified some tracks that contain particles on their ends. As initial investigation of such captured particles, we selected three aerogel tiles retrieved in 2002, 2004, and 2005. First track is in SM1\_3RA1, a tile facing to the RAM side and retrieved in 2002. Second track is in SM2\_4WD1, a tile facing to the WAKE side and retrieved in 2004. Third one is in SM3\_3WC1, facing to the WAKE and retrieved in 2005. As shown in Fig. 8, the sizes and shapes of the tracks are various. In the first sample, the track is straight and 3.95 mm in length. According to [8], entry speed of the particle that makes this track was estimated to be < 2 km/s. The other two are typical “carrot-shaped” tracks. Their lengths are 9.43 and 14.74 mm, respectively. Their entry

speeds was estimated to be from 6 to 8 km/s [8]. Recent studies revealed that the effect of frictional heating during capture of fine-grained particles is quite different [9], [10]. The surfaces of the captured particles are heated around 1250 °C when they are shot at > 6 km/s. On the contrary, particles shot at about 2 km/s, their surfaces are not heated higher than 450 °C. Therefore, we investigated not only constituent materials of each captured grains but also compared the results with those of the capture experiments. Because all the captured particles investigated in this study exist at the end of the tracks, they are terminal particles. Their sizes are about 5, 50, and 40 μm in length, respectively.

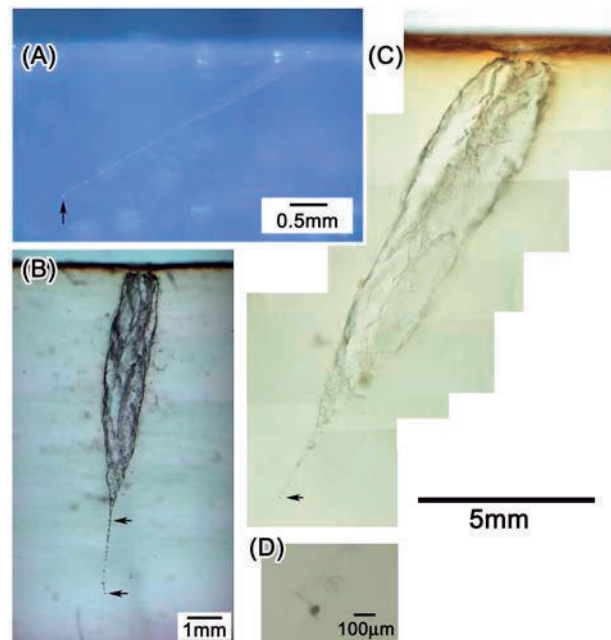


Fig. 8 Photomicrographs of tracks investigated in this study. Terminal particles are indicated by black arrows. (A) SM1\_3RA1, (B) SM2\_4WD1, (C) SM3\_3WD1, (D) an enlarged image of the terminal particle in the track shown in (C).

Raman spectrum of the terminal particle, SM1\_3RA1\_TP, was obtained. Many Raman shift peaks were obtained from the terminal particle. Major peaks are 531.4, 670.1, 840.7, 980.0, 1092.1, 1284.9, 1593.0  $\text{cm}^{-1}$ . Because chemical compositions of the material that emitted these Raman shift peaks are unknown, it is difficult to attribute these peaks to specific vibrations at present. However, based on Raman characteristic group charts, some of these peaks may be related to S and/or N bearing characteristic groups [12]. After ultramicrotomy, a cross section of the terminal particle was investigated by SEM/EDS. EDS analysis of the cross section revealed that it contains S as well as abundant Al. Therefore, it is estimated that the particle is composed of Al- and S-bearing organic material.

Low magnification bright field image of an ultrathin section of the terminal particle is shown in Fig. 9A. It is composed of polycrystalline metallic Al and Al- and S-bearing amorphous material. Grain size of each Al crystal is < 200 nm across. The amorphous material has a vesiculated texture



throughout the particle. Because no vesiculation occurred during TEM observation, the vesiculation occurred before or during capture by aerogel. Very thin ( $< 50$  nm thick) and non-vesiculated layer of silica aerogel is attached to the surface of the particle. It is similar to attached silica aerogel when projectiles were shot  $< 2$  km/s.

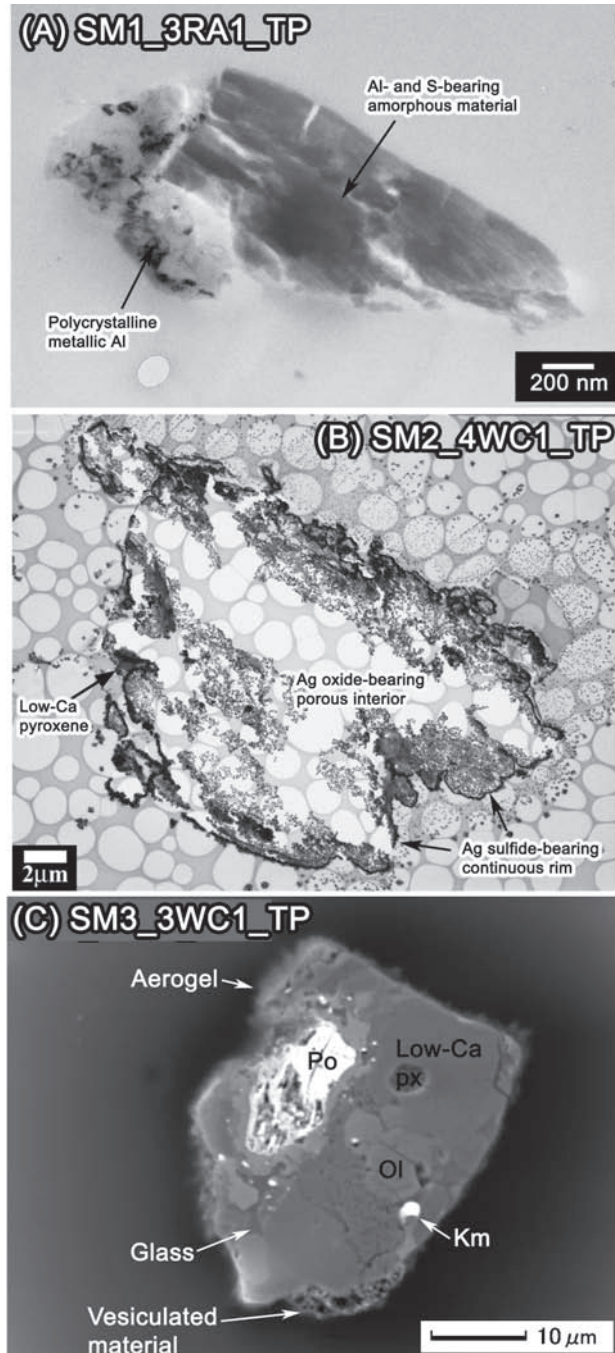


Fig. 9 Cross sections of the terminal particles investigated in this study. (A) and (B) low magnification bright field images of SM1\_3RA1\_TP and SM2\_4WD1\_TP. (C) BSE image of SM3\_3WC1\_TP. Network in (B) is a plastic film containing many holes, which support ultrathin sections. Many aligned sub- $\mu\text{m}$ -sized particles shown in the upper right side of the ultrathin section are Ag oxide, which were fallen out of the loose interior of the terminal particle.

There are two terminal particles in the silica aerogel retrieved in 2004. As indicated by two arrows in Fig. 8B, they were trapped in the funnel-shaped narrow part of the track. A black and opaque grain was trapped in the middle of the narrow channel and another colorless and transparent one was set near the end of the channel. After extraction from silica aerogel, they were investigated by SR-XRD. The black particle was a mixture of silver oxide and sulfide. However, the other one is amorphous. SEM/EDS analysis of these grains after SR-XRD indicates that the latter is basically composed of Si and O. Therefore, in the following section, only the black grain is described. TEM observation of the grain revealed that it has a continuous rim ( $< 500$  nm thick) and a quite porous interior. The rim is composed of S-rich amorphous material and silver sulfide  $\text{Ag}_2\text{S}$ . Its crystal structure is the same as acanthite. Because it is stable below  $179^\circ\text{C}$ , it was transformed from a high temperature form. Amorphous S-rich material among  $\text{Ag}_2\text{S}$  was quite unstable and decomposed under electron beam.

It is quite interesting that the terminal particle contains a  $2\text{-}\mu\text{m}$ -wide low-Ca pyroxene crystal near an edge of the particle (Fig. 9B). Because this particle is comprised of a mixture of natural and artificial materials, this particle is secondary debris, which was formed by a collision of a micrometeoroid with an artificial object. Selected area electron diffraction (SAED) pattern and high magnification images of the low-Ca pyroxene crystal show that it is orthopyroxene with many stacking disorders normal to  $a^*$  direction. Chemical composition of the pyroxene crystal is plotted in Fig. 10. Its composition is  $\text{Wo}_1\text{En}_{84.7}\text{Fs}_{14.3}$ . Its origin will be discussed in chapter 4.

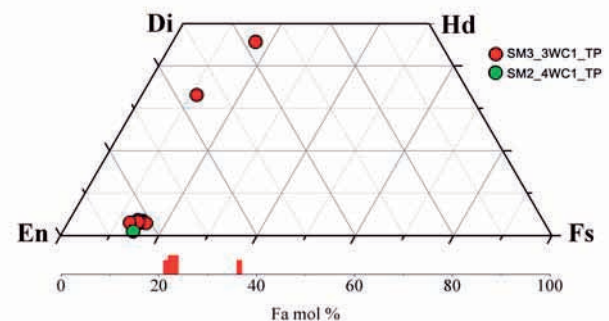


Fig. 10 Chemical compositions of pyroxene and olivine in SM3\_4WC1\_TP and a pyroxene crystal in SM2\_4WD1\_TP.

Third terminal particle retrieved in 2005 was set in the end of one of the largest tracks found among silica aerogel tiles retrieved in this year. It was back and opaque and has vitreous luster, suggesting abundant glass on its surface. Micro Raman spectrum of the particle has weak peaks of olivine, low-Ca pyroxene, and amorphous carbon as well as large background probably due to abundant glass on its surface. Presence of olivine and pyroxene suggests that this is a micrometeoroid (natural extraterrestrial particle). Figure 9C is a BSE image of the cross section of the particle. By considering EDS spectra of the particle, the most abundant mineral is low-Ca pyroxene. Most of the olivine crystals are poikilitically enclosed in low-Ca pyroxene. There is glass among these low-Ca pyroxene and olivine crystals. The texture of low-Ca

pyroxene, olivine, and glass strongly suggests that the glass was not formed during frictional heating during capture in silica aerogel. Fe-bearing sulfide and Fe-Ni metal (probably kamacite) are also observed. Aerogel is observed as ~2- $\mu\text{m}$ -thick layer on the surface of the particle. In the lower middle of Fig. 9C, vesiculated material is attached on the surface of the particle. It was probably formed by melting and vesiculation of fine-grained material that enclosed this coarse-grained (> 30  $\mu\text{m}$  across) terminal particle before colliding a silica aerogel tile.

SEAD patterns of constituent minerals in this particles revealed that it is composed of orthopyroxene, olivine, Ca-rich plagioclase, Ni-bearing pyrrhotite, troilite, and taenite. Orthopyroxene and high-Ca pyroxene have homogeneous chemical compositions. The average composition of orthopyroxene is  $\text{Wo}_{3.1}\text{En}_{82.7}\text{Fs}_{14.2}$ . Average  $\text{Al}_2\text{O}_3$ ,  $\text{Cr}_2\text{O}_3$ , and MnO contents of orthopyroxene are 2.6, 1.4, and 0.6 wt %, respectively. Diopsidic high-Ca pyroxene contains 1.7 wt %  $\text{TiO}_2$ , 2.2 wt %  $\text{Al}_2\text{O}_3$ , 1.9 wt %  $\text{Cr}_2\text{O}_3$ , and 0.7 wt % MnO. Most olivine crystals are also equilibrated except for one crystal. Their average Fa mol % is 25.1 and their average MnO is 0.9 wt %. Unfortunately, stoichiometry of plagioclase is bad probably due to partial decomposition by frictional heating during capture in silica aerogel. Ni-bearing pyrrhotite exists with troilite. Its composition is  $\text{Fe}_{32.7}\text{Ni}_{12.1}\text{S}_{55.2}$ . SAED pattern of the crystal shows  $a=2A$  and  $c=3C$  super lattice diffraction. Such super lattice diffractions are often observed among Fe-rich sulfides in interplanetary dust particles, typically ~15- $\mu\text{m}$ -sized extraterrestrial material captured in the stratosphere [12].

## 4. Discussion

### 4.1 Contamination on the silica aerogel tiles

Brown coloring has been also reported in the SM/MPAC & SEED experiments (e. g. [5], [6], [7]). They found that (1) contamination is more severe on the RAM side than on the WAKE side, (2) major contamination on the RAM side is continuous  $\text{SiO}_x$  layer, whose thickness increased with the increase of exposure duration, (3) that on the WAKE side are brown coating and many spotty stains. The  $\text{SiO}_x$  layer was estimated to have been produced by atomic oxygen (AO) reaction with siloxane. Based on the morphology, numerous colored spots were expected to have been formed by the particles and/or liquid droplets. Because two brown spots contained abundant N or F, fuel/oxidizer reaction products (FORP) were thought to be causes of these spots.

Our observation and a simple simulation experiment suggest that craters with wrinkled bottoms were formed by low-speed impact of liquid droplets. It is consistent with the above investigations. However, our observation revealed number density of such craters is much higher on the RAM facing tiles than on the WAKE facing ones. Because abundant "spots" were not detected on the RAM facing surface of aluminum plates by optical inspection and XPS analysis, chemical compositions of liquid droplets impinged between on the RAM side and on the WAKE side would have been different. Because the silica aerogel tiles are hydrophobic, the aqueous solution droplets would not have formed the craters.

We also found that the impact speeds of liquid droplets on the WAKE side were probably higher than those on the RAM side. This estimation is consistent with the previous works because the WAKE facing MPAC & SEED must have severely experienced thruster plumes of Progress braking thrusters [5]. This means that the WAKE facing silica aerogel tiles suffered impacts by higher speed droplets and/or particles from the plumes. However, it is still an enigma that why the RAM facing tiles experienced more abundant impacts of liquid droplets than the WAKE facing tiles although the speeds of droplets were lower than the latter. One important fact that may serve to estimate the origin of "projectiles" of the craters on the RAM side is that most of the wrinkled area in each crater offsets in the same direction (Fig. 4A). It means that the liquid droplets always came from almost the same direction or formed by single event. We need to search the sources of the projectiles of the craters on the RAM side, other than FORP.

SEM observation of the surface of the WAKE facing tiles revealed that contamination layer that probably corresponds to the brown coating under optical microscope proceeded several times based on the texture of cracks coated by contamination (Fig. 6). If the coated material and "projectiles" of the craters had been formed by the same material, thickness of the coated material and the number density of the craters would have increased in a discontinuous manner. If the origin of this material had been thrust plumes, liquid droplets directly reached the surface of the tiles would have made deep craters and gaseous material reached the surface of the tiles at a low speed would have made a continuous layer.

### 4.2 Origin of the space debris and the secondary debris

The main purpose of MPAC is capture of space debris and micrometeoroids on the ISS. In spite of the severe contamination on silica aerogel tiles as described above, there are tracks that capture fine-grained particles on their ends. Our investigation of the terminal particles confirmed that both space debris and micrometeoroids can be captured and that we can obtain important information from the particles. First terminal particle retrieved in 2002 is a mixture of metallic aluminum and Al- and S-rich amorphous material. Second one is a mixture of silver oxide and sulfide as well as a small fragment of orthopyroxene (natural crystal). Their origins are hard to estimate because there is no database of materials that can be obtained as fine-grained space debris. An idea of the origin of the first particle is partially reacted solid propellant because metallic Al is used as a metallic fuel. The origin of second particle is even hard to be deduced. One possible idea of its origin might be an electrode of a solar panel.

### 4.3 Origins of orthopyroxene in the secondary debris and the micrometeoroid

We could obtain a micrometeoroid from an aerogel tile retrieved in 2005. There are only a few micrometeoroids investigated by TEM [2]. All micrometeoroids investigated in [2] were aggregates composed of more than two kinds of minerals. They contained olivine exhibiting sharp electron-diffraction spots indicative of well crystalline and of minimal shock-deformation. One terminal particle contained

olivine, high-Ca pyroxene (augite and diopside), troilite, spinel-group minerals (chromite, magnetite, and hercynite). Olivine was contained in two terminal particles and compositional ranges of olivine were  $Fo_{60-70}$  and  $Fo_{39-53}$ , respectively. On the other hand, the micrometeoroid found in this study has a texture similar to porphyritic olivine pyroxene chondrules, some coarse-grained Antarctic micrometeorites (AMMs) [13], and some coarse-grained terminal grains retrieved from Wild2 comet by STARDUST spacecraft [14]. In other words, the micrometeoroid was once melted in space. This is the first successful comparison of the texture of a micrometeoroid and the other extraterrestrial material. The particle contains abundant orthopyroxene, suggestive of equilibrated ordinary chondrites in origin. However, average ferrosilite mol % of the orthopyroxene is 14.2 and below the range of H chondrites ( $Fs_{15-17.5}$ ). Minor elements concentrations ( $Al_2O_3$ ,  $Cr_2O_3$ , and  $MnO$ ) of the orthopyroxene and high-Ca pyroxene are considerably higher than those in H chondrites. Average chemical composition of olivine ( $Fa_{25.1}$ ) coexisting orthopyroxene is also different from that of equilibrated H chondrites ( $Fa_{16-20}$ ). If orthopyroxene and olivine in the particle was equilibrated, olivine should be more magnesian. Therefore, it is clear that this particle did not experience thermal metamorphism that resulted in equilibrated Fe-Mg partition between them.

The micrometeoroid contains Ca-rich plagioclase and Ni-bearing pyrrhotite, both of which are absent among equilibrated ordinary chondrites. These lines of evidences definitely indicate that this micrometeoroid has no genetic relationship with equilibrated ordinary chondrites. Ni-bearing pyrrhotite is common among carbonaceous chondrites and hydrated interplanetary dust particles, and phyllosilicate-rich AMMs that experienced heavy aqueous alteration on their parent bodies [15]. In this micrometeoroid, primary glass and Ca-rich plagioclase do not show the evidence of aqueous alteration although glass and plagioclase are susceptible to suffer aqueous alteration. Therefore, presence of Ni-bearing pyrrhotite suggests the possibility of aqueous alteration to a minor degree.

On the other hand, orthopyroxene found in the secondary debris has overlap chemical composition of orthopyroxene in ordinary chondrites. Therefore, there is a possibility that the micrometeoroid that made the secondary debris was derived from H chondrite parent body.

These particles collided to the WAKE facing tiles. The shapes of tracks that these two particles were trapped are carrot-shaped and the relative speed to the tiles was from 6 to 8 km/s based on ground-based experiments [8]. Because orbital speed of the ISS is 7.7 km/s, the speeds of the particles at the orbit of the ISS were probably 13.7 to 15.7 km/s. Interplanetary dust particles having atmospheric entry velocities from 14 to 18 km/s are difficult to estimate their parent bodies (asteroidal or cometary) [16]. Therefore, further investigations of the micrometeoroid such as TEM investigation of fine-grained matrix and oxygen isotopic analysis by SIMS are needed to confine its origin.

## 5. Comments for future MPAC experiment

As shown in the previous section, we often felt difficulty to estimate the origins of fine-grained space debris. Before start of future MPAC experiment such as JEM/MPAC & SEED, it is desired to make a database of materials that can be obtained as fine-grained space debris. At the same time, further investigation of surface contamination by XPS, TOF-SIMS, and so on are also desired. Another important thing to improve is to develop the method to cutout silica aerogel slabs from tile in order to decrease large-sized destruction of tiles during cutout.

## 6. Conclusions

We investigated silica aerogel tiles faced both the RAM and WAKE sides retrieved in 2002, 2004, and 2005. Although all the tiles suffered contamination, tiles retrieved in 2004 and 2005 were severely contaminated. On the surface of the RAM facing tiles, they experienced heavy bombardment of low speed impacts of liquid droplets. Thick  $SiO_x$  layer reported from the other researchers (e. g. [6], [7], [8]) could not be identified because silica aerogel is composed mainly of  $SiO_2$ . On the surface of the WAKE facing tiles, brown colored thin film coated the surface. In spite of its identification by both optical microscope and BSE images, we could not identify specific elements derived from the coating. As well as the thin coating, the surface also experienced bombardment of liquid droplets. Even the deep craters on the WAKE side tiles were not formed by hypervelocity impacts because none of them are not carrot-shape or bulbous-shape, indicative of hypervelocity. The depth/crater diameter ratios increase as the speeds of projectiles increase in such velocity range. Because the craters on the WAKE side have larger depth/crater ratios, the craters were probably formed by higher speed liquid impingent than on the RAM side. It is consistent with the severe effect of thruster plume from Progress on the WAKE side.

We could investigate three terminal particles that trapped on the end of tracks in the tiles retrieved in 2002, 2004, and 2005 irrespective of severe contamination. They are space debris, secondary debris, and micrometeoroid based on TEM and the other microanalyses. An orthopyroxene grain found in the artificial material (a mixture of silver oxide and sulfide) testifies that it is a secondary debris. This is the first identification of secondary debris by using microanalysis.

Mineralogy and petrography of the micrometeoroid were investigated in detail. Its texture is similar to chondrules, crystalline AMMs, and coarse-grained terminal particles retrieved by STARDUST. Its constituent minerals are similar to carbonaceous chondrites experienced minor aqueous alteration although no hydrated minerals were identified. However, at present, it is difficult to state whether this micrometeoroid is asteroidal or cometary in origin. Further investigation is needed to restrict the possible origin.

## References

- [1] M. J. Burchell, R. Thomson, and H. Yano: Capture of hypervelocity particles in aerogel: in ground laboratory and



- low Earth orbit, *Planet. Space Sci.* 47, 189-204 (1999).
- [2] F. Hörz, M. E. Zolensky, R. P. Bernhard, T. H. See, and J. L. Warren: Impact Features and Projectile Residues in Aerogel Exposed on Mir, *Icarus* 147, 559-579 (2000).
- [3] D. E. Brownlee and 182 coauthors: Comet 81P/Wild 2 Under a Microscope, *Science* 314, 1711-1716 (2006).
- [4] M. E. Zolensky and 74 coauthors: Mineralogy and Petrology of Comet 81P/Wild 2 Nucleus Samples, *Science* 314, 1735-1739 (2006)
- [5] C. Pankop, K. Smith, C. Soares, R. Mikatarian, and N. Baba: Induced contamination onto JAXA's micro-particle capturer and space environment exposure device – Comparison of predictions and measurements, *Proc. 10th ISMSE*, ESA-SP-616 (2006).
- [6] N. Baba, M. Suzuki, I. Yamagata, Y. Kimoto, and J. Ishizawa: Experimental Contamination Observation on the Micro-particles Capturer and Space Environmental Exposure Device, *Proc. 10th ISMSE*, ESA-SP-616 (2006).
- [7] J. Ishizawa, K. Mori, F. Imai, I. Yamagata and M. Suzuki: Results of the space-environment exposure experiment “SM/MPAC&SEED” on the international space station (2): Siloxane coated polyimide films, and silicone based paints and adhesives, *Proc. 10th ISMSE*, ESA-SP-616 (2006).
- [8] Y. Kitazawa, A. Fujiwara, T. Kadono, K. Imagawa, Y. Okada, and K. Uematsu: Hypervelocity impact experiments on aerogel dust collector, *J. Geophys. Res.* 104, E22035-22052 (1999).
- [9] K. Okudaira, T. Noguchi, T. Nakamura, S. Sugita, and H. Yano: Evaluation of mineralogical alteration of micrometeoroid analog materials captured in aerogel. *Adv. Space Res.* 34, 2299-2304 (2004).
- [10] T. Noguchi, T. Nakamura, K. K. Okudaira, H. Yano, S. Sugita, M. J. Burchell: Thermal alteration of hydrated minerals during hypervelocity capture to silica aerogel at the flyby speed of Stardust. *Meteoritics Planet. Sci.* 42, 357-372 (2007).
- [11] G. Socrates; Infrared and Raman characteristic group frequencies, John Wiley and Sons, Ltd, New York, 347 pp. (2001).
- [12] J. P. Bradley: Interplanetary dust particles, In: *Meteorites, Comets, and Planets* (A. M. Davis, ed.), Elsevier-Pergamon, Oxford, 689-711 (2005).
- [13] G. Kurat, C. Koebel, T. Presper, F. Brandstätter, and M. Maurette: Petrology and geochemistry of Antarctic micrometeorites, *Geochim. Cosmochim. Acta* 58, 3879-3904 (1994).
- [14] T. Nakamura and 11 coauthors: Mineralogy, Three Dimensional Structure, and Oxygen Isotope Ratios of Four Crystalline Particles from Comet 81P/Wild 2 *Lunar Planet. Sci. XXXIX*, Abstract #1695 [CD-ROM] (2008).
- [15] M. E. Zolensky and K. Thomas: Iron and iron-nickel sulfides in chondritic interplanetary dust particles. *Geochim. Cosmochim. Acta* 59, 4707-4712 (1995).
- [16] D. J. Joswiak, D. E. Brownlee, R. O. Pepin, and D. J. Schlutter: Characterization of asteroidal and cometary IDPs obtained from stratospheric collectors: Summary of measured He release temperature, velocities, and descriptive mineralogy, *Lunar Planet. Sci. XXXI* Abstract #1500 [CD-ROM] (2001).

#### Publication list related SM/MPAC&SEED

- Y. Kitazawa, T. Noguchi, M.J. Neish, I. Yamagata, Y. Kimoto, J. Ishizawa, A. Fujiwara, M. Suzuki, Y. Yamaura, S. Yamane; Passive Measurement of Dust Particles on the ISS (MPAC): Status report of the post flight analysis european Geosciences Union, General Assembly 2007 Vienna, Austria, 15-20 April 2007, CD-ROM (EGU2007-A-01406) (Abstract), (2007).
- Y. Kitazawa, M. J. Neish, T. Noguchi, I. Yamagata, Y. Kimoto, J. Ishizawa, A. Fujiwara, M. Suzuki, Y. Yamaura, Y. Watanabe, S. Yamane; Passive measurement of dust particles on the ISS (MPAC): Third report on aerogel dust collectors, 57th Meeting of the Aeroballistic Range Association, Venice, Italy, 18-22 Sept. 2006 CD-ROM, (2007)
- T. Noguchi, Y. Kitazawa, M. J. Neish, I. Yamagata, Y. Kimoto, J. Ishizawa, M. Suzuki, A. Fujiwara, Y. Yamaura, S. Yamane; Passive Measurement of Dust Particles on the ISS (MPAC): Fourth report on aerogel dust collectors, Committee on Space Research, 36th COSPAR Scientific Assembly, Beijing, China, 16 -23 July 2006, CD-ROM (PEDAS1-0008-06), (Abstract), (2006)
- Y. Kitazawa, M. J. Neish, T. Noguchi, T. Inoue, J. Ishizawa, A. Fujiwara, K. Imagawa, Y. Yamaura, S. Yamane, S. Nakazato; Passive measurement of dust particles on the ISS (MPAC): Second report on aerogel dust collectors, Preprints of The 25th International Symposium on Space Technology and Science, (CD-ROM), Kanazawa, Japan, 30 May - 6 June 2006, (2006)
- T. Noguchi, Y. Kitazawa, M. J. Neish, I. Yamagata, Y. Kimoto, J. Ishizawa, M. Suzuki, A. Fujiwara, Y. Yamaura, S. Yamane; Passive measurement of dust particles on the ISS (MPAC): Third report on aerogel dust collectors, European Geosciences Union General Assembly 2006 Vienna, Austria, 02 - 07 April 2006, CD-ROM (Abstract),(2006)
- M. J. Neish, Y. Kitazawa, T. Noguchi, T. Inoue, K. Imagawa, T. Goka, Y. Ochi; Passive measurement of dust particles on the ISS Using MPAC: experiment summary, particle fluxes and chemical analysis, ESA Proceedings of the 4th European Conference on Space Debris, p 221-226, Darmstadt, Germany, 18-20 April 2005 (SP-587, August, 2005), (2005)
- Y. Kitazawa, T. Noguchi, M. J. Neish, T. Inoue, J. Ishizawa, A. Fujiwara, K. Imagawa, Y. Yamaura, Y. Watanabe, A. Murakami; First year mission results of passive measurement experiment of dust particles on ISS (MPAC), Preprints of 24th International Symposium on Space Technology and Science, Miyazaki, Japan, 30 May - 6 June 2004 (CD-ROM), (2004)



## INFLUENCE ON POLYMER MATRIX COMPOSITE EXPOSED TO SPACE ENVIRONMENT

Yoji ARAKAWA<sup>1</sup>

<sup>1</sup> Aerospace Company, Fuji Heavy Industries LTD.,  
Utsunomiya, Tochigi 320-8564, Japan

Polymer matrix composites such as carbon fiber reinforced plastic (CFRP) are lightweight materials which have good mechanical properties and are applied widely as basic structural materials for spacecraft, especially reusable launch vehicle. However the degradation data of the CFRP after exposed in space environment for long period was not obtained in ground experiment. Therefore understanding the process of degradation for CFRP is very important to maintain structural reliability. In this study we evaluate the two heat resistant CFRP which are candidates for the reusable launch vehicle.

**Keywords:** CFRP, Polycyanate, Polyimide, Delamination, Micro crack

### 1. Introduction

Composite materials such as CFRP were applied to spacecraft especially reusable launch vehicle (RLV) more and more because of their high specific strength and specific elasticity. However effective data have not obtained although polymer matrix is degraded by space environment factors such as electron beam, ultra violet ray, high vacuum, thermal cycle and atomic oxygen, effective data were very few for difficulty of simulating space condition (Fig.1).

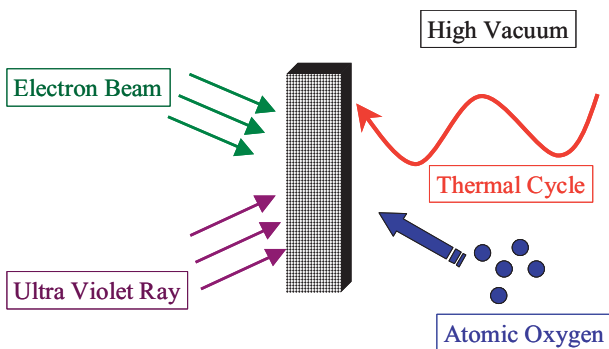


Fig.1 Space environmental factors to composite material

It is possible to conduct an experiment under each environment condition, but the experiment which includes all space environment factors is very difficult to conduct. Moreover it is known that the results which are obtained by simultaneous condition and sequential condition are different. The material experiments conducting under the actual space environment give us very important data for space development (Fig.2)

In case of RLV, the structure bears large mechanical and thermal load repeatedly. Therefore material degradation data under the space environment factor is very essential.

In this study we, Fuji Heavy Industries LTD. (FHI), selected two heat resistant materials which are the candidates for RLV structure, offered for the MPA&SEED experiment and evaluated surface and internal quality of the materials using 5 evaluation method

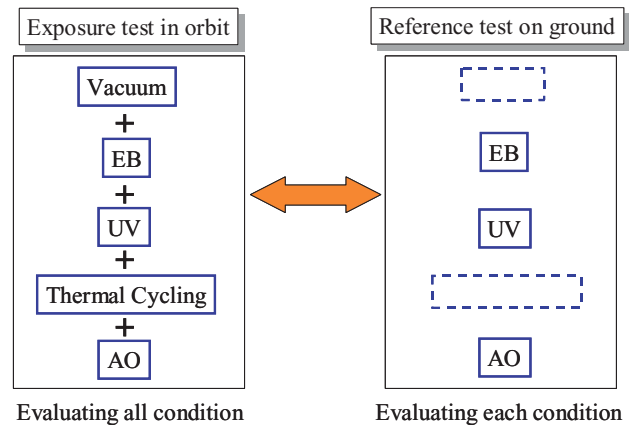


Fig.2 Difference of experiment condition between in orbit and on ground

### 2. Material Properties

Two heat resistant composite materials are evaluated in the experiment. One is YS90A/RS-3 which consist of pitch based carbon fiber and polycyanate resin, and the other is IM600/PIXA which consist of PAN based carbon fiber and the thermo plastic polyimide resin.

#### 2.1 CF/Polycyanate

CF/Polycyanate (CF/PC) is more durable in heat condition compared with epoxy based CFRP using pitch based high tensile modulus carbon fiber and Polycyanate heat resistant resin named YS90A. CF/PC has good heat cycle durability because of low micro crack.

The properties of the material are following.

- Fiber: YA90A, High tensile modulus carbon fiber.
- Resin: RS-3, Polycyanate resin.
- Resin composition: Thermo set resin with cyan group (CN).
- Main characteristic:
  - 1) Low out gas
  - 2) Low micro crack
  - 3) Heat resistant temperature : 190°C  
( Tg : 206~254)

**2.2 CF/Polyimide**

CF/Polyimide (CF/PX) is high heat resistant composite using PAN based carbon fiber and polyimide, which is one of the highest heat durable resin

The properties of the material are following.

- Fiber: IM600, High strength carbon fiber.
- Resin: PIXA-M, Polycyanate resin.
- Resin composition: Thermoplastic polyimide resin with imide group (NHO2)
- Main characteristic:
  - 1) Resistance to high temperatures  
(thermal deformation temperature : 220、Tg : 240)
  - 2) High resistance to radiation
  - 3) High CAI strength

**2.3 Specimens size and exposure period**

The specimen size for the each material is 17mm sq. and 3mm thickness. The specimens were exposed out of ISS Russian service module on three different periods (10, 28, 46months). In addition, ground experiments which were applied space environment factors such as electron beam, ultraviolet ray, and atomic oxygen were conducted separately as reference experiment.

For each space environment factor, the specimens were irradiated for 0.5 and 1.0 year in orbit equivalent.

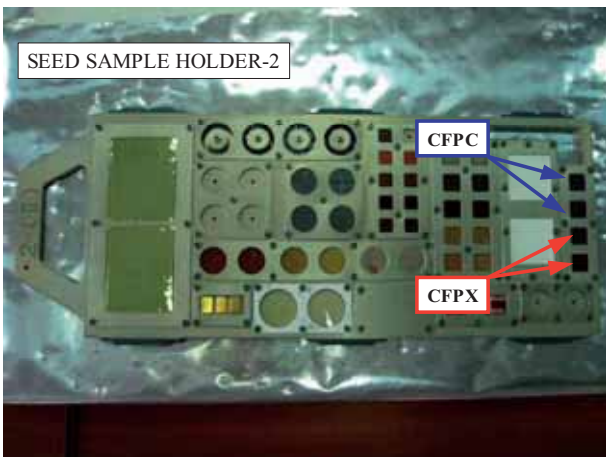


Fig.3

**3. Evaluation**

**3.1 Evaluating method**

Following observations were conducted in order to evaluate the specimens which were unexposed any condition, exposed in space environment and irradiated space environment factors.

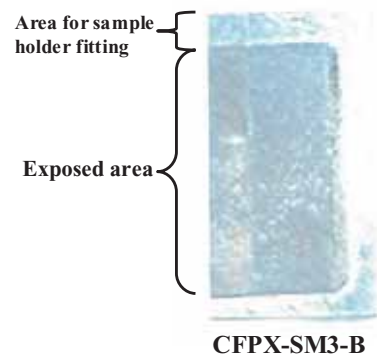
1. Visual Observation (VO)
2. Microscope Observation (MO)
3. Cross section Observation (CO)
4. Ultra Sonic Observation (USO)
5. Fourier Transform Infrared Spectroscope (FT-IR)

In the evaluation methods, VO and MO were conducted in order to obtain surface condition of the materials. CO and USO were conducted to get the internal data and FT-IR is for the data of composition change on the surface of the materials. The details of the evaluation are described in following next item.

**3.2 Visual Observation**

From results of VO, surface fading of the space-exposed specimens and atomic-oxygen-irradiated specimens were confirmed. Fig.4 shows the fading area of CFPX exposed for 46months. This picture is not clear to find changes. But the surface lost luster and changed to brawn color in the area exposed in space environment while the area for sample holder fitting had luster clearly and was not find any change. In addition, the surface of exposed area is rougher than that of the area for sample holder fitting.

In consideration of the above results, we think that the fading was caused by atomic oxygen in the space environment.



CFPX-SM3-B  
(46 months exposed)  
Fig.4 Fading of CFRP

**3.3 Microscope Observation**

Further research in the surface degradation we conducted microscope observation (MO). The MO results of CF/PC and CF/PX were shown in Fig.5, Fig.6. The rough surface was observed in either of the two materials under the condition of space environment exposure and atomic oxygen irradiation. On the other hand, any change was not observed among the unexposed and EB and UV irradiation


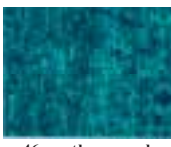
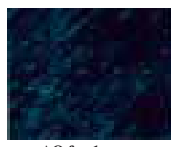


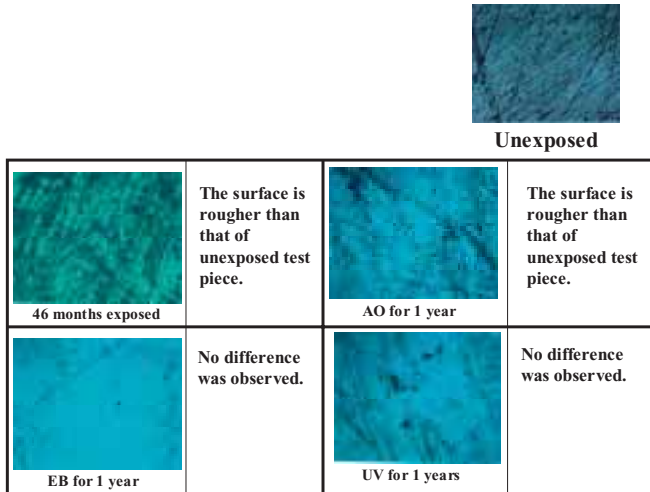
			
<b>Unexposed</b>			
	The surface is rougher than that of unexposed test piece.		The surface is rougher than that of unexposed test piece.
46 months exposed		AO for 1 year	
	No difference was observed.		No difference was observed.
EB for 1 year		UV for 1 years	

Fig.5 Results of CFPC for MO



**Fig.6 Results of CFPX for MO**

**3.4 Cross section Observation**

Cross section Observation (CO) was conducted in order to research on the internal quality such as micro crack and delamination. Table 1 shows the result of counting the numbers of cracks and delamination. The delamination was observed in all CFPC including the unexposed specimen. Therefore we think that the delamination was generated for manufacturing process.

Cracks were not observed in CFPC. This result supports the characteristic of this material that micro cracks were very low.

On the other hand, many cracks were observed in CFPX which was made using thermoplastic polyimide. Thermoplastic polyimide resin is thought as ductile material. And the results are not same compared with a prior prediction.

In consideration that the space environment factor in which the number of cracks is the largest is EB condition, it is thought that the cracks were generated because the resin became brittle by EB that permeated into the internal and changed the polymer composition of the specimen.

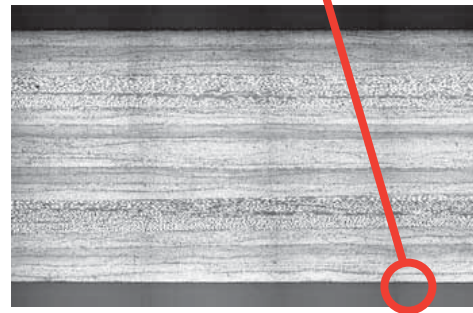
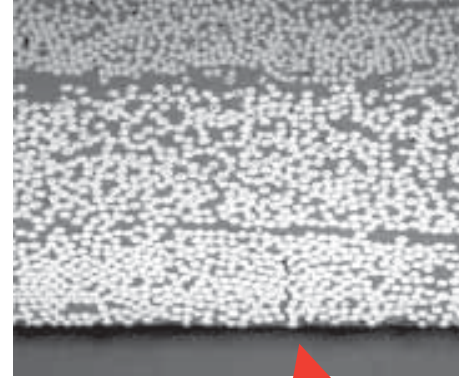
**Table1 The numbers of cracks and delaminations**

Material	Environment	Crack	Delamination
CFPC	10 months	0	1
	28 months	0	1
	46 months	0	0
	EB for 1 year	0	1
	AO for 1 year	0	1
	UV for 1 year	0	1
	Unexposed	0	1
CFPX	10 months	0	0
	28 months	1	0
	46 months	7	0
	EB for 1 year	9	0
	AO for 1 year	3	0
	UV for 1 year	5	0
	Unexposed	0	0

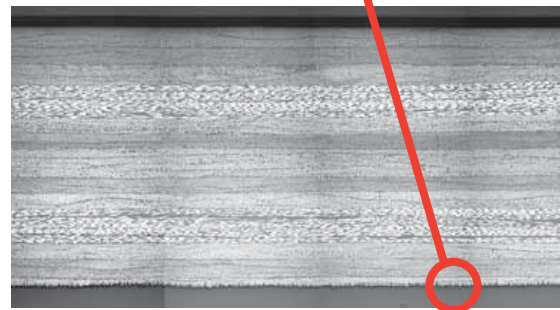
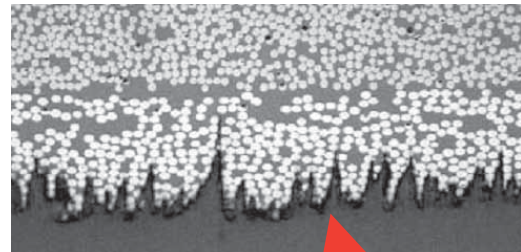
Fig.7 and Fig.8 show the picture of CO for CFPX exposed for 46months in orbit and AO irradiation 1 year equivalent.

Supporting the result of VO, resin damage and carbon fiber without resin was observed on the surface of the specimen in Fig.7, Fig.8

Resulting from CO, the roughness of the CFRP surface was caused by AO.



**Fig.7 CFPX 46 months exposed**



**Fig.8 CFPX AO for 1 year**



### 3.5 Ultrasonic Observation

Ultrasonic Observation (USO) is the general inspection method using aerospace composite parts for quality assurance.

In this study, USO was conducted in order to detect foreign objects and delamination.

Fig.9 and Fig.10 show the results of CFPC. The indication which exists directed to fiber was observed in all results including unexposed specimen. Although no clear indication was observed except the small delamination indication, clear trend among unexposed, space exposed and space environment factor was not found by using USO.

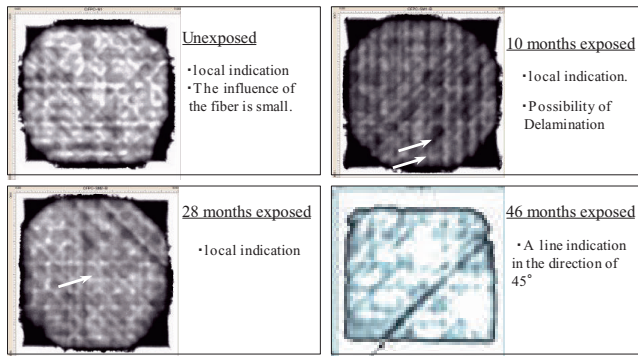


Fig.9 Result of CFPC for 4 period in orbit

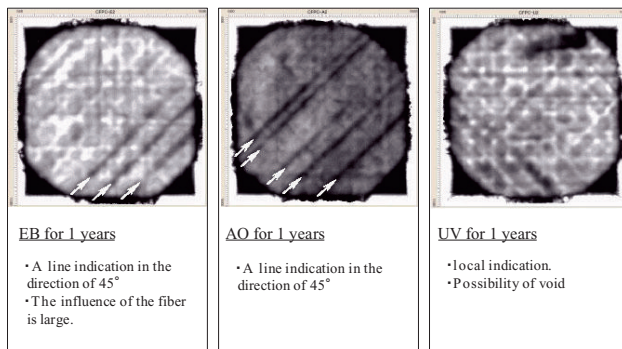


Fig.10 Result of CFPC irradiated space environment factors

The same trend was obtained in the results of CFPX. Fig.11 and Fig.12 show the results of CFPX.

No indication was observed in the specimen exposed for 46 months in orbit, although the indication which exists directed to fiber was observed in the results including unexposed specimen.

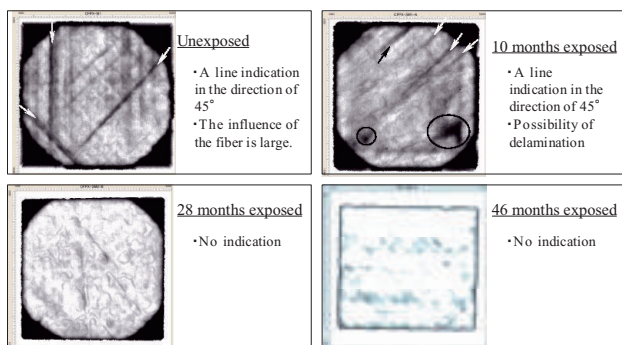


Fig.11 Result of CFPX for 4 period in orbit

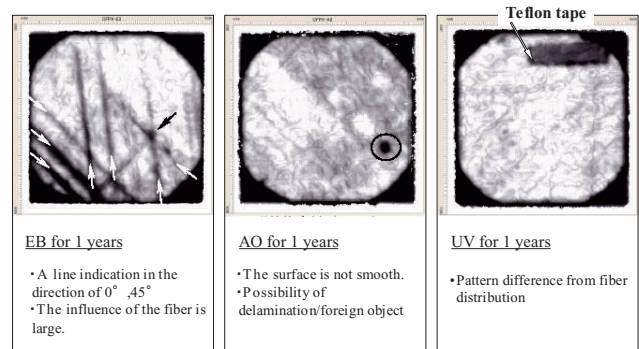


Fig.12 Result of CFPX irradiated space environment factors

### 3.6 Fourier Transform Infrared

Fourier Transform Infrared (FT-IR) spectroscopic analysis is the chemical analyzing method, and can get the resin degradation by measuring a organic composition change.

Fig.13 to 16 show the FT-IR results for CFPC and Fig.17 to 20 show the results for CFPX. In these graphs blue, orange, green, pink line show the unexposed, 10 months, 28 months, 46 months in orbit respectively.

Fig.14 to 16 also show the results of AO, EB, and UV respectively. In these graphs blue line shows the result of unexposed specimen. In the same way, orange and green line shows the result of equivalent irradiation for 0.5 year and 1.0 year respectively.

Same trend was confirmed in the result of CFPC and CFPX. As compared Fig.15 with Fig.16 and Fig.19 with Fig.20, no change of organic composition was found.

On the other hand, the sharp peak which indicates organic composition was low and almost disappear the result for 46 months in orbit and 1 year equivalent AO irradiation. The results show degradation of resin especially in CFPC.

In the result for 46 months in orbit, indication of ozone compound was found. But the phenomenon was not seen in the results of AO. I think this phenomenon to be the combined effect of the space environment, but the mechanism of the generation is not elucidated

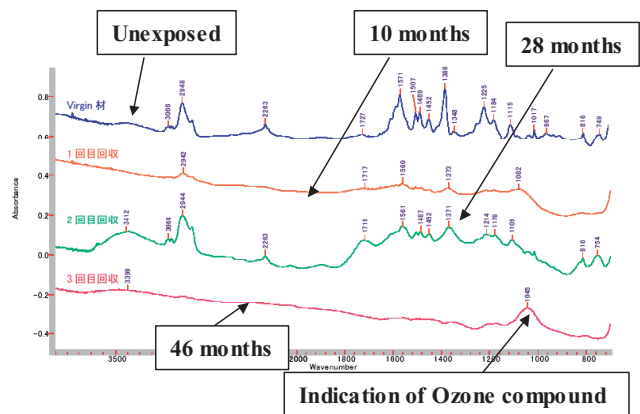


Fig.13 FTIR for CFPC in orbit



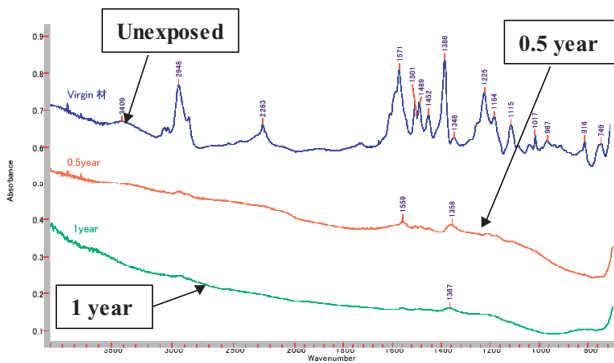


Fig.14 FTIR for CFPC AO irradiation

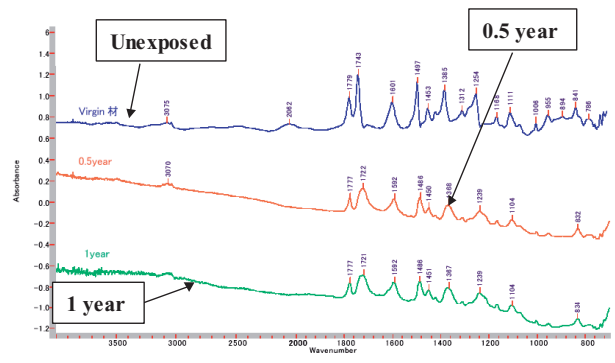


Fig.18 FTIR for CFPX AO irradiation

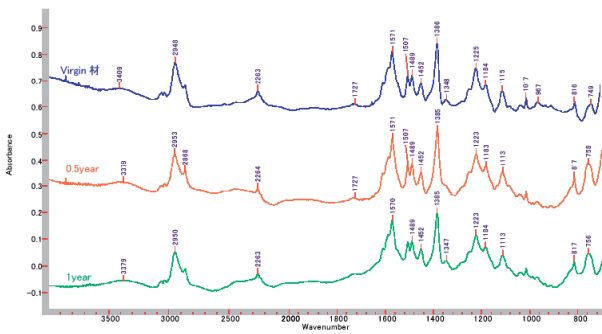


Fig.15 FTIR for CFPC EB irradiation

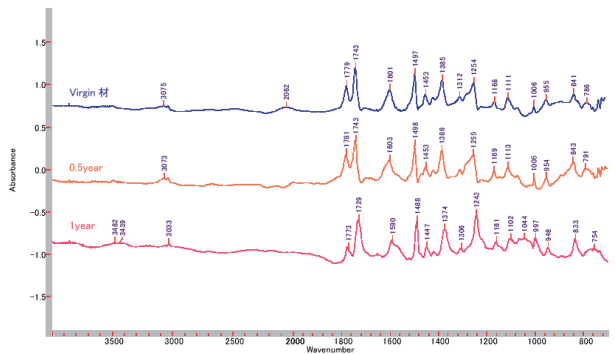


Fig.19 FTIR for CFPX EB irradiation

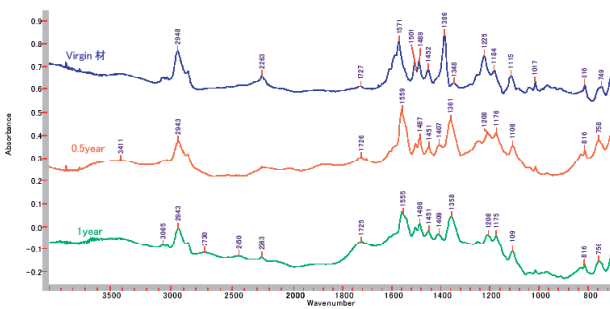


Fig.16 FTIR for CFPC UV irradiation

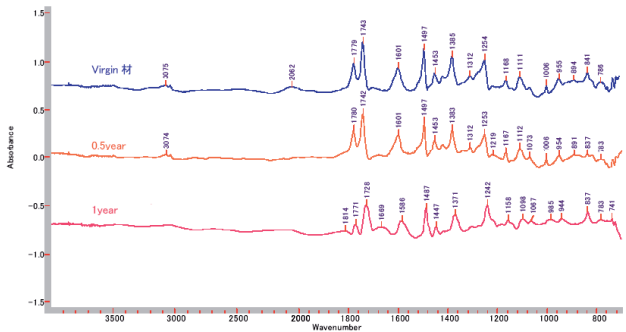


Fig.20 FTIR for CFPX UV irradiation

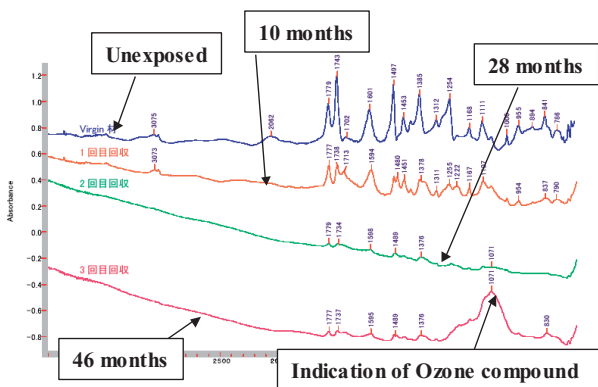


Fig.17 FTIR for CFPX in orbit

#### 4 Summary

In the Space environment exposure experiment two kinds of composite materials which are candidates for future spacecraft were evaluated as follows.

As a result of visual and optical microscope inspection, resin damage and carbon fiber without resin were observed on the exposed surface for each specimen. We think that AO gives main influence for the lack of resin because the same result was observed in the reference experiment of AO.

The clear degradation of the resin was not observed in the internal structure for each materials and conditions as a result of ultrasonic inspection and cross section observation.

As space environment exposure period became long, the resin degradation and the ozone compound were observed from the results of FT-IR.

## EFFECTS OF LEO ENVIRONMENT ON MECHANICAL PROPERTIES OF PEEK FILMS UNDER TENSILE STRESS

Takashi NAKAMURA<sup>1</sup> and Osamu FUJITA<sup>1</sup>

<sup>1</sup> *Mechanical and Space Engineering, Hokkaido University,  
North13, West8, Kita-ku, Sapporo, Hokkaido, 060-8628, Japan*

The environment of LEO is extremely harsh for polymer materials because of detrimental factors such as atomic oxygen (AO), ultraviolet light (UV), and charged particle radiation. Although many researches regarding LEO environment on physical and chemical properties of polymers were reported, those on mechanical behaviors are still insufficient. For the long term use of polymers in LEO, it is necessary to elucidate the strength properties systematically. This study exposed Poly-ether-ether-ketone (PEEK) films under tensile stresses into LEO by using ISS Russian service module. In parallel, ground tests were carried out by using JAXA facilities, which irradiated AO, UV, and electron beam (EB) to the specimens individually. By comparing the results of flight tests with ground tests, degradation properties and the mechanisms were studied.

**Keywords:** Atomic Oxygen, Ultraviolet Light, Electron Beam, PEEK, Tensile Properties, International Space Station

### 1. Introduction

In recent years, deployable structures have been acknowledged to be a leading edge technology for the construction of space facilities. Their use is expected in many space structures, such as large space antennas, photovoltaic generation systems, solar sails, etc. Polymeric films are one of the candidate materials for these deployable structures. In these applications, polymer films have to hold a certain amount of load in space for a long term. Therefore, the reliability of mechanical properties in space is one of the most important factors for them. However, space is extremely harsh to polymers due to the presence of several types of radiation and atomic oxygen (AO). In particular, it is well known that many polymeric materials are damaged by AO in LEO from 200 to 700 km altitude [1]. Although space exposure experiments of polymer films have been conducted [2]-[3], we have insufficient data of the relation between mechanical properties and LEO environment.

To investigate these phenomena, two different experiments were organized: one was a space exposure experiment and the other was a ground control experiment [4]. The space exposure experiment exposed Poly-ether-ether-ketone (PEEK) films with tensile loads in LEO environment. This research is a part of the Micro-Particles Capturer and Space Environment Exposure Device (MPAC&SEED) experiment implemented by the Japan Aerospace Exploration Agency (JAXA) [5]. The space experiment started in October 2001 utilizing the ISS Russian Service Module, and finished with the final retrieval of the samples in August 2005. The ground control experiments also started in 2001 by using JAXA facilities, which exposed individual irradiation of AO, ultraviolet light (UV) and electron beam (EB) to the reference PEEK films.

The exposed samples of both experiments were analyzed focusing on the following material properties at Hokkaido University:

(1) Physical properties: Change in mass, thickness, surface morphology.

(2) Chemical properties: Change in chemical structure.

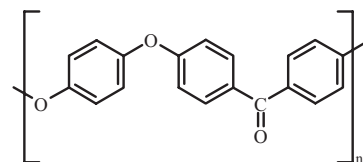
(3) Mechanical properties: Change in tensile properties.

This study mainly introduced the change in mechanical properties of PEEK films after space exposure, and investigated the influential factors on the degradation by comparing the flight and ground experiments.

### 2. Experimental procedures

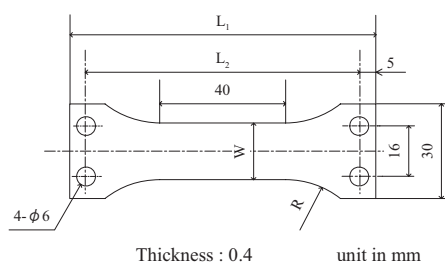
#### 2.1 Flight tests

The material used was PEEK film with 0.4mm thickness (FS-1100C, Sumitomo Bakelite Co., Ltd.). The repeating unit of PEEK is shown in Fig.1. PEEK is not a commonly used spacecraft material compared with polyimide; however, it has many attractive properties due to thermoplastic characteristics. In particular, it is expected for heat resistant films and/or matrix of composite materials because of its high formability. Besides, by comparing the degradation of PEEK with those of polyimide (thermosetting polymer), useful insights can be derived on the relation between polymer structures and changes of mechanical properties.



**Fig.1 Repeating unit of PEEK.**

Three types of specimens with different widths were machined as shown in Fig.2. The axial direction of the specimens was set to the extruded direction of the film. The specimens were loaded by a tension spring with initial setting stresses of 0, 1.6, and 4.7MPa during the experiments. These



W (mm)	R (mm)	L <sub>1</sub> (mm)	L <sub>2</sub> (mm)	Initial stress (MPa)
30	-	100	90	0
18	28	97	87	1.6
6	14	97	87	4.7

**Fig.2 Specimens of flight tests.**

values corresponded to about 0, 2 and 5% of yield strength ( $\approx 85\text{MPa}$ ).

In the space exposure experiment, the three types of specimens were installed on a same sample holder, and three sets of the sample holders were attached on the exterior of the Russian service module. Each sample holder was retrieved to the Earth after 10-months (315 days), 28-months (865 days), and 46-months (1403 days) exposures. The average values of the altitude and the velocity of the ISS were 371km and 8.1km/s, respectively.

## 2.2 Ground tests

In the ground tests, individual irradiation of AO, UV, and EB were carried out [4] by using the facilities of JAXA. The Combined Space Effects Test Facility [6] was used for AO and EB irradiation, and the UV test system (Yamashita Denso

**Table 1 Conditions of the AO, UV, and EB irradiations**

AO	AO velocity	(km/s)	8.11
	AO flux	(atoms/cm <sup>2</sup> ·s)	$1.95\sim 3.50\times 10^{15}$
	Vacuum pressure in the test chamber	(Pa)	$\approx 10^{-3}$
EB	Accelerating voltage	(kV)	200
	Vacuum pressure in the test chamber	(Pa)	$< 10^{-8}$
UV	Light intensity	(ESD/day)	10
	Wave length	(nm)	250-500
	Vacuum pressure in the test chamber	(Pa)	$< 10^{-8}$

ESD: Equivalent Solar Day =  $1.02\times 10^3 \text{ J/cm}^2$

**Table 2 Irradiance level of each irradiation**

	Irradiance level				Unit
AO	$2.79\times 10^{20}$	$1.31\times 10^{21}$	<sup>(a)</sup> $4.08\times 10^{21}$ <sup>(b)</sup> $3.97\times 10^{21}$	<sup>(a)</sup> $7.55\times 10^{21}$ <sup>(b)</sup> $7.75\times 10^{21}$	atoms/cm <sup>2</sup>
EB	—	$1.64\times 10^{12}$ (1.63)	$3.30\times 10^{12}$ (3.29)	$9.89\times 10^{12}$ (9.84)	Electrons/cm <sup>2</sup> (kGy)
UV	—	34 ( $3.47\times 10^4$ )	69 ( $7.04\times 10^4$ )	—	ESD (J/cm <sup>2</sup> )
Equivalent time in the LEO	0.1	0.5	1	3	year

Notes. (a):Stress=0MPa  
(b):Stress=1.6MPa, 4.7MPa

Corporation) was used for UV irradiation. The condition of each irradiation is shown in Table 1. The irradiation level (Table 2) was set to be equivalent with 0.1, 0.5, 1 and 3 years in LEO environment based on the calculation by the Space Environments & Effects System (SEES) [7] of JAXA.

## 2.3 Analyses methods

After the space and ground control experiments, specimens were analyzed by using mass measurements, AFM analyses, DSC analyses, EPMA analyses, and XPS analyses to investigate physical and chemical properties. The following equipments were used for the analyses.

**Mass measurement:** Mass of the specimens was measured by the electron balance (ME215P, Sartorius) at a temperature of  $23\pm 2^\circ\text{C}$  and a humidity of  $50\pm 2^\circ\text{C}$  after conditioned in the same environment for 48 hours. The repeatable precision is within  $\pm 0.015\text{mg}$ .

**AFM analysis:** Surface morphology was measured by using the atomic force microscope (SPA-400, SPI3800N, SII Nano Technology Inc.).

**DSC analysis:** Heat properties of the specimens were measured by the differential scanning calorimeter (DSC-6200, Seiko Instruments Inc.) to clarify the glass transition temperature, melting temperature, etc. Measurements were done in N<sub>2</sub> environment with a heating and cooling rate of  $10^\circ\text{C}/\text{min}$ .

**XPS analysis:** X-ray photoelectron spectroscopy was carried out to measure the chemical structure at specimen surface (ESCALAB 220i-XL, FI Surface Systems Inc.).

In addition to the physical and chemical analyses, mechanical properties were investigated by tensile tests. Specimens for tensile tests were cut into the width of 1mm from the samples by using a sharp razor blade. After conditioned at a temperature of  $23\pm 2^\circ\text{C}$  and a relative humidity of  $50\pm 5\%$ , tensile tests were conducted in the same environment with a strain rate of 0.1 /min, conforming to ASTM D882-95a.

## 3. Results of flight tests

Various changes were seen in the specimens after space exposure compared with pristine ones. In this section, main features of the flight specimens will be shown focusing on the surface appearance, thickness, and tensile properties.

### 3.1. Surface appearance

Fig. 3 shows the surfaces of the flight samples after space exposure. The color of the exposed areas clearly changed into brown. The browning became deeper with increasing exposure period; however, the amount of browning had no relation with tensile stress. In addition to the browning of the sample, specimen surfaces were slightly covered with the pale whitish matter. The detail of this feature is shown in Fig. 4. The pale whitish region was observed in about 70~80% of the exposed area regardless of applied stress and exposure period (the arrow A in Fig.4). The EPMA analyses showed that Si and O element were mainly detected; therefore, this region can result from the chemical reaction between Si-derived contamination and atomic oxygen.

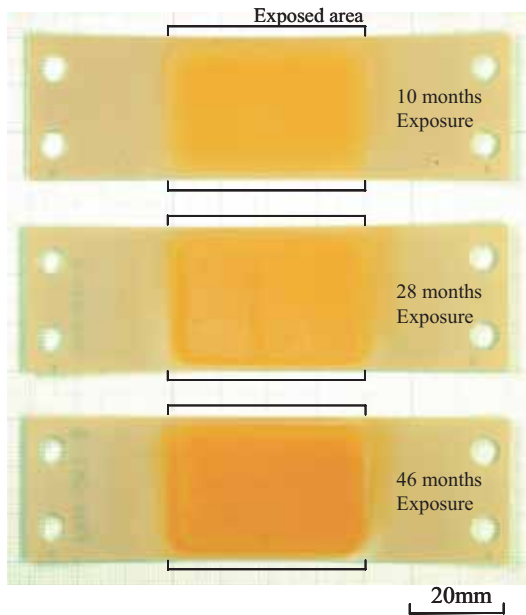


Fig.3 Surface appearances after space exposure under no tension.

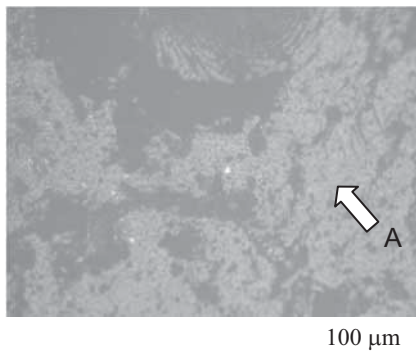


Fig.4 Magnified photograph of the 28-months flight sample under 1.5MPa. The arrow A shows the pale whitish region.

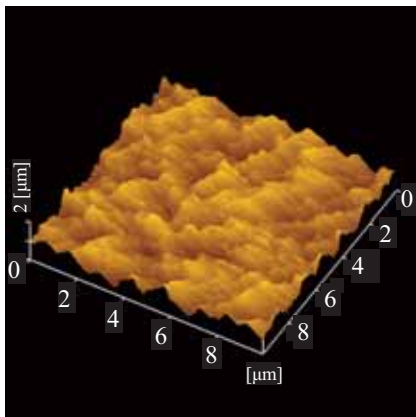


Fig.5 Surface morphology of the flight sample after 10-months exposure.

Fig. 5 shows the AFM surface topography of the sample exposed for 10 months. The exposed area was distinctively

eroded showing a cone-like pattern. This eroded feature is generally observed on the polymer surfaces attacked by AO. The maximum difference in the height of the conical pits was  $2.5 \mu\text{m}$  in the area of  $20 \mu\text{m} \times 20 \mu\text{m}$ . The amount of the roughness seemed to have no significant relation with tensile stress during exposure.

### 3.2 Thickness reduction

The mass of the specimens decreased with increasing exposure period, which resulted from thickness reduction caused by AO attack. The average thickness decrease,  $\Delta h$ , was calculated by using next equation,

$$\Delta h = \frac{\Delta m}{\rho \cdot A} \quad \dots (1)$$

where  $\Delta m$ : mass loss,  $\rho$ : density of PEEK= $1.3\text{g}/\text{cm}^3$ ,  $A$ : exposed area. Fig.6 shows the relation between  $\Delta h$  and exposure period.  $\Delta h$  increased with increasing exposure period; however, it tended to deflect from a straight line. Stresses during exposure seemed to have no significant effect on  $\Delta h$ .

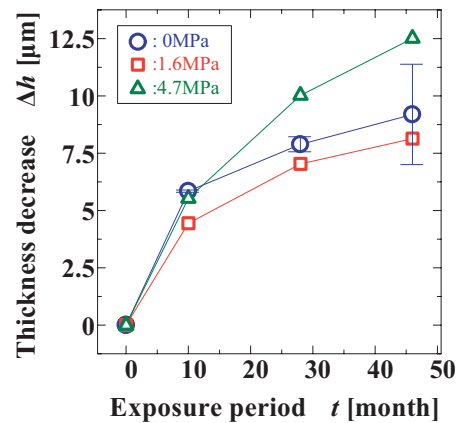


Fig.6 Thickness decrease of the flight samples.

### 3.3 Tensile properties

Fig. 7 shows the stress strain curves. For making stress-strain curves, stress was calculated by using the reduced thickness ( $h-\Delta h$ ) after exposure by subtracting thickness

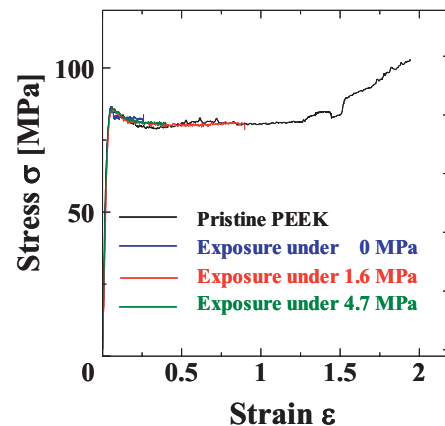


Fig.7 Stress-strain curves of the flight samples after 28-months exposure.



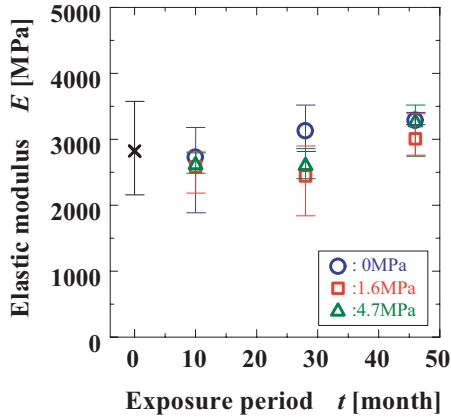


Fig.8 Relation between elastic modulus and exposure period of the flight samples.

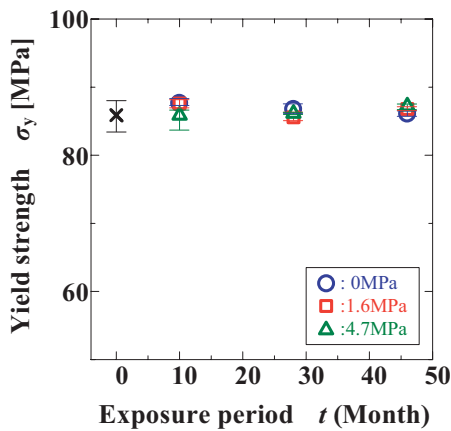


Fig.9 Relation between yield strength and exposure period of the flight samples.

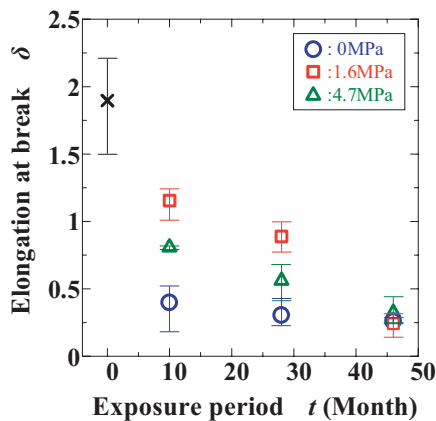


Fig.10 Relation between elongation at break and exposure period of the flight samples.

decrease  $\Delta h$  from initial thickness  $h$ . The stress strain curve of the pristine sample exhibited a clear yield point followed by a necking deformation. After the termination of the necking behavior, stress rose again and the specimen finally fractured. The strain at fracture point, elongation, was about 200 % showing large ductility of PEEK. The space exposed samples also exhibited yield point and necking deformation; however, elongation decreased compared with pristine sample.

The relation between elastic modulus and exposure period is shown in Fig.8. Although each elastic modulus had a wide distribution, the range of the flight samples was within that of the pristine ones. The space environment around the ISS had no clear effect on elastic behavior of PEEK. Fig.9 shows yield strength. Yield strengths of flight samples were almost same as the pristine one regardless of exposure period and tensile stress. Fig. 10 shows the relation between elongation and exposure period. Unlike with elastic modulus and yield strength, elongation was strongly affected by LEO environment. It decreased with increasing exposure time, and after 46 months, it dropped to about 15% of the pristine sample. The space environment clearly embrittled the specimens. As for 10- and 28-months exposures, elongations of the stressed samples were larger than those that were not stressed. However, elongations after 46-months exposure were similar regardless of stress. This suggests that a correlation between LEO environment and stress on mechanical properties are likely to exist in the early stage of exposures. Based on the results of the tensile tests, it can be said that elongation at break is the useful parameter to estimate the degradation of mechanical properties.

#### 4. Results of ground tests

Significant changes were observed in the flight samples as mentioned in the previous section. The following introduces the main results of AO, UV, and EB irradiation in the ground control experiments to clarify which factors in LEO environment caused the phenomena.

##### 4.1 Surface appearance

Fig.11 shows an example of the surface feature of AO irradiated sample in the ground tests. The cone-like morphology similar to the flight sample (Fig.5) was also observed. In contrast, there was no significant change in surface topography after UV and EB irradiations. Therefore, as anticipated, the surface erosion showing a cone-like pattern was caused by AO attack in LEO environment.

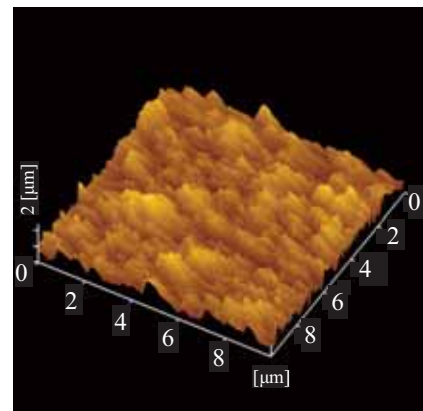


Fig.11 Surface morphology of the AO irradiated sample ( $2.79 \times 10^{20}$  atoms/cm<sup>2</sup>).

After the AO irradiation tests, maximum difference in height in the surface area ( $100 \mu\text{m} \times 100 \mu\text{m}$ ) were  $4 \mu\text{m}$ ,  $8 \mu\text{m}$ , and over  $10 \mu\text{m}$  with respect to the fluence of  $2.79 \times 10^{20}$ ,  $1.31 \times 10^{21}$ , and  $4.08 \times 10^{21}$  atoms/cm<sup>2</sup>. The surface roughness

increased with increasing AO fluence. On the other hand, the maximum difference in height of the surface of the flight sample after 10-months exposure was only 2.5  $\mu\text{m}$  (Section 3.1). This value is similar to the roughness of the sample (4 $\mu\text{m}$ ) irradiated with AO at  $2.79 \times 10^{20}$  atoms/cm<sup>2</sup>. According to the calculation by the SEES program [7],  $2.79 \times 10^{20}$  atoms/cm<sup>2</sup> was equivalent to the fluence of about 0.1 year in LEO (Table 2). Therefore, the actual fluence which the flight sample suffered from during 10 months in LEO can correspond to only 0.1 year. This discrepancy will be discussed in Section 5.

The surface color of the AO irradiated samples at  $2.79 \times 10^{20}$  atoms/cm<sup>2</sup> remained unchanged. The EB irradiated ones also showed no color change. In contrast, the UV irradiation changed the surface color into dark brown. Fig.12 shows the surface appearance after UV irradiation. The browning of the sample was clearly seen. Therefore, UV constituent in LEO can be the main reason for the surface browning of the flight samples.



Fig.12 Surface appearance of the UV irradiated sample (34ESD ( $3.47 \times 10^4$  J/cm<sup>2</sup>), under 4.7MPa).

#### 4.2 Thickness reduction

Mass change occurred only in the AO irradiated sample in the ground tests. The average thickness reduction  $\Delta h$  after AO irradiation was calculated by using Eq. (1). Fig. 13 shows the relation between  $\Delta h$  and AO fluence.  $\Delta h$  was directly proportional to the AO fluence. The tendencies in Fig.13 are very different from Fig.6, and the possible reasons for the discrepancy will be discussed in Section 5. Both UV and EB irradiation caused no significant change in mass and in thickness; therefore, the thickness decrease of the flight samples resulted from AO constituent in LEO.

The stress during irradiation had no significant effects on thickness decrease. The tendency is different from the report by Verker et al., which showed that stress during AO irradiation increased the erosion damage [8]. The reason of the discrepancy

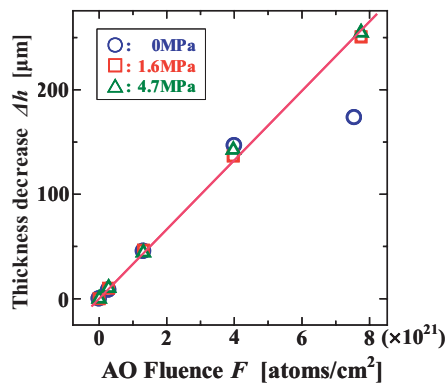


Fig.13 Relation between thickness decrease of the samples and AO fluence in the ground tests.

is still under examination; however, the very low stresses used in this study (2, 5 % of yield stress,) compared with their experiment may relate with the behavior.

#### 4.3 Tensile properties

As shown in Fig.7 and Fig.10, the elongation of the flight samples decreased after space exposure. Since the surface of the flight sample showed cone-like pattern, the concavities may relate with these phenomena due to stress concentration effects. To check this problem, stress-strain diagram of the AO irradiated samples were measured. Fig.14 shows the stress-strain curves of the samples irradiated with AO at  $2.79 \times 10^{20}$  atoms/cm<sup>2</sup>. As mentioned in Section 4.1, these samples had a similar roughness with 10-months flight samples, and are suitable for the comparison from the view point of stress concentration. From Fig. 14, stress-strain curves after AO irradiation are almost same with pristine sample regardless of tensile stress. The results suggested that the elongation at break was not affected by AO irradiation with this fluence level.

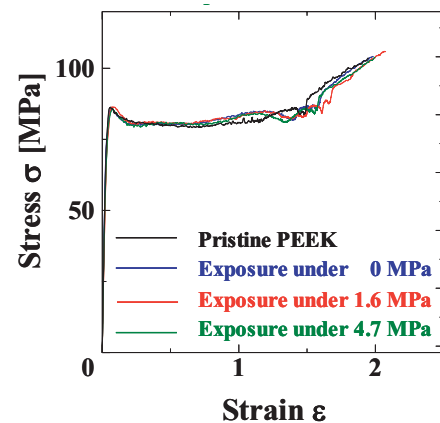


Fig.14 Stress-strain curves of the AO irradiated samples with a fluence of  $2.79 \times 10^{20}$  atoms/cm<sup>2</sup>.

In addition to AO irradiation, EB irradiation also had no effect on stress-strain curves of PEEK. Some researchers reported that EB irradiation decreased the elongation of PEEK; however, it was obtained under the high dose level over 100kGy ~100MGy [9]-[10]. The EB dose used in this research (10kGy, Table 2) was much less than these values, therefore, it

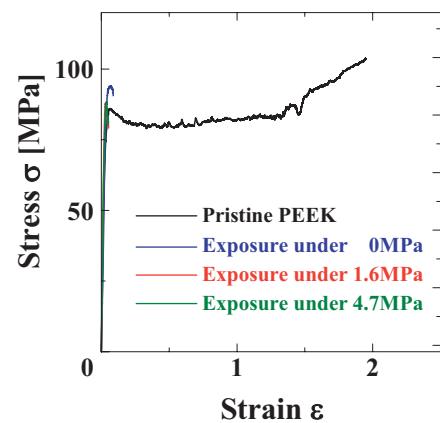
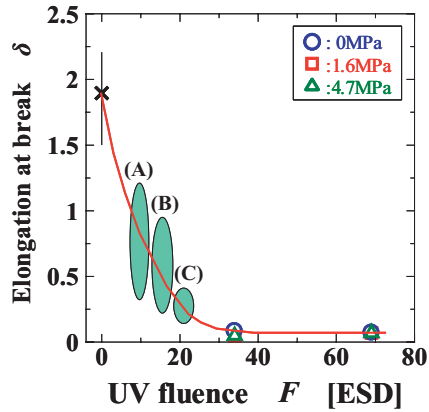


Fig.15 Stress-strain curves of the UV irradiated samples with a fluence of 34ESD ( $3.47 \times 10^4$  J/cm<sup>2</sup>).



**Fig.16** Relation between elongation at break and UV fluence. (A), (B) and (C) corresponds to the range of elongation of flight samples after 10, 28, and 46-months exposure, respectively.

was too low to affect the tensile properties of PEEK.

Different from the results of AO and EB irradiation, UV had significant effects on tensile properties. Fig.15 shows the stress-strain curves after UV irradiation with a fluence of 34ESD ( $3.47 \times 10^4 \text{ J/cm}^2$ ). The elongation at break decreased dramatically. Fig.16 shows the relation between elongation at break and UV fluence. The UV irradiation decreased the elongation to 3~5% of that of pristine sample. The reduction of the elongation seems to be already saturated at the fluence of 34ESD. Although the decrease of elongation was larger in ground UV tests (Fig.16) than in flight tests (Fig.10), the main factor which degrades mechanical properties of PEEK can be attributable to the UV constituent in LEO.

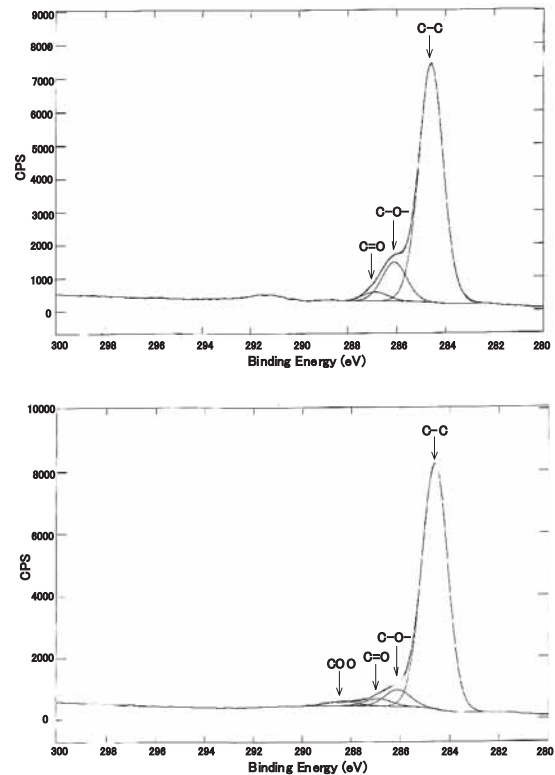
## 5. Discussion

### 5.1 The mechanism of degradation of PEEK induced by UV constituent in LEO environment

Based on the comparison between flight tests and ground tests of PEEK films, the harshest factor in LEO affecting the tensile properties was considered UV. It caused the embrittlement of the material as shown in Fig.10 and Fig.16. To investigate the reason, the XPS analysis of the UV irradiated sample in the ground tests [11] was shown in Fig.17. A new chemical structure of O=C-O was generated as well as the reduction of the C-O and C=O bonding after UV irradiation. This result suggested that both scissions and crosslinking of polymer chains occurred. The results of DSC analyses were given in Table 3. Glass transition temperature ( $T_g$ ) increased while heat of crystallization  $\Delta H_c$ , melting temperature  $T_m$ , and heat of melting  $\Delta H_m$  decreased after UV irradiation. These data corresponds to the result of XPS analyses (Fig.17). In particular, both the increase of  $T_g$  and the decrease of  $\Delta H_c$  indicated the formation of crosslinking [12]-[13]. Crosslinking generally results in the embrittlement of polymer materials [12]; therefore, the changes in mechanical properties of the flight samples were mainly caused by this mechanism.

As for the 10-months and 28-months exposures in space, elongations of the stressed samples were larger than those that were not stressed. The detail mechanism of the phenomenon is

still unclear; however, the similar tendencies were reported in the mechanical properties of polypropylene exposed with UV [14]. In the literature, tensile stress during UV exposure tended to reduce the decrease of elongation, especially in the early stage of UV irradiation. This suggests that tensile stress has the possibility to prevent the crosslinking during UV irradiation. However, when the fluence of UV increases, the ability to cause crosslinking can be much larger. As a result, the effect of tensile stress to prevent the decrease of elongation might diminish as shown in the 46-month exposed samples.



**Fig.17** XPS analyses before and after UV irradiation.

**Table 3** Heat properties before and after UV irradiation measured by DSC (34ESD, under no tension).

	$T_g$ (°C)	$\Delta H_c$ (J/g)	$T_m$ (°C)	$\Delta H_m$ (J/g)
Pristine	142.3	14.5	340.5	45.3
After UV irradiation	153.1	6.08	333.7	33.8

### 5.2 The discrepancies between the degradation of flight samples and those of reference samples in the ground tests

Comparison between flight and ground tests clarified that AO in LEO environment caused surface erosion and thickness decrease, and that UV induced the degradation of mechanical properties. However, there are several discrepancies between flight and ground samples quantitatively. As for thickness decrease  $\Delta h$ , the tendencies were different between the flight (Fig.6) and the ground tests (Fig.13). In the flight tests,  $\Delta h$  tended to deflect from a straight line with increasing exposure period; however,  $\Delta h$  was proportional to AO fluence in the ground tests. In addition,  $\Delta h$  in flight samples without tension were only 5.9 $\mu\text{m}$ , 7.9 $\mu\text{m}$ , and 9.2 $\mu\text{m}$  with respect to 10, 28, and

46-months exposures. In contrast,  $\Delta h$  of AO irradiation with a fluence of  $7.6\sim 7.8\times 10^{21}$  atoms/cm<sup>2</sup>, which corresponded to 3 years in ISS orbit (Table 2), was about 250 $\mu$ m. To investigate the discrepancies, the actual AO fluence of the flight samples were estimated by using both  $\Delta h$  of flight tests (Fig.6) and the results of AO irradiation tests (Fig.13). Then,  $1.8\times 10^{20}$ ,  $2.4\times 10^{20}$ , and  $2.8\times 10^{20}$  atoms/cm<sup>2</sup> were obtained with 10, 28, 46-months flight, respectively. These values are much smaller than the AO fluence calculated by SEES program [7] of JAXA (Table 2). In addition, the roughness of the flight samples (Fig.5) was similar to that of AO irradiated sample with a fluence of  $2.79\times 10^{20}$  atoms/cm<sup>2</sup> (Fig.11). From these results, the actual fluence of the flight samples can be about  $2\sim 3\times 10^{20}$  atoms/cm<sup>2</sup>. These values correspond to the AO fluence of about 1month in LEO environment.

As for tensile properties, the elongations at break after UV irradiation over 34ESD (Fig.16) were smaller than those of flight samples (Fig.10). To compare the difference, the range of elongation of flight samples were replotted as (A)~(C) on the curve in Fig. 16. As a result, the actual UV fluences of flight samples were estimated to be less than 20ESD. These values correspond to only about 2~3.5 months in LEO environment (Table 2).

Based on the above discussion, it can be said that the actual fluence of AO and UV which flight samples suffered from in LEO was much smaller than the value estimated by SEES program. The following two were possible reasons for the discrepancy. One was the attitude change of the ISS during the flight and the other was the attachment of SiO<sub>x</sub> contamination on the sample. The ISS had been under construction during the space experiment; therefore, the actual time, for which the normal of the sample surface coincided with the ISS traveling direction, was not always proportional to the exposure period. Besides, EPMA analyses confirmed that sample surfaces were covered by SiO<sub>x</sub> layer. This contamination has the ability to prevent the AO attack. In addition, SiO<sub>x</sub> has very low light transmission [15]. Therefore, the contamination composed of SiO<sub>x</sub> has the possibility to reduce the effect of AO and UV on the flight samples.

## 6. Conclusion

To clarify the effects of LEO environment on mechanical properties of polymers, exposure experiments were conducted utilizing the International Space Station Russian Service Module. Poly-ether-ether-ketone (PEEK) films under tensile stresses were exposed to LEO, and reference samples were irradiated with AO, EB, and UV by using ground facilities of JAXA. Comparing the results of flight and ground tests, degradation behaviors of the samples and those influential factors were investigated. The main results obtained in this study were summarized as follows:

- (1) The surface color of the flight samples changed into dark brown, and the browning became deeper with increasing exposure period. The similar phenomenon was not seen in AO and EB irradiations but in UV irradiation of ground tests. UV constituent in LEO environment can be the main reason of the browning of the sample surface.
- (2) The thickness of the flight samples decreased with showing

a surface morphology of cone-like pattern. These phenomena were only observed in AO irradiation of ground tests; therefore, it can result from AO in LEO environment.

- (3) Elastic modulus and yield strength of the flight samples remained unchanged; however, the elongation at break decreased to about 15% of pristine sample after 46-months exposure. The UV irradiations in the ground tests only showed similar tendencies. XPS and DSC analyses suggested that crosslinking induced by UV in LEO was the main factor for the change of elongation.
- (4) As for 10-months and 28-months exposures, the decrease of elongation of stressed samples was smaller than that of unstressed samples; however, the phenomena diminished after 46-months exposures. This indicated that tensile stress had a tendency to prevent the embrittlement in the early stage of exposure.
- (5) Based on the ground tests, it was clarified that EB constituent in the ISS orbit hardly influenced the tensile properties.
- (6) The amount of degradation of the flight samples was much smaller than estimated by using SEES program. The attitude change of the ISS during flight and the formation of contaminated layer of SiO<sub>x</sub> were presented for the reason.

## Acknowledgement

The authors express sincere appreciation to all the members of the Space Materials Section, Advanced Materials Group of JAXA for their devoted support on this study.

## References

- [1] R.C. Tennyson: Atomic Oxygen Effects on Polymer-Based Materials, *Can. J. Phys.*, Vol.69, (1991), pp.1190-1208.
- [2] Kim, K. de Groh, Bruce A. Banks: MISSE Peace Polymers: An International Space Station Environmental Exposure Experiment, *AIAA-2001-4923*, *NASA/TM-2001-211311*, (2001).
- [3] J.B. Whiteside, D. Giangano, R.L. Heuer, E. Kamykowski, M. Kesselman, W.D. Rooney, R. Schulte, and M. Stauber: Effects of the Space Environment on Space-Based Radar Phased-Array Antenna; Status and Preliminary Observations (LEDF Experiment A0133), *Proceedings of LDEF-69 Months in Space First Post-Retrieval Symposium*, (1991), pp.1227-1240.
- [4] T. Nakamura, H. Nakamura, O. Fujita, T. Noguchi, and K. Imagawa: The Space Exposure Experiment of PEEK Sheets under Tensile Stress, *JSME International Journal, Ser.A*, Vol.47, No.3, (2004), pp.365-370.
- [5] F. Imai, and K. Imagawa: NASDA's Space Environment Exposure Experiment on ISS - First Retrieval of SM/MPAC&SEED-, *Proceedings of the 9th International Symposium on "Materials in a Space Environment"*, (2003), pp.589-594.
- [6] JAXA Homepage, [http://www.ard.jaxa.jp/info/facility/capacity/vacuum/vacuum\\_d\\_j.html](http://www.ard.jaxa.jp/info/facility/capacity/vacuum/vacuum_d_j.html)
- [7] JAXA Homepage, [http://seesproxy.tksc.jaxa.jp/fw\\_e/dfw/SEES/English/index2.html](http://seesproxy.tksc.jaxa.jp/fw_e/dfw/SEES/English/index2.html).
- [8] R. Verker, E. Grossman, I. Gouzman, and N. Eliaz: Residual Stress Effect on Degradation of Polyimide under Simulated



- Hypervelocity Space Debris and Atomic Oxygen, *Polymer*, Vol.48, (2007), pp.19-24.
- [9] J.G. Funk, and G.F.Jr. Sykes: Space Radiation Effects on Poly [Aryl-Ether-Ketone] Thin Films and Composites, *SAMPE quarterly*, Vol.19, No.3, (1988), pp.19-26.
- [10] M. Oyabu, Y. Kobayashi, T. Seguchi, T. Sasuga, and H. Kudoh: Analysis of Electron-Irradiated Poly-Ether Ether Ketone by X-ray Photoelectron Spectroscopy, *Bunseki Kagaku*, Vol.44, No.3, (1995), pp.195-201, in Japanese.
- [11] H. Nakamura, T. Nakamura, T. Noguchi, and K. Imagawa, and T. Inoue: Photodegradation of PEEK Sheets under Tensile Stress, *Polymer Degradation and Stability*, Vol.91, (2006), pp. 740-746.
- [12] B. Claude, L. Gonon, J. Duchet, V. Verney, and J.L. Gardette: Surface Cross-linking of Polycarbonate under Irradiation at Long Wavelengths, *Polymer Degradation and Stability*, Vol.83, (2004), pp. 237-240.
- [13] A.S. Vaughan, G.C. Stevens: Irradiation and the Glass Transition in PEEK, *Polymer*, Vol.42, (2001), pp. 8891-8895.
- [14] Li. Tong, and J.R. White: Photo-oxidation of Thermoplastics in Bending and in Uniaxial Compression, *Polymer Degradation and Stability*, Vol.53, (1996), pp. 381-396.
- [15] E. Grossman, and I. Gouzman: Space Environment Effects on Polymers in Low Earth Orbit, *Nucl Instr and Meth B* Vol.208, (2003), pp. 48-57.
- Publication list related SM/MPAC&SEED**
- [1] T. Nakamura, O. Fujita, T. Noguchi, and H. Nakamura: Space Exposure Experiment of PEEK Sheets Under a Tensile Load Utilizing an International Space Station, *Proceedings of the First Taiwan-Japan Workshop on Mechanical and Aerospace Engineering*, Vol.1, (2001), pp.107-113.
- [2] T. Nakamura, O. Fujita, H. Nakamura, and T. Noguchi: AO Irradiation Damage on PEEK Sheet under Tensile Loads, *Proceedings of the 18th Space Station Conference*, (2002), pp.57-58, in Japanese.
- [3] H. Nakamura, T. Nakamura, T. Noguchi, O. Fujita, K. Imagawa, and Y. Tachi: Atomic Oxygen Irradiation on PEEK Sheet under Tensile Loads, *Proceedings of the 42th Conference of JSME Hokkaido Branch*, No.022-1, (2002), pp.122-123, in Japanese.
- [4] M. Sawaya, T. Nakamura, T. Noguchi, O. Fujita, K. Imagawa, and Y. Tachi: Electron Beam Irradiation on PEEK Sheet under Tensile Loads, *Proceedings of the 42th Conference of JSME Hokkaido Branch*, No.022-1, (2002), pp.124-125, in Japanese.
- [5] T. Nakamura, H. Nakamura, O. Fujita, T. Noguchi, and K. Imagawa: The Degradation of PEEK Sheets Accelerated by Stress in a Real Space Environment Based on the Space Exposure Experiment, *Proceedings of the International Conference on Advanced Technology in Experimental Mechanics*, CD-ROM, (2003).
- [6] T. Nakamura, H. Nakamura, O. Fujita, T. Noguchi, and K. Imagawa: The Space Exposure Experiment of PEEK Sheet under Tensile Loads, *Proceedings of the 52th Annual Meeting of the Society of Materials Science, Japan*, (2003), pp.143-144, in Japanese.
- [7] T. Nakamura, H. Nakamura, T. Noguchi, K. Imagawa, H. Takebayashi, T. Tojo, K. Mori, and H. Sasaki: Resistance Properties of Direct-Fluorinated-PEEK Sheets to the Space Environment, *Proceedings of the Mechanical Engineering Congress, 2003 Japan*, No.03-1, Vol.1, (2003), pp.115-116, in Japanese.
- [8] T. Nakamura, H. Nakamura, T. Noguchi, O. Fujita, and K. Imagawa: The Space Exposure Experiment of PEEK Sheets Utilizing the International Space Station, *Proceedings of the Joint Symposium of the University of Alberta and the Hokkaido University, "Mechanics of New Materials"*, (2003), pp.17-18.
- [9] T. Nakamura, H. Nakamura, O. Fujita, T. Noguchi, and K. Imagawa, T. Inoue: Damage Properties of PEEK Films Irradiated by Atomic Oxygen, *Key Engineering Materials*, Vols. 261-263, (2004), pp.1617-1622.
- [10] T. Nakamura, H. Nakamura, O. Fujita, K. Imagawa, T. Noguchi, and T. Inoue: The Space Exposure Experiment of Tension Loaded PEEK Sheets Utilizing the International Space Station, *Proceedings of the 24th International Symposium on Space Technology and Science (Selected Papers)*, (2004), pp.756-759.
- [11] T. Nakamura, H. Nakamura, O. Fujita, T. Noguchi, and K. Imagawa: The Space Exposure Experiment of PEEK Sheets Under Tensile Stress, *JSME International Journal, Ser.A.*, Vol.47, No.3, (2004), pp 365-370.
- [12] T. Nakamura, H. Nakamura, O. Fujita, K. Imagawa, and T. Inoue: Strength Properties of PEEK Sheet Exposed in the Low Earth Orbit, *Proceedings of the Mechanical Engineering Congress, 2005 Japan*, No.05-1, Vol.5, (2005), pp.451-452, in Japanese.
- [13] H. Nakamura, T. Nakamura, T. Noguchi, O. Fujita, K. Imagawa, and T. Inoue: Mechanical Properties of PEEK Films Irradiated by Atomic Oxygen, *Transactions of the JSME, Ser.A.*, Vol.71, No.710, (2005), pp 1327-1332, in Japanese.
- [14] H. Nakamura, T. Nakamura, T. Noguchi, and K. Imagawa, and T. Inoue: Photodegradation of PEEK Sheets under Tensile Stress, *Polymer Degradation and Stability*, Vol.91, (2006), pp 740-746.
- [15] K. Mori, H. Shimamura, T. Nakamura, and M. Suzuki: Evaluation of Space Materials by Space Environment Exposure Device, *Aeronautical and Space Sciences Japan*, Vol.54, No.633, (2006), pp.298-305.
- [16] T. Nakamura, H. Nakamura, and H. Shimamura: Effects of LEO Environment on Tensile Properties of PEEK Films, *ICPMSE-9*, (2008), to be published.

## EFFECTS OF LEO ENVIRONMENT ON MECHANICAL PROPERTIES OF POLYIMIDE FILMS UNDER TENSILE STRESS

Hiroyuki SHIMAMURA<sup>1</sup>

<sup>1</sup> *Institute of Aerospace Technology, Japan Aerospace Exploration Agency,  
Tsukuba, Ibaraki 305-8505, Japan*

Mechanical properties of polyimide films after exposure to a low earth orbit (LEO) environment were investigated using tensile tests. Polyimide films were placed in a tensile stress state during space exposure to evaluate the effects of tensile stress state on degradation of mechanical properties. Atomic oxygen (AO), ultraviolet (UV), and electron beam (EB) irradiation tests were also conducted for polyimide films to enable comparison to the degradation behavior of the flight samples. Results show that the tensile strength and elongation were decreased by space exposure. The reduction of the mechanical properties became marked as the exposure period increased. The AO irradiation was considered to be the main degrading factor; both UV and EB had only slight effects on the mechanical properties. The tensile strength and elongation of the AO irradiated samples decreased with increased AO fluence. Moreover, the surface roughness of the AO irradiated samples developed dependently on the increased AO fluence. Consequently, surface roughness is one of the leading causes of degradation of mechanical properties. Excessive stress might concentrate at a concave region on the rough surface, leading to formation of surface cracks and initiation points of destruction. No obvious difference attributable to the tensile stress state (below 7 MPa) was apparent in the degradation of mechanical properties.

**Keywords:** MPAC&SEED, Polyimide film, Mechanical property, Atomic oxygen, Surface roughness

### 1. Introduction

Space environmental factors such as orbital thermal cycling, high-energy ultraviolet (UV) and various types of radiation (protons, electrons, and X-rays) can strongly impact the performance of polymer materials used on spacecrafts. Thermal cycling accumulates heat strain in polymer materials, causing geometric variation, delamination, and cracks. Generally, a polymer material irradiated by UV or radiation changes its chemical construction with decompositions and cross-links of polymer bonds. The chemical construction change engenders brittleness and discoloration. In a low earth orbit (LEO), polymer materials exposed to a space environment are also degraded by atomic oxygen (AO). When a polymer material collides with AO at high velocity of about 8 km/s, its surface is deeply eroded by oxidative decomposition and a gasification reaction [1]. Then the polymer material thins and exhibits a rough texture, changing the optical reflectance of the material from specular to diffuse. The surface texture change increases the solar absorptance, which is an important parameter for a spacecraft's thermal control. Additionally, the surface texture can cause crack initiation and tearing of thin polymer films [2].

Among polymer materials, polyimide has considerable resistance to high temperatures and can function well in large operating temperature ranges; it also has a large tolerance against intense UV and radiation. For those reasons, polyimide has been applied predominantly to thermal control films such as the outermost layer film of multilayer insulation (MLI). The thermal control films are attached where they are exposed to a space environment. For thermal control applications, it is important to evaluate the degradation of thermo-optical properties by space exposure. Space exposure experiments and

ground simulations for investigation of thermo-optical properties degradation have collected many data and have facilitated estimation of the degree of degradation in some orbits [3–5].

Polyimide has also been applied as a base film of deployable structures of spacecraft, such as large flexible solar arrays, large deployable antenna and solar sails, because of its high specific strength and rigidity, high dimensional accuracy, and low rate of thermal expansion [6–9]. Base films are used under tensile stress states to maintain their structural shapes at low gravity when deployable structures are fully expanded [10]. The initial tensile stress state is expected to be altered by orbital thermal cycling. For application as a structural material, it is indispensable to evaluate the space environmental effects on mechanical properties. The impacts of tensile stress states should also be understood if they hasten degradation of mechanical properties in a space environment.

Mechanical properties of polyimide films exposed to space environments have been studied in the Long Duration Exposure Facility (LDEF) experiment and the Materials International Space Station Experiment (MISSE) [11, 12]. Results of these experiments indicated that space exposure can degrade the mechanical properties of polyimide films. However, these experiments include large variations in their results. Another problem is that the sample number is insufficient to support statistical significance. Further study is needed to confirm which space environmental factors impart serious damage to mechanical properties, the extent to which degradation proceeds, and whether or not the tensile stress state affects the degradation.

In this study, polyimide films under a tensile stress state were exposed to a space environment with the Micro-Particles

Capturer and Space Environment Exposure Device on the International Space Station Russian Service Module (SM/MPAC&SEED); the polyimide films were included in the SM/SEED experiment samples. The overview of the experiment is described in [13]. Polyimide films were also irradiated by AO, UV, and electron beams (EB) in ground reference tests. After the space exposure and the ground reference tests, tensile tests of samples were conducted to evaluate changes of mechanical properties.

This paper reports the tensile test results of polyimide films after space exposure and each irradiation test. Then, the main space environmental factor affecting the mechanical properties of polyimide films are investigated through comparison of the sample's degradation behavior. Degradation mechanism of mechanical properties and effects of tensile stress state on the degradation are also discussed.

## 2. Experimental Procedures

### 2.1 Material

The tested polyimide films were 125- $\mu\text{m}$ -thick UPILEX-S (UBE Industries Ltd.); UPILEX-S has been applied as a base film for the flexible solar array of the Space Flyer Unit (SFU) and the Advanced Earth Observing Satellite-I and II (ADEOS-I and II).

The sample dimensions are presented in Fig. 1. The sample has a dog-bone-shape which resembles the "Type IV" specimen of American Society for Testing and Materials (ASTM) Standard D-638-03 [14], punched out from a sheet using a die. For polymer sheet production, sheets are drawn to the rolling direction and polymer chains are aligned in the same direction. Then, tensile strength and elongation depend on the drawing direction. Therefore, the longitudinal direction of all samples was arranged to the drawing direction to prevent the influence of anisotropy.

As described above, a polymer material is eroded by AO attacks and thins with increased exposure. Before the beginning of the SM/SEED experiment, the sample erosion depth during the experimental duration of approximately 3 years was estimated at about 250  $\mu\text{m}$  from the total AO fluence, which was calculated by the Space Environments and Effects System (SEES) simulation. For the 125- $\mu\text{m}$ -thick polyimide film, a single layer is completely eroded away during the experiment. Additionally, the retrieval date can be delayed; then the samples are exposed to LEO environment much longer than the planned duration. Therefore, the flight samples consisted of four stacked layers to survive the SM/SEED experiment; total thickness of the stacked layers was 500  $\mu\text{m}$ . The samples for ground reference tests have same configuration as the flight samples.

### 2.2 Tensile stress states

During the SM/SEED experiment and the ground reference tests, the samples were mounted on a tension-loading mechanism. Figures 2 and 3 show post-flight photographs of the tension-loading mechanism used in the SM/SEED experiment and a cross-sectional schematic view of the mechanism, respectively. The mechanism can apply unidirectional tensile stress to samples by pulling one end of the sample using a spring. The tensile stress applied to the samples was set to 0 MPa, 1.4

MPa, and 7.0 MPa by adjusting the spring elongation. The tensile stress level of 1.4 MPa was based on the nominal stress of the base films of the ADEOS-I solar paddles; 7.0 MPa was set five times as large as 1.4 MPa.

### 2.3 SM/SEED experiment

The SM/SEED experiment has three periods of exposure to a LEO environment: 315 days, 865 days, and 1403 days [13]. The first, second and third retrieval samples are designated as Flight #1, Flight #2, and Flight #3 in this paper, respectively.

The polyimide films mounted on a tension-loading mechanism were set in the RAM side of the SM/MPAC&SEED unit, as presented in Fig. 4. The number of the flight samples was two for each tensile stress state.

The estimated environmental conditions for the flight samples on the RAM side are shown in Table 1. The AO and UV fluence and the total ionizing dose for the flight samples resulted from the evaluations of monitoring samples, which were mounted on the SM/SEED experiment, and SEES simulations [15].

**Table 1 Environmental conditions for the flight samples [15]**

		Flight #1	Flight #2	Flight #3
Exposure duration, days		315	865	1403
AO fluence, atoms/cm <sup>2</sup>	Vespel	$2.04 \times 10^{20}$	$2.57 \times 10^{20}$	$2.70 \times 10^{20}$
	SEES	$2.85 \times 10^{21}$	$5.70 \times 10^{21}$	$8.41 \times 10^{21}$
UV fluence, ESD*	Polyurethane	18.1	15.8	13.4
	SEES	73.8	167	271
Total ionizing dose**, Gy	Alanine dosimeter	1.95	15.3	32.0
	SEES	67.6	181	234
Maximum temperature***, °C		60	90	90

\* Equivalent Solar Day, 1 ESD =  $1.02 \times 10^7$  J/m<sup>2</sup>

\*\* Shield thickness; 0.04 g/cm<sup>2</sup>

\*\*\* Temperature at approximately 1 mm depth

### 2.4 Ground reference irradiation tests

In ground reference tests, the samples were irradiated by AO, UV, and EB. Respective irradiation test conditions are presented in Tables 2, 3, and 4.

The AO irradiation testing was performed using the "Combined Space Effects Test Facility" of JAXA Tsukuba Space Center [16]. This facility has a laser detonation AO beam source. The AO velocity was controlled to approximately 8 km/s to simulate the LEO environment; the translational energy was 5 eV at the velocity. Kapton H (DuPont) films were adopted as AO monitoring sample with a well-known erosion yield of  $3.0 \times 10^{-24}$  cm<sup>3</sup>/atom [17]. The AO fluence was estimated from the mass loss of Kapton H after AO irradiation tests using the following equation.

$$F = \frac{\Delta m_K}{A_K \rho_K E_K} \quad (1)$$

where

- $F$  = total AO fluence  
 $\Delta m_K$  = mass loss of Kapton H  
 $A_K$  = exposure area of Kapton H  
 $\rho_K$  = density of Kapton H  
 $E_K$  = erosion yield of Kapton H,  $3.0 \times 10^{-24}$  cm<sup>3</sup>/atom [17]

A high-vacuum chamber equipped with a Xe lamp was used for UV irradiation tests. The UV flux and fluence levels at a wavelength of 200–400 nm were measured using a multispectral radiometer. The Xe lamp light includes an infrared wavelength region. Then samples are expected to be heated during UV irradiation. Therefore, the backsides of the samples were cooled by water flow to prevent sample heating. The temperature of the sample surfaces was monitored using thermocouples.

The Combined Space Effects Test Facility was also used for EB irradiation tests. The accelerating voltage and the electron current for the irradiation tests were set at 200 kV and 2.0 mA, respectively. The total doses for samples were monitored by cellulose triacetate (CTA) films mounted with irradiated samples.

**Table 2 AO irradiation test conditions**

AO flux, atoms/cm <sup>2</sup> ·s	$1.0\text{--}5.0 \times 10^{15}$
AO fluence, atoms/cm <sup>2</sup>	$0.3 \times 10^{21}$ $1.3 \times 10^{21}$ $4.1 \times 10^{21}$
AO velocity, km/s	8.0
Vacuum, Pa	$10^2\text{--}10^3$

**Table 3 UV irradiation test conditions**

UV flux, ESD*/day	10
UV fluence, ESD*	20 35 69
Sample surface temperature, °C	10–30
Vacuum, Pa	$10^4\text{--}10^5$

\* Equivalent Solar Day, 1 ESD =  $1.02 \times 10^7$  J/m<sup>2</sup>

**Table 4 EB irradiation test conditions**

EB dose, kGy	1.6 (26)
(Irradiation time, s)	3.3 (53)
Vacuum, Pa	$10^4\text{--}10^5$

## 2.5 Calculation of thickness change

Thickness changes of each sample were calculated using the following equation from the mass loss after space exposure or ground reference tests:

$$\Delta t_S = \frac{\Delta m_S}{A_S \rho_S}, \quad (2)$$

where

- $\Delta t_S$  = thickness loss of samples  
 $\Delta m_S$  = mass loss of samples  
 $A_S$  = exposure area of samples  
 $\rho_S$  = density of samples  
 (UPILEX-S: 1.47 g/cm<sup>3</sup> [18])

## 2.6 Tensile tests

Mechanical properties of samples were evaluated by tensile testing using Autograph AG-5kNI (Shimadzu Corp.) and Instron 5565 (Instron Corp.). Four-layer stacked samples were used for tensile tests. Grip sections of the samples were mutually bonded using an adhesive to prevent interlayer slippage during tensile tests. Before testing, tensile tests results for stacked samples were compared to that for one-layer samples in order to confirm that tensile tests using stacked samples can properly evaluate tensile characteristics of samples. In consequence, no difference was apparent between stress-strain curves of four-layer stacked samples and those of one-layer samples.

Tensile tests were conducted according to ASTM D-638-03 [14], at room temperature and 50±5% relative humidity under a constant strain rate of 50 mm/min. The strain was obtained based on the crosshead travel distance. The tensile strength and elongation were determined as the maximum stress and the strain at the first failure of four-layer stacked films, respectively. For the calculation of tensile strength, the thickness loss defined by Eq. (2) was considered.

## 3. Results and Discussion

The thickness loss of flight samples is expected to become larger with increased exposure duration. There is, however, no remarkable difference of the thickness loss among flight samples, as presented in Fig. 5. In addition, the thickness loss of Flight #3 was about 8 μm, a much lower than expected value, which is approximately 250 μm for three years of space exposure. In ground reference tests, only AO irradiation decreased the sample thickness; there was almost no variation in the mass of UV and EB irradiated samples. The thickness loss of AO irradiated samples increased in direct relation to AO fluence in Fig. 6. No considerable change attributable to tensile stress state was found in either the flight or AO-irradiated samples.

Tensile strength and elongation changes of the flight samples for exposure duration are portrayed in Fig. 7. The tensile strength of the flight samples had decreased slightly from the value of control samples. A major reduction in elongation was detected, showing 70% loss compared to the control samples at a maximum. Samples of Flights #2 and #3 showed more serious degradation than Flight #1 in both tensile strength and elongation.

The AO irradiated samples deteriorated considerably with increasing AO fluence, as portrayed in Fig. 8. The samples at AO fluence of  $4.1 \times 10^{21}$  atoms/cm<sup>2</sup> showed a large reduction of 40% in tensile strength and a reduction of 80% in elongation compared to the control samples, which indicated considerable degradation as a polymer material. Both tensile strength and elongation at AO fluence of  $0.3 \times 10^{21}$  atoms/cm<sup>2</sup> are within the deviation of control samples. According to this result, AO irradiation cannot affect mechanical properties of polyimide films at low fluence.

As shown in Fig. 9, minor changes of tensile strength and elongation occurred in UV irradiated samples. Because polyimides have a high absorption in the UV region, UV irradiation causes extensive surface degradation, leaving the inside intact [19]. Therefore, it is conceivable that UV irradiation imparted no considerable deleterious effect on



mechanical properties of polyimide films.

In addition, EB irradiation little affected tensile strength and elongation of polyimide films, as shown in Fig. 10. Generally, polyimide has a high concentration of imide rings in the main chain, rendering it resistant to EB irradiation because of pi-electron conjugation. The EB dose level, by which the elongation of UPILEX-S declines to 50% of its initial value, is approximately 30 MGy [20]. The dose levels in present EB irradiation tests, 1.6 kGy and 3.3 kGy, are extremely small compared to 30 MGy. Therefore, noticeable degradation of mechanical properties by EB irradiation was not detected at these EB dose levels.

For the flight and ground reference samples, there was no marked difference depending on the tensile stress state in tensile strength and elongation. This result means that a tensile stress state of less than 7.0 MPa has no impact on polyimide films' degradation of mechanical properties. The tensile stress of 7.0 MPa is only a few percent of the yield stress of control samples. It is conceivable that the tensile stress states used for this study are too weak to degrade samples. Further experiments using higher stress are needed to clarify the effects of tensile stress state on the degradation of mechanical properties of polyimide films. This result, however, demonstrated that the practical tensile stress states for spacecrafts contribute no degradation of the mechanical properties.

Ground reference tests showed considerable degradation of mechanical properties of polyimide films only in AO-irradiated samples. Consequently, AO irradiation is considered to be the main degrading factor for mechanical properties. In addition, according to the fact that the degradation became noteworthy only with the AO fluence increase, as presented in Fig. 8, it can be argued that mechanical properties of polyimide films degrade with increased space exposure duration, but that the tensile strength and elongation of Flight #3 are nearly equal to those of Flight #2, as shown in Fig. 7.

The degradation behavior of flight samples for AO fluence is compared to that of the AO irradiated samples in Fig. 11, which shows the tensile strength and elongation for the samples under a no-tensile-stress state. Flight samples were plotted for two kinds of AO fluence: one is determined by the analysis of the AO monitoring sample on the SM/SEED experiment; the other is estimated by the simulation using SEES [15]. An enormous discrepancy pertains between these two kinds of AO fluence. The tensile strength and elongation of flight samples were decreased as the AO fluence increases, denoting the same tendency of the AO irradiated samples. However, it is difficult to interpret the consistency of the degree of degradation between the flight samples and the AO irradiated samples because of the large discrepancy of the flight samples' AO fluence.

The flight sample surfaces that had been exposed to the space environment were observed using SEM, as presented in Fig. 12. The samples were tilted 45 degrees to facilitate viewing of the surface topography. All flight sample surfaces showed a rough texture, which is typical for an AO-irradiated polyimide [1]. No obvious differences between Flight #1, #2, and #3 were detected in surface texture, even though these flight samples had different exposure durations. Some contamination was visible on all flight samples' surfaces.

The other samples on SM/SEED were also contaminated by outgassing from organic materials used in the ISS; the main components of contamination were found to be SiO<sub>x</sub> [21, 22]. The SiO<sub>x</sub> contamination layer on the flight sample surface can serve as the anti-AO coating; the flight samples were prevented from AO erosion because of the contamination layer. As described above, the thickness losses of each flight sample were far below the expected value. Moreover, thickness loss and surface texture of flight samples were approximately equivalent, irrespective of the space exposure duration. These phenomena stem from the SiO<sub>x</sub> contamination layer.

The contamination thickness for Flight #3 was estimated as about 120 nm [21], which is quite small compared to the amount of thickness loss for the flight samples. Consequently, the mass increase by contamination attachment is sufficiently smaller than the mass loss by AO erosion. Therefore, the influence of contamination attachment is negligible in the thickness loss calculation using Eq. (2).

The surface topography of AO irradiated samples was also evaluated with SEM observation at a 45-degree tilt, as presented in Fig. 13. The sample surfaces were deeply eroded by AO irradiation, exhibiting a rough texture. The surface roughness of the AO irradiated sample,  $1.3 \times 10^{21}$  atoms/cm<sup>2</sup>, was remarkable compared to that of the AO irradiated sample,  $0.3 \times 10^{21}$  atoms/cm<sup>2</sup>. This result indicates that surface roughness develops as AO fluence increases. The relation between the roughness of the AO irradiated surface and AO fluence has been investigated through surface observations using SEM or AFM, or Monte Carlo computational modeling [23–25]. Our current results are consistent with past investigation results.

Results of SEM observation revealed that the amount of surface roughness increases concomitant with the AO fluence. In addition, the degradation of tensile strength and elongation of samples was enhanced by increasing AO fluence, as presented in Fig. 8. From these results, surface topography transformation to greater roughness might correlate with the degradation of tensile strength and elongation. It is generally assumed that excessive stress concentrates at a concave region on the rough surface during deformation; then the concave region can develop into surface cracks and become the initiation point of the polymer film's destruction. The increased surface roughness facilitates crack formation and hastens destruction.

Flight #3 showed a significant decrease that was greater than that of the AO irradiated sample of  $1.3 \times 10^{21}$  atoms/cm<sup>2</sup>, as presented in Fig. 11. Nevertheless, a broad distinction of surface topography was made between Flight #3 and the AO irradiated sample of  $1.3 \times 10^{21}$  atoms/cm<sup>2</sup>, as revealed by surface observations using SEM; the surface roughness of Flight #3 was a much lower than that of the AO irradiated sample of  $1.3 \times 10^{21}$  atoms/cm<sup>2</sup>. Then, cross-section observation was conducted to identify the surface topography for Flight #3. The samples for cross-section observation were embedded in epoxy and then cut with a microtome.

The three cross-sections for Flight #3 under no tensile stress during space exposure are presented in Fig. 14. The boundary between the sample and the embedding agent is traced in Fig. 14 to clarify the surface texture. Numerous blunt and short cones are formed on the Flight #3 surface. The average

surface roughness,  $R_z$ , was approximately 1  $\mu\text{m}$ . It should be noted that the Flight #3 surface exhibits some extremely deep concavities compared to its surroundings, as indicated by the white arrow in Fig. 14. Stress can readily concentrate at the deep concavities compared with surroundings; these deep concavities can exert a large reduction in mechanical properties of Flight #3.

#### 4. Conclusions

Degradation of mechanical properties for polyimide films exposed to a LEO environment was investigated using tensile tests. Some polyimide films were under a tensile stress state during space exposure to evaluate the effects of the tensile stress state on degradation.

The tensile strength and elongation of polyimide films decreased during space exposure. The reduction of the mechanical properties became marked as the exposure period increased. Ground reference tests demonstrated that the AO irradiated samples underwent considerable degradation of tensile strength and elongation; the samples exhibited no marked degradation of mechanical properties by either UV or EB. This result clearly suggests that AO attack is the main cause of decreased tensile strength and elongation in a LEO environment. A tensile stress state of less than 7.0 MPa, which was applied to the samples during space exposure and irradiation tests, had little effect on the degradation of the mechanical properties of any sample.

The tensile strength and elongation were decreased with increased AO fluence. In addition, the surface roughness developed dependently on the increased AO fluence. Consequently, the rough surface was regarded as a cause of degradation of mechanical properties. It is generally assumed that excessive stress concentrates at a concave region on the rough surface during deformation, leading to formation of surface cracks and initiation points of destruction.

The flight samples' surfaces showed a rough texture by AO erosion. Additionally, some extremely deep concavities compared to surroundings were found on the surface. These deep concavities have the potential to reduce mechanical properties considerably.

#### Acknowledgments

The author gratefully acknowledges the experimental support of the Advanced Engineering Services staff, and greatly appreciates the work of all people involved in the development and operation of the SM/MPAC&SEED project.

#### References

- [1] R. C. Tennyson, "Atomic Oxygen and Its Effects of Materials," *The Behavior of Systems in the Space Environment*, edited by R. N. DeWitt, Kluwer Academic, Amsterdam, 1993, pp. 233–357.
- [2] Bruce A. Banks, Aaron Snyder, and Sharon K. Miller, "Issues and Consequences of Atomic Oxygen Undercutting of Protected Polymers in Low Earth Orbit," NASA TM-211577, 2002.
- [3] Joseph Marco and Stephanie Remaury, "Evaluation of Thermal Control Coatings Degradation in Simulated Geo-Space Environment," *High Performance Polymers*, Vol. 16, 2004, pp. 177–196.
- [4] Youichi Nakayama, Kichiro Imagawa, Minoru Tagashira, Muneaki Nakai, Hisaaki Kudoh, Masaki Sugimoto, Noboru Kasai, and Tadao Seguchi, "Evaluation and Analysis of Thermal Control Materials under Ground Simulation Test for Space Environment Effects," *High Performance Polymers*, Vol. 13, 2001, pp. S433–S451.
- [5] Edward M. Silverman, "Space Environment Effects on Spacecraft: LEO Materials Selection Guide," NASA Contractor Report 4661 Part 1 & 2, 1995.
- [6] Mark J. Forkapa, Curtis R. Stidham, Bruce A. Banks, Sharon K. Rutledge, David H. Ma, and Edward A. Sechkar, "Atomic Oxygen Durability Testing of an International Space Station Solar Array Validation Coupon," NASA TM-107212, 2001.
- [7] Y. Shibayama, H. Arai, K. Matsui, K. Hama, A. Ushirokawa, M. Natori, K. Takahashi, N. Wakasugi, and T. Anzai, "SFU Solar Array," *Proceedings of European Space Power Conference*, Madrid, Oct, 1989.
- [8] [http://www.jaxa.jp/press/2004/05/20040521\\_midori2-03\\_j.pdf](http://www.jaxa.jp/press/2004/05/20040521_midori2-03_j.pdf) (in Japanese)
- [9] Yuichi Tsuda, Osamu Mori, Shinsuke Takeuchi, and Junichiro Kawaguchi, "Flight Result and Analysis of Solar Sail Deployment Experiment Using S-310 Sounding Rocket," *Proceedings of 56<sup>th</sup> International Astronautical Congress* [CD-ROM], Fukuoka, Japan, 17–21 Oct., 2005.
- [10] David L. Edwards, William A. Hollerman, Whitney S. Hubbs, Perry A. Gray, George E. Wertz, David T. Hoppe, Mary K. Nehls, and Charles L. Semmel, "Electron Radiation Effects on Candidate Solar Sail Materl," *High Performance Polymers*, Vol. 16, No. 2, 2004, pp. 277–288.
- [11] J. B. Whiteside, D. Giangano, R. L. Heuer, E. Kamykowski, M. Kesselman, W. D. Rooney, R. Schulte, and M. Stauber, "Effects of the Space Environment on Space-Based Radar Phsed-Array Antenna; Status and Preliminally Observations (LEDF Experiment A0133)," *Proceedings of LDEF-69 Months in Space First Post-Retrieval Symposium*, Kissimmee, Florida, 2–8 June, 1991.
- [12] Joyce A. Dever, Sharon K. Miller, and Edward A. Sechlar, "Effects of the Space Environment on Polymer Film Materials Exposed on the Materials International Space Station Experiment (MISSE 1 and MISSE 2)," *Proceedings of the 10<sup>th</sup> International Symposium on "Materials in a Space Environment" & the 8<sup>th</sup> International Conference on "Protection of Materials and Structures in a Space Environment"* [CD-ROM], Collioure, France, 19–23 June, 2006.
- [13] Yugo Kimoto, Junichiro Ishizawa, Eiji Miyazaki, and Mineo Suzuki, "SM/MPAC&SEED Experiment Overview," *Proceedings of International Symposium on "SM/MPAC&SEED Experiment"*, Tsukuba, Japan, 10–11 March, 2008.
- [14] American Society for Testing and Materials (ASTM) Standard D-638-03, "Standard Test Method for Tensile Properties of Plastics," 2003.

- [15] Yugo Kimoto, Keiichiro Yano, Junichiro Ishizawa, and Eiji Miyazaki, "Post Retrieval Analyses of Space Environment Monitoring Samples: Radiation Effects, UV, and Atomic Oxygen Fluence," *Proceedings of International Symposium on "SM/MPAC&SEED Experiment,"* Tsukuba, Japan, 10–11 March, 2008.
- [16] Yasuo Tanaka, Masanori Iwaki, Singo Obara and Hiroyuki Nagata, "New High Vacuum Test Facilities for Mechanical Components (part 1) -UHV Surface Properties Test Facility and Combined Space Effects Test Facility," *Proceedings of 21<sup>st</sup> International Symposium on Space Technology and Science,* 1998.
- [17] American Society for Testing and Materials (ASTM) Standard E-2089-00, "Standard Practices for Ground Laboratory Atomic Oxygen Interaction Evaluation of Materials for Space Application," 2000.
- [18] UBE Industries, Ltd., UPILEX-S Catalog.
- [19] David J. T. Hill, Firas A. Rasoul, John S. Forsythe, James H. O'Donnell, Peter J. Pomery, Graeme A. George, Philip R. Young, and John W. Connell, "Effect of Simulated Low Earth Orbit Radiation on Polyimides (UV Degradation Study)," *Journal of Applied Polymer Science,* Vol. 58, 1995, pp. 1847–1856.
- [20] Tsuneo Sasuga, Naohiro Hayakawa, Kenzo Yoshida, and Miyuki Hagiwara, "Degradation in Tensile Properties of Aromatic Polymers by Electron Beam Irradiation," *Polymer,* Vol. 26, 1985, pp. 1039–1045.
- [21] Eiji Miyazaki, Junichiro Ishizawa and Hiroyuki Shimamura, "Evaluation of F-OSR Exposed to Space on SM/SEED Experiment," *Proceedings of International Symposium on "SM/MPAC&SEED Experiment,"* Tsukuba, Japan, 10–11 March, 2008.
- [22] Naoko Baba, and Yugo Kimoto, "Contamination Effect on SM/MPAC&SEED Experiment," *Proceedings of International Symposium on "SM/MPAC&SEED Experiment,"* Tsukuba, Japan, 10–11 March, 2008.
- [23] Deborah L. Waters, Bruce A. Banks, Stephen D. Thorson, Kim K. de Groh and Sharon K. R. Miller, "Comparison of the Atomic Oxygen Erosion Depth and Cone Height of Various Materials at Hyperthermal Energy," *Proceedings of the 10<sup>th</sup> International Symposium on "Materials in a Space Environment" & the 8<sup>th</sup> International Conference on "Protection of Materials and Structures in a Space Environment"* [CD-ROM], Collioure, France, 19–23 June, 2006.
- [24] R. Vered, G. D. Lempert, E. Grossman, Y. Haruvy, G. Marom, L. Singer, and Y. Lifshitz, "Atomic Oxygen Erosion of Teflon FEP and Kapton by Oxygen from Different sources: Atomic Force Microscopy and Complementary Studies," *Proceedings of the 6<sup>th</sup> International Symposium on "Materials in a Space Environment,"* Noordwijk, The Netherlands, 19–23 September, 1994.
- [25] Bruce A. Banks, Thomas J. Stueber, Scott A. Snyder, Sharon K. Rutledge, and Mary J. Norris, "Atomic Oxygen Erosion Phenomena," AIAA-1997-3903, 1997.
- Tension-Loaded Polyimide Films in a Space Environment: Results of the SM/MPAC&SEED Mission," *Proceedings of the 10<sup>th</sup> International Symposium on "Materials in a Space Environment" & the 8<sup>th</sup> International Conference on "Protection of Materials and Structures in a Space Environment"* [CD-ROM], Collioure, France, 19–23 June, 2006.
2. Hiroyuki Shimamura and Takashi Nakamura, "Evaluation of Tension-Applied Polyimide Films Exposed to Space Environment on ISS Russian Service Module/Space Environment Exposure Device," *Proceedings of 51<sup>st</sup> Space Sciences and Technology Conference,* Sapporo, Japan, 29–31 October, 2007. (in Japanese)

#### Publication list related SM/MPAC&SEED

1. Hiroyuki Shimamura, and Ichiro Yamagata, "Degradation of

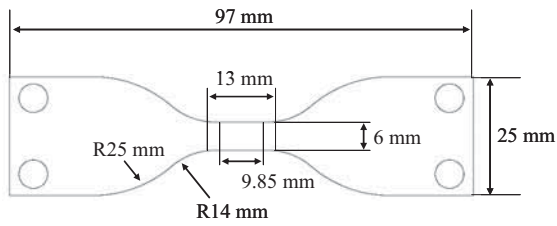


Fig. 1 Schematic view of the sample.

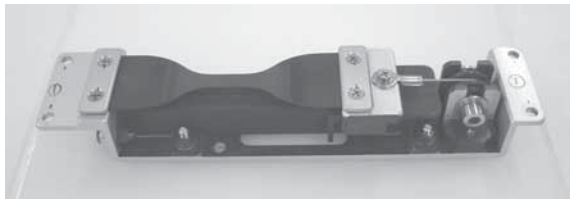


Fig. 2 Post-flight photograph of the tension-loading mechanism with a sample.

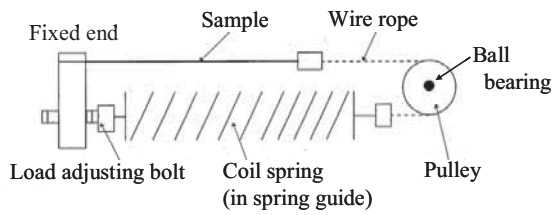


Fig. 3 Cross-sectional view of the tension-loading mechanism.

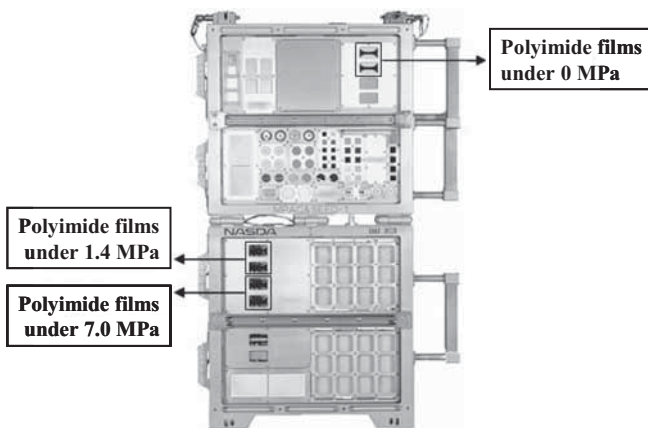


Fig. 4 Mounting location of polyimide films in the RAM side of the SM/MPAC&SEED unit.

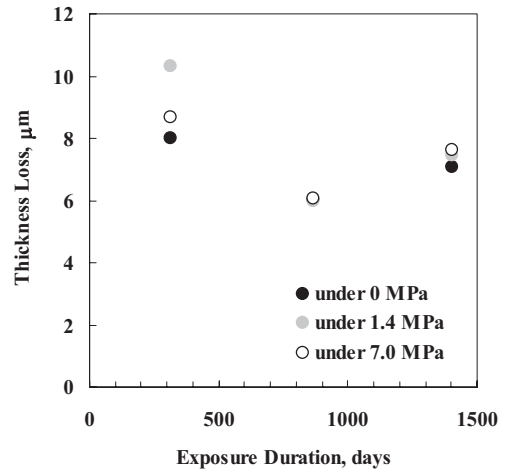


Fig. 5 Thickness loss of the flight samples.

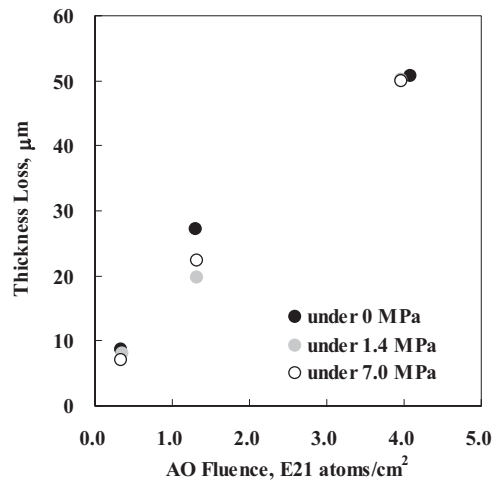


Fig. 6 Thickness loss of the AO irradiated samples.



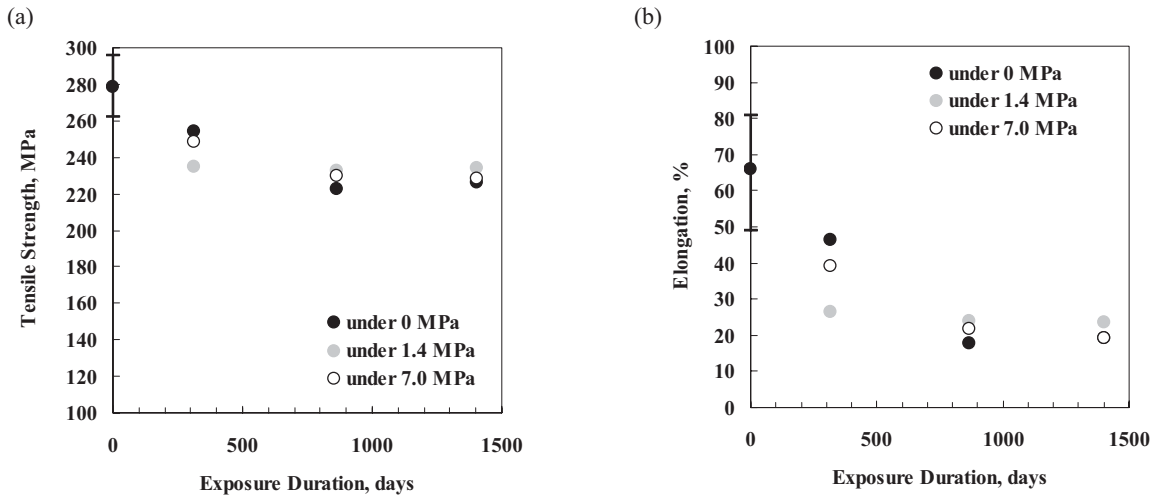


Fig. 7(a) Tensile strength and (b) elongation of the flight samples.

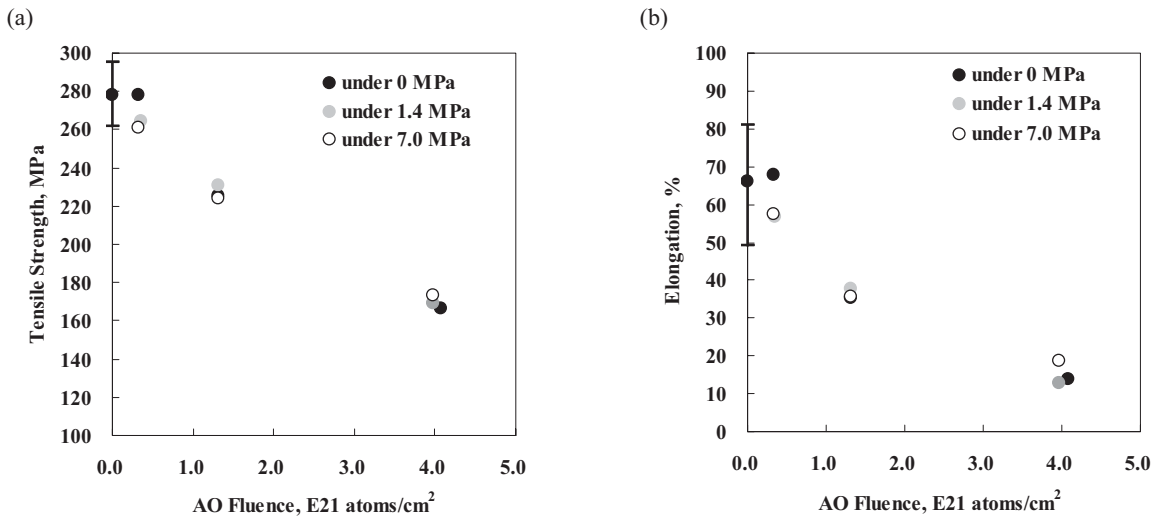


Fig. 8(a) Tensile strength and (b) elongation of the AO irradiated samples.

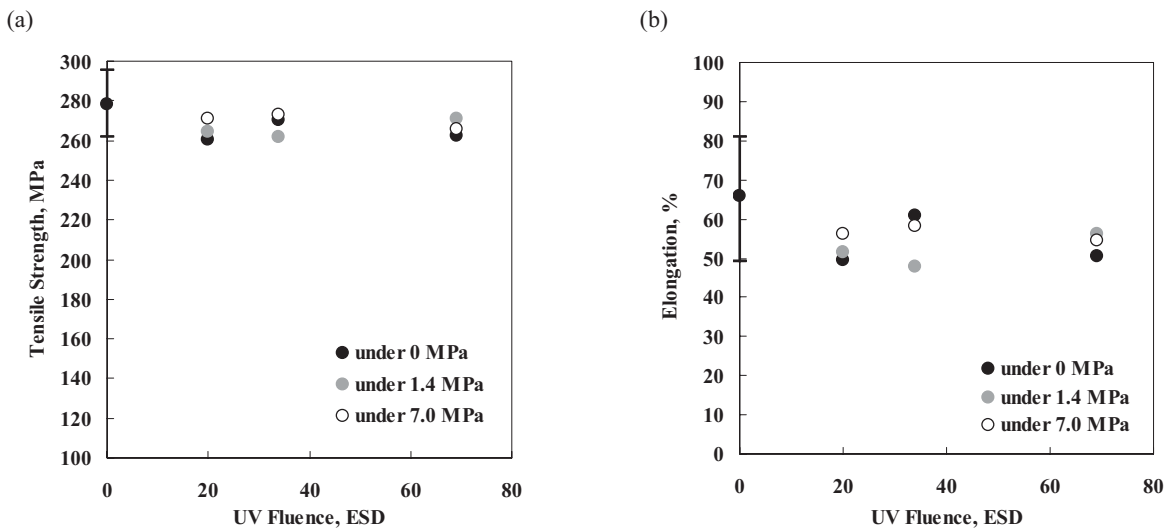


Fig. 9(a) Tensile strength and (b) elongation of the UV irradiated samples.

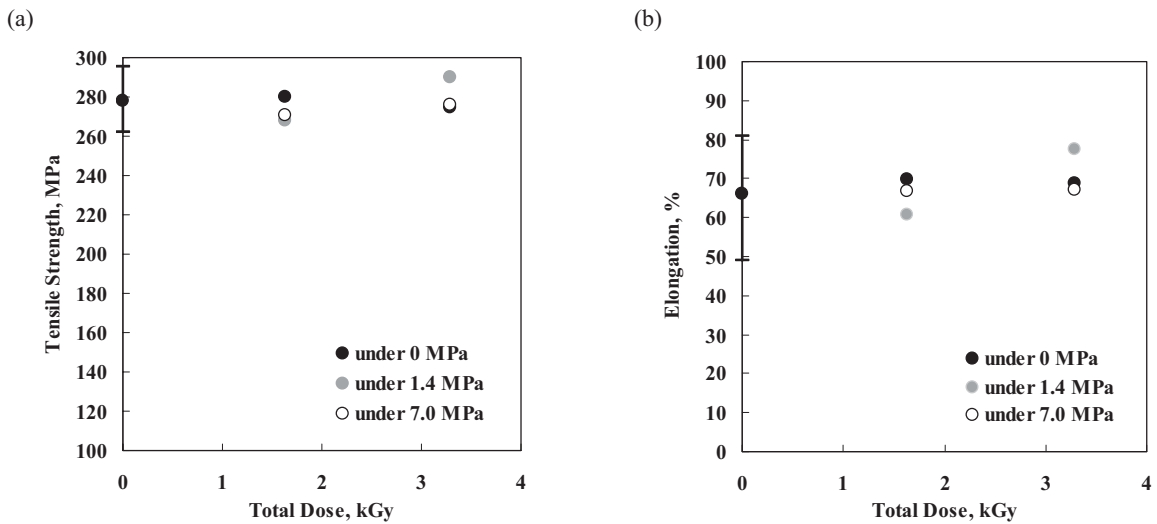


Fig. 10(a) Tensile strength and (b) elongation of the EB irradiated samples.

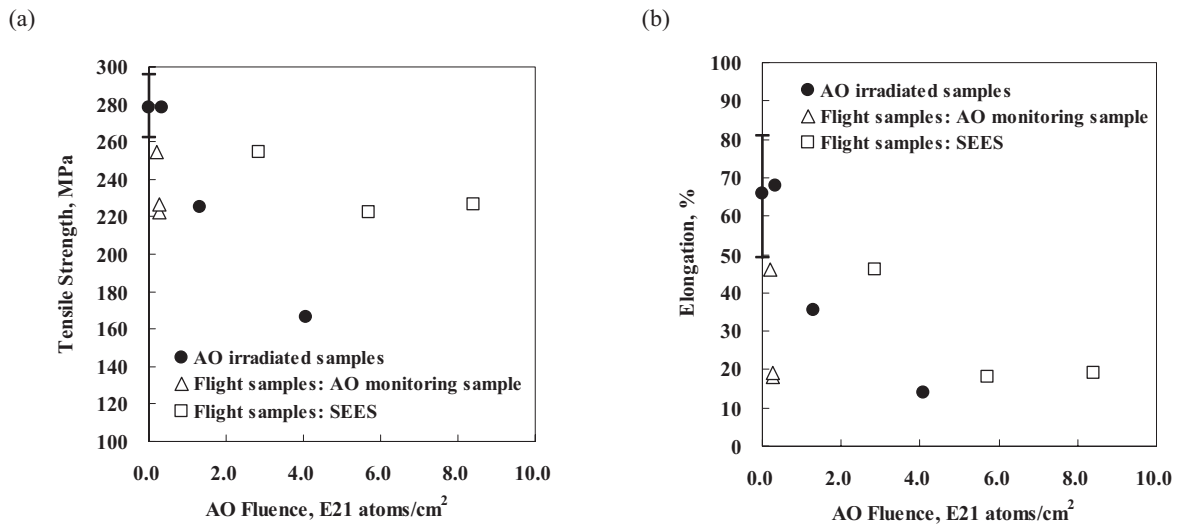


Fig. 11 (a) Tensile strength and (b) elongation of flight samples and AO irradiated samples for AO fluence. These figures show data for the samples under no tensile stress. Flight samples were plotted for two kinds of AO fluence: one is determined by the analysis of the AO monitoring sample on the SM/SEED experiment; the other is estimated by the simulation using SEES [15]

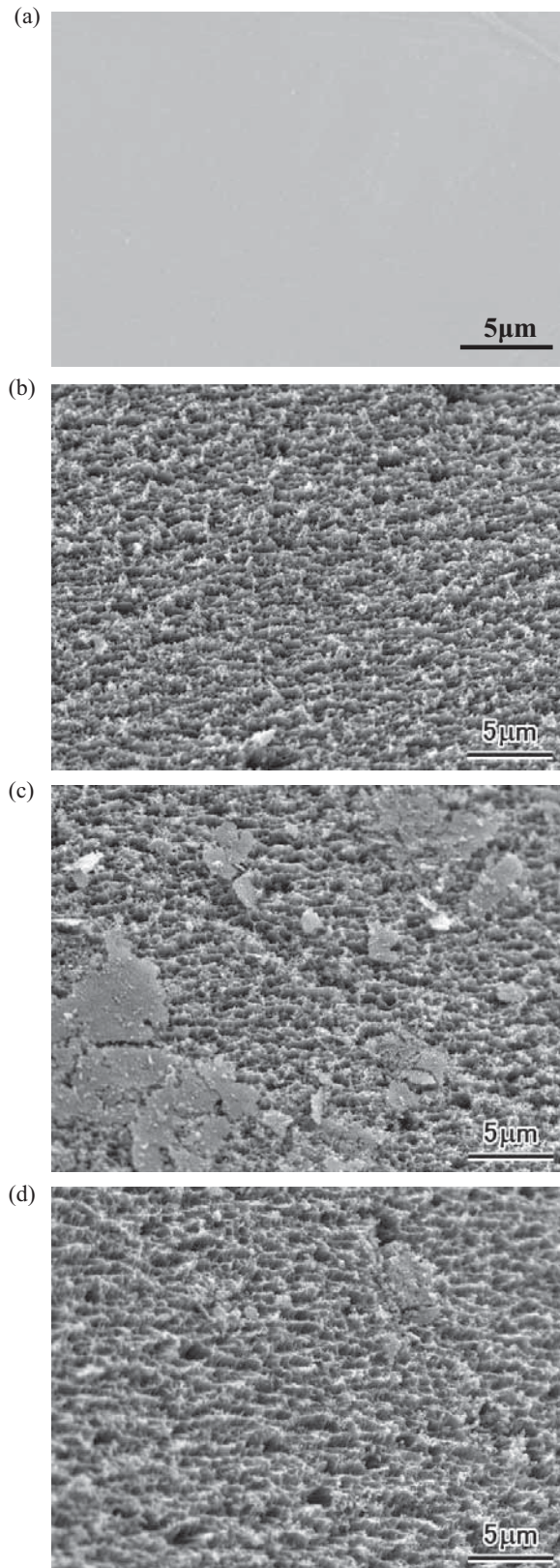


Fig. 12 SEM images of (a) the control sample, (b) Flight #1 and (c) Flight #2, and (d) Flight #3. The flight samples were under no tensile stress state during space exposure.

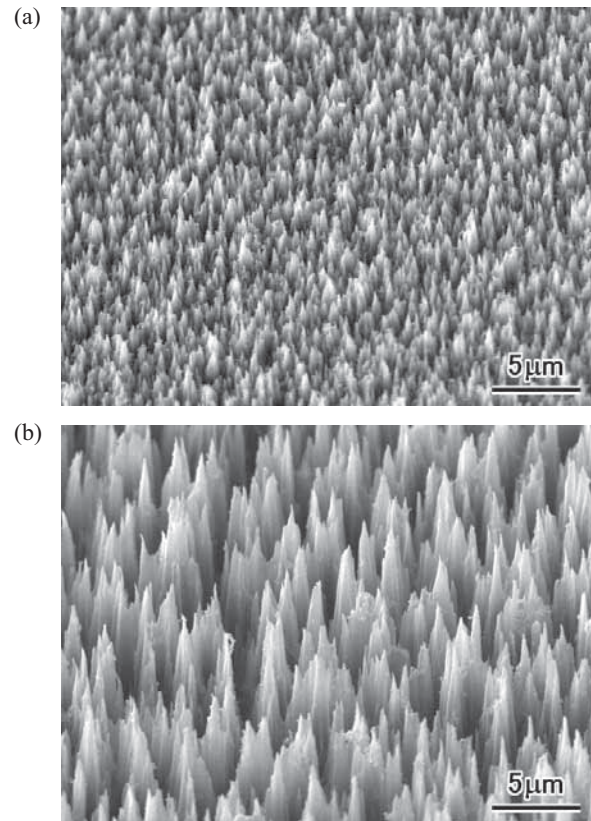


Fig. 13 SEM images of (a) the AO irradiated sample at  $0.3 \times 10^{21}$  atoms/cm<sup>2</sup> and (b) the AO irradiated sample at  $1.3 \times 10^{21}$  atoms/cm<sup>2</sup>. These samples were under no tensile stress during AO irradiation tests.

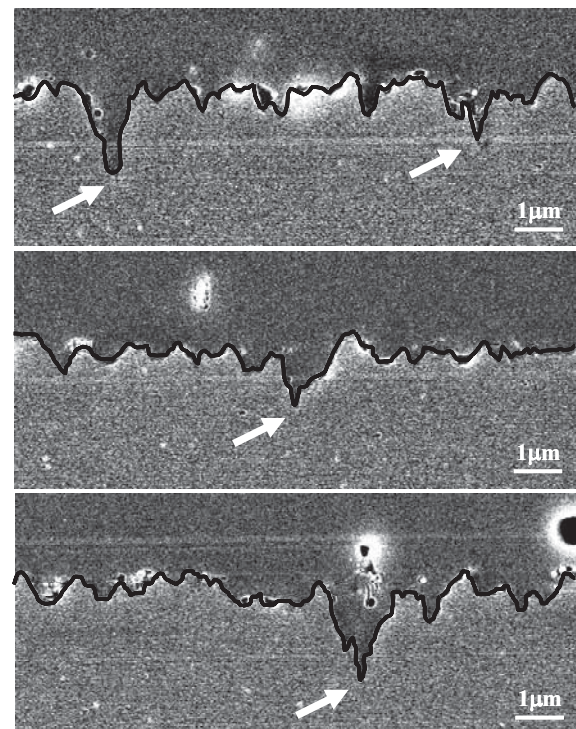


Fig. 14 Cross-sections of Flight #3 under no tensile stress during space exposure. The boundary between the sample and the embedding agent was traced to clarify the surface aspect.



**NASA GLENN RESEARCH CENTER'S  
MATERIALS INTERNATIONAL SPACE STATION EXPERIMENTS (MISSE 1-7)**

Kim K. DE GROH<sup>1</sup>, Bruce A. BANKS<sup>2</sup>, Joyce A. DEVER<sup>3</sup>, Donald A. JAWORSKE<sup>1</sup>, Sharon K. MILLER<sup>1</sup>,  
Edward A. SECHKAR<sup>4</sup> and Scott R. PANKO<sup>4</sup>

<sup>1</sup>Space Environment and Experiments Branch, NASA Glenn Research Center

<sup>2</sup>Consultant to Alphaport, Inc. at NASA Glenn Research Center

<sup>3</sup>Durability and Protective Coatings Branch, NASA Glenn Research Center

<sup>4</sup>ASRC Aerospace Corp. at NASA Glenn Research Center

21000 Brookpark Rd., Cleveland, OH 44135, USA

NASA Glenn Research Center (Glenn) has 39 individual materials flight experiments (>540 samples) flown as part of the Materials International Space Station Experiment (MISSE) to address long duration environmental durability of spacecraft materials in low Earth orbit (LEO). MISSE is a series of materials flight experiments consisting of trays, called Passive Experiment Carriers (PECs) that are exposed to the space environment on the exterior of the International Space Station (ISS). MISSE 1-5 have been successfully flown and retrieved and were exposed to the space environment from one to four years. MISSE 6A & 6B were deployed during the STS-123 shuttle mission in March 2008, and MISSE 7A & 7B are being prepared for launch in 2009. The Glenn MISSE experiments address atomic oxygen (AO) effects such as erosion and undercutting of polymers, AO scattering, stress effects on AO erosion, and in-situ AO fluence monitoring. Experiments also address solar radiation effects such as radiation induced polymer shrinkage, stress effects on radiation degradation of polymers, and radiation degradation of indium tin oxide (ITO) coatings and spacesuit fabrics. Additional experiments address combined AO and solar radiation effects on thermal control films, paints and cermet coatings. Experiments with Orion Crew Exploration Vehicle (CEV) seals and UltraFlex solar array materials are also being flown. Several experiments were designed to provide ground-facility to in-space calibration data thus enabling more accurate in-space performance predictions based on ground-laboratory testing. This paper provides an overview of Glenn's MISSE 1-7 flight experiments along with a summary of results from Glenn's MISSE 1 & 2 experiments.

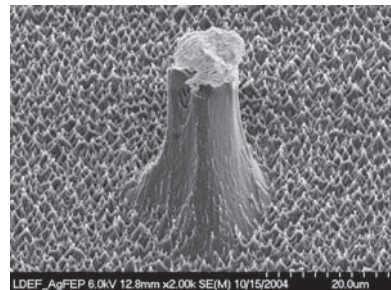
**Keywords:** Materials International Space Station Experiment, International Space Station, low Earth orbit, flight experiments, atomic oxygen, radiation, degradation

## 1. Introduction

Functional materials used on the exterior of spacecraft are subjected to many environmental threats that can cause degradation in materials properties, possibly threatening spacecraft mission success. In LEO these threats include AO, photon radiation, charged particle radiation, temperature effects and thermal cycling, impacts from micrometeoroids and debris, and contamination. Atomic oxygen is the most predominant species in LEO and is present in other planetary orbital environments. At spacecraft velocities, LEO AO is energetic enough ( $\approx 4.5$  eV) to cause bond breakage and subsequent oxidation. The oxidation products of most polymers are gas species, therefore material erosion occurs. Atomic oxygen can produce serious structural, thermal or optical degradation of spacecraft components. Figure 1 shows AO erosion of Teflon<sup>®</sup> fluorinated ethylene propylene (FEP) around a small protective particle. To assess the AO durability of a material for mission applicability, the erosion yield (volume loss in  $\text{cm}^3$  per incident oxygen atom) needs to be characterized using actual space flight data, as ground AO facilities do not perfectly simulate the space environment.

The most common approach to protecting susceptible spacecraft materials from AO erosion is to coat the material with a thin AO protective film, such as  $\text{SiO}_x$ . Unfortunately, microscopic scratches, dust particles or other imperfections in

the substrate surface can result in defects in the protective coating. These coating defects can provide pathways for AO attack and undercutting erosion of the substrate can occur. Undercutting erosion can be a serious threat to component survivability. An example is shown in Figure 2, where AO undercutting erosion has severely degraded the P6 Truss port solar array wing two-surface aluminized-Kapton<sup>®</sup> blanket box cover on the ISS.[1]

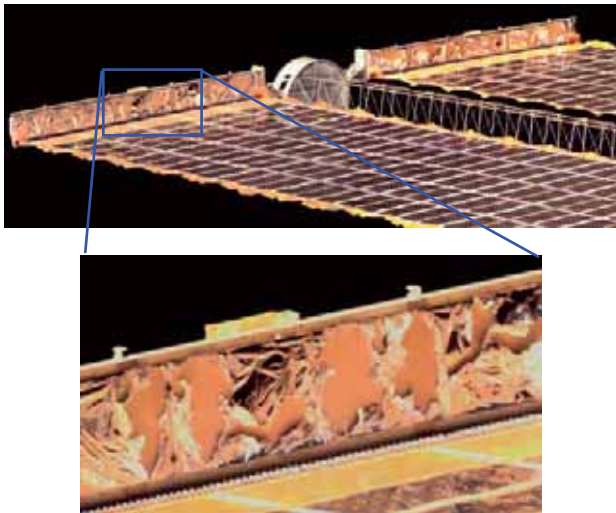


**Fig. 1 Atomic oxygen erosion of Teflon FEP in space.**

An example of radiation induced polymer degradation is found through extensive embrittlement of thermal control insulation on the Hubble Space Telescope (HST). During the second servicing mission (SM2), after 6.8 years in space, severe cracking was observed in the aluminized-Teflon



fluorinated ethylene propylene (Al-FEP) outer layer of the multilayer insulation (MLI) covering the HST Light Shield. Astronaut observations combined with photographic documentation revealed extensive cracking of the MLI in many locations, with the solar facing surfaces being heavily damaged.[2] Figure 3 shows two large cracked areas. Extensive testing was conducted on retrieved HST insulation, combined with ground-based testing, which revealed that embrittlement of FEP on HST is caused by radiation exposure (electron and proton radiation, with contributions from solar flare x-rays and ultraviolet (UV) radiation) combined with thermal effects.[2]



**Fig. 2 Atomic oxygen undercutting degradation of the solar array wing blanket box cover on ISS.**



**Fig. 3 Large cracks in HST MLI after 6.8 years in space.**

Unfortunately, accelerated laboratory testing often does not accurately simulate degradation caused by combined on-orbit environmental exposures. One example was the inability to reproduce the extent of embrittlement of Al-FEP insulation on the HST based on mission fluence requirements.[3] The fact that highly accelerated ground-laboratory testing did not replicate the on-orbit degradation highlights the necessity of actual long-duration space flight data.

NASA Glenn Research Center has 39 individual materials flight experiments, with over 540 samples, being flown as part of the MISSE series to address long duration environmental

durability issues for spacecraft materials in the LEO space environment. The Glenn MISSE experiments address AO effects such as erosion and undercutting of polymers, AO scattering, stress effects on AO erosion, and in-situ AO fluence monitoring. Experiments were also designed to address solar radiation effects such as radiation induced polymer shrinkage, stress effects on radiation degradation of thin film polymers, and radiation degradation of ITO coatings and spacesuit fabrics. Several NASA Glenn experiments also address combined AO and solar radiation effects on thermal control films, paints and cermet coatings. Experiments with Orion CEV Low Impact Docking System (LIDS) seals materials and UltraFlex solar array materials are also being flown. Several of the experiments were designed to provide ground-facility to in-space calibration data, thus enabling more accurate in-space performance predictions based on ground-laboratory testing. NASA Glenn's participation on MISSE 5 also included a substantial contribution to MISSE 5's primary experiment, the Forward Technology Solar Cell Experiment (FTSCE). The Glenn MISSE 1 & 2 materials experiments have already had a direct impact on the Exploration space program, the space industry, the military and education. This paper provides an overview of Glenn's MISSE 1-7 flight experiments and their relevance to various NASA missions. A summary of the results from NASA Glenn's MISSE 1 & 2 experiments are provided, along with the use of the data for ground-facility calibration and improved LEO environmental durability prediction.

## **2. Materials International Space Station Experiment (MISSE) Overview**

MISSE is a series of materials flight experiments consisting of trays, called PECs, which are exposed to the space environment on the exterior of the ISS providing long-duration space exposure. Each PEC consists of two trays, hinged like a suitcase, as shown in Figure 4. The PECs are closed with the samples facing each other and protected for launch on the shuttle and then are attached to the outside of ISS during an extravehicular activity (EVA) and opened back-to-back, exposing the samples to space. The trays are typically positioned with one surface facing the ram direction thus receiving AO and solar radiation (Tray 1), and the back surface facing the wake direction thus receiving solar radiation with minimal AO exposure (Tray 2). The overall objective of MISSE is to test the stability and durability of materials and devices in the space environment in order to gain valuable knowledge on the performance of materials in space as well as to enable lifetime prediction of new materials and components that may be used in future space flight. Figure 5 shows MISSE PEC 1 during an EVA in January 2003 after 17 months of space exposure. Five MISSE PECs (MISSE 1-5) have been successfully flown and retrieved to date. Table 1 provides a summary of the MISSE 1-5 launch and retrieval missions, and the space exposure durations. MISSE 6A & 6B were deployed during the STS-123 shuttle mission in March 2008 and were planned as a one-year mission. At the time of writing this paper, MISSE 7A & 7B are being prepared for a 2009 launch.



Fig. 4 Pre-flight photo of MISSE 2.

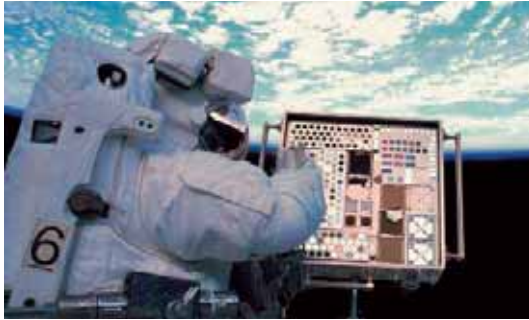


Fig. 5 MISSE 1 being examined during a spacewalk in January 2003.

### 3. Glenn's MISSE 1-7 Experiments

Researchers at Glenn are principal investigators (PI) for seven materials experiments, with a total of 80 samples, flown for nearly 4 years on the exterior of the ISS as part of MISSE 1 & 2. These Glenn experiments investigated AO erosion of unprotected polymers, AO scattering characteristics, and effects of the overall LEO environment on optical and mechanical properties of polymer films. Experiments were also flown to provide data to calibrate ground-based facilities for simulating LEO AO effects on polymers with protective coatings. Results of these experiments are provided, along with an example of how the data are being used to improve LEO environmental durability prediction. The use of MISSE 1 & 2 data for durability prediction for specific missions is also provided.

Glenn has eight spacecraft materials durability experiments (with a total of 71 samples) that were flown as part of MISSE 3 & 4, and four experiments (with 105 samples) flown as part of MISSE 5. Glenn was also actively involved in the MISSE 5 FTSCE experiment. The MISSE 5 mission, which received 13 months of space exposure, flew directly after retrieval of MISSE 1 & 2. MISSE 3 & 4, which was deployed before retrieval of MISSE 5, received 1 year of space exposure. Post-flight sample documentation and analyses have begun on these experiments.

MISSE 6 and 7 differ from the prior trays in that many of the experiments are active experiments. The MISSE 6 active experiments are powered by ISS and the data are being stored on data loggers and will be available when the experiments are retrieved. NASA Glenn has six active experiments and six passive experiments on MISSE 6, with a total of 168 samples that are integrated into the two MISSE 6 PECs (6A & 6B). MISSE 6 was delivered to ISS during the STS-123 mission,

and both 6A and 6B were placed outside of the Columbus Module on March 22, 2008. MISSE 7 will be powered by, and will have communication links through ISS. Hence, the active data will be retrieved daily via telemetry. Glenn has a total of nine experiments (three active and six passive), with a total of 120 samples that are being developed for integration into the MISSE 7 PECs, with a planned launch in 2009. MISSE 7A will be placed in a zenith/nadir orientation and MISSE 7B will be placed in a ram/wake orientation. The Glenn MISSE 6 & 7 experiments include Exploration Mission relevant materials such as spacesuit fabrics, thermal control blanket polymers and paints, solar array blanket materials, o-ring seals, and dust mitigation materials.

### 4. MISSE 1 & 2 Experiments and Flight Results

Table 2 provides a list of Glenn's MISSE 1 & 2 materials experiments along with the on-orbit orientation, the individual experiment objective and the number of samples.

Estimated environmental conditions of AO, solar exposure, tray temperatures, and ionizing radiation doses on MISSE 1 & 2 are described in detail by Pippin.[4] Black light inspection of the trays showed minimal to no contamination on the MISSE surfaces.[4] Results of x-ray photoelectron spectroscopy (XPS) contamination analysis of two MISSE 2 sapphire witness samples in MISSE 2 ram sample tray E6 indicated an extremely thin silica contaminant layer (1.3 and 1.4 nm on each slide, respectively).[5] A small amount of fluorine was also detected.[5] The MISSE 2 environment was found to be an unusually clean environment with very low spacecraft induced molecular contamination. This is due to low outgassing of other MISSE 2 Tray 1 materials and also due to the position of MISSE 2 on ISS. Therefore, the flight data was not affected by contamination. This further increases the importance of this long duration flight data.

#### 4.1. Polymer Erosion and Contamination Experiment (PEACE) Polymers Experiment (MISSE 2)

The PEACE Polymers experiment included 41 – 1" (2.54 cm) diameter samples (39 polymer samples and 2 Kapton H AO fluence witness samples). The experiment (sample tray E5) was flown on the ram side of MISSE 2 and was exposed to AO along with solar and charged particle radiation (see Figure 6). The objective of the MISSE 2 PEACE Polymers experiment was to accurately determine the AO erosion yield ( $E_y$ ) of a wide variety of polymeric materials exposed for an extended period of time to the LEO space environment. The polymers range from those commonly used for spacecraft applications, such as Teflon FEP, to more recently developed polymers, such as high temperature polyimide PMR (polymerization of monomer reactants). Additional polymers were included to explore erosion yield dependence upon chemical composition so that an AO erosion yield predictive tool could be developed. The majority of samples were comprised of thin film polymers, with numerous layers stacked together to last a minimum of 3 years in LEO. The MISSE 2 PEACE Polymers experiment is unique because it contains the widest variety of well-documented polymers exposed to identical long duration LEO AO conditions.

Table 1. MISSE 1-6 Mission and Space Exposure Summary

MISSE PEC	Launch Mission	Date Placed Outside ISS	Location on ISS	Orientation	Retrieval Mission	Date Retrieved from ISS	LEO Exposure Duration
1 & 2	STS-105	8/16/2001	PEC 1: High Pressure Gas Tank PEC 2: Quest Airlock	Ram & Wake	STS-114	7/30/2005	3.95 years
3 & 4	STS-121	8/3/2006	PEC 3: High Pressure Gas Tank PEC 4: Quest Airlock	Ram & Wake	STS-118	8/18/2007	1 year
5	STS-114	8/3/2005	Aft P6 Trunion Pin Handrail	Solar & Anti-Solar	STS-115	9/15/2006	13 months
6A & 6B	STS-123	3/22/2008	Columbus Module	Ram & Wake	-	-	-

Table 2. Glenn's MISSE 1 &amp; 2 Materials Experiments (80 Samples)

Glenn Experiment	Orientation	# Samples	Experiment Objective
PEACE Polymers	Ram	41	To determine the AO erosion yield of a wide variety of polymers with and without solar radiation
Spacecraft Silicones	Ram	4	To determine changes in optical properties and nanomechanical hardness for ground-testing
AO Scattering Chamber	Ram	1	To determine scattered AO erosion characteristics for undercutting modeling
Double SiO <sub>x</sub> -Coated Kapton (Mass Loss)	Ram	2	To determine AO undercutting rate dependence in space as compared to ground-facility (mass loss)
AO Undercutting Erosion (Undercut Cavities)	Ram	2	To determine AO undercutting rate dependence in space as compared to ground-facility (undercut cavities)
Polymer Film Thermal Control (PFTC)	Ram & Wake	20	To assess radiation and temperature effects on a variety of currently used and candidate thermal control materials
Gossamer Materials	Ram & Wake	10	To assess solar exposure, radiation, and temperature effects on candidate materials for gossamer structures



Fig. 6 MISSE 2 on the ISS Quest Airlock (the PEACE Polymers experiment is outlined).

Figure 7 provides photos of the MISSE 2 PEACE Polymers experiment prior to, and after, LEO space exposure. Although MISSE 2 was supposed to be a 1.5 year mission, planning for a three-year mission exposure was crucial in the success of this experiment, as it was exposed to LEO AO for four years. The AO fluence for the experiment was determined to be  $8.43 \times 10^{21}$  atoms/cm<sup>2</sup> based on mass loss of the two polyimide Kapton H witness samples. Atomic oxygen erosion yield values have been determined for each of the MISSE 2 PEACE polymers based on mass loss obtained from pre-flight and post-flight vacuum dehydrated samples. Table 3 provides

a list of each of the MISSE 2 PEACE Polymer samples, the MISSE 2 mass loss, the sample density, the exposure area and the MISSE 2 erosion yield data.[6] Details on the specific polymers flown, flight sample fabrication, pre-flight and post-flight characterization techniques, AO fluence calculations and AO erosion yield results are reported by de Groh et al.[6,7]



a.



b.

Fig. 7 MISSE 2 PEACE Polymers experiment (Sample Tray E5), a). Prior to flight, and b). After space flight.



Table 3. MISSE 2 PEACE Polymers Erosion Yield Data [6]

MISSE Serial #	Material	Polymer Abbrev.	MISSE 2 Mass Loss (g)	Density (g/cm <sup>3</sup> )	Area (cm <sup>2</sup> )	MISSE 2 Erosion Yield (cm <sup>3</sup> /atom)
2-E5-6	Acrylonitrile butadiene styrene	ABS	0.033861	1.05	3.4944	1.09E-24
2-E5-7	Cellulose acetate	CA	0.191482	1.2911	3.4831	5.05E-24
2-E5-8	Poly-(p-phenylene terephthalamide)	PPD-T (Kevlar)	0.026790	1.4422	3.5099	6.28E-25
2-E5-9	Polyethylene	PE	0.102760	0.918	3.5489	>3.74E-24
2-E5-10	Polyvinyl fluoride	PVF (Tedlar)	0.132537	1.3792	3.5737	3.19E-24
2-E5-11	Crystalline polyvinylfluoride w/white pigment	PVF (White Tedlar)	0.004714	1.6241	3.4176	1.01E-25
2-E5-12	Polyoxymethylene; acetal; polyformaldehyde	POM (Delrin)	0.378378	1.3984	3.5119	9.14E-24
2-E5-13	Polyacrylonitrile	PAN	0.047281	1.1435	3.4768	1.41E-24
2-E5-14	Allyl diglycol carbonate	ADC (CR-39)	0.267295	1.3173	3.5392	>6.80E-24
2-E5-15	Polystyrene	PS	0.115947	1.0503	3.5043	3.74E-24
2-E5-16	Polymethyl methacrylate	PMMA	0.194588	1.1628	3.5456	>5.60E-24
2-E5-17	Polyethylene oxide	PEO	0.066395	1.1470	3.5591	1.93E-24
2-E5-18	Poly(p-phenylene-2,6-benzobisoxazole)	PBO (Zylon)	0.056778	1.3976	3.5526	1.36E-24
2-E5-19	Epoxide or epoxy	EP	0.140720	1.1150	3.5576	4.21E-24
2-E5-20	Polypropylene	PP	0.072357	0.907	3.5336	2.68E-24
2-E5-21	Polybutylene terephthalate	PBT	0.036429	1.3318	3.5619	9.11E-25
2-E5-22	Polysulphone	PSU	0.105948	1.2199	3.5010	2.94E-24
2-E5-23	Polyurethane	PU	0.057227	1.2345	3.5182	1.56E-24
2-E5-24	Polyphenylene isophthalate	PPPA (Nomex)	0.030549	0.72	3.5626	1.41E-24
2-E5-25	Pyrolytic graphite	PG	0.02773	2.22	3.5703	4.15E-25
2-E5-26	Polyetherimide	PEI	0.126853	1.2873	3.5352	>3.31E-24
2-E5-27	Polyamide 6 or nylon 6	PA 6	0.118376	1.1233	3.5646	3.51E-24
2-E5-28	Polyamide 66 or nylon 66	PA 66	0.065562	1.2252	3.5249	1.80E-24
2-E5-29	Polyimide	PI (CP1)	0.080648	1.4193	3.5316	1.91E-24
2-E5-30	Polyimide (PMDA)	PI (Kapton H)	0.124780	1.4273	3.4590	3.00E-24
2-E5-31	Polyimide (PMDA)	PI (Kapton HN)	0.121315	1.4346	3.5676	2.81E-24
2-E5-32	Polyimide (BPDA)	PI (Upilex-S)	0.038127	1.3866	3.5382	9.22E-25
2-E5-33	Polyimide (PMDA)	PI (Kapton H)	0.129250	1.4273	3.5773	3.00E-24
2-E5-34	High temperature polyimide resin	PI (PMR-15)	0.118887	1.3232	3.5256	>3.02E-24
2-E5-35	Polybenzimidazole	PBI	0.082708	1.2758	3.4762	>2.21E-24
2-E5-36	Polycarbonate	PC	0.142287	1.1231	3.5010	4.29E-24
2-E5-37	Polyetheretherketone	PEEK	0.107764	1.2259	3.4821	2.99E-24
2-E5-38	Polyethylene terephthalate	PET (Mylar)	0.125187	1.3925	3.5432	3.01E-24
2-E5-39	Chlorotrifluoroethylene	CTFE (Kel-f)	0.052949	2.1327	3.5452	8.31E-25
2-E5-40	Ethylene-chlorotrifluoroethylene	ECTFE (Halar)	0.088869	1.6761	3.5103	1.79E-24
2-E5-41	Tetrafluoroethylene-ethylene copolymer	ETFE (Tefzel)	0.049108	1.7397	3.4854	9.61E-25
2-E5-42	Fluorinated ethylene propylene	FEP	0.012479	2.1443	3.4468	2.00E-25
2-E5-43	Polytetrafluoroethylene	PTFE	0.008938	2.1503	3.4841	1.42E-25
2-E5-44	Perfluoroalkoxy copolymer resin	PFA	0.010785	2.1383	3.4570	1.73E-25
2-E5-45	Amorphous Fluoropolymer	AF	0.012352	2.1463	3.4544	1.98E-25
2-E5-46	Polyvinylidene fluoride	PVDF (Kynar)	0.066860	1.7623	3.4993	1.29E-24

Note: Erosion yields listed with a > symbol indicate polymers that were eroded partially or completely through all layers.



An extensive error analysis was conducted to determine the error in the erosion yield values for each of the MISSE 2 PEACE Polymers flight samples. Three different equations were needed for determining mass loss of the flight samples, which is a factor in determining erosion yield. Therefore, it was necessary to develop three different equations for determining the fractional uncertainty in the erosion yield. Six of the 41 samples were partially or completely eroded through all layers, hence the erosion yield values for these samples are greater than those computed. These six polymers are being re-flown in the MISSE 6 Stressed PEACE Polymers experiment (see Section 7.1 below).

#### 4.1.1. Atomic Oxygen Erosion Yield Predictive Tool

The MISSE 2 PEACE Polymers experiment consisted of 40 structurally different polymers (including the Kapton H witness samples) not only to allow accurate measurement of the AO erosion yields of commonly used polymers, but also to allow the development of a space validated AO erosion yield predictive tool that can approximate the LEO erosion yields of polymers based on structural chemistry and physical properties. The value of such a predictive tool is that as new polymers emerge, one would not have to wait for several years for flight experiment results to obtain AO durability information. A Glenn Atomic Oxygen Erosion Yield Predictive Tool has been developed based on best fit criteria for the MISSE 2 PEACE Polymers erosion yield data. The predictive tool utilizes polymer structural and physical properties, such as number and types of chemical bonds, density and ash content. The Atomic Oxygen Erosion Yield Predictive Tool is described in detail by Banks et al.[8]

#### 4.1.2. Ground-Laboratory to In-Space Correlation

Although space flight experiments, such as the MISSE 2 PEACE experiment, are ideal for determining LEO environmental durability of spacecraft materials, ground-laboratory testing is most often relied upon for durability evaluation and prediction. Unfortunately, significant differences exist between LEO AO and AO in test facilities. These differences include variations in species, energies, thermal exposures and radiation exposures, all of which can result in different reactions and erosion rates. In an effort to improve the accuracy of ground-based durability testing, ground-laboratory to in-space AO correlation experiments have been conducted based on the MISSE 2 PEACE polymers flight data. In these tests, the AO erosion yields of the 39 PEACE polymers were determined relative to Kapton H using a radio-frequency (RF) plasma asher operated on air with the samples in metal holders. The asher erosion yields were compared to the MISSE 2 erosion yields for the PEACE polymers to determine the correlation between erosion rates in the two environments. The asher erosion yield of every polymer was higher than that of its in-space counterpart, and the asher to in-space erosion yield ratios ranged from 1.0 (1.02) to 37.1. The fluoropolymers in particular had higher ratios, ranging from 6.1 to 8.0. Kevlar, a woven fabric, had a ratio of 24.0, and White Tedlar, a

material containing AO durable filler particles, had a ratio of 37.1. Details of this research, along with the asher-to-space Ey ratios, are provided by Stambler et al.[8]

#### 4.1.3. Application to the Commercial Orbital Transportation System (COTS)

As one example of the use of MISSE data for Exploration Mission applications, the MISSE 2 PEACE Polymers Ey data has been used to evaluate the effects of AO texturing of a potential solar cell polymer cover being considered for the COTS mission solar array. The candidate polymer, polyvinyl fluoride (PVF, Tedlar), was subjected to end Hall AO (~70 eV O<sub>2</sub><sup>+</sup> ions) and then vacuum ultraviolet (VUV) radiation to determine the effects of the combined AO and VUV radiation (from deuterium lamps) on solar cell performance. The erosion yield of PVF from the MISSE 2 PEACE Polymers experiment was used along with the mission fluence requirement to determine the expected mass loss per area. This mass loss per area was then replicated in the end Hall AO facility to properly simulate the LEO erosion expected. The directed AO produced cones which slightly darkened the surface upon VUV exposure causing a slight loss in solar transmittance.

#### 4.1.4. PEACE Team Collaboration

Glenn has numerous collaborative MISSE experiments with Hathaway Brown School in Shaker Heights, Ohio. These experiments include the MISSE 2 and MISSE 5 PEACE Polymers experiments, the MISSE 6A Stressed PEACE Polymers Experiment, and the MISSE 7B Polymers Experiment. Hathaway Brown School is Ohio's oldest independent day school for girls. Through Hathaway Brown's Science Research & Engineering Program (SERP) students join the Glenn/HB "PEACE" team, where they can work on MISSE research at NASA Glenn throughout their entire high school career. Over the past 10 years, 20 students have been part of the Glenn/HB PEACE team. To date the student involvement has included: MISSE pre-flight research, MISSE 2, 5, 6A and 7B flight sample fabrication, pre-flight characterization, and MISSE 2 post-flight characterization and error analyses. The students have authored research papers, presented their work at an international conference, and entered their research in science fairs, winning over \$80,000 in scholarships and awards through this collaboration.

#### 4.1.5. The Handbook of Atomic Oxygen Erosion

Glenn plans to write a Handbook of Atomic Oxygen Erosion, as a NASA Special Publication or NASA Standard, which will document the MISSE 2 PEACE Polymers AO erosion yield data, allowing proper selection of materials and thickness for future long-duration space flight missions. The Handbook will include an extensive background on LEO AO and will document the AO erosion yield of the MISSE 2 PEACE Polymers. Details on the specific polymers flown, flight sample fabrication techniques, pre-flight and post-flight characterization, and mission AO fluence calculations

will be documented along with a summary of the AO erosion yield results. Details of the corresponding erosion yield error analyses will also be included along with the Glenn Atomic Oxygen Erosion Yield Predictive Tool. The handbook will inform users on how to use the predictive tool and how to use the erosion yield data for spacecraft durability prediction.

#### 4.2. Spacecraft Silicones Experiment (MISSE 2 & 4)

The objective of the Spacecraft Silicones Experiment was to determine changes in optical properties and nanomechanical surface hardness of silicones exposed to various LEO AO and UV radiation fluence levels. Silicones are widely used on spacecraft, such as the use of DC 93-500 to bond cover glasses to solar cells for the ISS photovoltaic array blankets or as protective coatings on the back of solar arrays. Silicones have previously been thought of as being AO durable because they typically do not lose weight in an AO environment and the surface converts to a glassy  $\text{SiO}_x$  layer.[10] Unfortunately, the oxidized glassy layer eventually shrinks as it densifies and cracks form, exposing the underlying silicone or coated substrate to AO.[10] Surface hardness measurements for silicones exposed to various AO fluences are desired so that comparisons of equivalent fluences can be made with AO ground-laboratory exposed samples. These comparisons will allow ground-facility to in-space AO equivalent fluences to be determined, such as those reported by de Groh, Banks & Ma.[11] It is important to find a technique which enables effective fluences in ground facilities to be determined based on space data because traditional mass loss techniques do not work for silicones. Obtaining microhardness data on MISSE flown silicone samples will allow this correlation to be made for high fluence exposures. Therefore, the MISSE 2 and MISSE 4 Spacecraft Silicones Experiments each included four DC 93-500 silicone samples. Three of the four samples were covered with different thickness layers of Kapton H (0.3 mil, 0.5 mil and 0.8 mil) in order for each of the samples in the same experiment to receive different AO fluences, as the AO needs to erode through the over-laying Kapton before attacking the underlying silicone. Because the 10 mil thick silicone samples are rubbery and can stick to smooth surfaces, they were placed on 1/16" (0.16 cm) thick fused silica slides to allow post-flight optical properties to be made without the samples bending and hence inducing cracking in the glassy oxidized layer. Silicones can darken with AO and UV radiation exposure increasing the solar absorptance of the material, and hence knowledge of the degree of darkening on-orbit is desired. The MISSE 2 Spacecraft Silicones Experiment samples were flown in PEC 2 sample tray E5 (samples 2-E5-1 to 2-E5-4), along with the MISSE 2 PEACE Polymers experiment, and were exposed to ram exposure for 4 years. The MISSE 4 Spacecraft Silicones Experiment samples were exposed to ram exposure for 1 year in MISSE 4 sample tray E22 (samples 2-E22-2 to 2-E22-5).

The MISSE 2 samples all crazed due to AO exposure, which cause surface shrinking. Figure 8 shows the "mud-tile" surface that developed due to conversion of the silicone

surface to a silicate glassy layer. Pre-flight and post-flight optical properties were obtained for each of the MISSE 2 samples with the fused silica base. Two of the back-up samples were also measured post-flight as control samples, with little change from the pre-flight measurements eight years earlier. The AO fluence for the MISSE 2 samples ranged from  $8.43 \times 10^{21}$  atoms/cm<sup>2</sup> (no cover) to  $7.08 \times 10^{21}$  atoms/cm<sup>2</sup> (0.8 mil thick Kapton cover). The fluence values are provided in Table 4 along with the pre-flight and control sample optical properties. Figure 9 is a graph of the total transmittance spectral data for flight sample 2-E5-1 (no Kapton H cover) and for a control sample. Although the reflectance did not change significantly, the diffuse transmittance increased, the specular transmittance decreased, the total transmittance decreased, and the solar absorptance increased significantly from 0.005 to 0.033-0.037.

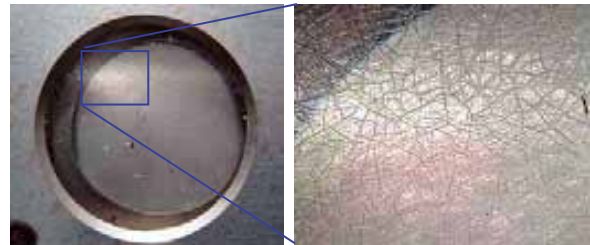


Fig. 8 Post-flight photograph of MISSE 2 DC 93-500 sample 2-E5-1 showing the crazed surface.

#### 4.3. Scattered Atomic Oxygen Characterization Experiments (MISSE 2 & 4)

When AO impinges upon a typical spacecraft surface (such as anodized aluminum) it can scatter with a lower flux and lower energy than the incoming AO. Yet scattered AO can react with, and hence, erode spacecraft components not in AO direct line of site. Therefore, it is desirable to characterize scattered AO with respect to its scattering distribution and effective erosion yield. Small (1" (2.54 cm) diameter) passive Scattered Atomic Oxygen Characterization Experiments have been designed to allow measurement of the distribution and effective erosion yield of scattered AO (see Figure 10a).

In these simple scattering chambers, ram AO passes through an aperture (0.12" (3 mm) diameter) in a  $\text{SiO}_2$ -coated polyimide Kapton H orifice plate. The AO impinges upon an aluminum disk at the bottom of the chamber and the ejected, scattered, AO can oxidize the bottom side of the Kapton H orifice plate (see Figure 10b). Sodium chloride salt particles have been dusted onto the bottom surface of the orifice plate to provide isolated protected areas. Post-flight the salt particles are washed off and profilometry is used to accurately measure the erosion as a function of ejection angle. The results of the MISSE 2 Scattered Atomic Oxygen Characterization Experiment were rather surprising in that the AO scattered almost exclusively, from the bottom aluminum plate at a 45 degree angle rather than being a cosine (Lambertian) distribution (see Figure 10c).

Table 4. MISSE 2 DC 93-500 Flight Sample Optical Property Summary Table

	DC 93-500 Flight Samples				DC93-500 Control (Back-ups)		
	2-E5-1	2-E5-2	2-E5-3	2-E5-4	Control 1	Control 2	Average
AO Fluence (atoms/cm <sup>2</sup> )	8.43 E+21	8.18 E+21	7.75 E+21	7.08 E+21	0	0	
Total Reflectance, TR	0.074	0.072	0.070	0.071	0.071	0.071	0.071
Diffuse Reflectance, DR	0.039	0.038	0.035	0.036	0.011	0.013	0.012
Specular Reflectance, SR	0.036	0.034	0.035	0.035	0.061	0.058	0.059
Total Transmittance, TT	0.893	0.892	0.894	0.894	0.924	0.924	0.924
Diffuse Transmittance, DT	0.249	0.237	0.228	0.230	0.013	0.013	0.013
Specular Transmittance, ST	0.644	0.655	0.666	0.664	0.912	0.911	0.911
Solar Absorptance, A	0.033	0.037	0.037	0.035	0.005	0.005	0.005

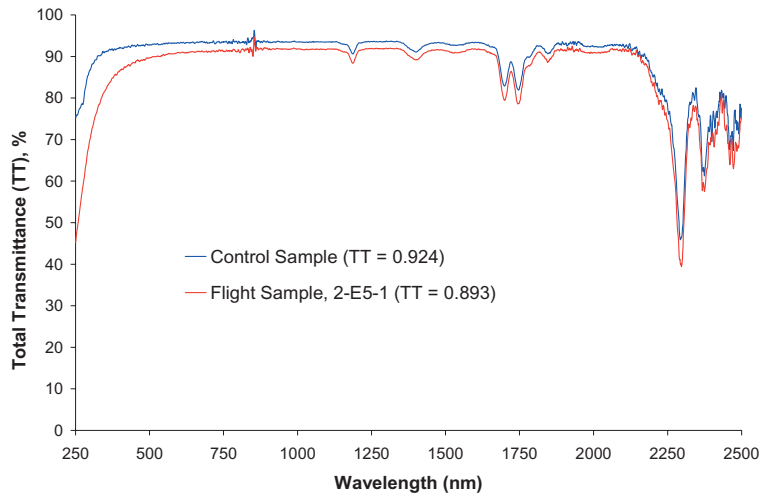


Fig. 9 Total transmittance spectral data for flight sample 2-E5-1 (no Kapton H cover) and for a back-up control sample.

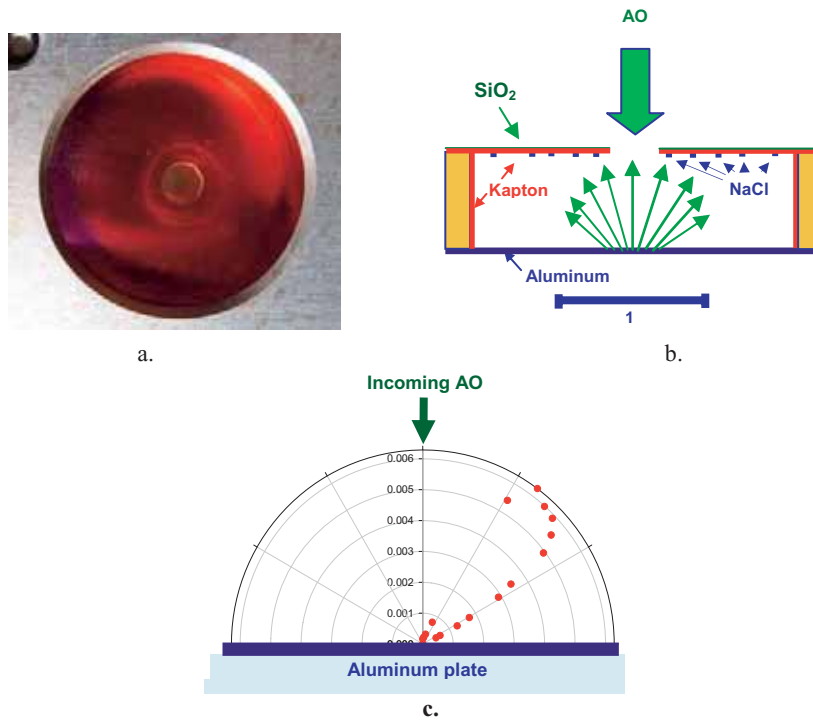


Fig. 10 MISSE 2 Scattered Atomic Oxygen Characterization Experiment: a). Post-flight photograph of the scattering chamber inside MISSE 2 E5 tray, b). Cross-section illustration of experiment, and c). Scattered AO angular erosion distribution.

The effective erosion yield for Kapton H of the scattered AO was found to be  $6.54 \times 10^{-25} \text{ cm}^3/\text{atom}$  which is 21.8% of that of LEO AO for Kapton H. Details of the experiment and the results are reported by Banks et al., 2006.[12]

#### 4.4. Double SiO<sub>x</sub>-Coated Kapton Ground to Space Erosion Correlation Experiment (Mass Loss) (MISSE 2 & 4)

##### 4.4.1. Experiment Description and Results

The ability to predict the durability of materials in the LEO environment by exposing them in ground-based facilities is important because one can achieve test results sooner, expose more types of materials, and do it much more cost effectively than to test them in flight. Flight experiments to determine the durability of groups or classes of materials that behave similarly are needed in order to provide correlation of how much time in ground-based facilities represents a selected duration in LEO for the material type of interest. An experiment was designed and flown on the ram facing surfaces of MISSE 2 (approximately 4 years of exposure in LEO) and MISSE 4 (approximately 1 year of exposure in LEO) in order to develop this type of correlation between ground-based radio frequency (RF) plasma exposure, ground-based thermal energy directed AO beam exposure, and LEO exposure for coated Kapton based on mass loss. The experiment consisted of four samples (two for each MISSE flight) of Kapton H polyimide coated with approximately 1300 angstroms of silicon dioxide by Sheldahl, Inc. Two of the samples were exposed to an AO effective fluence of approximately  $6 \times 10^{19} \text{ atoms/cm}^2$  in a RF plasma prior to flight and the remaining two were exposed to a thermal energy directed beam to an AO effective fluence of

approximately  $1 \times 10^{21} \text{ atoms/cm}^2$  prior to flight. Mass change for each sample was measured for the ground facility exposures. One of the RF plasma exposed samples, and one of the directed beam exposed samples was then flown on MISSE 2 and the remaining pair was flown on MISSE 4 for comparison. The directed beam exposed samples have not been analyzed yet but the pre-flight RF plasma exposed samples were exposed again post-flight in the RF plasma and the mass loss was recorded. This second exposure was performed in order to determine if the erosion would be the same as it had been in the same facility pre-flight, which would indicate if the sample had been damaged or not during flight, and hence if defects on the surface were those that were resident pre-flight. The slopes of the mass change vs. fluence plots were then used to develop a correlation factor for predicting the durability of coated Kapton in a RF plasma.

Results of these tests are shown in Figure 11 for the RF plasma exposed samples. Comparison of the slopes on the plots shows that there is good agreement between the pre-flight and post-flight mass loss data. The correlation factor for RF ground-based exposure to in-flight exposure for coated Kapton is approximately  $18 \pm 2$ . [13] This would indicate that exposure in a ground-based RF plasma system for a particular effective AO fluence would produce the same amount of erosion for a coated Kapton sample with approximately a factor of 18 more fluence exposure in LEO. This knowledge can be used to more accurately predict the performance of coated polymers such as coated Kapton in LEO through ground-based exposure testing.

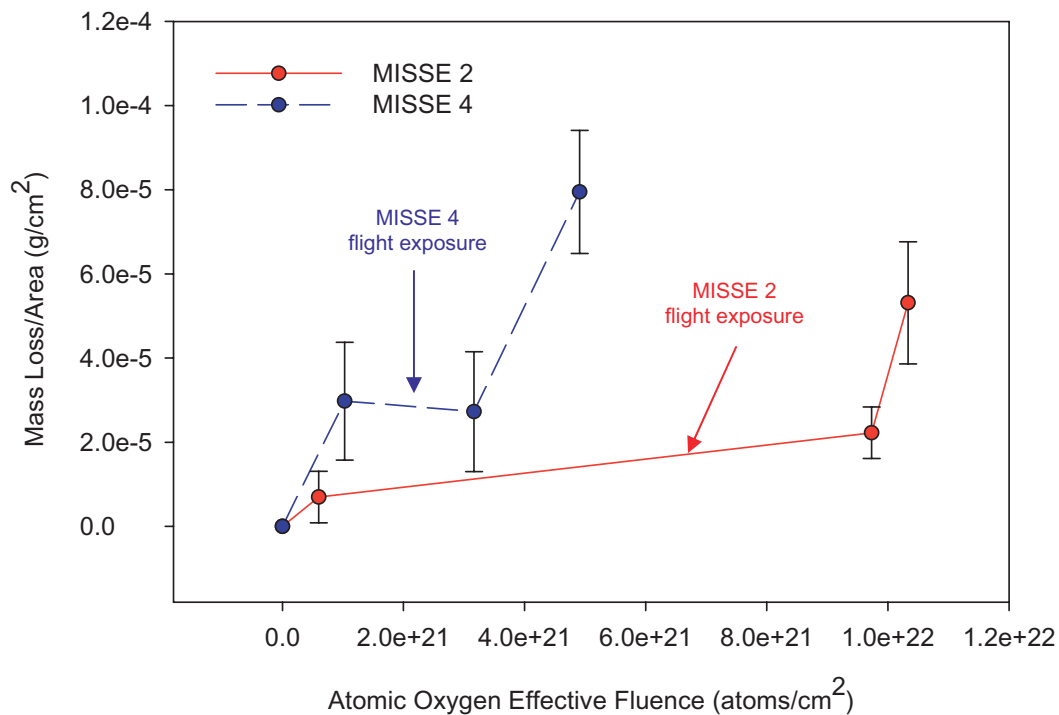
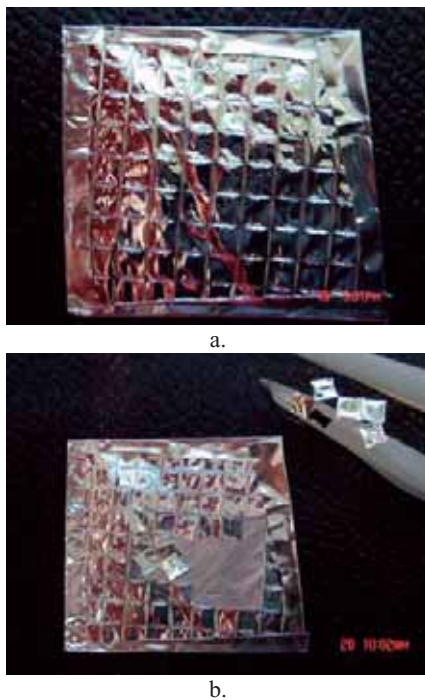


Fig. 11 Mass loss data for MISSE 2 and MISSE 4 RF plasma samples for ground pre-flight, during flight and ground post flight exposure to AO.



#### 4.4.2. Application of MISSE 2 Results to Hubble Space Telescope (HST) Servicing Mission 4 (SM4)

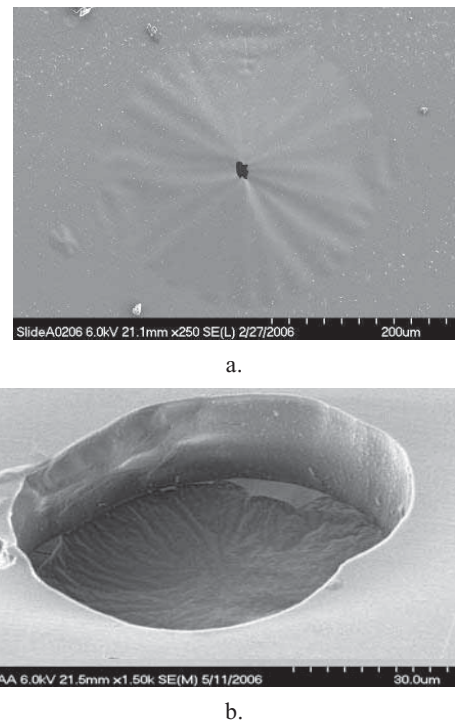
For HST SM4, it was necessary to determine if there would be a hazardous condition for astronauts and the equipment if the double aluminized Kapton thermal insulation blanket covering the outside of HST near the site of the proposed EVA would be damaged enough by exposure to the environment that pieces of the blanket would break off during the EVA. A section of the insulation blanket used on HST was exposed in an RF plasma to the point that the blanket began to break apart. In order to determine the amount of real time this would represent in LEO, the MISSE Double SiO<sub>x</sub> Coated Kapton Ground to Space Erosion Correlation Experiment correlation results were used comparing the RF plasma erosion for coated Kapton to that in LEO on MISSE. The effective fluence to make the blanket fail in the RF plasma facility was multiplied by the RF facility correlation factor 18 to obtain the space fluence that this would represent. Results were able to show that the condition of the thermal blanket at the time of servicing mission 4 would not pose a hazard for the EVA. Figure 12a and 12b show the thermal blanket after an equivalent exposure of that near the servicing mission and at failure, respectively. The fluence required to make the blanket fail was much greater than that which HST would experience prior to the servicing mission. These tests, which utilized the MISSE flight data for ground-facility calibration, directly impacted the decision to eliminate a planned SM4 EVA task (Bay 7 multilayer insulation coverage), thus freeing time to perform other crucial tasks and potentially reducing critical EVA time.



**Fig. 12** Photo of HST Kapton thermal blanket: a). Segment after effective AO exposure near that for HST servicing mission 4 and b). At point of failure showing segments of the quilted thermal blanket detaching.

#### 4.5. AO Undercutting Erosion SiO<sub>x</sub> Double-Coated Kapton H (Undercut Cavities) (MISSE 2 & 4)

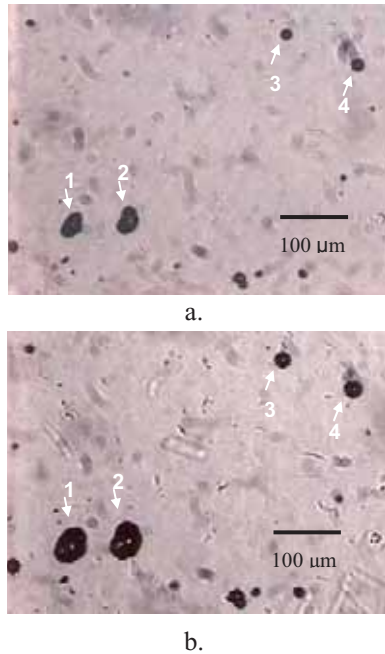
The AO Undercutting Erosion SiO<sub>x</sub> Double-Coated Kapton H investigation is similar to the Double SiO<sub>x</sub>-Coated Kapton Ground to Space Erosion Correlation Experiment, but the erosion characterization in this experiment was based on undercut cavity growth in addition to mass loss, for both in-space AO exposure (hyperthermal) and RF plasma AO exposure (thermal). There are a total of four samples of 0.001” (0.025 mm) thick Kapton H polyimide coated with ≈1300 angstroms of silicon dioxide by Sheldahl, Inc. that were flown on MISSE 2 and MISSE 4. Two of the four samples were exposed to an AO effective fluence of  $4.03 \times 10^{21}$  atoms/cm<sup>2</sup> in a RF plasma prior to flight, and the undercut cavities and mass loss were documented prior to flight. One of the pre-exposed samples and one unexposed sample were flown on MISSE 2, and one of the pre-exposed samples and one of the unexposed samples were flown on MISSE 4. Mass and defect cavities (same cavities as documented pre-flight) were characterized after MISSE LEO AO exposure and the rate of undercut growth was determined. Figure 13a shows a defect site in the protective coating of the MISSE 2 flight sample. Figure 13b shows an image of the shape of an undercut cavity post-flight.



**Fig. 13** Protective coating defect and undercut cavities: a). Undercut cavity at a protective coating defect site in MISSE 2 flight sample, and b). Undercut cavity after removal of top SiO<sub>x</sub> protective coating.

The growth of the undercut cavities was found to be significantly smaller in LEO than in a RF plasma asher environment. Figure 14 compares optical microscope photos of a pair of defect sites after two different RF plasma AO fluences. In most cases of pin window defect sites in the SiO<sub>x</sub> protective coating, the AO exposure in space did not cause the pin windows to tear or open up in any manner which suggests that the mass loss in the protected polymer is a rather uniform

and linear progression with time. Results of this experiment are reported by Snyder et al.[14]



**Fig. 14 Optical photos showing growth in undercut cavities after two fluences in a RF Plasma Asher: a).  $2 \times 10^{21}$  atoms/cm<sup>2</sup>, and b).  $4 \times 10^{21}$  atoms/cm<sup>2</sup>.**

#### 4.6. Polymer Film Thermal Control (PFTC) & Gossamer Materials Experiments (MISSE 1-4)

The main objective of the Glenn Polymer Film Thermal Control (PFTC) and Gossamer Materials experiments on MISSE 1-4 was to assess radiation and temperature effects on optical and mechanical properties of a variety of currently used and candidate thermal control materials. The materials included: traditionally used Teflon® FEP and Kapton®, various thin polymer film materials with and without coatings for light-weight inflatable and deployable structures, and polymer films with conductive coatings for charge dissipation. The development of these experiments is fully described by Dever et al., in reference 15 and is summarized here. Coatings are listed and defined in Table 5 and samples are listed in Table 6. For polymers with coatings, the material description indicates the various layers from the front space-facing surface to the back surface in the following format: front surface

coating(s) if used/ polymer/back surface coating(s). Also shown in Table 6 are the MISSE experiment PECs and whether the samples were on a carrier surface which was AO-facing (ram facing) or non-AO facing (wake facing). The various analyses that were planned for each material type are also indicated.

Tensile test samples were fabricated using a die manufactured according to specimen “Type V” under the American Society for Testing and Materials (ASTM) Standard D-638. In order to occupy the least area possible on the MISSE trays, tensile specimen holders were designed to allow the gage area of samples to receive full space exposure while the grip ends were wrapped around mandrels (~4.8 mm diameter) at the edges of the gage area and secured underneath the exposed gage area. Specimens for optical property measurements were approximately 1” (2.54 cm) diameter. Results of optical properties analysis and tensile testing of MISSE 1 and MISSE 2 specimens are summarized in the sections below. Full details on the analyses of the MISSE 1 & 2 PFTC and Gossamer Materials experiments are provided by Dever et al., 2006.[16]

#### 4.6.1. Optical Results

Tables 7 and 8 show optical properties changes for the MISSE 2 PFTC (AO-facing) samples and Gossamer Materials (non-AO-facing) samples, respectively. As shown in Table 7, the uncoated FEP/VDA sample on the MISSE 2 AO exposure tray experienced a significant decrease in thermal emittance, a likely result of AO erosion, which had caused a loss in FEP thickness for this non-coated sample. Among samples on the AO-facing holder, the most significant increase in solar absorptance was for the TOR LM material ( $\Delta\alpha \sim 0.15$ ), which had undergone significant visible darkening, as shown in Figure 15.



**Fig. 15 TOR LM, 38.1 μm thickness post-flight (left) compared to a pristine control (right).**

Table 5. Coatings used on MISSE Glenn PFTC and Gossamer Materials Samples

Coating Name	Description
VDA	Vapor deposited aluminum (VDA)
SiO <sub>x</sub> -8% PTFE (NASA GRC)	Ion beam co-sputter-deposited coating: 92 % (vol.) SiO <sub>x</sub> (where $x \approx 2$ ) and 8% (vol.) polytetrafluoroethylene (PTFE)
SiO <sub>2</sub> /Al <sub>2</sub> O <sub>3</sub> /Ag/Al <sub>2</sub> O <sub>3</sub>	Silver composite coating (CCAg) with sputter deposited coating layers of Al <sub>2</sub> O <sub>3</sub> , followed by silver, Al <sub>2</sub> O <sub>3</sub> , and SiO <sub>2</sub>
Ge	Sputter deposited germanium coating
Ag/Niobium	Sputter deposited silver followed by a niobium layer
ATO/PbO	Sputter deposited coating layers of antimony tin oxide (ATO) and lead oxide (PbO)
ATO	Sputter deposited antimony tin oxide

Table 6. Glenn Polymer Film Thermal Control and Gossamer Materials Samples on MISSE 1-4 and Planned Analyses

MISSE PEC: Direction Experiment Facing: Experiment:	MISSE 1 & 2 Ram PFTC	MISSE 1 & 2 Wake Gossamer	MISSE 3 & 4 Ram PFTC	MISSE 3 & 4 Wake Gossamer
Material				
25.4 μm CP1/VDA		O, T		O
SiO <sub>x</sub> -8%PTFE/25.4 μm CP1/VDA	O, T		O, T(3)	
25.4 μm CP1 (stack)	E [6+3]		E [18+3]	
25.4 μm CP1 strip without seam				T
25.4 μm CP1 strip with seam				T
25.4 μm Upilex-S/VDA		O, T		O, T(2)
92% SiO <sub>x</sub> -8% PTFE/25.4 μm Upilex-S/VDA	O, T		O, T(3)	
25.4 μm Upilex-S (stack)	E [6+3]		E [18+3]	
25.4 μm Kapton HN/VDA		O, T		O, T
92% SiO <sub>x</sub> -8% PTFE/25.4 μm Kapton HN/VDA	O, T		O, T(3)	
CCAg/25.4 μm Kapton HN/VDA	O, T		O, T(2)	
127 μm Kapton HN (stack)	E [2+1]		E [6+1]	
127 μm Kapton H (stack)	E [2+1]		E [6+1]	
25.4 μm Kapton E/VDA				O, T
Ge/25.4 μm Kapton XC (black)/Nomex scrim	OE [1]		OE [1]	
127 μm FEP/VDA	OE [1]			
50.8 μm FEP/VDA		O, T		T
50.8 μm FEP (stack of 10)				OT
50.8 μm FEP/VDA with 50.8 μm FEP cover layer				T
127 μm FEP/Ag/Niobium			OE [1]	
ATO/PbO/127 μm FEP/Ag/Niobium				T
ATO/ 127 μm FEP/Ag/Niobium	O			
92% SiO <sub>x</sub> -8% PTFE/127 μm FEP/VDA	O, T		O, T(3)	
92% SiO <sub>x</sub> -8% PTFE/127 μm FEP/VDA, in tension			T(3)	
92% SiO <sub>x</sub> -8% PTFE/50.8 μm FEP/VDA			O, T(3)	
25.4 μm polyphenylene benzobisoxazole (PBO)		O, T		O, T
38.1 μm TOR LM	O		O, T(2)	
Sapphire (Al <sub>2</sub> O <sub>3</sub> ) disk	W(2)		W(2)	

E = erosion yield specimen

[#] = Number of sample layers stacked together as 1 sample

O = optical properties specimen

OE = sample used for both optical and erosion yield measurements

T = tensile specimen

OT = specimen for optical and mechanical properties measurements

W = witness for contamination

(#)= Number of samples included in experiment

Table 7. Solar Absorptance and Thermal Emittance of Ram-Facing MISSE 2 PFTC Experiment Samples

Sample Description	Solar Absorptance			Thermal Emittance		
	Flight	Control	$\Delta \alpha$	Flight	Control	$\Delta \epsilon$
92% SiO <sub>x</sub> -8% PTFE/127 μm FEP/VDA	0.139	0.149	-0.010	0.858	0.862	-0.004
127 μm FEP/VDA	0.133	0.126	0.007	0.833	0.857	-0.024
ATO/127 μm FEP/Ag/Niobium	0.083	0.087	-0.004	0.868	0.872	-0.004
92% SiO <sub>x</sub> -8% PTFE/25.4 μm Kapton HN/VDA	0.368	0.361	0.007	0.699	0.698	0.001
CCAg/25.4 μm Kapton HN/VDA	0.105	0.088	0.017	0.578	0.615	-0.037
Ge/25.4 μm Black Kapton/Nomex scrim	0.539	0.502	0.037	0.877	0.874	0.003
92% SiO <sub>x</sub> -8% PTFE/25.4 μm Upilex S/VDA	0.509	0.464	0.045	0.751	0.690	0.061
92% SiO <sub>x</sub> -8% PTFE/25.4 μm CP1/VDA	0.283	0.233	0.050	0.660	0.661	-0.001
38.1 μm TOR LM*	0.287	0.136	0.151	Not Measured		

\* TOR LM was non-opaque. Solar absorptance was calculated based on reflectance and transmittance. Thermal emittance, measured with an infrared reflectometer, was not measured for this non-opaque sample.

Table 8. Solar Absorptance and Thermal Emittance of Wake-Facing MISSE 2 Gossamer Materials Experiment Samples

Sample Description	Solar Absorptance			Thermal Emittance		
	Flight	Control	$\Delta \alpha$	Flight	Control	$\Delta \epsilon$
50.8 $\mu\text{m}$ FEP/VDA	0.128	0.120	0.008	0.706	0.741	-0.035
25.4 $\mu\text{m}$ Kapton HN/VDA	0.400	0.346	0.054	0.648	0.677	-0.029
25.4 $\mu\text{m}$ Upilex S/VDA	0.487	0.437	0.050	0.649	0.675	-0.026
25.4 $\mu\text{m}$ CP1/VDA	0.255	0.223	0.032	0.544	0.637	-0.093

As shown in Table 8, polymer films, Kapton HN, Upilex S, and CP1, all showed moderate increases in solar absorptance ( $\Delta\alpha \sim 0.03$  to  $0.05$ ). Also, as shown in Table 8, all of these “non-AO” wake facing polymer films experienced significant decreases in thermal emittance, the likely result of the AO erosion. Whereas these samples were on wake-facing trays, unexpected ISS maneuvers caused brief ram-exposure of the wake-facing surfaces, resulting in exposure to some AO ( $\approx 2 \times 10^{20}$  atoms/cm<sup>2</sup>). Also, note that no optical properties are given for the PBO sample which was completely eroded/degraded post-flight.

#### 4.6.2. Tensile Results

Figure 16 shows photographs of the MISSE 1 tensile samples post-flight. Mechanical properties are provided in Table 9 for the tensile test samples which were intact post-flight. For samples already broken by the time of sample de-integration, samples were not tensile tested, and their condition is noted in the table.

### 5. MISSE 3 & 4 Experiments

Glenn has eight materials durability experiments (with a total of 71 samples) that were flown as part of MISSE 3 & 4.

Table 10 provides a list of the Glenn MISSE 3 & 4 experiments along with the on-orbit orientation, the individual experiment objective and the number of samples. As stated before, the Glenn MISSE 3 & 4 experiments were all passive experiments. The MISSE 3 & 4 trays were successfully flown and retrieved after 1 year of space exposure. Figure 17 shows on-orbit photos of both ram- and wake-facing surfaces of MISSE 3 & 4 (Trays 1 and 2, respectively). Post-flight sample documentation and analyses have begun on some of these experiments.

The following MISSE 3 & 4 experiments were very similar to experiments flown on MISSE 1 & 2, and thus are described in the MISSE 1 & 2 Experiment sections above: Double SiO<sub>x</sub>-Coated Kapton (Mass Loss), AO Undercutting Erosion (Undercut Cavities), AO Scattering Chamber, Spacecraft Silicone Experiment, Polymer Film Thermal Control & Gossamer Materials Experiments (2 experiments) and Stacked FEP Experiment (listed as part of the Polymer Film Thermal Control & Gossamer Materials Experiments). The Electromagnetic Interference Shielding experiment was the only experiment flown on MISSE 3 & 4, which was not also flown on MISSE 1 & 2. The following section describes this experiment.

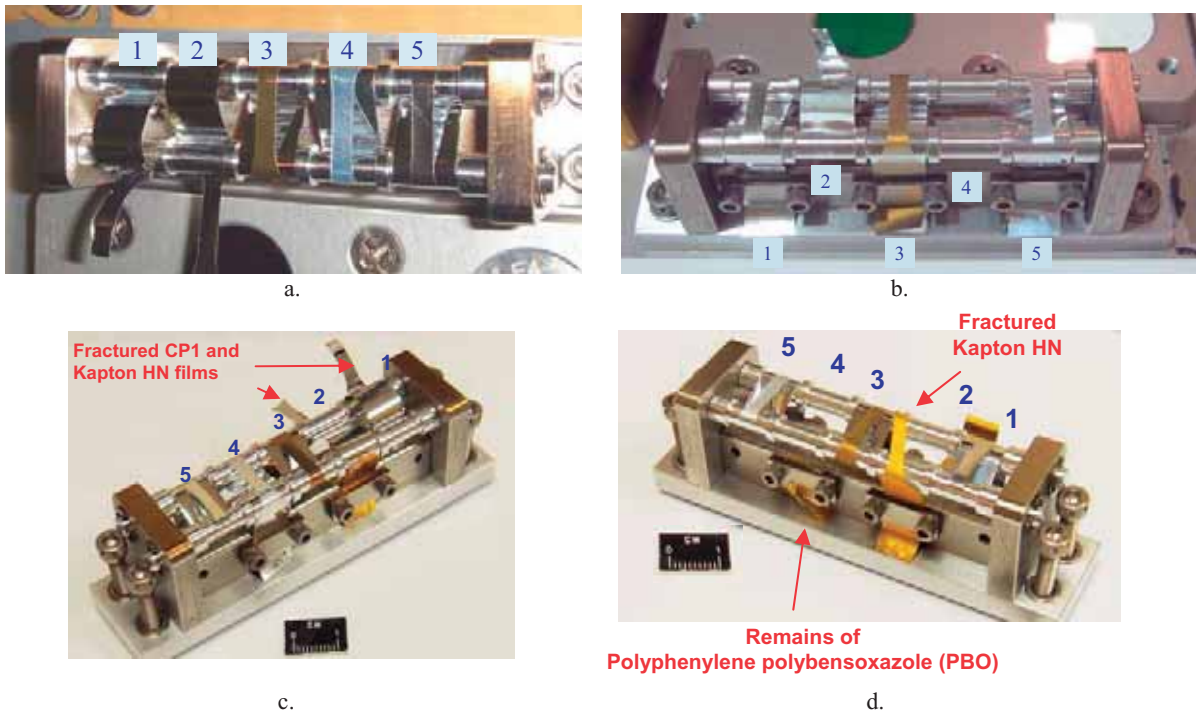


Fig. 16. Post-flight Photographs of MISSE 1 tensile holders: a). 1-Q1 at time of de-integration, b). 2-Q2 at time of de-integration, c). 1-Q1 showing broken samples, and d). 2-Q2 showing broken samples.



Table 9. Mechanical Properties of MISSE 1 (1-Q1 and 2-Q2 Holder) PFTC and Gossamer Materials Samples

Sample Description	UTS (MPa)			Elongation (%)		
	Flight	Controls, Avg. (2)	% Loss	Flight	Controls, Avg. (2)	% Loss
<i>MISSE 1, 1-Q1 Holder (AO-Facing):</i>						
1 - 92% SiO <sub>x</sub> -8% PTFE/25.4 μm CPI/VDA	Sample broken during flight due to AO erosion at coating crack					
2 - 92% SiO <sub>x</sub> -8% PTFE/25.4 μm Kapton HN/VDA	Sample broken during flight due to AO erosion at coating cracks					
3 - 92% SiO <sub>x</sub> -8% PTFE/25.4 μm Upilex S/VDA	210.5	330.2	36.2	4.1	12.6	67.5
4 - 92% SiO <sub>x</sub> -8% PTFE/127 μm FEP/VDA	13.6	19.4	29.7	62.2	234.2	73.4
5 - CCAg/25.4 μm Kapton HN/VDA	133.8	203.7	34.3	7.9	36.2	78.2
<i>MISSE 1, 2-Q2 Holder ("Non-AO" Tray):</i>						
1 - 25.4 μm CPI/VDA	88.9	87.4	-1.8	6.7	7.9	14.6
2 - 25.4 μm Kapton HN/VDA	AO eroded due to unplanned ISS maneuvers – too eroded to test					
3 - 25.4 μm Upilex-S/VDA	AO eroded due to unplanned ISS maneuvers – too eroded to test					
4 - 25.4 μm PBO	Sample observed to be broken during flight					
5 - 50.8 μm FEP/VDA	13.9	18.2	23.4	26.7	181.1	85.3

Table 10. Glenn's MISSE 3 &amp; 4 Experiments (71 Samples)

Glenn Experiment	Orientation	# Samples	Experiment Objective
Double SiO <sub>x</sub> -Coated Kapton (Mass Loss)	Ram	2	To determine AO undercutting rate dependence in space as compared to ground-facility (mass loss)
AO Undercutting Erosion (Undercut Cavities)	Ram	2	To determine AO undercutting rate dependence in space as compared to ground-facility (undercut cavities)
AO Scattering Chamber	Ram	1	To determine scattered AO erosion characteristics for undercutting modeling
Spacecraft Silicones	Ram	4	To determine changes in optical properties and nanomechanical hardness for ground-testing
Polymer Film Thermal Control (PFTC)	Ram & Wake	42	To assess radiation and temperature effects on a variety of currently used and candidate thermal control materials
Gossamer Materials	Ram & Wake	15	To assess solar exposure, radiation, and temperature effects on candidate materials for gossamer structures
Stacked FEP	Wake	1	To determine gradient in FEP embrittlement as a function of depth into the stack
Electromagnetic Interference Shielding	Wake	4	To determine the environmental durability of radiation shielding composites

#### 6. MISSE 5 Experiments (4 experiments, 105 samples)

MISSE 5 was placed in a zenith/nadir position on the ISS during the STS-114 mission, shortly after retrieval of MISSE 1 & 2. Hence MISSE 5 was launched before MISSE 3 & 4, which were launched and placed outside of ISS in August 2006 during the STS-121 mission. MISSE 5 contained two active and one passive investigations: The FTSC, an active experiment that tested the performance of 36 current and advanced generation solar cells for use on future spacecraft; The active Second Prototype Communication Satellite System (PCSat-2) that provided a communications system and tested the Amateur Satellite Service off-the-shelf solution for telemetry command and

control; and the passive MISSE 5 Thermal Blanket Materials Experiment, which consisted of several individual experiments to measure the degradation of more than 200 materials in the space environment. Figure 18 shows a pre-flight photograph of MISSE 5 and an on-orbit photo taken during the STS-114 mission. MISSE 5 was exposed to the LEO space environment for 13 months. It was retrieved during the STS-115 mission in September 2006. The flight experiment was examined post-flight at the Naval Research Laboratory in October 2006. Figure 19 shows on-orbit and post-flight photos of the Thermal Blanket Materials Experiment.

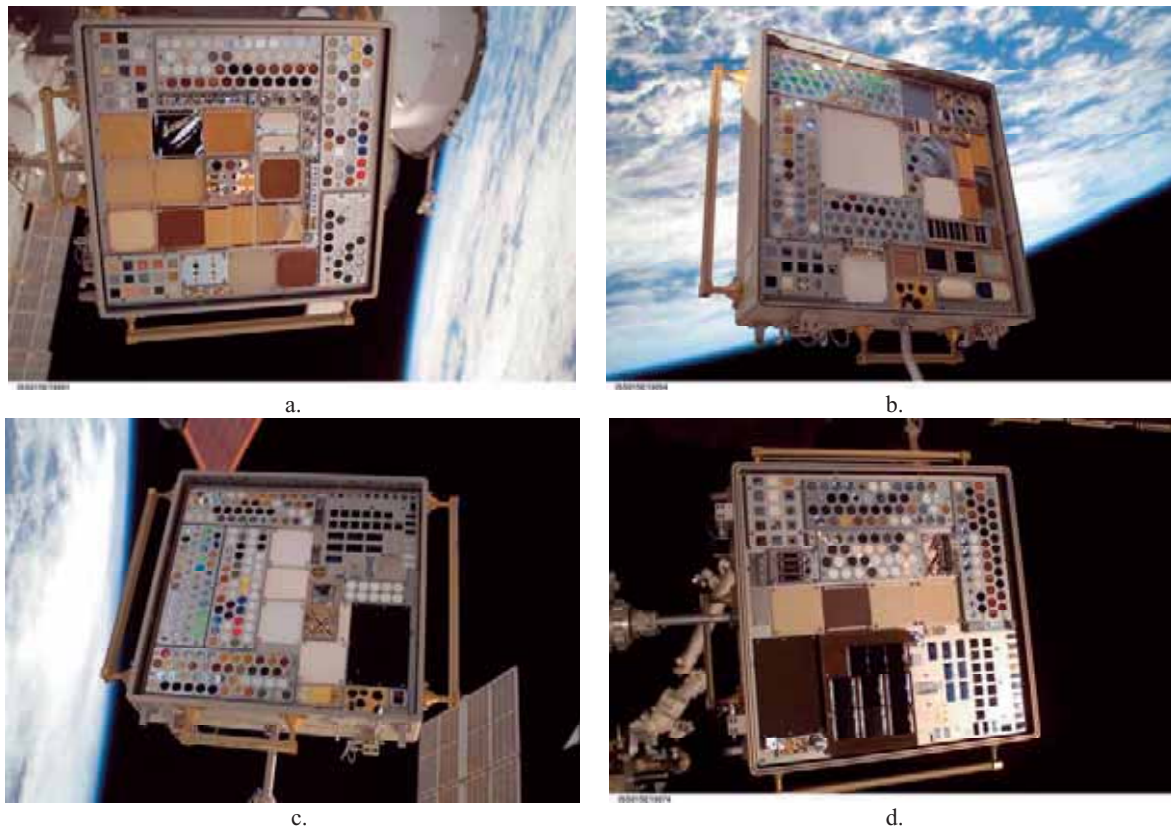


Fig. 17 On-orbit photos of MISSE 3 & 4 taken during Expedition 15: a). PEC 3 Tray 1 (ram facing), b). PEC 3 Tray 2 (wake facing), c). PEC 4 Tray 1 (ram facing), and d). PEC 4 Tray 2 (wake facing).

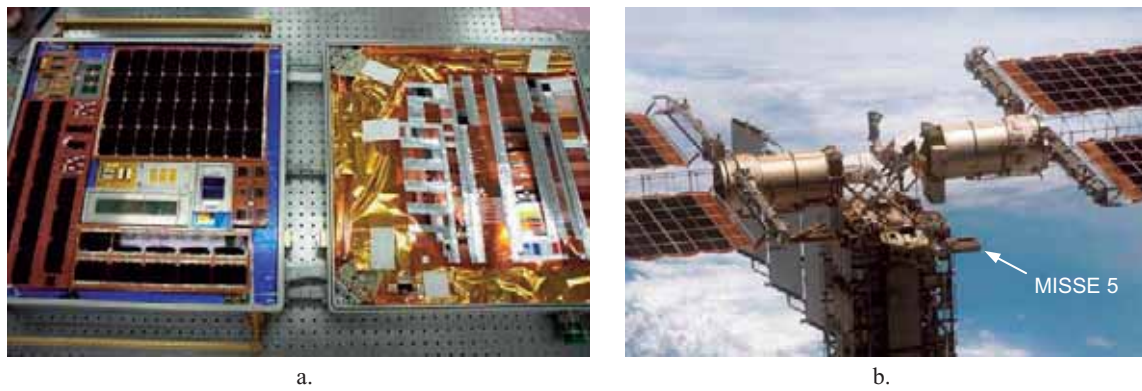


Fig. 18 MISSE 5: a). Pre-flight, and b). On-orbit photo taken during STS-114 of the zenith facing experiments.

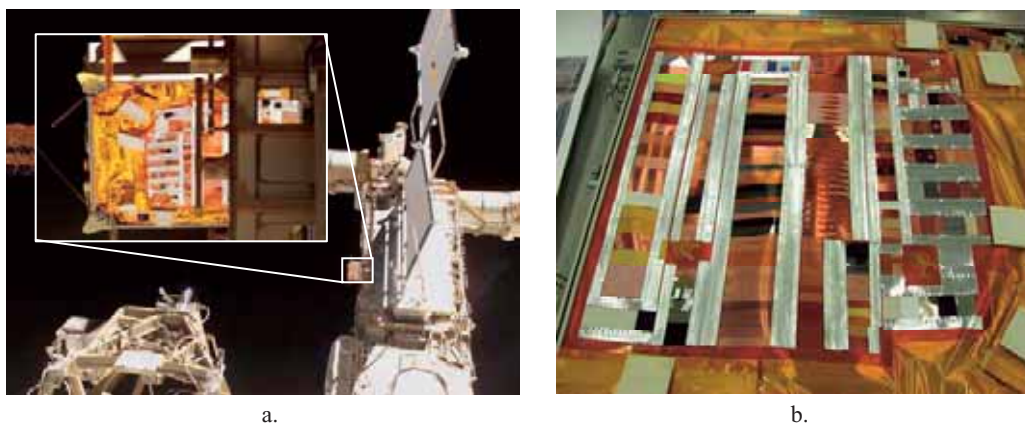


Fig. 19 MISSE 5 Thermal Blanket Experiment: a). On-orbit photo taken during STS-114, and b). Post-flight.

Table 11. Glenn's MISSE 5 Thin Film Polymers Experiments (85 Glenn &amp; 20 Team Cooperative Samples)

Glenn Experiment	# Samples	Experiment Objective
Polymer Film Thermal Control (PFTC)	33	Assess solar exposure, radiation, and temperature effects on currently used and candidate thermal control materials
PEACE Polymers	49	Determine AO erosion yield of a wide variety of polymers with low solar radiation
Spacecraft Silicones	3	Determine changes in optical properties and nanomechanical hardness for ground-testing
Team Cooperative (Fluorinated Polymers)	20	Determine space environmental durability of fluorinated polymers (w/ Boeing, NASA MSFC & Montana State University)

NASA Glenn has four thin film polymer durability experiments (with 105 samples) flown as part of the MISSE 5 Thermal Blanket Materials Experiment. These experiments are listed in Table 11 along with the number of samples and the individual experiment objective. The Thermal Blanket Materials Experiment consists of thin film or flexible samples that were taped and then stitched onto a Kapton blanket. Post-flight sample documentation and analyses have begun on the Glenn MISSE 5 experiments.

### 6.1. PEACE Polymers and Spacecraft Silicones Experiments (MISSE 5)

The MISSE 5 PEACE Polymers experiment consists of 49 - 0.5" (1.27 cm) x 1.5" (3.81) rectangular samples, with a total of 53 different polymer materials, exposed to the space environment on the exterior of ISS as part of the MISSE 5 Thermal Blanket Experiment. The majority of samples were thin film flexible polymers, as required. But, a few samples were rigid. Those samples were cut into small pieces and sandwiched between two pieces of either Kapton H or Kapton HN using Y966 acrylic adhesive, and a window was cut into the space exposed Kapton cover providing a window for exposure. Because the samples were taped and then sewn on the Kapton blanket substrate, and hence mass loss was not possible, all samples were dusted with fine salt-spray particles to provide protection from AO erosion, so that recession depth measurements could be made post-flight for Ey determination.

The MISSE 5 PEACE Polymers experiment contains the same set of polymers as the MISSE 2 experiment, with numerous additional polymers. While the MISSE 2 polymers were exposed to high AO fluence along with solar radiation exposures, the MISSE 5 polymers were exposed to low AO with very low solar radiation exposure.[17] Table 12 provides a comparison of the two experiments and their various on-orbit exposures. Hopefully, with the two experiments receiving different AO/solar radiation ratios (provided in Table 12), the combined data will provide highly desired space-flight information on the synergistic effects of solar exposure on the AO erosion of polymers. The MISSE 5 PEACE Polymers experiment has been returned to Glenn for post-flight analyses and post-flight photo-documentation has been conducted.

The Spacecraft Silicones Experiment contains three different spacecraft silicones: DC 93-500 (1.0 x 1.5" (2.54 x 3.81 cm)), CV 1144 (1.0 x 1.5" (2.54 x 3.81 cm)) and MD944 adhesive tape (0.5 x 1.5" (1.27 x 3.81 cm)). It is desired to evaluate the changes in surface hardness with space exposure and compare the data with other flight data and ground-laboratory exposed samples.

### 6.2. Polymer Film Thermal Control (PFTC) (MISSE 5)

The MISSE 5 PFTC materials experiment consists of 33 tensile specimens including many of the same types of polymer films exposed in the Glenn MISSE 1-4 Gossamer Materials and PFTC experiments. The goal of this experiment is to examine effects of the anti-solar, or nadir facing, space environment on mechanical properties changes of polymer films. Eleven types of specimens were included, each in triplicate. Configurations of these polymer film samples are shown in Table 13. Results from this experiment will be compared to ram and wake facing polymers in the MISSE 1-4 Gossamer Materials and PFTC experiments.

### 6.3. Team Cooperative Experiment (MISSE 5)

The Team Cooperative Fluorinated Polymers Experiment is a collaborative effort between NASA Glenn, NASA Marshall Space Flight Center, Boeing Phantom Works and Montana State University. The objective of this experiment was to determine the space environmental durability of fluorinated polymers in a nadir-facing orientation. Specifically, it is desired to provide evidence of degradation mechanisms, to relate degradation rates to structural features, to provide selected property measurements of the material specimens, and to correlate the results with other flight experiments. The experiment consists of 20 - 0.75" (1.91 cm) x 2.5" (6.35 cm) rectangular samples. The MISSE 5 Team Cooperative Experiment samples are listed in Table 14. Each of the samples was salt-spray dusted in a ¼" wide strip at one end, to allow for post-flight recession depth measurements to be made. Recession rate measurements using Kapton H indicate an AO fluence exposure of  $\sim 1.8 \times 10^{20}$  atoms/cm<sup>2</sup>. [17] Initial results of analyses can be found in reference 17.

Table 12. Comparison of the MISSE 2 &amp; MISSE 5 PEACE Polymers Experiments

	MISSE 2 PEACE	MISSE 5 PEACE
# Samples	41	52 (56 materials)
Ey Characterization Technique	Mass loss	Recession depth
Orientation	Ram	Nadir
AO Fluence (atoms/cm <sup>2</sup> )	8.43 x 10 <sup>21</sup>	1.81 x 10 <sup>20</sup>
Solar Exposure (Equivalent Sun Hours, ESH)	6300 (≈770 albedo, 5530 direct)	525 (≈360 albedo, 165 direct)
AO/Solar Ratio (atoms/cm <sup>2</sup> ESH)	1.3 x 10 <sup>18</sup>	3.5 x 10 <sup>17</sup>

Table 13. MISSE 5 PFTC Samples

Polymer (Film Thickness)	Sample Configurations Exposed		
	Uncoated	Coated (SiO <sub>x</sub> -8% PTFE)	Coated (other)
Teflon FEP (50.8 μm)	X	X	
Upilex S (25.4 μm)		X	
CP1 (25.4 μm)		X	
Kapton E (50.8 μm)	X		Si (front), VDA (back)
PTFE (76.2 μm)	X	X	
Kapton HN (50.8 μm)	X	X	
TOR LM (50.8 μm)	X		

Table 14. MISSE 5 Team Cooperative Experiment Sample List

MISSE 5	Chemical Name	Trade Name
B-01	Polytetrafluoroethylene (PTFE)	PTFE T-100
B-02	0.1 mil Kapton over PTFE	PTFE T-100
B-03	0.3 mil Kapton over PTFE	PTFE T-100
B-04	Fluorinated ethylene propylene (FEP)	Teflon FEP
B-05	0.3 mil Kapton over FEP	Teflon FEP
B-06	0.3 mil Kapton over THV	AMD 313
B-07	Crystalline polyvinylfluoride (PVF) w/ white pigment	White Tedlar
B-08	Ethylene-tetrafluoroethylene (ETFE) or Tetrafluoroethylene-ethylene copolymer	Tefzel LZ
B-09	Perfluoroalkoxy (PFA)	Teflon PFA LP
B-10	Tetrafluoroethylene/ hexafluoro propylene/vinylidene fluoride (THV)	AMD 313
B-11	Ethylene-chlorotrifluoroethylene (ECTFE)	Halar 300
B-12	Polyvinylidene fluoride (PVDF)	Kynar 740
B-13	Amorphous fluoropolymer (AF)	Teflon AF 1601
B-14	Polyimide (PMDA)	Kapton H
B-15	0.3 mil Kapton over PVDF	Kynar 740
B-16	Polyethylene (PE)	Alathon
B-17	Polypropylene (PP)	Profax, C28 PP
B-18	0.3 mil Kapton over PVF w/ white pigment	White Tedlar
B-19	Polychlorotrifluoroethylene (PCTFE)	Aclar, Kel-F, Neoflon M-300
B-20	Ag/Fluorinated ethylene propylene (FEP)	Silvered-Teflon

#### 6.4. The Forward Technology Solar Cell Experiment (MISSE 5)

Glenn's participation on MISSE 5 also included a substantial contribution to MISSE 5's primary experiment, the "Forward Technology Solar Cell Experiment" (FTSCE) built by the Naval Research Lab.[18] The goal of FTSCE was to rapidly put current and future generation space solar cells on orbit and provide in-situ performance measurements for these technologies. Glenn designed and built the measurement electronics and software for the FTSCE.[19] Figure 20 shows

the FTSCE measurement electronics consisting of nine data acquisition (DAC) boards and a motherboard that managed communication and data storage and measurement acquisition. Additionally, Glenn provided thin film solar cells and GaAs/Si cells for the experiment.[20] Results for many of the solar cells are detailed in reference 21 and 22.

For MISSE 7 Glenn is designing a communications interface board to route and manage communications of 20 active experiments. It provides a bi-directional RS485 bus to experiments and routes data and commands via the ISS 1553B



low rate telemetry bus to and from the ground for both 7A and 7B. Glenn also has four active experiments on MISSE 7A consisting of AO fluence monitors (discussed in Section 8.2), a Makel hydrogen/oxygen sensor, a demonstration of SiC Junction Field Effect Transistors (JFETs) designed for low-power analog and digital circuits in extreme environments, and a re-flight of the MISSE 5 FTSCE, called FTSCE-II on MISSE 7A.

#### 7. MISSE 6A & 6B Experiments (6 active & 5 passive experiments, 168 samples)

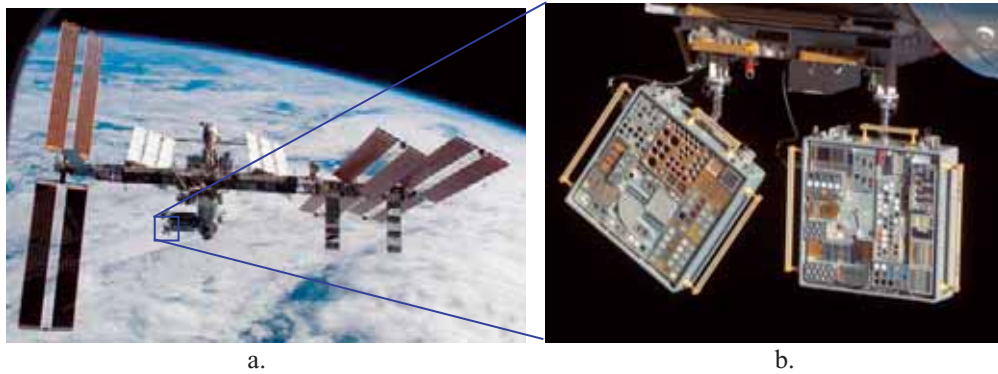
Table 15 provides a list of the Glenn MISSE 6A & 6B experiments along with the objective, number of samples, the on-orbit orientation, and whether it is an active or passive experiment. There are a total of 11 Glenn experiments, six are active and 5 are passive. As noted previously, MISSE 6 was delivered to ISS during the STS-123 mission, and both 6A and 6B were placed outside of the Columbus Module on March 22, 2008 in ram/wake orientations. Figure 21 is a photo showing the location of MISSE 6A & 6B on the Columbus module, and includes a close-up image of the ram surfaces of both PECs. These images were taken during the STS-123 mission.



**Fig. 20** Photograph of the DAC (1-9) boards and main microprocessor board (0) that perform the FTSCE electrical measurements. The metal box in the upper right is the power control unit (PCU). The metal boxes in the center route wires from the solar cells mounted on the opposite side and serve to maintain a Faraday cage around the measurement electronics.[18]

Table 15. Glenn's MISSE 6A & 6B Experiments (168 Samples)

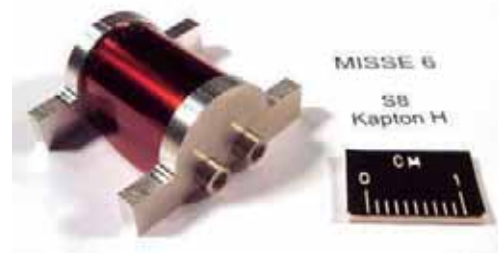
Glenn Experiment	6A or 6B Orientation	# Samples	Experiment Objective	Active / Passive
Stressed PEACE Polymers Experiment	6A Ram	27	To determine if the AO Ey is dependent upon stress	P
AO Pinhole Camera (Stressed PEACE)	6A Ram	1	To document the arrival direction of AO impinging upon the MISSE 6A ram tray	P
Solar Cells for Exploration Missions (Stressed PEACE)	6A Ram	2	To evaluate silicone (DC 93-500) coated triple junction solar cells with and without polyhedral oligomeric silsesquioxane (POSS) coatings	P
Polymer Film Tensile Experiment	6A Wake & 6B Ram	3 Active & 38 Passive	To measure radiation induced tensile failure of stressed and unstressed thin film polymer tensile samples	A & P
Indium Tin Oxide (ITO) Degradation Experiment	6A Wake & 6B Ram	4	To investigate the effects of space solar exposure on optical and electrical properties on ITO coatings	A
Cermet Coatings and Thermal Control Paints Experiments	6A Wake & 6B Ram	8	To evaluate the LEO durability of Cermet coatings	A
Atomic Oxygen Fluence Monitor	6B Ram	1	To actively measure the cumulative AO fluence arriving at the surface of the PEC	A
Scattered Space Atomic Oxygen Experiment (SSAOE)	6B Ram	4 Active & 9 Passive	To actively measure direct ram & scattered AO erosion and to passively measures angular distribution of AO scattered from inclined angle	A & P
LIDS Seals for CEV	6B Ram & Wake	50	To evaluate 3 candidate elastomers for the primary mating interface seal for LIDS	P
New Thermal Control Paints Experiment	6B Wake	15	To evaluate the LEO durability of newly developed thermal control paints	P
Polymer Strain Experiment	6B Wake	6	To measure radiation-induced strain in thin film polymers as a function of exposure time on-orbit	A



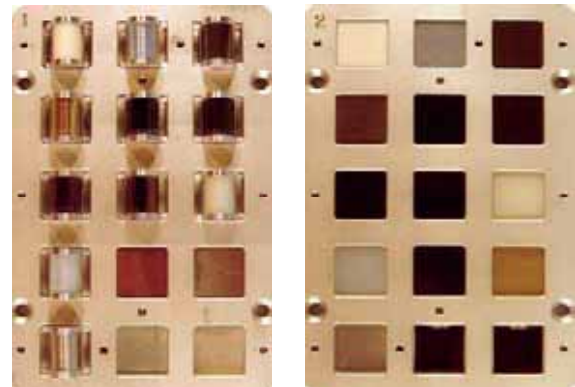
**Fig. 21 Photographs of MISSE 6A and 6B: a). Location on the ISS Columbus Module, and b). Close-up image of the ram surfaces of 6A (left) and 6B (right).**

### 7.1. Stressed PEACE Polymers Experiment (MISSE 6A)

Several retrieved MISSE 1 & 2 samples appeared to have preferentially eroded at high stress locations; an example of this is observed in several of the tensile samples in the Glenn PFTC & Gossamer Materials Experiments. Therefore, the objective of the Stressed PEACE Polymers Experiment is to compare the AO Ey of stressed and non-stressed polymers to determine if the AO erosion rate is dependent upon stress while in LEO. This experiment utilizes 2 passive experiment trays that each hold 15 – 1” (2.54 cm) square samples. Stressed sample holders were designed to fit into the 2.54 cm square area. One of the stressed sample holders loaded with a flight sample is shown in Figure 22. The experiment includes 11 stressed/non-stressed polymer pairs (PTFE, FEP, Upilex-S, CP1, Kapton CB, Kapton XC, Kapton E, Kapton H, Mylar A, low oxygen PE, and DC 93-500 silicone) and 4 polymer samples that were partially or completely eroded through all sample layers during the MISSE 2 PEACE Polymers experiment (high temperature polyimide resin PMR-15, PEI, PBI, ADC). The samples for erosion yield were thin film polymers (1 - 20 mils or 0.0254 - 0.508 mm thick) and were stacked to survive a multiple year mission (ADC was 47 mils or 1.2 mm thick). The total thickness of the stressed samples was chosen to be 20 mils (0.508 mm), so that the surface flexural stress on each sample would be the same. The samples for Ey will be characterized based on pre-flight and post-flight mass. Also included in this experiment are 2 passive solar cells with silicone and POSS coatings being evaluated for short duration or CEV-type missions, a Kapton H AO fluence witness sample and an Atomic Oxygen Pinhole Camera. The pinhole camera will document the arrival direction of AO during the mission. Atomic oxygen will pass through an orifice in a thin aluminum plate and impinge upon a Kapton H disk. The Kapton H disk will have sodium chloride salt particles on it to allow profilometry of the eroded Kapton surface to measure the amount of fluence in any particular direction. A pre-flight photograph of the Stressed PEACE Polymers Experiment is provided in Figure 23.



**Fig. 22 A Stressed PEACE Polymers Experiment stressed sample holder with the Kapton H flight sample.**



**Fig. 23 Pre-flight photograph of the Stressed PEACE Polymers Experiment.**

### 7.2. Polymer Film Tensile Experiment (MISSE 6A & 6B)

The MISSE 6 Polymer Film Tensile Experiment will measure radiation induced tensile failure of stressed and unstressed thin film polymer tensile samples. Forty-one tensile specimens were installed flat in samples holders. Twenty-nine samples were loaded with no tension and 10 samples were installed with an applied stress through a spring-loading mechanism. Examples of samples loaded under these stressed and non-stressed conditions are shown in Figure 24. Two additional samples were pulled tight when loaded. The polymer film samples in these experiments included Kapton HN, Kapton E, Kapton XC, Teflon FEP, CP1 and DC 93-500 silicone. The spring-loaded samples were mounted with stresses that represent the functional stresses expected on the James Webb Space Telescope (JWST) sunshield and potential stresses on solar sails. Depending on the application being studied, backside or front surface aluminum coatings were applied and/or other protective coatings, such as SiO<sub>x</sub>-PTFE,

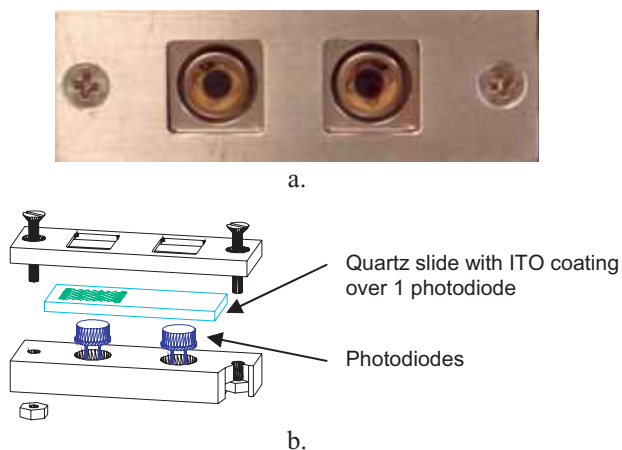
were included. The resistance across the length of three samples is actively monitored on-orbit to document tensile failure versus exposure. Seven stressed and 17 unstressed samples are mounted on MISSE 6A Tray 2 (wake facing) and are being exposed to solar radiation with minimal AO. Three stressed, 12 unstressed and 2 tightly pulled samples are mounted on MISSE 6B Tray 1 (ram facing) and are being exposed to AO and solar radiation.



**Fig. 24 Two sets of tensile test samples in fixtures on MISSE 6 Polymer Film Tensile Experiment. For each set, the left hand sample is installed in a spring-loaded fixture to apply stress and the right hand sample is installed with no tensile stress applied.**

### 7.3. Indium Tin Oxide (ITO) Degradation Experiment (MISSE 6A & 6B)

The purpose of the ITO Degradation Experiment is to investigate the effects of space solar exposure on optical and electrical properties of transparent conductive ITO coatings. Two experiment fixtures will be included on MISSE 6; one is located on MISSE 6A Tray 2 (wake facing) receiving solar radiation with minimal AO, and one is located in MISSE 6B Tray 1 (ram facing) receiving AO and solar radiation. These experiments will actively measure changes in transmittance of quartz with and without an ITO coating and will actively monitor the resistance of the ITO coating over time on-orbit. Figure 25a shows an exploded drawing of the experiment and Figure 25b is a pre-flight photograph showing a top view of one of the experiment fixtures.



**Fig. 25 Indium Tin Oxide Degradation Experiment showing: a). a breakout schematic of the experiment, and b). a photograph showing a top view of the experiment.**

### 7.4. Cermet Coatings and Thermal Control Paints Experiment (MISSE 6A & 6B)

The objective of the Cermet Coatings and Thermal Control Paints Experiment is to evaluate the in-space durability of newly developed cermet coatings and thermal control paints. It is an active experiment with two sets of four samples (each 0.5" (1.27 cm) in diameter). One set is being flown on the wake side of 6A and the second is being flown on the ram side of 6B. The cermet coatings (2 samples per set) were developed originally for solar Stirling space power systems and may have terrestrial applications.[23] One sample has a titanium and aluminum oxide cermet coating. The second sample has a molybdenum and aluminum oxide cermet coating. The thermal control paints (2 samples per set) are described in the New Thermal Control Paints Experiments section (Section 7.8). These thermal control paints were developed under the Small Business Innovative Research (SBIR) Phase II entitled "Next Generation Advanced Binder Chemistries for High Performance, Environmentally Durable Thermal Control Material Systems". In this SBIR effort, thermal control coating development was based on lithium silicate chemistry. The coatings in the Cermet Coatings and Thermal Control Paints Experiment were applied to thermally isolated nickel disks that are each instrumented with a thermocouple and the temperature data will be stored in on-board data loggers. A pre-flight photograph of one set of samples is shown in Figure 26.



**Fig. 26 Pre-flight photograph of one set of Cermet Coatings and Thermal Control Paints Experiment samples.**

### 7.5. Atomic Oxygen Fluence Monitor (MISSE 6B)

A Glenn developed Atomic Oxygen Fluence Monitor is being flown on the ram side of MISSE 6B to actively measure the AO fluence accumulated with time. The sensor utilizes two wedge shaped sheets of pyrolytic graphite, which erode with AO exposure allowing sunlight to increasingly enter into a photodiode, as shown in Figure 27. The short circuit current from a photodiode under two pyrolytic graphite wedges is compared the short circuit current from an identical photodiode, which is exposed to unobstructed sunlight in the Glenn ITO experiment to measure the erosion of the graphite. Because the erosion yield of pyrolytic graphite is known to be  $4.15 \times 10^{-25} \text{ cm}^3/\text{atom}$  from MISSE 2 [6,7] the AO fluence can be measured by knowing the ratio of short circuit currents. One significant advantage of this measurement technique is that the geometry of the pyrolytic graphite produces a linear dependence upon AO fluence using a material with a well characterized LEO erosion yield. A pre-flight photo of the Atomic Oxygen Fluence Monitor is provided in Figure 28.



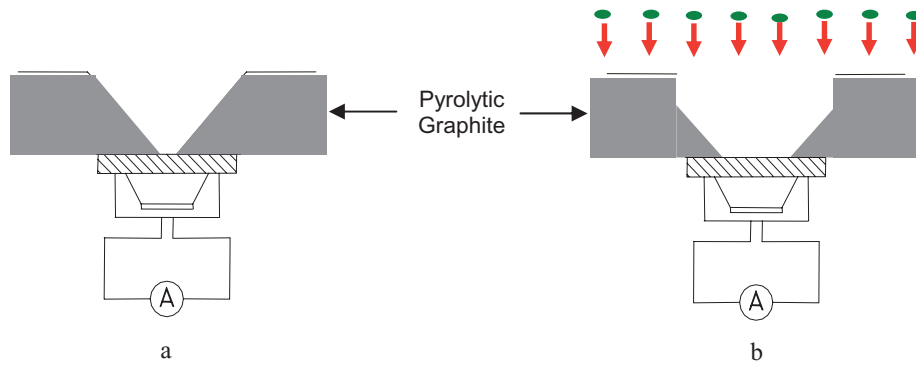


Fig. 27 Schematic diagram of the Atomic Oxygen Fluence Monitor: a). Prior to AO exposure, and b).. After AO exposure.



Fig. 28 MISSE 6B Atomic Oxygen Fluence Monitor.

#### 7.6. Scattered Space Atomic Oxygen Experiment (SSAOE) (MISSE 6B)

The objective of the SSAOE is to actively measure direct ram and scattered AO erosion in LEO, and to passively measure the angular distribution and relative erosion rate of LEO ram AO scattered from an inclined angle. The SSAOE is being flown on the ram side of MISSE 6B. To measure, and thus be able to compare direct ram and scattered AO erosion, this experiment compares the in-situ erosion of opaque diamond-like carbon (DLC) exposed to direct ram AO to DLC exposed to only thermally accommodated scattered space AO. The scattered AO experiment is set inside a cylindrical scattering chamber where ram AO scatters off a fused silica slide tilted at a 45° angle from the incoming flux. Photodiodes are placed behind DLC coated fused silica slides and the  $E_y$  of direct ram and scattered AO will be determined by increases in the transmittance of light through the eroded DLC coatings. The light sources for the ram and scattered experiments are the sun and a light bulb, respectively. Uncoated fused silica covered photodiodes are placed next to the DLC-coated fused silica covered photodiodes for light calibration. To passively measure the angular distribution of LEO ram AO scattered from an inclined angle, salt-dusted Kapton H polyimide lines a second passive cylindrical scattering chamber, again with a fused silica slide set at a 45° angle. From this chamber the effective  $E_y$  of Kapton H will be determined as a function of ejection angle. A schematic diagram of the SSAOE is provided in Figure 29. Pre-flight photos of the inside of the SSAOE are provided in Figure 30. This experiment also includes 8 ram-facing small passive samples for  $E_y$  determination (Kapton H, CV-1144 silicone, polyphosphazene, carborane-siloxane, FEP, Teflon AF-1600, HRG-3/AB (epoxy-silane), HRG-3/AO (epoxy-silane)).

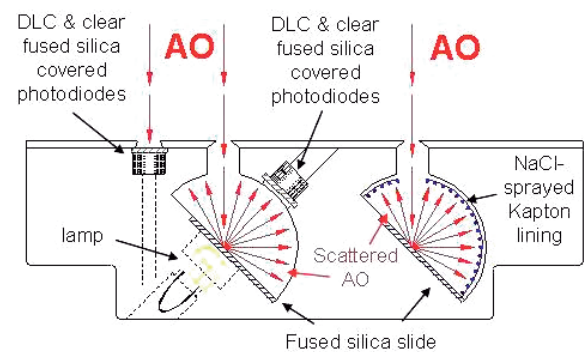
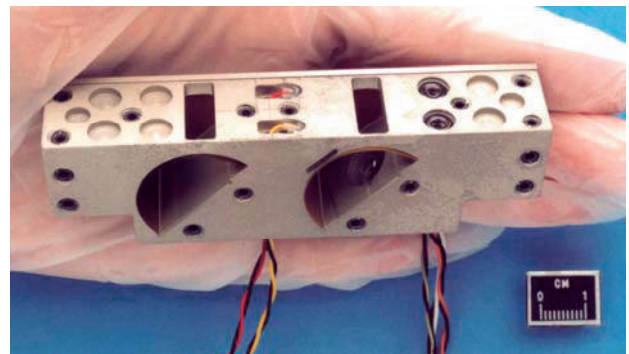


Figure 29. Schematic diagram of the SSAOE.



a.



b.

Fig. 30 Photographs of SSAOE: a). Experiment with side panel removed (the internal light bulb is visible), and b). Close-up of photodiodes inside the scattering chamber.



### 7.7. Low Impact Docking System (LIDS) Seals for Crew Exploration Vehicle (CEV) (MISSE 6B)

The objective of the LIDS Seals for CEV experiment is to expose three candidate elastomers to the space environment in LEO to evaluate their applicability as material for the primary mating interface seal for the LIDS. The mating interface seal, shown in Figure 31, is a mission critical, life support subsystem. Leakage through this interface seal results in an unrecoverable loss of breathable air for astronauts. Understanding the durability of materials that comprise LIDS seals is critical to fulfilling proposed Constellation missions. The materials used between mating spacecraft to help seal in cabin air will be exposed to the space environment prior to docking. The AO, radiation, and meteoroid and debris impacts found in space have been shown to damage seal materials. Individual space environments can be simulated on Earth. However, in-space testing is an essential part of assessing the synergistic effects of combined exposures to the LEO environment in the development of durable seal materials. The LIDS experiment on MISSE 6B utilizes two types of hardware, specimen holder A and specimen holder B. Specimen holder A, shown in Figure 32a, holds 15 o-ring samples and is being flown on both the ram and wake sides of 6B. These trays of samples will be used to evaluate the effects of the combined space environment on candidate seal materials, including leakage rate, weight, durometer & dimensional changes. Specimen holder B, shown in Figures 32b and 32c, holds 1 set of two o-rings under compression. A total of 20 sets of samples are being flown on the wake side of 6B to evaluate the seal-on-seal adhesion forces (pre & post-flight) to assess effect of long term engagement in the space environment.

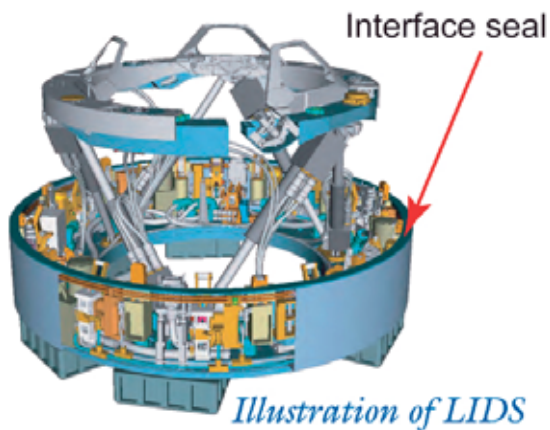
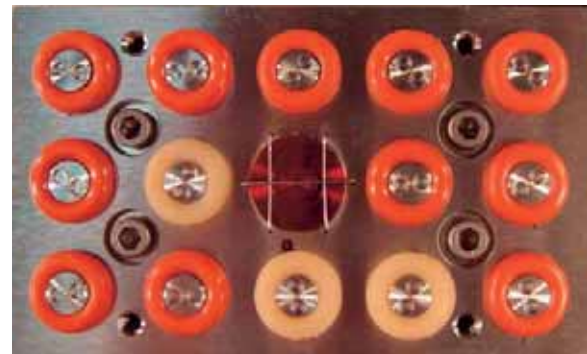


Fig. 31 Illustration of LIDS showing the primary mating interface seal.

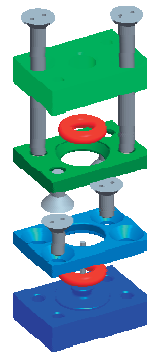
### 7.8. New Thermal Control Paints Experiments (MISSE 6B & 7B)

The objectives of the MISSE 6 & 7 New Thermal Control Paints Experiments are to evaluate the in-space durability of newly developed thermal control paints. The MISSE 6 New Thermal Control Paints Experiment is a passive experiment flown on the wake side of MISSE 6B. It consists of 15 – 1” square (2.54 cm) samples. The MISSE 7 Thermal Control

Paints Experiment is similar to the MISSE 6 Cermet Coatings and Thermal Control Paints Experiment. It is an active experiment consisting of two sets of four samples each 0.5” (1.27 cm) in diameter. One set of samples will be flown on the ram side of 7B, and the second will be flown on the wake side of 7B. The coatings are applied to thermally isolated nickel disks. In the 7B experiment each sample is instrumented with a temperature transducer and the temperature data will be sent through a communications interface to the ISS and then back to Earth by telemetry. The New Thermal Control Paints Experiment includes new thermal control paints that are being developed for light weight composite radiators for Fission Surface Power applications.[24]



a.



b.



c.

Fig. 32 LIDS Seals for CEV experiment: a). Specimen holder A with 15 o-ring samples (the center sample is a control sample covered with a Kapton H AO fluence sample), b). Exploded view of specimen holder B with 1 set of o-ring samples, and c). Pre-flight photograph of specimen holder B.

The New Thermal Control Paints Experiments thermal control paint technology is derived from two Phase II Small Business Innovative Research (SBIR) investments: 1) next generation thermal control paint matrix materials based on lithium silicate chemistry, and 2) next generation thermal control paint pigment materials based on microgel encapsulation.[25] The first effort focused on Zn assisted lithium alumino silicate nano-cluster binders that provided interconnecting channels as percolating paths for electrical conductivity. The goal was to provide increased space

radiation stability by creating binders that prevent surface charging and deep charging via percolating paths and appropriate secondary emission mechanisms for the desired reliability in high radiation environments. The nano-clusters in the matrix materials also offered the advantage of having a negative coefficient of thermal expansion (CTE), which facilitates CTE-tailoring to match the paint to the underlying composite. The second effort, developed under SBIR Phase II entitled “Robust Engineered Thermal Control Material Systems for Crew Exploration Vehicle (CEV) and Prometheus Needs” focused on developing pacified beta alumina coated with lithium silicate nanoclusters suitable for plasma spraying. The goal was to develop new thermal control material systems which can be dielectrically engineered, tailored for CTE matching to composite substrates, and which are durable to space radiation exposure at elevated operating temperatures up to 600 °C.

The passive MISSE 6B Thermal Control Paints Experiment contains thermal control material systems developed in the first SBIR effort (with Zn assisted lithium alumino silicate nano-cluster binders). In this experiment, the Zn assisted lithium alumino silicate nano-cluster binders that provided interconnecting channels were applied to aluminum and composite samples, all utilizing a heritage zinc oxide pigment. Some samples were prepared by conventional water spraying while others were prepared by plasma spraying. Selected samples were prepared having the heritage zinc oxide pigment encapsulated in glass-frit. All samples were evaluated before flight for their optical properties and any changes in optical properties will be documented by post-flight optical properties characterization. A pre-flight photograph of the MISSE 6B New Thermal Control Paints Experiment is shown in Figure 33. The MISSE 7B active Thermal Control Paints Experiment contains thermal control materials developed in the second SBIR effort on microgel encapsulated pigment particles capable of being plasma sprayed.



Fig. 33 Pre-flight photograph of the MISSE 6B New Thermal Control Paints Experiment.

#### 7.9. Polymer Strain Experiment (MISSE 6B)

One of the observations of degraded polymers of retrieved MISSE 1 & 2 flight trays was environmentally induced shrinkage that contributes to polymer cracking and/or curling.

This shrinking, cracking and curling phenomenon was observed in-space in the aluminized-Teflon FEP multilayer insulation covering the HST. On Hubble, the magnitude of cracks induced in the Teflon insulation has been observed to be on the order of meters in length. Curling of cracked insulation through environmental induced surface strain of the Teflon has allowed the underlying components to be directly exposed to the space environment; hence the insulation is no longer functioning properly for thermal control. The objective of the MISSE 6 Polymer Strain Experiment, being flown on the wake side of MISSE 6B, is to measure radiation and thermal exposure-induced strain in thin film polymers as a function of exposure time in LEO.

In the Polymer Strain Experiment six long thin opaque rectangular polymer film samples are positioned in the hardware such that one end of the polymer sample is held securely in place, while the other end is left unattached and hence free to shrink or expand. The free end is positioned inside one end of the hardware that contains a small light emitting diode (LED) and a photodiode, placed above and below the free end of the sample, respectively, as shown in Figure 34. As the polymer sample shrinks (or expands) due to environmentally induced interactions, the photodiode short circuit current will change in proportion to the strain of the sample. Small gauge wires lay over the polymer film samples to keep the samples from curling on-orbit. The experiment has been calibrated and can measure length changes as small as ~ 1%. Table 16 lists the thin film samples along with their mission relevance. A pre-flight photograph of the Polymer Strain Experiment is provided in Figure 35.

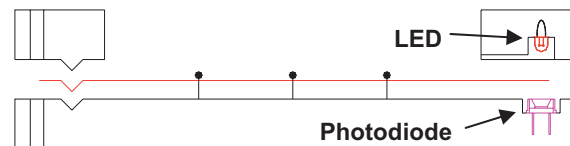


Fig. 34 Cross-section schematic view of the Polymer Strain Experiment.

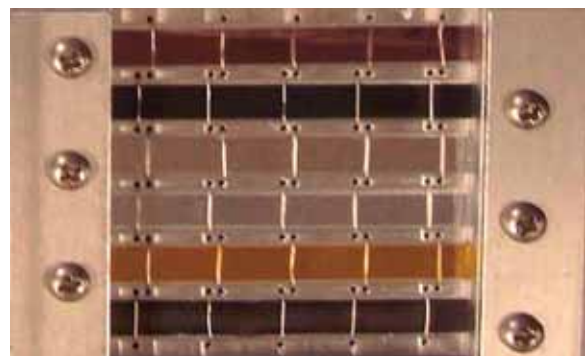


Fig. 35 Pre-flight photograph of the MISSE 6B Polymer Strain Experiment.

Table 16. MISSE 6B Polymers Strain Experiment Samples

Sample #	Material	Mission Relevance
1	Si/2 mil Kapton E/VDA/Inconel/VDA	JWST sunshield candidate
2	1 mil Kapton XC	JWST wiring insulation material
3	VDA/1 mil CP1	Solar sail material
4	2 mil FEP/VDA	Common thermal control material
5	1 mil Kapton HN/VDA	Common thermal control material
6	2 mil FEP/carbon coating	Elevated temperature FEP

Table 17. Glenn's MISSE 7A &amp; 7B Materials Experiments (120 Samples)

MISSE 7 Experiment	7A or 7B Orientation	# Samples	Objective	Active or Passive
Zenith Polymers Experiment	7A Zenith	15	To determine the effect of solar exposure on the AO Ey of fluoropolymers (high solar/low AO exposure)	P
AO Fluence Monitor	7A & 7B Ram & Wake	4	To actively measure the cumulative AO fluence arriving at the surface of the PEC	A
LIDS Seals for CEV	7A Zenith, 7B Ram & Wake	34*	To characterize the performance of candidate seal materials when subjected to the synergistic effects of the space environment in low Earth orbit (LEO)	P
Polymers Experiment	7B Ram & Wake	27	For AO Ey determination and to determine if AO erosion of high & low ash containing polymers is dependent on fluence	P
AO Scattering Chamber (Polymer Experiment)	7B Ram	1	To determine scattered AO erosion characteristics for undercutting modeling (30° tilt base)	P
AO Pinhole Camera (Polymer Experiment)	7B Ram	1	To document the arrival direction of AO impinging upon the MISSE 7 experiment tray	P
Flexural Stress Effects Experiment	7B Wake	24	To examine the role of surface flexural stress on space environment induced polymer degradation	P
New Thermal Control Paints Experiment	7B Wake	8	To evaluate the durability of next generation white thermal control paints developed under a GRC Phase II SBIR for Fission Surface Power applications	A
Spacesuit Fabrics Exposure Experiment	7B Wake	6	To identify and evaluate the effect of long term ultraviolet radiation upon pristine and dust-damaged spacesuit fabric.	P

\* Four LIDS o-ring seal samples will be flown as 1 sample on the Zenith Polymers Experiment

## 8. MISSE 7A & 7B Experiments (3 active & 6 passive, 120 samples)

Table 17 provides a list of the Glenn MISSE 7A & 7B materials experiments along with the on-orbit orientation, the objectives, number of samples and whether they are active or passive. There are a total of nine experiments; three will be active and six will be passive. As noted before, the MISSE 7A experiments will be placed in a zenith/nadir orientation and MISSE 7B will be placed in a ram/wake orientation. In addition to these materials experiments, Glenn is designing the communications interface board to route and manage communications between 20 active experiments on MISSE 7A and the ISS.

### 8.1. Zenith Polymers Experiment (MISSE 7A)

The objective of the Zenith Polymers Experiment is to determine the effect of solar exposure on the AO Ey of fluoropolymers under high solar/low AO exposure. This passive experiment will be flown in the zenith facing orientation as part of MISSE 7A, and includes 15 - 1" (2.54

cm) square samples. Seven different fluoropolymers: (PTFE, FEP, CTFE (Kel-f), ETFE (Tefzel), PVDF (Kynar), ECTFE (Halar) and PVF (clear Tedlar), are being flown along with low oxygen PE. These polymers were flown as part of the MISSE 2 and MISSE 5 PEACE Polymers experiments, and therefore the Ey for the same polymers under 3 different LEO solar/AO exposures should provide data on whether or not there is a synergistic effect of solar radiation on the AO erosion, as is currently being debated in the space environmental durability community. Samples of Al-FEP and silvered-Teflon FEP (Ag-FEP) are also being flown to determine the effect of metallization on AO Ey, and to characterize changes in optical properties. A Kapton H witness sample will be included for AO fluence characterization.

Four additional samples are included in the Zenith Polymers Experiment: JWST sunshield material (Si/2 mil Kapton E/VDA), Orion LIDS seal sample and two barrier coating samples. The Orion LIDS seal sample will include four small o-rings mounted together in a 1" (2.54 cm) area. The o-rings will be comprised of 2 types of materials: Parker



S0383-70 and Esterline ELA-SA-401. These four zenith facing o-rings are part of the LIDS Seals for CEV experiment. The barrier coating samples include two samples of coated Teflon FEP to evaluate AO and VUV barrier coatings. One sample is sectioned in half with two different thicknesses (~10 and ~40 nm) of  $\text{Al}_2\text{O}_3$  coatings on FEP. This coating will protect against oxygen atoms, but will transmit VUV light. The coating should also act as a barrier to the escape of volatile reaction products. The second sample is a multilayer coated FEP sample. The coating consists of a thin layer (~30 nm) of  $\text{TiO}_2$  on top of a thinner layer (~10 nm) of  $\text{Al}_2\text{O}_3$ . This multilayer coating should protect against AO and VUV light. These samples will be compared with an identical  $\text{TiO}_2$  (~30 nm)/ $\text{Al}_2\text{O}_3$  (~10 nm) coated FEP sample being flown in the ram facing direction as part of the MISSE 7B Polymers Experiment (see Section 8.4).

### 8.2. Atomic Oxygen Fluence Monitor (MISSE 7A & 7B)

Four Glenn Atomic Oxygen Fluence Monitors are being flown on MISSE 7 to actively measure the cumulative AO fluence arriving at the surface of the PEC. Monitors will be positioned on each of the 4 PEC surfaces (7A zenith & nadir and 7B ram & wake). Whereas the MISSE 6 AO fluence monitor uses reference photodiodes from other experiments to compare the output from the pyrolytic graphite photodiode, the MISSE 7 fluence monitor was designed with its own reference photodiode next to the pyrolytic graphite photodiode. The geometry is almost identical for each MISSE 7 AO fluence monitor diode, which should result in more accurate fluence versus time data. A photograph of a MISSE 7 AO fluence monitor is provided in Figure 36.

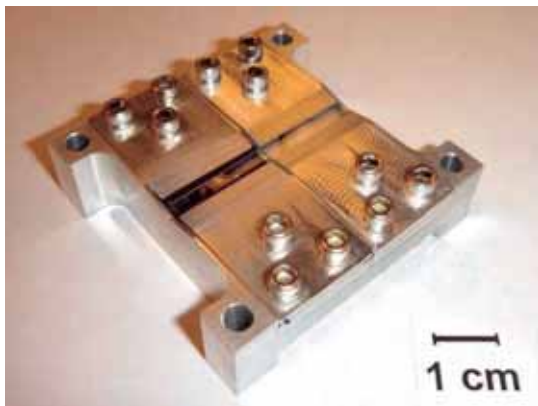


Fig. 36 MISSE 7A & 7B AO fluence monitor.

### 8.3. Low Impact Docking System (LIDS) Seals for Crew Exploration Vehicle (CEV) (MISSE 7A & 7B)

The objective of the MISSE 7 LIDS Seals for CEV experiment is similar to MISSE 6, namely to characterize the performance of candidate seal materials when subjected to the synergistic effects of the space environment in LEO. The materials used between mating spacecraft to help seal in cabin air will be exposed to the space environment prior to docking. Figure 37 shows the specimen holder that will be utilized on MISSE 7B, and will be flown on both the ram and wake sides of MISSE 7B. The differences between the MISSE 6 and 7

seals experiments are as follows: 1) MISSE 6 is flying as-received material and MISSE 7B will fly 10 seals that have received the same AO pre-treatment planned for LIDS seal, 2) ISS side of the LIDS will be an aluminum flange and hence MISSE 7B will test ISS aluminum with the correct surface coatings and finishes (12 samples), and 3) other seal applications employ RTV adhesives, therefore MISSE 7B will include one of these adhesives, thus helping with its flight qualification (6 samples). Figure 37 shows only 1 large RTV sample, but 3 samples will be flown on each holder. Kapton H AO fluence samples are also included in each holder (2 samples). As mentioned previously, the LIDS Seals for CEV experiment includes 4 small o-rings that will receive zenith exposure as part of the MISSE 7A Zenith Polymers Experiment.

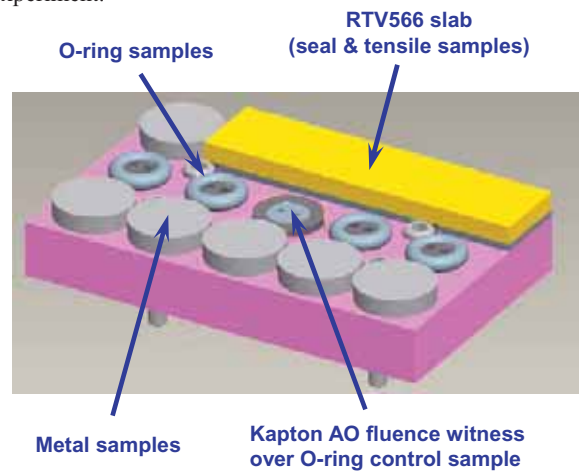


Fig. 37 MISSE 7B LIDS Seals for CEV experiment holder.

### 8.4. Polymers Experiment (MISSE 7B)

The MISSE 7B Polymers Experiment includes a variety of passive samples to investigate the effects of AO and radiation (ram samples) or radiation with minimal AO (wake samples). This experiment includes 29 samples: 26 on the ram side of 7B and 3 on the wake side of 7B. Table 18 provides a list of each of the MISSE 7B Polymers Experiment samples along with the individual sample objectives, the sample sizes and the on-orbit orientations. The Polymers Experiment is a collaborative effort with researchers from the Japan Aerospace Exploration Agency (JAXA), Towson University, Montana State University, ManTech SRS Tech., Inc., ATK, NASA Langley Research Center (LaRC), the National Institute of Aerospace, and Hathaway Brown School. Several of the samples are being co-investigated with Hathaway Brown School and Towson University as educational outreach efforts.

The MISSE 7B AO Scattering Chamber, flown as part of the MISSE 7B Polymers Experiment, will differ from the MISSE 2 and MISSE 4 AO Scattering Chamber experiments in that scattering in the 7B experiment will be off an aluminum surface that provides an angle of attack  $30^\circ$  from normal, rather than  $0^\circ$  from normal. The  $30^\circ$  tilted base will provide information on the angular distribution of scattered AO with respect to incident angle.



Table 18. MISSE 7B Polymers Experiment (29 Samples)

Sample	Sample Objective	Square (inch)
<i>Ram Side Samples</i>		
Kapton H	AO Fluence witness	1
Vespel	JAXA: For AO Ey determination (compare to Kapton H)	1
White Tedlar	To determine if AO erosion of high ash containing polymers is dependent on fluence (compare MISSE 2)	1
0.5 mil Kapton H/White Tedlar		1
1.0 mil Kapton H/White Tedlar		1
Kapton HN	To determine if AO erosion of low ash containing polymers is dependent on fluence (compare to MISSE 2 Ey)	0.75
0.5 mil Kapton H/Kapton HN		0.75
1.0 mil/Kapton H/Kapton HN		0.75
Polyethylene (low oxygen PE)	For AO Ey determination & predictive model verification	0.75
Polymethylpentene (PMP)		0.75
Polyethersulfone (PES)		0.75
Polyamide-imide (Torlon)		0.75
Polyvinyl alcohol (PVOH)		0.75
Cellulose Nitrate (CN)		0.75
Aluminized-Teflon FEP		To determine the effect of metallization on AO Ey & characterize changes in optical properties
HOPG parallel to AO/HOPG perpendicular to AO/Single crystal Class 2A diamond	Highly oriented pyrolytic graphite HOPG: for AO Ey crystal orientation determination & Diamond: verify Ey = 0	1
FEP/PTFE/POM/PEO	Towson University Education: "Quartered" salt-sprayed samples for recession depth & AO morphology studies	1
Kapton H/Mylar/PE/PG		1
AO Scattering Chamber	AO scattering chamber with 30° tilted base to check angular distribution of scattered AO	1
Atomic Oxygen Pinhole Camera	To track the arrival direction of AO during the mission	1
Kapton H	AO Fluence witness	0.75
TiO <sub>2</sub> /Al <sub>2</sub> O <sub>3</sub> /FEP	Montana State University: To study AO & VUV barrier coatings	1
CORIN (AO resistant polyimide)	ManTech SRS Tech., Inc.: To determine AO Ey	0.75
Urethane/Vectran Mesh	ATK: Demonstrate alternative AO protection for Vectran	0.75
Orion UltraFlex solar array sample (blanket & cell frontside material)	ATK: To validate the survivability in LEO key UltraFlex solar array blanket materials	1.5
Orion UltraFlex solar array sample (blanket & cell backside material)		1.5
<i>Wake Side Samples</i>		
POSS coated Kapton HN	NASA LaRC: Dust mitigation for Exploration Mission Systems	0.75
POSS coated abraded Kapton HN		0.75
CORIN (AO resistant polyimide)	ManTech SRS Tech., Inc.: To assess UV degradation without the effects of AO	0.75

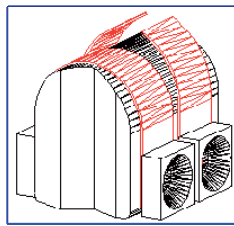
Included in the MISSE 7B Polymers Experiment are several Exploration Mission relevant samples. ATK Orion UltraFlex passive samples are being flown to validate the survivability in the LEO environment of key UltraFlex solar array blanket materials. Two 1.5" samples are being flown: one sample composed of front side blanket assembly materials, and one sample composed of backside blanket assembly materials. An ATK urethane/Vectran mesh sample will also be included for durability assessment. Also being flown are

POSS coated Kapton HN samples from NASA LaRC/National Institute of Aerospace. These samples are being investigated for lunar dust mitigation applications.

#### 8.5. Flexural Stress Effects Experiment (MISSE 7B)

The objective of the MISSE 7B Flexural Stress Effects Experiment is to examine the role of surface tensile flexural stress on space environment induced polymer cracking. The experiment includes two sets of 12 polymer thin film samples

wrapped around mandrels of two different diameters (see Figure 38). The samples, as shown in Fig. 38b from left to right, are: DC 93-500 silicone (1), SiO<sub>x</sub>/Kapton HN (1), Kapton HN/VDA (1), FEP/VDA (2), CP1/VDA (1), VDA/CP1 (1), Si/Kapton E/VDA/Inconel/VDA (3) and Kapton XC (2). The mandrel diameters are 0.25” (0.635 cm) and 0.375” (0.953 cm). The Flexural Stress Effects Experiment will be flown on the wake side of MISSE 7B. This experiment includes the same sample materials (and of the same thickness) flown as part of MISSE 6 Polymer Film Tensile Experiment. Between the two experiments, performance of flat and unstressed films can be compared with performance of tensile stressed and flexural stressed films.



a.



b.

**Fig. 38 Flexural Stress Experiment: a). Illustration of sample mounting and failure, and b). Pre-flight photo of one mandrel.**

#### 8.6. New Thermal Control Paints Experiment (MISSE 7B)

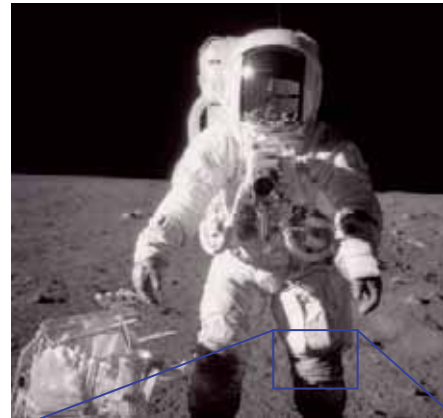
The active MISSE 7B New Thermal Control Paints Experiment is summarized along with the MISSE 6 New Thermal Control Paints Experiment in Section 7.8 above.

#### 8.7. Spacesuit Fabrics Exposure Experiment (MISSE 7B)

The Spacesuit Fabrics Exposure Experiment is a passive experiment to fly on the wake side of MISSE 7B. The objective is to evaluate the long term space exposure durability of state-of-the-art orthofabrics and Apollo era fabrics, both pristine and damaged by dust abrasion. Spacesuits for use at a future lunar outpost are envisioned to be used for a much longer time than those for Apollo. Indeed, one concept is to have the spacesuits reside outside the lunar habitat and have the astronauts climb in through the back of the spacesuit. In such a case, the suit itself would be exposed to the ultraviolet (UV) radiation environment for a long time, even when not in use. It is well known that lunar dust is a serious issue. Figure 39 shows Apollo 12 astronaut Alan Bean in a heavily dust covered spacesuit. Therefore, there is a concern of UV radiation degradation of both pristine, and dust abraded, spacesuit fabrics.

A total of six 0.47” (12 mm) square fabric samples will be flown. Three state-of-the-art orthofabrics will be flown, including one pristine sample, one lightly dust damaged

sample, and one heavily dust damaged sample. The dust damaged samples will be abraded with lunar simulant. Three Apollo era fabrics will be flown, including one pristine sample, one lightly dust damaged sample (lunar simulant), and one sample damaged by actual lunar dust (a section of the left knee of Alan Bean’s Apollo 12 spacesuit). The fabric samples were documented photographically, and by both atomic force microscopy (AFM) and scanning electron microscopy (SEM), prior to flight. These techniques were chosen because they are non-destructive analysis techniques. Upon return, the coupons will be re-photographed and re-submitted for AFM and SEM analyses to identify and evaluate the effect of long term UV radiation upon the fabric. A photograph of the Spacesuit Fabrics Exposure Experiment is provided in Figure 40.



**Fig. 39 Apollo 12 photograph showing the extent of lunar dust on Alan Bean’s spacesuit; with a close-up of his left knee.**



**Fig. 40 Spacesuit Fabrics Exposure Experiment: the top row contains modern orthofabrics and the bottom row contains Apollo era  $\beta$ -cloth. The bottom middle sample is from Alan Bean’s Apollo 12 spacesuit left knee.**

## 9. Summary and Conclusions

This paper introduces space environmental durability issues in LEO and provides an overview of Glenn's 39 passive and active MISSE 1-7 materials flight experiments. The Glenn MISSE experiments address AO effects such as erosion and undercutting of polymers, AO scattering, stress effects on AO erosion, and in-situ AO fluence monitoring. Several experiments address solar radiation effects such as radiation induced polymer shrinkage, stress effects on radiation degradation of polymers, and radiation degradation of ITO coatings and spacesuit fabrics. Experiments also address combined AO and solar radiation effects on thermal control films, paints and cermet coatings. Experiments with Orion CEV seals and UltraFlex solar array materials are also being flown. Several experiments, such as the MISSE 2 & 4 Double SiO<sub>x</sub>-Coated Kapton Ground to Space Erosion Correlation Experiments were designed to provide ground-facility to in-space calibration data thus enabling more accurate in-space performance predictions based on ground-laboratory testing. Numerous experiments, such as the MISSE 6A Stressed PEACE Polymers and the MISSE 6B Polymer Strain Experiment were designed based on observations of materials damage from prior retrieved MISSE experiments. The MISSE 2 PEACE Polymers experiment contains the widest variety of well-documented polymers exposed to identical long duration LEO AO conditions, and provides AO Ey data for 39 different polymers. Results from Glenn MISSE experiments have impacted spacecraft missions, such as the HST SM4 and Exploration Mission spacecraft such as COTS.

## 10. Acknowledgments

The authors would like to acknowledge and thank numerous additional principal and co-investigators for their involvement in the Glenn MISSE experiments, and for their contributions to this paper. In particular we thank: Bruce Steinetz (NASA Glenn), Henry de Groh (NASA Glenn), Aaron Snyder (NASA Glenn), James Gaier (NASA Glenn), Frank Lam (Jacobs Sverdrup), Debbie Waters (ASRC Aerospace Corp. at NASA Glenn), Phil Jenkins (Naval Research Laboratory), Mike Krasowski (NASA Glenn), Norman Prokop (NASA Glenn), Patty Hunt (Hathaway Brown School) and the entire PEACE team. In addition, with great appreciation we acknowledge the many students and NASA summer interns who have made significant contributions to many of these experiments over the years.

We also gratefully acknowledge the opportunity to fly these MISSE experiments and give our thanks to the MISSE program sponsors and managers. In particular, we would like to thank the following for their support of our experiments: Gary Pippin (Boeing Phantom Works), Bill Kinard (Retired, NASA Langley Research Center), Rob Walters (Naval Research Laboratory) and Phil Jenkins (Naval Research Laboratory). Lastly, we would also like to acknowledge that part of this work was sponsored by NASA Glenn Research Center's Independent Research & Development (IR&D) Program.

## 11. References

- [1] B. A. Banks, K. K. de Groh and S. K. Miller, "Low Earth Orbital Atomic Oxygen Interactions with Spacecraft Materials," Materials Research Society Symposium Proceedings 2004, NN8.1; also NASA/TM-2004-213400, November 2004.
- [2] J. A. Townsend, P. A. Hansen, J. A. Dever, K. K. de Groh, B. A. Banks, L. Wang and C. He, "Hubble Space Telescope Metallized Teflon FEP Thermal Control Materials: On-Orbit Degradation and Post-Retrieval Analysis," High Performance Polymers 11 (1999) 81-99.
- [3] J. Townsend, C. Powers, M. Viens, M. Ayres-Treusdell and B. Munoz, "Degradation of Teflon FEP following Charged Particle Radiation and Rapid Thermal Cycling" Proc. Space Simulation Conf. NASA CR-1998-208598, 201-209.
- [4] G. Pippin, "Summary Status of MISSE-1 and MISSE-2 Experiments and Details of Estimated Environmental Exposures for MISSE-1 and MISSE-2," AFRL-ML-WP-TR-2006-4237, Technical Operations Support (TOPS) II (Delivery Order 0011), Air Force Research Laboratory, Wright-Patterson Air Force Base, OH 45433-7750
- [5] J. A. Dever, S. K. Miller, E. A. Sechkar and T. N. Wittberg, "Preliminary Analysis of Polymer Film Thermal Control and Gossamer Materials Experiments on MISSE 1 and MISSE 2," Proceedings of the 2006 National Space & Missile Materials Symposium in conjunction with the 2006 MISSE Post-Retrieval Conference, June 26-30, 2006, Orlando, FL.
- [6] K. K. de Groh, B. A. Banks, C. E. McCarthy, R. N. Rucker, L. M. Roberts and L. A. Berger, "MISSE 2 PEACE Polymers Atomic Oxygen Erosion Experiment on the International Space Station," High Performance Polymers, 2008 (in-print).
- [7] K. K. de Groh, B. A. Banks, C. E. McCarthy, R. N. Rucker, L. M. Roberts and L. A. Berger, "MISSE PEACE Polymers Atomic Oxygen Erosion Results," Proceedings of the 2006 National Space & Missile Materials Symposium, Orlando, Florida, June 26 - 30, 2006; also NASA TM-2006-214482, November 2006.
- [8] B. A. Banks, K. K. de Groh and J. A. Backus, "Atomic Oxygen Erosion Yield Predictive Tool for Spacecraft Polymers in Low Earth Orbit," NASA TM, 2008 (in-print).
- [9] A. H. Stambler, K. E. Inoshita, L. M. Roberts, C. E. Barbagallo, K. K. de Groh and B. A. Banks, "Ground-Laboratory to In-Space Atomic Oxygen Correlation for the PEACE Polymers," Proceedings of the 9th International Space Conference "Protection of Materials and Structures From Space Environment" (ICPMSE-9), May 19-23, 2008 in Toronto, Canada, 2008 (in-print).
- [10] K. K. de Groh and T. A. McCollum, "Low Earth Orbit Durability of Protected Silicone for Refractive Photovoltaic Concentrator Arrays," Journal of Spacecraft and Rockets, Vol. 32, No. 1, Jan-Feb 1995, 103-109.
- [11] K. K. de Groh, B. A. Banks and D. Ma, "Ground-to-Space Effective Atomic Oxygen Fluence Correlation for

- DC 93-500 Silicone," *Journal of Spacecraft and Rockets*, Vol. 43, No. 2, March-April 2006, 414-420.
- [12] B. A. Banks, K. K. de Groh and S. K. Miller, "MISSE Scattered Atomic Oxygen Characterization Experiment," *Proceedings of the 2006 National Space & Missile Materials Symposium*, Orlando, Florida, June 26 - 30, 2006; also NASA TM-2006-214355, May 2006.
- [13] S. K. Miller, B. A. Banks and G. Tollis, "MISSE Results Used for RF Plasma Ground Testing to Space Correlation for Coated Kapton," *Proceedings of the 9th International Space Conference "Protection of Materials and Structures From Space Environment" (ICPMSE-9)*, May 19-23, 2008, Toronto, Canada, 2008 (in-print).
- [14] A. Snyder, B. A. Banks and D. L. Waters, "Undercutting Studies of Protected Kapton H Exposed to In-Space and Ground-Based Atomic Oxygen," *Proceedings of the 10th International Symposium on Materials in a Space Environment & 8th International Conference on Protection of Materials and Structures in a Space Environment*, Collioure, France, June 19 - 23, 2006, ESA SP-616, Sept. 2006.
- [15] J. Dever, S. Miller, R. Messer, E. Sechkar and G. Tollis, "Exposure of Polymer Film Thermal Control Materials on the Materials International Space Station Experiment (MISSE)," AIAA 2001-4924, October 2001; also NASA TM-2002-211363, February 2002.
- [16] J. A. Dever, S. K. Miller and E. A. Sechkar, "Effects of the Space Environment on Polymer Film Materials Exposed on the Materials International Space Station Experiment (MISSE 1 and MISSE 2)," *Proceedings of the 10th International Symposium on Materials in a Space Environment & 8th International Conference on Protection of Materials and Structures in a Space Environment*, Collioure, France, June 19 - 23, 2006, ESA SP-616, Sept. 2006.
- [17] M. Finckenor, K. de Groh, T. Minton, A. Brunsvold and G. Pippin, "Post-Flight Analysis of Selected Fluorocarbon and other Thin Film Polymer Specimens Flown on MISSE-5," Presentation given at the National Space and Missiles Materials Symposium (NSMMS), held June 25-29, 2007 in Keystone, Colorado.
- [18] R. J. Walters, J. C. Garner, S. N. Lam, J. A. Vazquez, W. R. Braun, and R. E. Ruth, J. R. Lorentzen, R. Bruninga, P. P. Jenkins, J. M. Flatico, D. M. Wilt, M. F. Piszczor, L. C. Greer, and M. J. Krasowski, "Materials on the International Space Station Experiment-Forward Technology Solar Cell Experiment," NASA CP-2005-213431, 2005.
- [19] M. Krasowski, L. Greer, J. Flatico, P. Jenkins, D. Spina, "A Hardware and Software Perspective of the Fifth Materials on the International Space Station Experiment (MISSE-5)," NASA Technical Memorandum, NASA TM-2005-213840, August, 2005.
- [20] D. Wilt, M. Piszczor, M. Krasowski, P. Jenkins, R. Walters and S. Messenger, "Advanced Solar Cell Technology Testing Aboard Materials International Space Station Experiment 5 (MISSE5)," *Proceedings of the 2nd International Energy Conversion Engineering Conference*, AIAA-2004-5580, 2004.
- [21] P. P. Jenkins, R. J. Walters, L. C. Greer, M. J. Krasowski, J. M. Flatico, CDR R. Bruninga (Ret.), CDR D. Myre, J. R. Lorentzen, K. Crist, K. Edmondson and A. Boca, "In-Flight Performance Of III-V Multi-Junction Solar Cells From The Forward Technology Solar Cell Experiment," *Proceedings of the 33rd IEEE Photovoltaics Specialists Conference*, May 11-15, 2008, to be published.
- [22] D. Wilt, A. Pal, S. Ringel, E. Fitzgerald, P. Jenkins and R. Walters, "Final Results from the MISSE5 GaAs on Si Solar Cell Experiment", *Proceedings of the 33rd IEEE Photovoltaics Specialists Conference*, May 11-15, 2008, to be published.
- [23] D. A. Jaworske and T. Raack, "Cermets Coatings for Solar Stirling Space Power," *Thin Solid Films*, Vol. 469-470, 2004, 24-30.
- [24] D. A. Jaworske, D. E. Beach and J. L. Sanzi, "Heat Rejection Systems Utilizing Composites and Heat Pipes: Design and Performance Testing," *5th International Energy Conversion Engineering Conference*, St. Louis, MO, AIAA-2007-80969, June 2007.
- [25] D. A. Jaworske, J. A. Dever and M.S. Deshpande, "Initial Evaluation of White Thermal Control Paints Incorporating Lithium Silicate Chemistry," *48th AIAA/ASME/ASCE/AHS/ASC Structures, Structural Dynamics, and Materials Conference 23 - 26 Apr 2007*, Waikiki, Hawaii, AIAA-2007-2200, April 2007.



## SM/SEED SPACE EXPOSURE EXPERIMENT OF BALL BEARING LUBRICATED BY TRIBO-COATING

Koshi ADACHI<sup>1</sup> and Koji KATO<sup>2</sup>

<sup>1</sup> School of Mechanical Engineering, Tohoku University, Sendai 980-8579, Japan

<sup>2</sup> College of Engineering, Nihon University, Koriyama 963-8642, Japan

Degradation of friction properties of three types of ball bearings (conventional vacuum ball bearing and two types of ball bearings lubricated by tribo-coating of indium) exposed to real space environment was investigated on SM/SEED experiment. Well-friction properties of ball bearings lubricated by tribo-coating of indium were maintained for one year exposure to real space field. Even after degradation of ball bearing due to exposure to the real space environment, friction properties could be restored by in-situ tribo-coating.

**Keywords:** Tribo-coating, SM/SEED, In-situ and On-demand Restoration, Tribology

### 1. Introduction

Lubrication is one of the most important key technologies for the reliability and long life of space systems.

In the present space systems, solid lubricants such as lead, indium, silver, gold and molybdenum disulfide are pre-coated with certain thickness before assembling. The life of present space systems is, therefore, determined by the wear life of the coating of lubricant.

If solid lubricants could be restored in-situ and on-demand during operation even under exposure to real space environment, the life of the space systems could be extended. It is believed that "a self-restoring lubrication system with in-situ and on-demand controllable lubrication method" is needed for the future space systems to improve reliability and overcome unexpected tribological troubles in space.

To reply to the requirements, a new solid lubrication method called "Tribo-coating" has been proposed [1-3]. And it has been clarified that this method gives the unique advantage of excellent tribological performance such as low friction and semi-permanent lifetime by in-situ and on-demand forming of an optimum tribo-coating film [1-3].

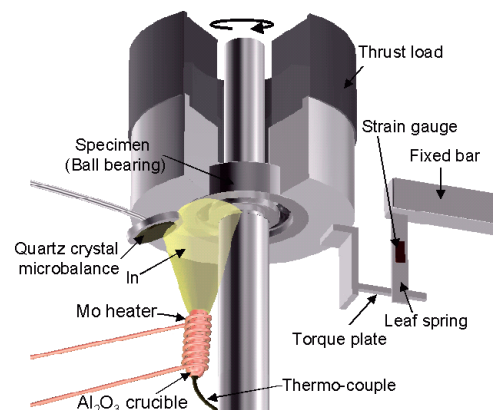
The purposes of this paper are to clarify the effect of the real space environment such as radiation and atomic oxygen etc. on friction properties of ball bearings lubricated by the tribo-coating of indium on SM/SEED space exposure experiment and to show possibility of restoration of lubricant which might be damaged by exposure to the real space environment.

### 2. Experimental apparatus and specimens

Fig. 1 shows the schematic illustration of friction apparatus with in-situ tribo-coating system, where solid lubricant (indium) is evaporated from the Al<sub>2</sub>O<sub>3</sub> crucible by heating of the Mo heater in vacuum of

10<sup>-6</sup> Pa during sliding. Two types of ball bearings coated by the tribo-coating of indium and conventional vacuum ball bearing coated by sputtered MoS<sub>2</sub> with special retainer of PTFE as shown in Table 1 were used as one set of specimens. Three sets were placed on a panel of SM/SEED (Service Module/Space Environment Exposure Device) [4], and it was attached on the outside of Russian Service Module in the International Space Station (Fig. 2). Individual set was exposed to the real space environment for about one year (10 months), two years (28 months) and three years (46 months). After experiment, each set was returned to earth to evaluate friction properties by using friction apparatus as shown in Fig. 1.

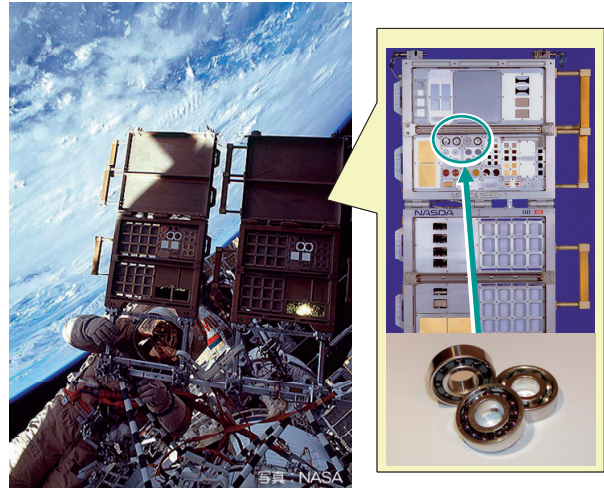
On the other hand, ground environment exposure test (Atomic Oxygen, Ultra Violet, EB (Electron Beam) bombardment) were conducted for each set to compare the friction properties against on orbit exposure effect.



**Fig. 1 Schematic illustration of friction apparatus for ball bearings with tribo-coating system**

**Table 1 Specification of three types of ball bearings used in the test**

ID	BR1	BR2	BR3
Size (t=8 mm)			
Inner & Outer race	SUS440C		
Ball	Si <sub>3</sub> N <sub>4</sub>		SUS440C (MoS <sub>2</sub> )
Retainer	—	SUS440C	Fluorine resin
Lubricant	Tribo-coated In		MoS <sub>2</sub> Fluorine resin
Weight	17.32 g	18.21 g	18.00 g

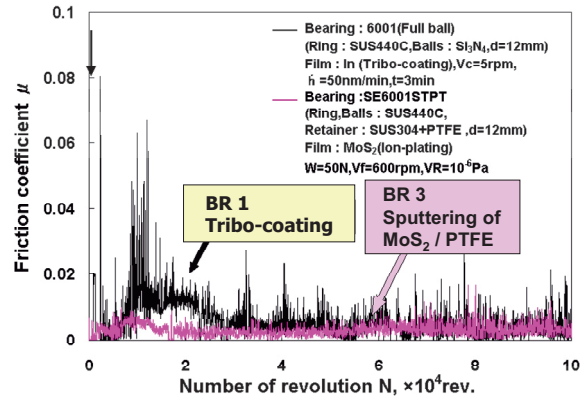


**Fig. 2 Installation of a SM/SEED unit**

**3. Experimental results**

**3.1 Friction properties of ball bearings before exposure**

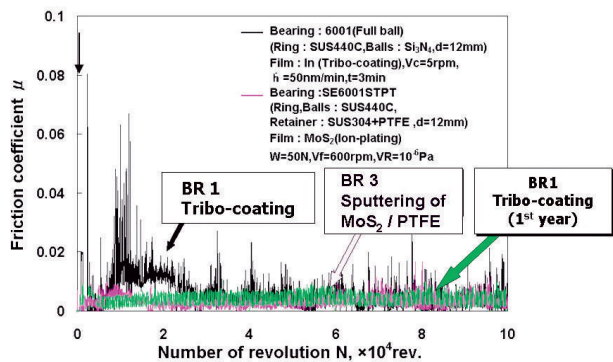
Figure 3 shows a representative friction curves of ball bearings lubricated by tribo-coating of indium (BR1) and conventional vacuum ball bearing (BR3). Friction coefficient of ball bearing lubricated by tribo-coating (BR1) increases and decreases after evaporation of indium at the initial running-in stage, and it reaches a low value. Although some variation of friction are observed, Tribo-coating of indium gives sufficient low value of friction coefficient (=0.005) which is similar as that of conventional vacuum ball bearing (BR3).



**Fig. 3 Representative friction curves of ball bearings of BR1 and BR3**

**3.2 Effect of exposure in space environment on friction properties of the ball bearings**

Friction curves of ball bearings of BR1 and BR3 before and after exposure in space environment for one year are shown in Figs. 4 and 5, respectively. It is clearly seen that friction coefficients of both bearings after one year exposure are kept similar values as those of before exposure. It is, therefore, considered that tribo-coating of indium is useful lubricant for space systems, which works for short time less than one year.



**Fig. 4 Friction curves of ball bearings of BR1 before and after exposure in the space environment for one year**

Figures 6 and 7 show effect of exposure period on friction properties of two types of ball bearings (BR1 and BR3), respectively. Although friction coefficients are kept low values after one year exposure as mentioned before, those values increase by exposure for more than two years. It is sure that life time of both bearings under exposure condition in space is less than two years. Indeed, friction property of conventional vacuum ball bearing (BR3) after two years exposure shows quite unstable with high variation of friction coefficient.

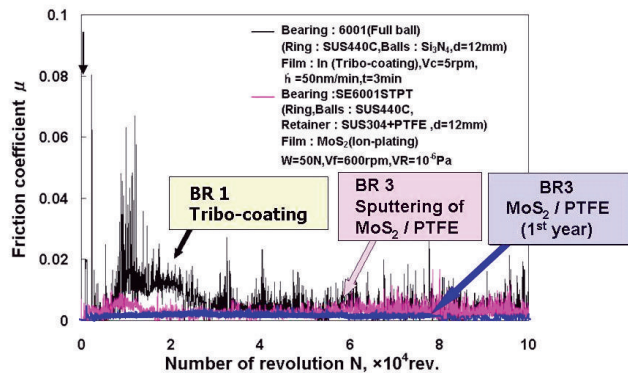


Fig. 5 Friction curves of ball bearings of BR3 before and after exposure in the space environment for one year

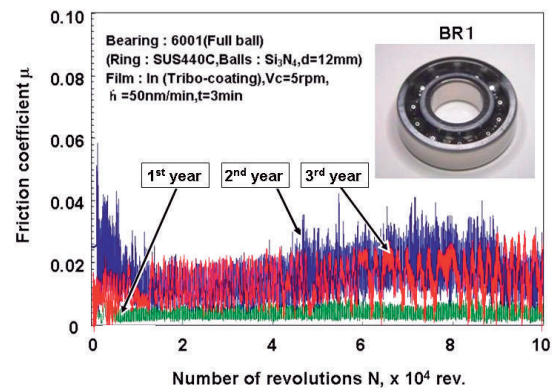


Fig. 6 Friction curves of ball bearings lubricated by tribo-coating (BR1) after exposure in the space environment for one, two and three years

However, friction curves of ball bearing lubricated by tribo-coating (BR1) after two years exposure shows relatively low and stable, in addition its value is almost no change even after three years exposure. These stable friction phenomena against long exposure period in space are considered as the reason of high seizure resistance of silicon nitride ball. It should be necessary for in-situ and on-demand restored system for future.

#### 4. Discussion

##### 4.1 Degradation of ball bearing performance by exposure in space environment

Figure 8 shows friction curves of ball bearing lubricated by tribo-coating of indium (BR1) after bombardment of affective two elements such as atomic oxygen and electron beam. Atomic oxygen is the most affective bombardment element on degradation of bearing performance comparison with those of ultra violet and electron beam. With increasing of amount of atomic oxygen bombardment (from  $1.32 \times 10^{25}$  to  $4.08 \times 10^{25}$  atoms/m<sup>2</sup>), its friction coefficient increases clearly as shown in Fig. 9. Atomic oxygen is believed to be a key element to control friction of ball bearing lubricated by tribo-coated In and sputtered MoS<sub>2</sub>.

Figure 10 shows atomic oxygen effect on friction properties of two types of ball bearings (BR1 and BR3). In case of conventional ball bearing (BR3), the value of friction coefficient drastically increases and becomes unstable by bombardment of atomic oxygen ( $4.08 \times 10^{25}$  atoms/m<sup>2</sup>). On the other hand, ball bearing lubricated by tribo-coating of In (BR1) shows 0.01 of friction coefficient even after bombardment of atomic oxygen. It is suggested from Figs. 6, 7 and 10 that degradation of ball bearing performance by exposure in space environment is mainly caused by atomic oxygen.

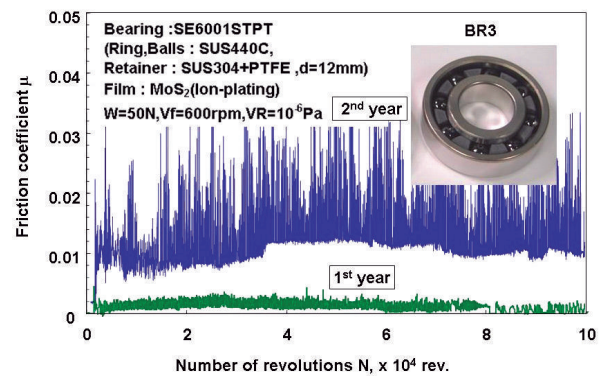


Fig. 7 Friction curves of conventional vacuum ball bearings (BR3) after exposure in the space environment for one and two years

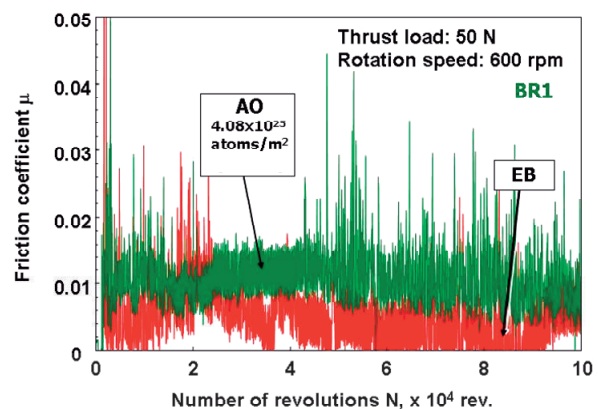


Fig. 8 Friction curves of ball bearing lubricated by tribo-coating (BR1) after bombardment of affective two elements of AO and EB



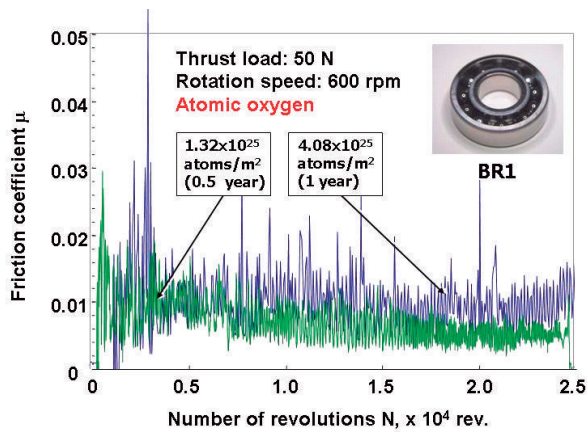


Fig. 9 Friction curves of ball bearing lubricated by tribo-coating (BR1) under different amount of atomic oxygen bombardment

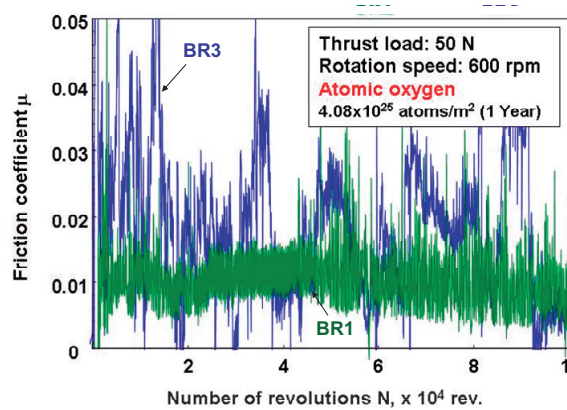


Fig. 10 Effect of atomic oxygen bombardment on friction properties of both ball bearing lubricated by tribo-coating (BR1) and conventional ball bearing (BR3)

#### 4.2 Possibility of in-situ and on-demand restoration of vacuum ball bearing

In Fig. 11, indium was evaporated when friction coefficient of ball bearing lubricated by tribo-coating (BR2) starts to increase due to its lifetime after exposure for one year. The friction coefficient is kept low value by re-tribo-coating (In-situ tribo-coating). This shows the possibility of in-situ and on-demand restoration of solid lubricant in lubrication system with tribo-coating for mechanical system in real space environment.

It is unique advantage of tribo-coating as in-situ and on-demand restoration of lubricant for space mechanisms, which might be damaged by exposure to the real space environment.

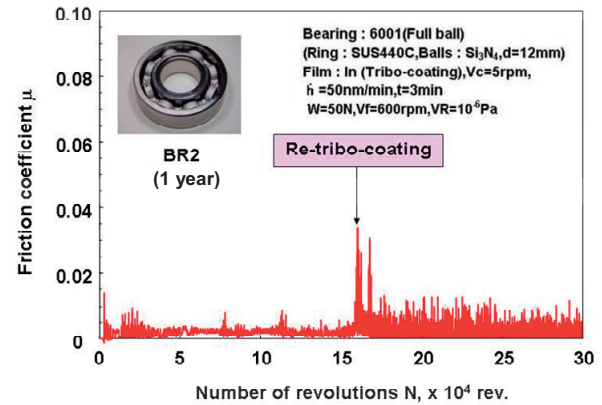


Fig. 11 Possibility in-situ restoration of lubricant for ball bearing after exposure to real space environment

#### 5. Conclusions

- 1) Well-friction properties of ball bearing lubricated by tribo-coating of indium were maintained for one year exposure to real space field.
- 2) Friction coefficient of conventional ball bearing after two years exposure to space showed much higher and unstable than those of ball bearing lubricated by tribo-coating of indium.
- 3) By tribo-coating of indium, possibility of in-situ restoration of friction property of ball bearing damaged by exposure to the real space environment was clearly shown.

#### Acknowledgements

Authors would like to express our appreciations to JAXA for their full support for SM/SEED project and to JTEKT Corporation for their support of the specimens.

#### References

- [1] K. Adachi, K. Kato: Reliable Design of Space System in Tribology Viewpoint, Proc. of the 22<sup>nd</sup> Int. Symp. on Space Technol. and Science, 1 (2000) 593.
- [2] K. Adachi, R. Suzuki, H. Shibuya, K. Kato: Lubrication of ball bearing by Tribo-coating of Indium in Ultra High Vacuum, Proc. of 1<sup>st</sup> Int. Conf. on Advanced Tribol. iCAT 2004 (2004) B-28.
- [3] K. Adachi, K. Kato, In-situ and On-demand Lubrication by Tribo-coating for Space Applications, IMechE, (2008) in press.
- [4] K. Mori, H. Shimamura, T. Nakamura and M. Suzuki: Evaluation of Space Materials by Space Environment Exposure Device, Aeronautical and Space Science Japan, 54 (2006) 298.



**Publication list related SM/MPAC&SEED**

- K. Adachi, R. Suzuki, H. Shibuya, K. Kato, "Lubrication of Ball Bearing by Tribo-coating of Indium in UHV," 1st Int. Conf. on Advanced Tribology 2004, (2004) B-28
- K. Adachi, H. Shibuya, S. Obara, K. Kato, "Film formation mechanisms of indium by tribo-coating on ball bearing in UHV," Synopses of the International Tribology Conference, Kobe, 2005 (2005) 227.
- K. Adachi, K. Kato, "Tribo-coating for Space Mechanisms-Tribologically-based Design for Reliable Space Mechanisms-," (in Japanese) Journal of Japan Society for Design Engineering, 42 (2007) 23-30
- K. Adachi, R. Suzuki, H. Shibuya, K. Kato, S. Obara, "Tribo-coating for Friction Control of Ball Bearings in Ultra High Vacuum," (in Japanese) Shinku, 51 (2008) 490-495.
- K. Adachi and K. Kato, "In-situ and On-demand Lubrication by Tribo-coating for Space Applications," Journal of Engineering Tribology, ImechE, (2008), in press.

## Evaluation of MoS<sub>2</sub> Bonded Film Degradation on ISS SM-SEED Experiment

Masahito TAGAWA<sup>1</sup>, Koji MATSUMOTO<sup>2</sup>,  
Katsuhiko KISHI<sup>3</sup> and Masao AKIYAMA<sup>4</sup>

<sup>1</sup> Associate Professor, Department of Mechanical Engineering, Faculty of Engineering,  
Kobe University, Rokko-dai 1-1, Nada, Kobe 657-8501 Japan

<sup>2</sup> Institute of Aerospace Technology, Japan Aerospace Exploration Agency,  
7-44-1, Jindaiji Higashi-cho, Chofu, Tokyo, 182-8522, Japan

<sup>3</sup> Japan Ultra-high Temperature Materials Research Institute Co., LTD.,  
573-3, Okiube, Ooaza, Ube, Yamaguchi, 755-0001, Japan

<sup>4</sup> Space Systems Department, IHI Aerospace Co., LTD.,  
900, Fujiki, Tomioka, Gunma, 370-2398, Japan

This paper describes upon the on orbit degradation of the MoS<sub>2</sub> Bonded Film which are applied to external mechanism of Japanese Experiment Module (JEM) of International Space Station (ISS). The Test articles were launched and kept on orbit for 1 year, 2 year and 3 year. Evaluation are performed by measuring adhesive property, friction property and surface properties of the MoS<sub>2</sub> bonded film, HMB-34. Also ground environment exposure test were conducted to compare the degradation against on orbit exposed environment effect.

**Keywords:** MPAC&SEED, ISS Service Module, JEM, ELM-ES, PAM, HMB-34

### 1. Introduction

As when the ISS program has been approved by Japanese government, IHI Aerospace (formerly NISSAN Motor Co., LTD.) has proposed to develop Payload Attach Mechanism (PAM) to carry the external payloads to Japanese Experiment Module (JEM) on ISS by Space Shuttle. Due to the external environment effect to the solid lubricant, Space exposure experiment has been expected to evaluate its durability compare to ground exposure experiment, such as Atomic Oxygen, Ultra-Violet and Electron Beams.

Authors has been joining JAXA's space exposure programs, EFFU, ESEM and SM-SEED upon MoS<sub>2</sub> bonded film, HMB-34.

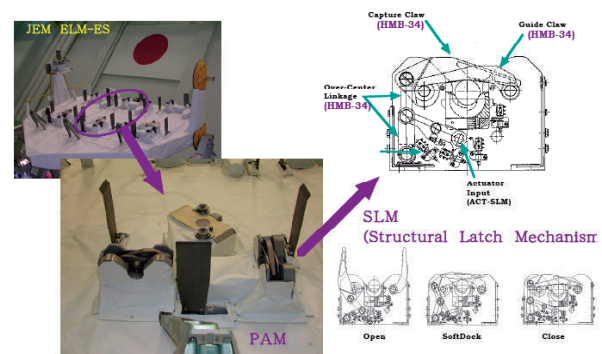


Fig.1 SLM on JEM ELM-ES

### 2. MoS<sub>2</sub> Bonded Film

HMB-34 MoS<sub>2</sub> bonded film has been selected for the JEM ELM-ES PAM from in-house research and development conducted by IHI Aerospace. HMB-34 is kind of MoS<sub>2</sub> with organic binder which are coated onto Ti-6Al-4V, CRES and Aluminum Alloys on JEM ELM-ES PAM.

Fig.1 describes the JEM ELM-ES and where the mechanisms are installed.

Structural Latch Mechanism (SLM) is one of the critical component on ELM-ES which has to withstand the launch and re-entry load and need to release / latch on orbit.

### 3. Post Exposure Evaluation

Evaluation has been conducted upon space exposure test article and also comparison has been conducted to evaluate the space exposed effects to the MoS<sub>2</sub> bonded film with Ti-6Al-4V bas material. Test Article which are evaluated as 3 year expose are described in Fig. 2

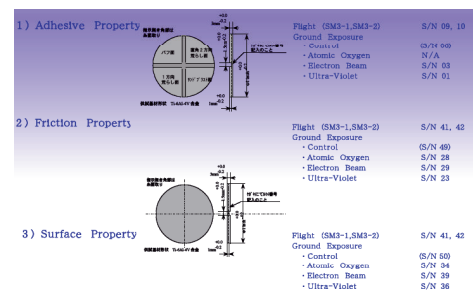


Fig.2 Test Article of MoS<sub>2</sub> Bonded Film

3.1 Adhesive Property

Adhesive property were evaluated according to JIS-K-5400 and the measured result is described in Tab. 1as,

- (1) There were clear degradation upon adhesive property after 3 year exposure to Space environment.
- (2) Compare to ground exposure test result, there seems no difference to adhesive property under single U.V. nor E.B. environment.

Table 1 Adhesive Property Result

Environment	S/N	Buff	1axis rough	2axis rough	Sand brust
U.V.	#1	8	8	8~10	8~10
E.B.	#3	6~10	6	8	8
Flight	#9	2	2	2~4	2~4
Flight	#10	2	2	2~4	2~4
Control	#6	8	8	8~10	8~10
Flight 1yr	#11, #12	8	8	8	8~10
Flight 2yr	#7, #8	6	8	8	8

Test Standard : JIS K-5400  
 Using qualified Tape to prove more Than F300 gf upon 18mm x10mm Area) and inspect X-cut area and point from ;  
 10 : No Peer  
 8 : No Peer in crossing area but some peer in X cut area

3.2 Friction Property

Friction property was evaluated according to ball on disk test as described in Fig.3 as,

- (1) LEO Exposed Environment  
 Due to decrease of initial friction and increase of on-orbit exposure duration has decreased the friction of MoS2 Bonded Film.
- (2) Atomic Oxygen Exposure  
 Decrease of initial friction were similar to on-orbit exposure , but no difference due to exposure duration.
- (3) Ultra-Violet Exposure  
 Decrease of initial friction were similar to on-orbit exposure , but no difference due to exposure duration and friction itself was not stable.
- (4) Electron Beam Exposure  
 No difference of the friction property were measured

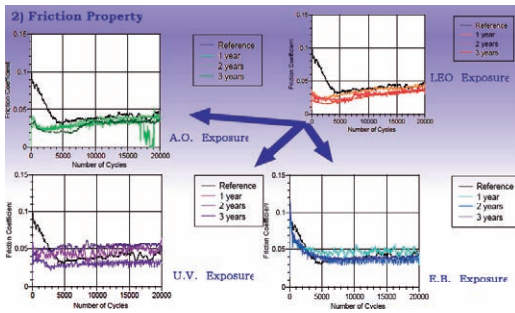


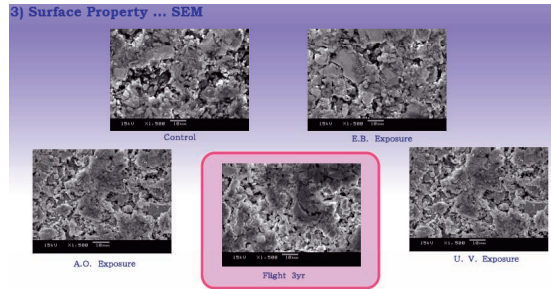
Fig.3 Friction Property Measurement

3.3 Surface Property

SEM, XPS and EDS evaluation were conducted to each test article and SiO2 were measured as contamination to MoS2 Bonded Film surface of space exposure samples as described in Fig.4 to Fig.6.

- (1) Surface of 3 year space exposure seems to have same contamination of Si (SiO2).
- (2) Cu and Fe were measured from A.O. exposure which seems to come from the A.O. generator.

- (3) SiO2 has been identified as Si on MoS2 Bonded Film exposed to space environment according to the measurement of Si4+ peak near 104 eV. (1) Si has been increasing on the surface of MoS2 Bonded Film. This means the surface has been contaminated by Si (SiO2).
- (4) Si has been increasing on the surface of MoS2 Bonded Film. This means the surface has been contaminated by Si (SiO2).
- (5) Si contamination seems to be only on very surface of Bonded Film compare XPS to EDS result.



(1) Surface of 3 year space exposure seems to be smooth compare to ground exposure surface.

Fig.4 SEM

Sample	C	O	S	Mo	Sb	Si	Cr	Fe	Ni	Cu
LEO	16.5	57.3	0.1	0.4	-	25.8	-	-	-	-
AO	24.2	50.5	1.7	4.5	0.2	1.6	0.9	7.6	1.3	7.6
UV	58.4	18.6	5.6	3.3	0.2	3.9	-	-	-	-
EB	72.7	17.2	5.5	4.0	0.2	0.4	-	-	-	-
Ref.	64.7	18.6	9.7	6.3	0.4	0.3	-	-	-	-

Note : Difficult to compare directly to both XPS result as condition is not same.

Fig.5 XPS

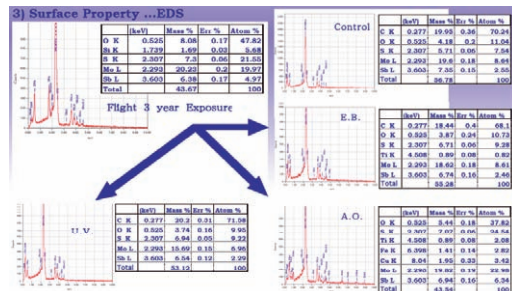


Fig.6 EDS

- b) Overall friction has decreased and Life time of HMB-34 Bonded Film seems to increase.
- c) This property change might have some relation with the SiO<sub>2</sub> contamination which is also proved not to change MoS<sub>2</sub> Bonded Film lubrication property.

#### 4. Conclusion

As from 3 years of exposure experiment with 1 and 2 year exposure as reference of degradation of MoS<sub>2</sub> Bonded Film, following are the conclusion we have got.

- (1) Adhesive property, friction property and surface property evaluation were conducted to all test articles including 1 year, 2 year and 3 year exposure to space environment and same effect were measured.
- (2) According to 3 year exposure to ISS exposed environment,
  - a) Initial friction of space exposed HMB-34 MoS<sub>2</sub> Bonded Film has been decreased compare to ground initial condition (Control) and not have changed during 1 to 3 year exposure.

- (3) This space exposure has proved that the HMB-34 Bonded Film have enough performance for JEM exposed mechanisms such as ELM-ES PAM SLM for 10 year life operation under ISS space exposed environment.

#### 5. Acknowledgments

The authors wish to thank Ms Yokota and other students at Kobe Univ. for their assistance in preparation of this paper..



## Evaluation of Solid Lubricative Coatings after Space Environment Exposure Test

Masahiro TOSA, Akira KASAHARA and Masahiro GOTO

*Micro-nano Materials Engineering group, Materials Reliability Center, National Institute for Materials Science, Tsukuba, Ibaraki 305-0047, Japan*

Moving components materials in orbit environment require surface modification with stable lubrication for preventing increase in friction due to oxidation and irradiation damages. We have prepared a stainless steel substrate and four kinds of lubricative coatings such as TiN, MoS<sub>2</sub>, mixture of Cu and BN and Cu on the substrates and installed them on the International Space Station in orbit for exposure test from about a year to three years. We have analyzed tribological properties, surface roughness, chemical concentration and so on. Most of a year exposed substrates generally decrease friction in a vacuum as well as at an atmospheric pressure and over years exposure increased friction of almost substrates. XPS analysis shows Si based contamination layer that might affect the change in tribological properties.

**Keywords:** MPAC&SEED, ISS Service Module, coatings, friction, vacuum, TiN, MoS<sub>2</sub>, mixture of Cu and BN, Cu

### 1. Introduction

Orbit environment about 400km above the ground of a space shuttle and a space station is an ultrahigh vacuum under  $10^{-5}$  Pa and usually suffers from atomic oxygen attack at a high speed as well as some particles irradiation. Moving components materials therefore require surface modification with stable lubrication for preventing increase in friction due to oxidation and irradiation damages. After preparation of a stainless steel substrate and four kinds of such lubricative coating films as titanium nitride, molybdenum disulfide, mixture of copper and boron nitride and copper on the stainless steel substrates, these substrates have been exposed in orbit for a year, two years and three years. Analyses have been carried out on tribological properties, surface micro roughness, structure, chemical concentration and so on in order to understand change in properties of lubricant coating by the exposure test in orbit and to develop surface modification for advanced smooth and reliable space solid lubrication.

### 2. Experimental

Commercial type 304 austenitic stainless steel sheet substrates (size; 14 mm x 14 mm x 1mm) have been coated with titanium nitride (TiN), molybdenum disulfide (MoS<sub>2</sub>), mixture of copper and boron nitride (Cu/BN) and copper (Cu) using a rf magnetron sputter deposition system with a film thickness about 50nm to 250nm [1] and were set on a panel then were installed onto the SM/MPAC&SEED (Service Module/ Micro-Particles Capturer and Space Environment Exposure Device) prepared by JAXA on the Russian service module in the International Space Station (ISS), then have been exposed in orbit and have recovered to the Earth.

The frictional properties of the substrates with and without exposure to orbit were observed with a system developed for measuring vacuum friction before and after annealing in a vacuum of  $10^{-5}$  Pa or less level. The design of the friction measurement system comes from the Bowden-Leben type as shown in Fig.1 [2]. The sample stage can move in x-y direction by two axes stepping motor and a manual axis in an ultrahigh

vacuum. A stainless steel ball or sapphire ball probe above the substrate holder has a load weight holder with 0.49N and has two strain gauges to detect frictional force.

Surface chemical characterization for the substrates was carried out on TiN coated substrate after exposure test for a year with a X-ray photoelectron spectroscopy with X-ray of excited from Al K  $\alpha$  (1486.6eV), constant pass energy of 69eV, X-ray beam size of 100  $\mu$ m in diameter and so on. Depth profiles of the substrates were also obtained with XPS using an argon ion sputtering.

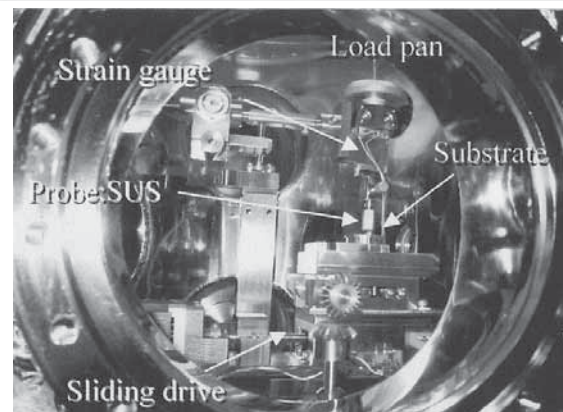
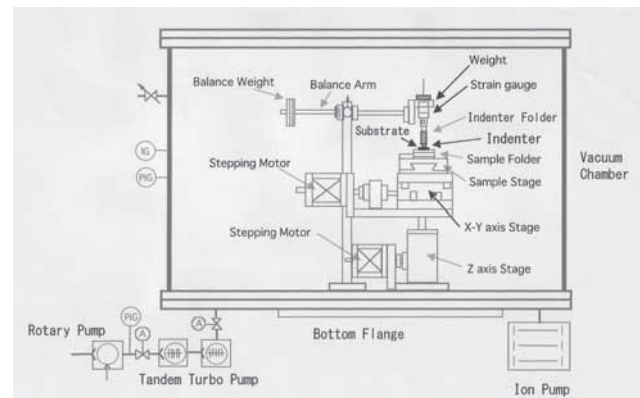


Fig.1 Schematic view of a vacuum friction measurement system and photo of a center system.

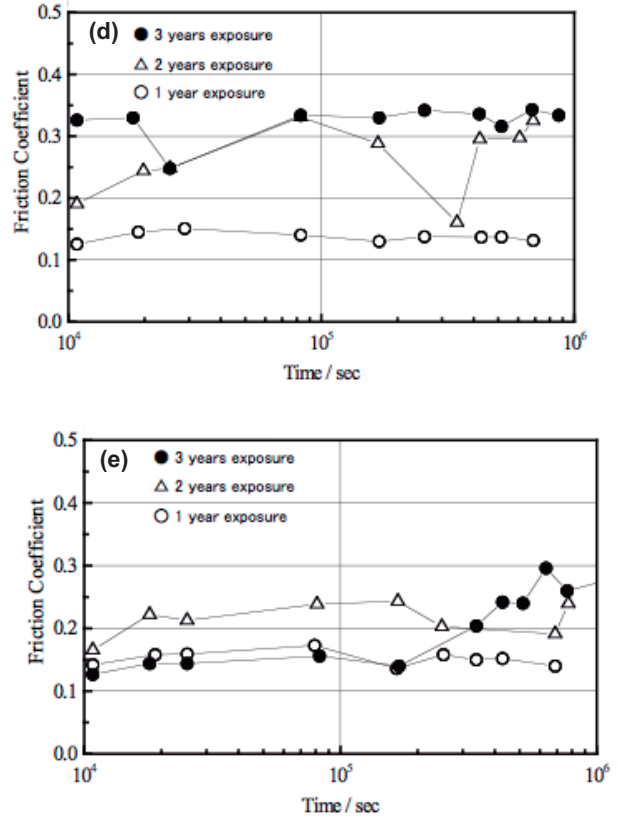
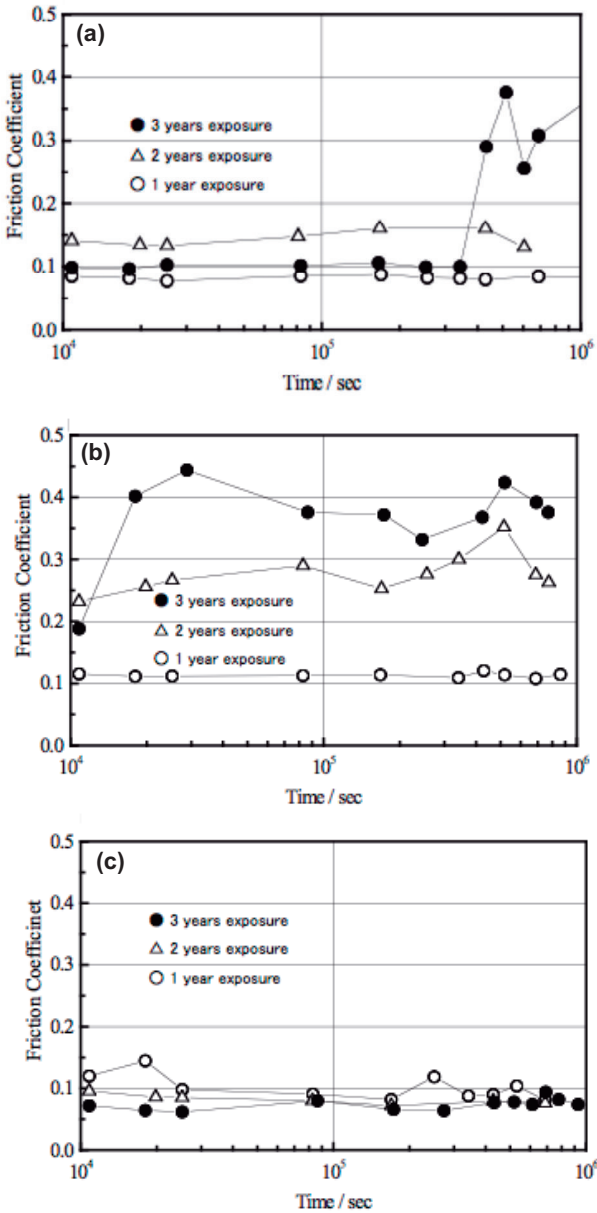


Fig.2 Effect of vacuum annealing on vacuum friction coefficients ( $\mu$ ) of substrates with a variety of exposure term; (a) SUS304 substrate, (b) TiN coating, (c) MoS<sub>2</sub> coating, (d) Cu coating, (e) mixture coating of Cu and BN.

**3. Results**

**3.1. Friction properties**

Figure 2 shows the effect of vacuum annealing on vacuum friction coefficients of coatings on substrates with a variety of exposure test years. A year exposure test made substrates keep almost low coefficient of friction ( $\mu$ ) even after vacuum annealing but two years exposure test made some substrates increase  $\mu$ . Three years exposure test makes obvious difference among substrates in increase in  $\mu$ . SUS304 substrate, TiN coating and Cu coating show a large increase in  $\mu$ , mixture coating of Cu and BN shows a small increase in  $\mu$  and MoS<sub>2</sub> coating shows little increase in  $\mu$  keeping good lubrication in spite of long time exposure in orbit.

**3.2. Surface analyses**

Surface chemical condition and depth profile were obtained with a X-ray photoelectron spectroscopy for two surface areas of TiN coated substrates, one for exposure and the other for screening against exposure test in orbit for a year.

Figure 3 shows survey spectra of exposed and screened stainless steel sheets coated with TiN. Silicon (Si) peaks and large oxygen (O) peaks are observed on the exposed area while large fluorine (F) peaks are observed on screened area of the TiN coated substrate. Figure 6 shows depth profiles of exposed and screened area of the substrate coated with TiN. Silicon and oxygen concentrated layer is observed at the surface of TiN coating layer at the exposed area in orbit.

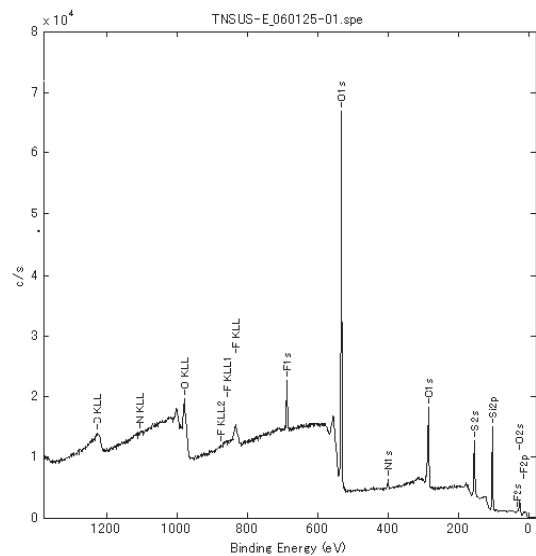


Fig.3 Survey spectra of exposed area of TiN coated substrate.

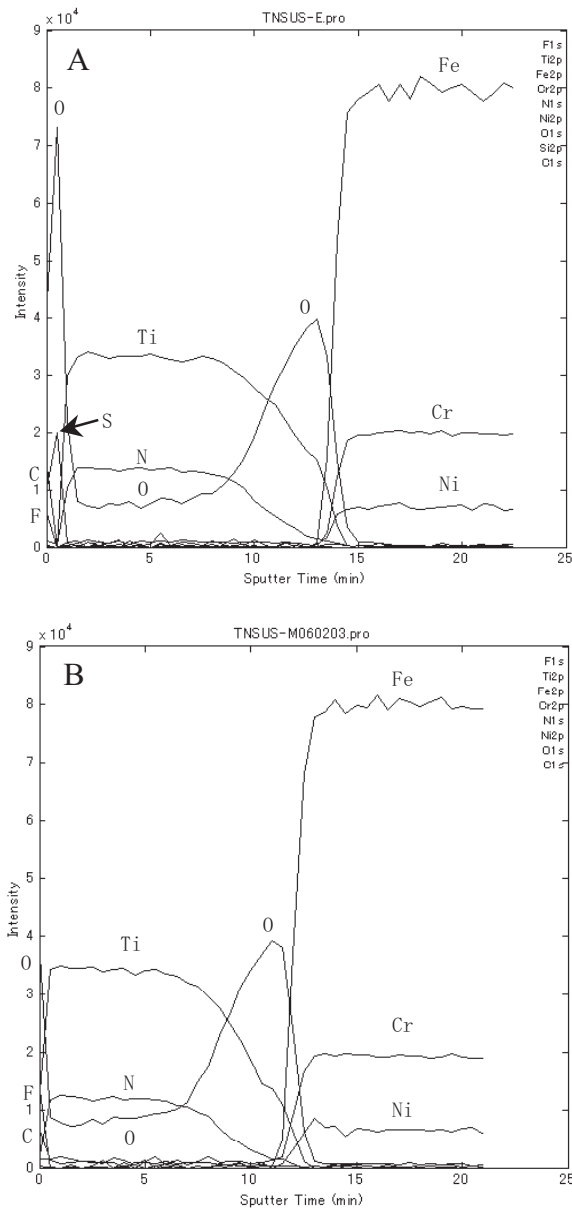


Fig.4 Depth profiles of a year exposed (A) and screened area (B) of TiN coated substrates.

Changes in chemical condition were obtained for elements composing TiN coated stainless steel sheets after exposure in orbit as shown in Fig.7 with main binding energies [7]. Titanium forms TiN with nitrogen mainly and also forms  $TiO_2$  with oxygen in part. Silicon forms  $SiO_2$  with oxygen at the surface of TiN coating layer.

Comparison between these surface analytical results of exposed and screened area of TiN coated stainless steel sheet indicates as follows.  $TiO_x$  layer formed during TiN film preparation. Silicon evaporated from silicone adhesives used for space station structure might react the atomic oxygen to form  $SiO_2$  during exposure in orbit. The mixed structure of  $SiO_2$  in coating film is considered to form a good lubricant

layer that can offer smooth and stable sliding against annealing in a vacuum.

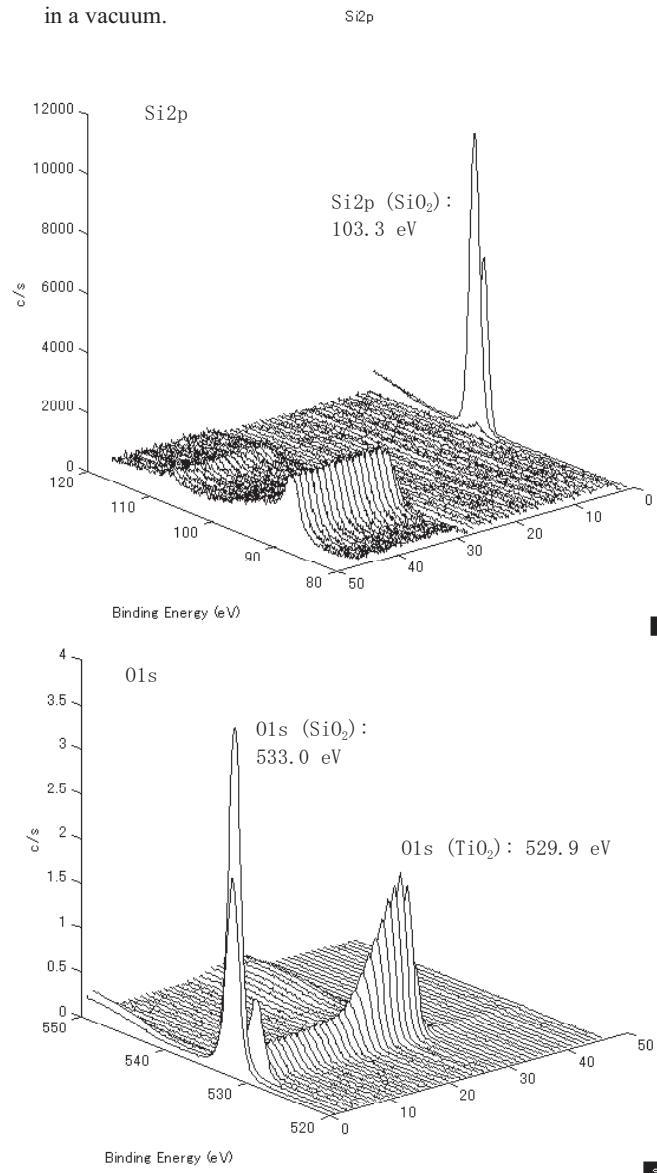


Fig.5 Changes in XPS spectra for silicon and oxygen with sputter time for obtaining depth profile

#### 4. Conclusion

Lubricative coatings such as TiN, MoS<sub>2</sub>, mixture of Cu and BN and Cu were prepared on the stainless steel substrates and installed them on the International Space Station in orbit for exposure test from about a year to three years. Most of a year exposed substrates generally decrease friction in a vacuum as well as at an atmospheric pressure but over years exposure increased friction of almost substrates except MoS<sub>2</sub> coating. XPS analysis shows Si based contamination layer that might affect the change in tribological properties and further analyses are required to understand the detail mechanism on change in friction by exposure test in orbit.

**References**

- [1] M.Goto, A.Kasahara, M.Tosa, J.Hobley, M.Kishimoto, K.Yoshihara and H.Fukumura, , J. Vacuum Science and Technol. A20 (2002)1458.
- [2] A.Kasahara, M.Goto, M.Tosa and K.Yoshihara, J. Electroanalytical Chemistry 45(2003)559.
- [3] J.Chastain and R.C.King,Jr., Handbook of X-ray Photoelectron Spectroscopy, Physical Electronics Inc., Minnesota (1995).

**Publication list related SM/MPAC&SEED**

- [1] M.Tosa, A.Kasahara, M.Goto, Y.Pihosh, S.Ota, T.Kinura, S.Fukushima, T.Inoue, E.Miyazaki and K.Imagawa:  
Characterization of Lubricative Coating after Exposure Test in Orbit, Journal of Surface Analysis, 13(2006)217.
- [2] M.Tosa, A.Kasahara, M.Goto, Y.Pihosh, S.Ota, T.Kinura, S.Fukushima, T.Inoue, E.Miyazaki and K.Imagawa: Characterization of Lubricative Coating Exposed in space Orbit, Proceedings of The Third Asia International Conference on Tribology, 2(2006)625.
- [3] M.Tosa, A.Kasahara, M.Goto, T.Inoue, E.Miyazaki and K.Imagawa: Characterization of Lubricative Coating after Exposure Test in Orbit, Proceedings of 25<sup>th</sup> International Symposium on Space Technology and Science, (2006) 2006-r-2-29-1
- [4]. M.Tosa, A.Kasahara, M.Goto, T.Inoue, E.Miyazaki and K.Imagawa: Effect of Exposure in Orbit on Friction of Lubricative Coating, Funal Papaers 56th nternational Astronautical Congress 2005 CD1, C2.5(2005)701.
- [5] M.Tosa, A.Kasahara, M.Goto, T.Ooishi, T.Inoue and K.Imagawa: Frictional change in lubricant coating by exposure in orbit, Proceedings of 24th International Symposium on Space Technology and Science, (2005)702



## SM/SEED Experiments of Carbide and Nitride Ceramics for Three Years

Osamu ODAWARA<sup>1)</sup>, Hiromichi AKIYAMA<sup>1)</sup>, Toshihide TOBITSUKA<sup>2)</sup>, and Toyohiko YANO<sup>2)</sup>

<sup>1)</sup> *Department of Innovative and Engineered Materials, Tokyo Institute of Technology*

<sup>2)</sup> *Research Laboratory for Nuclear Reactors, Tokyo Institute of Technology*

Space exposure tests of five ceramic samples have been carried out from October 15, 2001 to August 19, 2005 at the Service Module of the International Space Station; aluminum nitride, two kinds of silicon carbides fabricated by hot-pressing and reaction-sintering, and ion-plated titanium nitrides on aluminum and alumina plates. The samples were fixed on three sets of sample trays, which were set on to the external wall of the Service Module, which were retrieved after 315 days, 865 days and 1403 days, respectively. In the present experiments, the tested samples in the three series were examined to evaluate property changes due to atomic oxygen, cosmic-ray radiation, solar light exposure, thermal cycle, etc. As a result, the oxygen content of the surface of space-exposed samples was confirmed to be increased markedly compared with those of non-tested and atomic oxygen-irradiated ones, and the oxidized layers of the samples exposed in space were thicker than those irradiated by atomic oxygen.

**Keywords:** Exposure Test, Atomic Oxygen, Non-Oxide Ceramics, LEO, Surface

### 1. Introduction

Ceramic materials have advantages in their properties such as high specific strength, tolerance in high temperature, high hardness, low friction, etc. Such ceramic materials are useful for heat shield and/or insulator materials in fields of space explorations, where there exist many environmental factors, such as particles, radiations, gravity, pressure, temperature, etc. The factors are sometimes harmful to spacecrafts or materials consisting of a spacecraft. Large particles of centimeter order are catastrophic for spacecraft and small ones, which exists some kinds such as gas molecule, atom, heavy ion particle, etc, make small but cumulative damages. Radiations affect on electronic device and life. Low pressure causes out-gassing from materials. On orbit, temperature of a spacecraft changes in the range between 100 K and 400 K, resulting in thermal fatigue. It is also necessary to verify that the materials have enough tolerance for these factors and have enough life in space environments.

The research regarding the characteristic change of ceramics due to long period of exposure in space environment has been limited, although several space environment exposure missions haven performed in the past by NASA and JAXA. In the present work, five kinds of tests have been carried out with three ceramic materials: aluminum nitride (AlN), hot-pressed silicon carbide (SiC), reaction-sintered silicon carbide (SiC), titanium nitride (TiN) ion-plated on alumina plate, and titanium nitride (TiN) ion-plated on aluminum plate. The ceramic materials exposed in a space environment for three years on the surface of the International Space Station (ISS) have been evaluated through an SM/SEED (Service Module / Space Environment Exposure Device) mission. In the SM/SEED mission, it is unique that three exposed samples with three different durations of exposure have been obtained. Five tests with three ceramic materials have been proposed in the present experiments, and reference experiments on ground have also been carried out through the SM/SEED missions. By analyzing each tested sample, the influence of exposure

duration has been investigated with respect to the material resistance against the environment in durations. Such an environmental effect would be classified in two categories: dynamic effect and static effect. The dynamic effect occurs with high force in short time and the static one with low force in long time.

The main focus of the present SM/SEED mission is measuring the degradation of materials exposed to the environment. Since the orbit of ISS is LEO (Low Earth Orbit), the amount of atomic oxygen is much higher compared to that in higher orbit. Atomic oxygen (AO) generates through the dissociation of molecular oxygen under UV-ray. With the data of AO flux with altitude, the AO flux can be estimated to be  $10^{13}$  atoms/cm<sup>2</sup>-sec at the ISS altitude of about 400km, where the spacecraft goes round with the period of 90 minutes (8 km/s). This corresponds to a mean AO energy of about 5 eV. When the collision occurs between the surface of material and AO, the material would be damaged through its oxidation or erosion. The energy of sunlight at the ISS orbit is about 1.4 kW/m<sup>2</sup>, which includes strong UV-ray under low pressure of  $10^{-5}$ Pa resulting in some serious degradation of material surface characteristics.

### 2. Experimental Procedure

#### 2.1 Samples

All samples have been sized in the same dimension of 17mm x 17mm x 2mm as shown in Fig. 1. AlN is characterized with its high heat conduction, electrical insulation and translucency, which give the high potential to AlN as integrated circuit substrate, heater base, heating sink and light-emitting devise-package material. Grain sizes of the hot-pressed SiC are uniform, and those of the reaction-sintered SiC are not uniform. There exist some impurities in grain boundaries of the hot-pressed SiC because the hot-pressing process needs additives. SiC has been applied to bearing balls, refractory materials, mechanical seals and turbine blades. Recently, its potential as power devices has been highly

assessed and actively investigated world-widely. TiN is characterized with its hardness and low friction. The samples in the present work are ion-plated on Al and Al<sub>2</sub>O<sub>3</sub> plates. With its superior thermal properties, the surface treatment of cutting tool is a popular application.

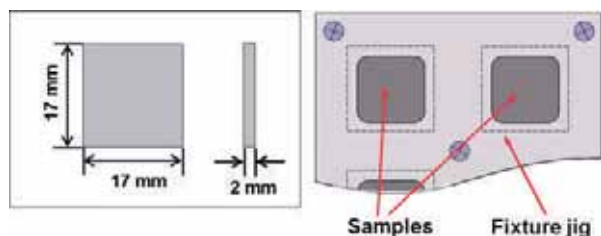


Fig. 1 Sample arrangement in the SM/SEED tests.

## 2.2 Experimental procedure

Samples are installed on sample trays which are inserted into the SM/SEED frame. Three SM/SEEDs were launched together by a Russian Progress Supply Ship from Kazakhstan in August, 2001. After the arrival at ISS, the SM/SEEDs were installed outside Service Module "Zvezda" on 15th of October in 2001 by an EVA (Extravehicular Activity) of an astronaut aboard on ISS, and the exposure tests have started in space environment. On 26th of August in 2002, astronauts on ISS collected only one set of sample trays by EVA from the SM/SEEDs, which means the first exposure duration 315 days. The collected sample trays returned to the earth by a Soyuz. The second sample trays were also collected on 27th of February in 2004(865 day exposure), and the third ones were collected on 19th of August in 2005(1403 day exposure).

Ground experiments were also conducted for comparing with the data of the space-exposed ones. Each kind of samples was irradiated by AO, UV ray and electron beam (EB) separately at room temperature under vacuum on the ground. Actual fluxes were roughly corresponding to half, one and three year exposures on the orbital as follows; AO:  $1.38 \times 10^{21}$ ,  $3.70 \times 10^{21}$  and  $6.39 \times 10^{21}$  atoms/cm<sup>2</sup>, UV ray: 401.2, 814.2 and 2448.5 mW/cm<sup>2</sup> and EB:  $1.64 \times 10^{12}$ ,  $3.86 \times 10^{12}$  and  $9.89 \times 10^{12}$  electrons/cm<sup>2</sup>, respectively. The AO irradiation was conducted using the FAST<sup>TM</sup> atomic oxygen irradiation apparatus (Physical Sciences Inc. USA) under vacuum of the order of  $10^{-2}$  Pa. Energy of AO was 5 eV, corresponding to the speed of 8 km/s, and an average flux of  $1.17 \times 10^{15}$  atoms/cm<sup>2</sup>·s at room temperature. The EB irradiation was conducted using an electron beam irradiation apparatus (Nisshin high-voltage Corp. Japan). The accelerating voltage of electron was 200 kV and the sample was irradiated at RT under  $<10^{-8}$  Pa. The UV irradiation was conducted using the ultraviolet-ray irradiation apparatus (Yamashita Electronic Inc.). Light source was 6 kW xenon lamps under vacuum of  $<10^{-8}$  Pa at lower temperature than 80°C.

The samples exposed for 315 days in space were labeled as ISS-1, for 865 days as ISS-2 and for 1403 days as ISS-3. About the AO-irradiated samples, those irradiated by AO up to the fluence corresponding to 0.5 year, 1.0 year and 3 years on the orbital were indicated as AO-0.5, AO-1 and AO-3,

respectively.

The tested samples were characterized with an electric micro-balance for mass change, a thermo-optical measuring unit for solar absorptance and IR emissivity, and a surface roughness. With a field-emission type scanning electron microscope (FE-SEM) and a wavelength-dispersive-type X-ray spectrometer (WDX) and a secondary ion mass spectrometer (SIMS) on exposed surfaces, the changes of composition are measured. The roughness average of each sample surface was measured along 10 mm in length and ten different positions near the center of each sample. An averaged value for ten measurements was obtained as a roughness average. The WDX measurement was performed for five positions (12.8 mm x 9.6 mm) of each sample and an averaged value was obtained.

## 3. Results and Discussion

### 3.1 Surface roughness

Change in roughness average of the SiC sample surfaces after the space exposure and the AO irradiation is shown in Fig. 2. Irradiation of AO increased surface roughness average with increasing the AO irradiation, although no correlation was found between the effect of AO irradiation and that of the space exposure. In the case of the space exposure, slight increase in roughness average was observed after 0.86 year exposure, but it decreased less than the blank sample after 2.4 year exposure, and again increased after 3.8 year exposure. Surface roughness average of the RS-SiC samples was generally larger than that of the HP-SiC samples.

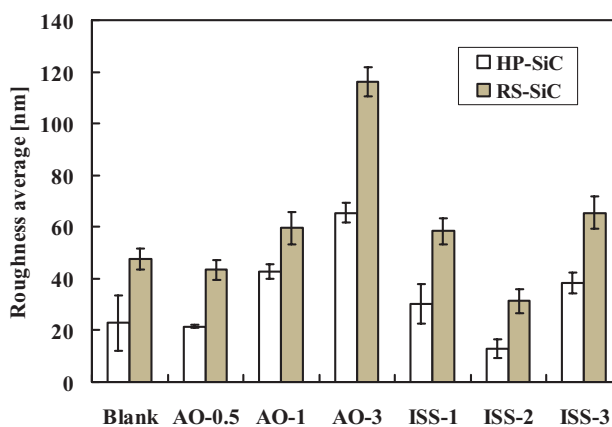


Fig. 2 Roughness of HP-SiC and RS-SiC samples.

### 3.2 Surface morphology

According to the SEM observation of the HP-SiC and the RS-SiC samples, the polishing damage which existed on the SiC surface before the space exposure gradually diminished with increasing space exposure duration. As shown in Fig. 3, the tiny particles which were thought to be SiC particles were observed for RS-SiC ceramics at the grain boundary silicon phase of the space-exposed samples. But it was rarely or never observed at the grain boundary of the sample irradiated by AO on the ground. In the cases of TiN/Al and TiN/Al<sub>2</sub>O<sub>3</sub> tests, the morphologies exposed in space were much different from those irradiated by AO as shown in Fig. 4.

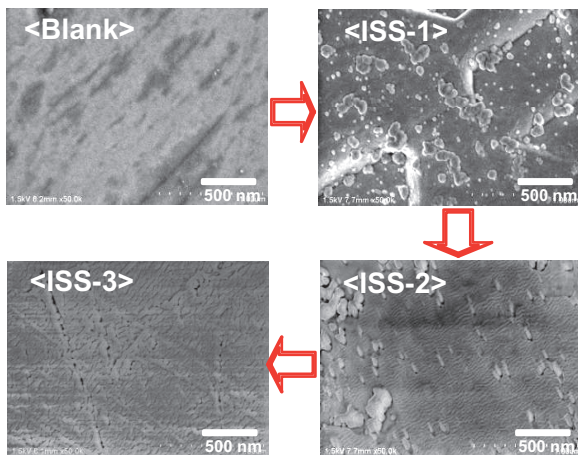


Fig. 3 Surface morphology changes of the RS-SiC samples during the exposed periods.

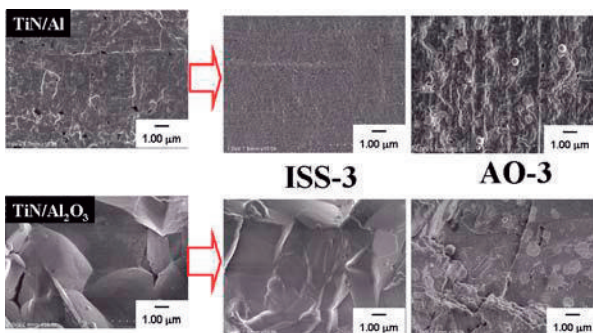


Fig. 4 Surface morphology changes of the TiN/Al and TiN/Al<sub>2</sub>O<sub>3</sub> samples.

### 3.3 Surface composition

Figs. 5(a) and 4(b) show the oxygen concentration of the sample surface of the HP-SiC and RS-SiC sample detected by WDX. The oxygen content of surface of the space-exposed samples (detection range  $\sim 1$  mm in depth), where was not covered by a fixture jig, increased markedly compared with those of the blank samples. The surface oxygen content of the samples irradiated by AO was also increased. Therefore, it is thought that AO is a principal factor of the oxidation of the sample. On the contrary, oxygen content of surface where was covered by the fixture jig was comparable or slightly higher values from those of the blank samples, and far lower values compared with the un-covered parts of the space-exposed samples. Therefore, direct bombardment of AO with 5 eV energy (8 km/s) is seemed to be essential for the surface oxidation of SiC. Carbon should become volatile components and be lost from the sample surface.

Figs. 6(a) and 5(b) show the depth profiles of the O/Si ratio observed by SIMS for the HP-SiC and RS-SiC samples. The 15 keV O<sub>2</sub><sup>+</sup> or 10 keV Cs<sup>+</sup> was used as a primary ion, and the beam current was about 10 nA or 100 nA, respectively. Its scanned area was 250 mm square. The measuring depth was more than 1.5 mm. Energy distributions of molecular ions were measured with secondary ion energy windows of 10 eV. The most candidate species for the present measurements are neutral atomic and molecular ions, so the secondary ions

measured are both in positive and negative treatments. The oxygen ion detection ratio was calculated as follows; (1) <sup>28</sup>Si silicon intensity was recorded at start and finish of the measurement. (2) These silicon intensities were averaged. (3) <sup>16</sup>O oxygen intensities were divided by the averaged silicon intensity, giving the O/Si ratio. Compared with the O/Si ratio along depth change of the 0.86 year space-exposed sample (ISS-1) and 1.0 year AO-irradiated sample (AO-1), the O/Si ratio profiles are mostly resemble each other, and the thickness of the oxygen-rich layer was less than 15 nm in both the HP-SiC and RS-SiC samples. In past years, two chemical vapor deposited SiC mirrors were exposed to the 5eV fast atomic oxygen environment in low Earth orbit on NASA's Long Duration Exposure Facility(LDEF) which remained in space for nearly 6 years. The XPS results showed the presence of SiO<sub>2</sub>-like species on surface with the thickness varying from 1 to 8 nm depending the location of the samples on the spacecraft.

It is obvious that the O/Si ratio of the space-exposed sample for 2.4 year (ISS-2) kept high values until depth of about 50 nm, which was deeper than that of the ISS-1 samples. The O/Si ratio of the ISS-1 sample until  $\sim 15$  nm was higher than that of the blank sample. The high oxygen concentration layer in the 3.8 year exposure (ISS-3), HP-SiC sample was thicker than that of the sample after 2.4 year exposure (ISS-2).

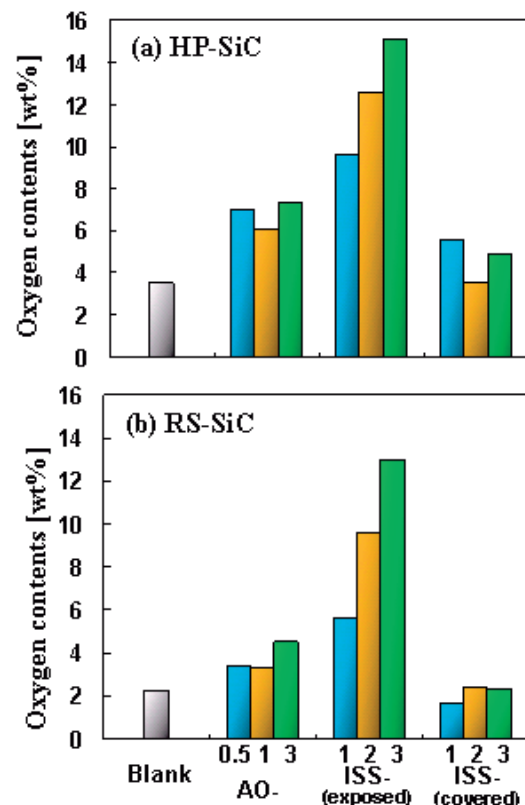


Fig. 5 Changes of oxygen contents in the HP-SiC and RS-SiC tested samples.

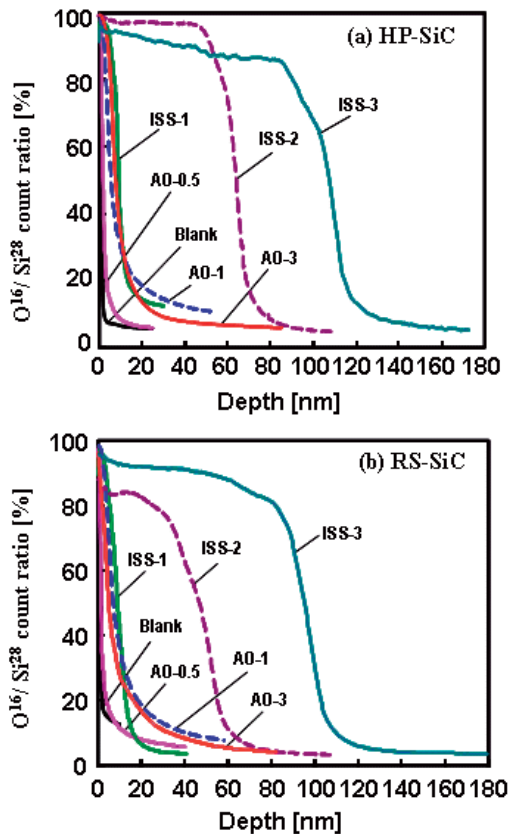


Fig. 6 Oxygen depth profiles from the surfaces of the HP-SiC and RS-SiC tested samples.

#### 4. Conclusion

As space utilization becomes broader, space activities not only on science and technology but also on culture and social applications have been designed. Therefore, greater technological development can make more reliable set-up for space infrastructures, which grow ideas of applications much more. A key technology would be in material development. Ceramic materials have advantages such as high specific strength, tolerance in high temperature, high hardness, low friction, etc. These properties must be useful to apply for spacecraft or payload.

Surface characteristics change of two types of SiC ceramics due to the space exposure up to three years was evaluated. The results were summarized as follows. (1) Surface of the SiC ceramics were oxidized continuously by the space

exposure up to three years. (2) Degree of oxidation was quite different between the exposed part and the covered part of the same space-exposed samples. (3) Oxidation should be caused by the collision of atomic oxygen, but another effect should be considered for accelerated oxidation in the present space exposure condition.

#### References

- [1] O. Odawara, E. Miyazaki, M. Imai and T. Yano, 24th International Symposium, Space Technology and Science, Miyazaki, Japan, ISTS 2004-H-08, 2004.
- [2] T. Tobitsuka, E. Miyazaki, M. Imai, O. Odawara and T. Yano, *Journal of the Japan Society of Microgravity Application*, 24, 1, 2007.

#### Publication list related SM/MPAC&SEED

- 1) Osamu Odawara and Eiji Miyazaki, "Space Exposure Tests of Carbide and Nitride Ceramics Carried out on ISS", *J. Jpn. Soc. Microgravity Appl.* 18[S], 37, 2001.
- 2) Eiji Miyazaki and Osamu Odawara, "Space Exposure Tests of Ceramic Materials on International Space Station", 2nd Pan-Pacific Basin Workshop Proceedings on Microgravity Science, PaperET-1038, 2001.
- 3) Osamu Odawara and Eiji Miyazaki, "Material Exposure Tests on ISS", *J. Jpn. Soc. Microgravity Appl.* 19[S], 19, 2002.
- 4) Osamu Odawara, Eiji Miyazaki, Masami Imai and Toyohiko Yano, "Material Exposure Tests for the First One Year on ISS", *J. Jpn. Soc. Microgravity Appl.*, 20[S], 43, 2003.
- 5) Osamu Odawara, Eiji Miyazaki, Masami Imai and Toyohiko Yano, "Exposure Tests of Carbide and Nitride Ceramics with SM/SEED on ISS", *Proc. 24th Int'l. Symp. Space Tech. Sci.*, 765-769, 2004.
- 6) Osamu Odawara, Eiji Miyazaki, Masami Imai and Toyohiko Yano, "ISS SM/SEED Exposure Tests of Ceramic Materials", *J. Jpn. Soc. Microgravity Appl.* 21[S], 59, 2004.
- 7) Osamu ODAWARA, Hiromichi AKIYAMA, Toshihide TOBITSUKA, and Toyohiko YANO, "SM/SEED Experiments of Carbide and Nitride Ceramics for Three Years", *Extended Abstract, Int'l. Symp. on SM/MPAC&SEED Experiments, Tsukuba (2008.3.10-11)*.



## MATERIAL AGING OF SILOXANE COATED POLYIMIDE FILM AND SILICONE-BASED WHITE PAINT ON SM/SEED EXPOSURE EXPERIMENTS

Junichiro ISHIZAWA

*Institute of Aerospace Technology, Japan Aerospace Exploration Agency, Tsukuba, Ibaraki 305-8505, Japan*

Thermal control polymeric films for spacecraft are required to achieve high tolerance against space environments because they are used as the outermost layer of spacecraft and are therefore exposed directly to space. Especially in low-Earth-orbit (LEO) environments, "erosion" by atomic oxygen (AO) attack is the dominant form of degradation for such materials. JAXA has assessed the effectiveness of several AO-barrier coatings to improve their AO-resistance. Silicone-based coatings form a passivating layer on the surface through oxidization with AO. Siloxane-coated polyimide film and silicone-based white paints were exposed to a LEO environment during Space Environment Exposure Device experiments on the Russian Service Module (SM/SEED exposure experiments). Both materials exhibited high space environment tolerance after exposure.

**Keywords:** MAPC&SEED, Polyimide white paint, Atomic oxygen, MPAC&SEED, Space exposure experiments, Silicone, Contamination

### 1. Introduction

A great demand exists for evaluating material degradation and developing materials tolerant to the low-Earth-orbit (LEO) environment for operation of manned spacecraft (ISS, space shuttle), Earth observation satellites, etc. Compared with geosynchronous orbit (GEO), the LEO environment is characterized by atmospheric atomic oxygen (AO). AO is generated by dissociation of oxygen or ozone molecules due to solar ultra violet rays (UV) and is very active on materials. AO strikes spacecraft surfaces at a relative velocity of 8 km/s and chemically reacts with materials as erosion on polymeric materials or metal oxidation.

We developed highly tolerant films consisting of polyimide coated with thin polyimidesiloxane (Silox) layers. Silox-coated polyimide films were evaluated for changes in material properties using the Combined Space Effects Test Facility (CSETF). Thermo-optical properties and mass changes of the films showed significant AO tolerance [1,2]. Furthermore, JAXA developed silicone-based white paint and certified it for space use. It has been demonstrated as a highly AO-tolerant material.

To evaluate material aging in real LEO environment, JAXA has conducted space experiments using the Micro-Particle Capturer (MPAC) and Space Environment Exposure Device (SEED) on the Russian Service Module (SM) in the ISS. Material exposure experiments are very important for understanding the effects of real environments consisting of AO, UV, radiation, micro-particle (debris and micrometeoroids) irradiation, and contamination derived from outgassing and propellants. They also synergistically affect materials, and it is still now difficult to simulate a space environment in ground test.

To clarify material-aging mechanisms with different exposure duration specimens, three identical sets of SM/MPAC&SEED were exposed together. The sets were retrieved at around one-year intervals. Exposure periods of the three SM/MPAC&SEED units are presented in Table 1.

Their high tolerance to the ISS environment was

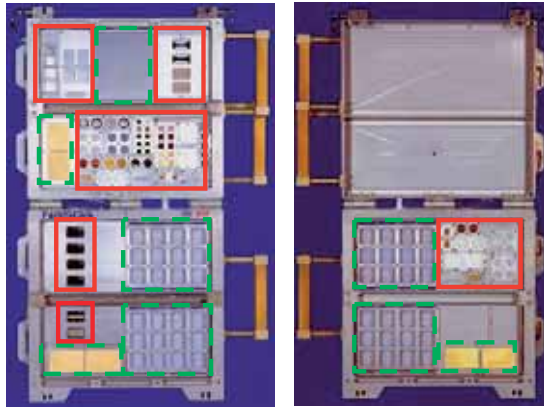
demonstrated by small changes of their thermo-optical properties and mass. We consider that silicone-based materials were stable in the ISS environment due to inorganic silicon oxide layers being converted from silicone by AO irradiation to provide protection against AO. The silicon-oxide layer, converted from the siloxane coating on polyimide film, was highly tolerant. In addition, the silicon-oxide layer produced from condensed on-orbit contamination consisting of silicon was observed on every exposed sample (among silicone-free materials). It also acted a barrier against AO attacks, although not to the extent of the siloxane coating.

### 2. Experimental

#### 2.1 Flight experiment

Each SM/MPAC&SEED contained 28 SEED specimens and 4 monitoring materials[3]. Silica aerogels, polyimide foams, and aluminum plates for MPAC were installed for MPAC [4,5]. The conditions of the exposure environment (e.g., the total fluence of AO, UV, and EB) were estimated using JAXA's Space Environments & Effects System (SEES) [6] analysis code (Table 3). In addition, they were extrapolated from property changes of monitoring samples [7]

Specimen changes in physical, chemical, and thermo-optical properties (e.g. solar absorptance ( $\alpha_s$ ) and normal infrared emittance ( $\epsilon_N$ )) before and after flight were evaluated using Atomic Force Microscopy (AFM), Scanning Electron Microscope (SEM), Transmission Electron Microscope (TEM), X-ray Photoelectron Spectroscopy (XPS), Energy Dispersive X-ray Spectroscopy (EDX), Fourier Transform Infrared Spectrophotometer (FT-IR), and thermo-optical measurement systems.



**Solid line:** SM/SEED and monitoring materials  
**Dashed line:** SM/MPAC

**Fig.1 SM/MPAC&SEED**

**Table 1 Ground simulation test conditions of SM/MPAC&SEED**

	Exposure Period (days)	AO (atoms·cm <sup>-2</sup> )	UV (ESD*)	Electrons (e·cm <sup>-2**</sup> )
1st	315	$2.85 \times 10^{21}$	66.5	$1.61 \times 10^{12}$
2nd	865	$5.70 \times 10^{21}$	150.5	$4.67 \times 10^{12}$
3rd	1403	$8.41 \times 10^{21}$	244.0	$6.57 \times 10^{12}$

\* 1 equivalent solar day (ESD) =  $1.02 \times 10^7$  J·m<sup>-2</sup>

\*\* Covering more than 0.1 MeV electron

## 2.2 Monitoring samples

Conditions of the second SM/SEED environment, as estimated from monitoring sample property changes and SEES database analysis data, are presented in Table 2 [7].

**Table 2 SM/SEED environment from monitoring sample changes and SEES database analysis**

	Sample/Model	RAM face	
		#1	#2
Maximum Temperature (°C)	Thermo label	#1	50–60
		#2	50–90
		#3	60–90
AO (atoms/cm <sup>2</sup> )	Vespel®	#1	$2.04 \times 10^{20}$
		#2	$2.57 \times 10^{20}$
		#3	$2.70 \times 10^{20}$
	SEES	#1	$2.85 \times 10^{21}$
		#2	$5.70 \times 10^{21}$
		#3	$8.41 \times 10^{21}$
UV (ESD)	Poly urethane	#1	18.1
		#2	15.8
		#3	13.4
	SEES	#1	73.8
		#2	167
		#3	271
TID (Gy)	Alanine Dosimeter	#1	1.95
		#2	15.30
		#3	32.0
	RADFET	#1	0.44
		#2	5.99
		#3	8.59
	SEES	#1	67.6
		#2	181
		#3	234

## 2.2 Ground experiment

JAXA conducted reference experiments on the ground simultaneously with on-orbit experiments to clarify the degradation mechanisms of retrieved materials. Specimens exposed to single AO, UV, and electron beam (EB) were compared for identical specimens from SM/SEED. Both AO and EB irradiations were performed at the combined space-effects test facility, which is equipped with PSI's FAST™ AO source [8] EB source, and a deuterium UV source. The AO flux was greater than  $10^{19}$  atoms·m<sup>-2</sup>·s. For irradiation of UV in this study, another UV irradiation facility with a conventional xenon UV-ray source that can emit 10 equivalent solar days (ESD)/day at wavelengths between 200 nm and 400 nm for solar UV radiation was used. The EB energy was 144.2 keV, beam current was 0.685 mA, and surface absorptance dose of the specimen was 1.633 kGy. Evaluation of changes in the material properties of ground specimens corresponded to evaluations of flight experiment specimens.

## 2.3. Specimen

### 2.3.1 Modified PI

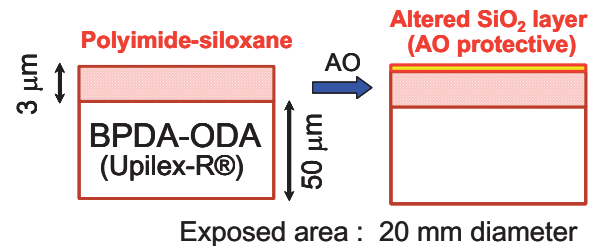
#### (Polyimide-siloxane coated UPILEX-R)

It is important to improve the durability of thin polymer thermal-control films against AO erosion. We have developed new polyimide films with high tolerance against AO attack. This 50 μm thick UPILEX-R® ([biphenyl tetra carboxylic dianhydride]-[4,4'-oxydianiline] BPDA-ODA) film is coated with a 3 μm thick polyimide siloxane layer as shown in Fig. 2 [1]. AO attack changes the coating to an inorganic oxide, which forms a protective skin that is highly resistant to AO erosion. These types of AO-tolerant materials are easy to apply to satellites because, during launch or assembly, the coat material is sufficiently flexible to withstand deformation, in contrast to inorganic coatings.

The polyimide siloxane layer was synthesized from 2,3,3',4'-biphenyl tetra carboxylic dianhydride (a-BPDA) as the acid component and bis(3-aminopropyl) polydimethylsiloxane (DAPSi), 2,2-bis[4-(4-aminophenoxy)phenyl] propane (BAPP) and 3,5-diaminobenzoic acid (DABA) as the amine component in a 1,2-bis(2-methoxyethoxy) ethane solvent. A cross-linking reagent composed of polyglycidyl ether of o-cresol-formaldehyde novolak (EOCN) and a hardener composed of 2-ethyl-4-methylimidazole (2E4MZ) were mixed into the polyimide siloxane solution to form a varnish. The varnish was then applied to UPILEX-R® film and thermo-set.

Two modified PI specimens with different treatments (coated or uncoated) were exposed as shown in Table 3. The uncoated specimen was equivalent to normal UPILEX-R®.

The specimen exposure area for flight and ground experiments was a 20-mm-diameter circle.



**Fig.2 Constitution and atomic oxygen protect concept of Modified PI**

**Table 3 Treatments of modified PI in each retrieved set**

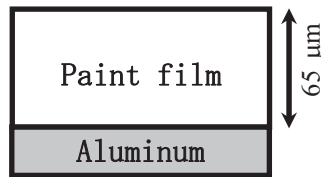
1st	Uncoated	Uncoated
2nd	Coated	Uncoated
3rd	Coated	Coated

### 2.3.2 White paint

JAXA has developed silicone-based white paint through collaboration with Nippon Paint Co. Ltd. The white paint (NOVA 500 Astro® White) was designed as a low-outgassing type for space use and qualified as NASDA-1049/101-S. It comprises a silicone-resin matrix with mainly zinc oxide (ZnO) as a white pigment.

JAXA has demonstrated its stability against space environments with ground test facility and space exposure experiments: Evaluation of Space Environment and effects on Materials (ESEM) [9]. In ESEM experiments, this material was exposed to a space environment on the cargo bay of the Space Shuttle 85 for 10 days. High stability was confirmed, but the exposure period was too short to evaluate its stability in a space environment.

For SM/SEED experiments, white paint specimens were coated to 65- $\mu\text{m}$  thickness onto aluminum alloy plates: a 21-mm-square area was exposed in orbit (Fig. 3). Each aluminum plate was weighed to ascertain the paint film's weight.

**Fig.3 Schematic of white paint specimen**

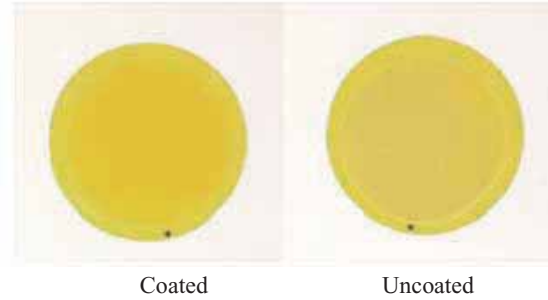
## 3. Results and discussion

### 3.1 Post flight evaluation

Samples of three different terms of exposure were retrieved. No defect such as peeling-off, cracks, etc. was detected in any specimen.

Figure 4 portrays the second retrieved Modified PI: coated and uncoated. The exposed area of the coated sample was browned slightly; that of the uncoated sample was lusterless, appearing to be eroded by AO. Figure 5 depicts a photograph of a 1403-day exposed white paint. The exposed area was browned lightly. This tendency was observed in longer-exposed specimens.

The changes in mass, solar absorptance ( $\alpha_S$ ), and infrared emittance ( $\epsilon_N$ ) of the retrieved specimens are presented in Table 4.

**Fig.4 Second retrieved Modified PI****Fig.5 Third retrieved white paint**

### 3.2 Modified PI

#### (Polyimide-siloxane coated UPILEX-R)

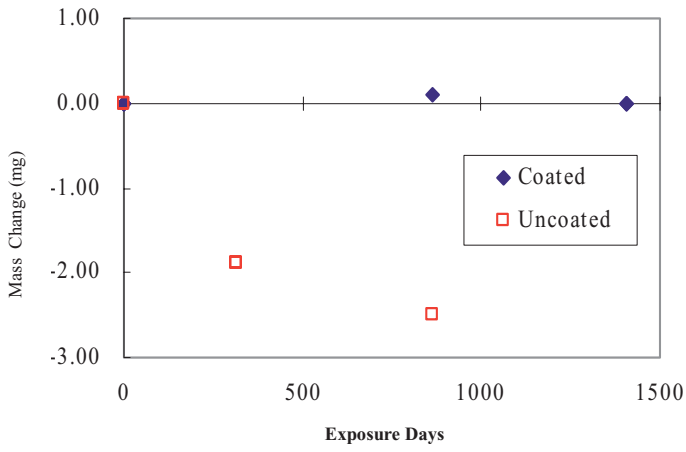
Figure 6 and Figure 7 depict changes in mass and thermo-optical properties of Modified PI. Uncoated specimen exhibited greater solar absorptance degradation and much greater mass loss than the coated specimen did. The coated sample demonstrated high AO erosion tolerance. The  $\alpha_S$  increased; however, it did so less than the uncoated sample.

Actually,  $\alpha_S$  changes in ground AO irradiation tests in Figure 8.  $\alpha_S$  were unaffected by AO fluences. Figure 9 shows  $\alpha_S$  changes in ground UV irradiation tests. The  $\alpha_S$  was increased by UV irradiation corresponding to the flown specimen.  $\alpha_S$  increasing during exposure is regarded as discoloration of UV. In addition, few  $\alpha_S$  changes in were observed in EB irradiation test.

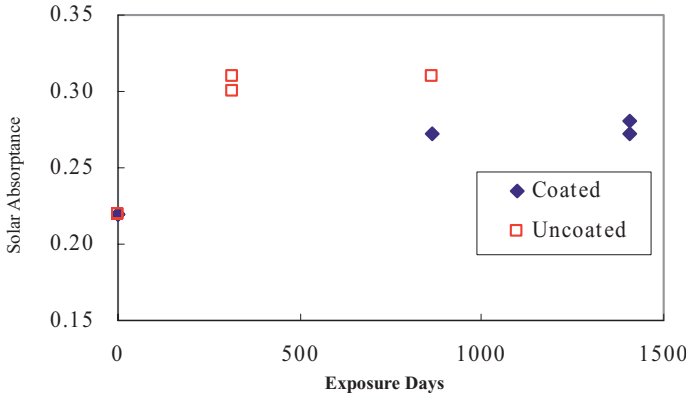
**Table 4 Changes in mass, solar absorptance ( $\alpha_S$ ), and infrared emittance ( $\epsilon_N$ ) of the second retrieved specimens**

Sample	Retrieval	Mass (mg)			Solar Absorptance ( $\alpha_S$ )			Infrared Emittance ( $\epsilon_N$ )		
		$M_{\text{control}}$	$M_{\text{flight}}$	$\Delta M$	$\alpha_{S \text{ control}}$	$\alpha_{S \text{ flight}}$	$\Delta \alpha_S$	$\epsilon_{N \text{ control}}$	$\epsilon_{N \text{ flight}}$	$\Delta \epsilon_N$
Upilex-R (Uncoated)	#1	36.9	35.0	-1.9	0.220	0.310	0.090	0.628	0.592	-0.036
		36.6	34.7	-1.9	0.220	0.303	0.083	0.628	0.588	-0.040
Modified PI (Coated)	#2	36.3	33.8	-2.5	0.220	0.305	0.085	0.628	0.599	-0.029
	#3	36.2	36.3	0.1	0.220	0.272	0.052	0.628	0.624	-0.004
White Paint	#1	36.7	36.7	0.0	0.220	0.280	0.060	0.630	0.630	0.000
		36.9	36.9	0.0	0.220	0.272	0.052	0.630	0.630	0.000
	#2	144.5	144.3	-0.2	0.275	0.280	0.000	0.865	0.870	0.005
		143.4	143.2	-0.2	0.275	0.280	0.000	0.865	0.870	0.005
	#3	143.2	142.9	-0.3	0.276	0.321	0.045	0.866	0.869	0.003
		144.4	144.0	-0.4	0.274	0.318	0.050	0.865	0.869	0.004
#3	138.0	137.6	-0.4	0.272	0.330	0.060	0.865	0.863	-0.002	
	142.4	142.0	-0.4	0.275	0.326	0.051	0.866	0.865	-0.001	

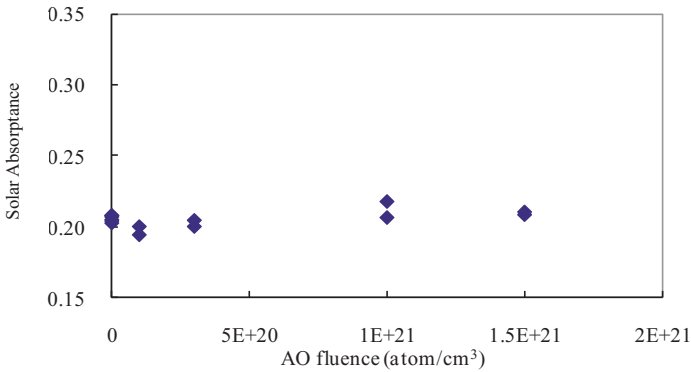
$$\Delta M = \text{mass}_{\text{flight}} - \text{mass}_{\text{control}}, \Delta \alpha_S = \alpha_{S \text{ flight}} - \alpha_{S \text{ control}}, \Delta \epsilon_N = \epsilon_{N \text{ flight}} - \epsilon_{N \text{ control}}$$



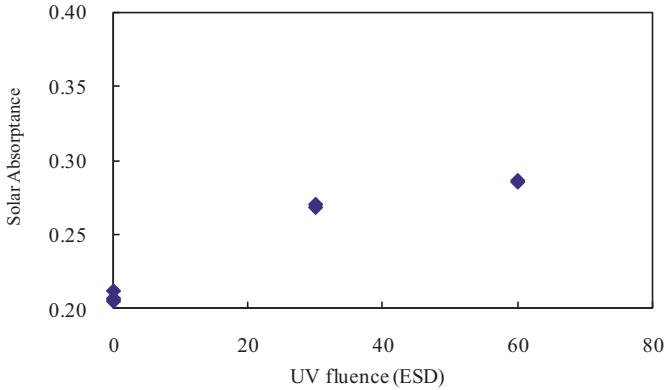
**Fig.6 Mass changes of Modified-PI on SM/SEED**



**Fig.7 Solar absorptance changes of Modified-PI on SM/SEED**

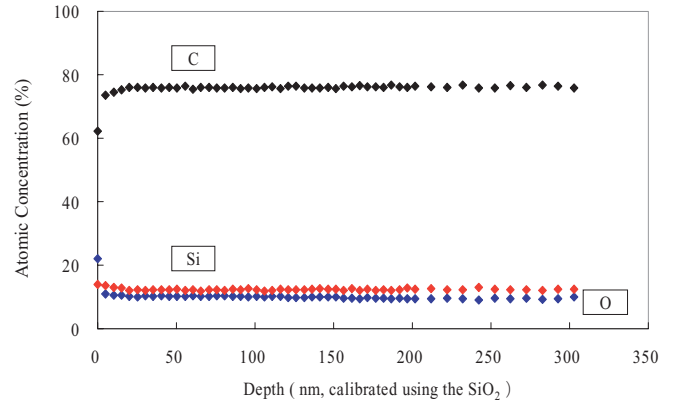


**Fig.8 Solar absorptance changes of Modified-PI on AO irradiation test**

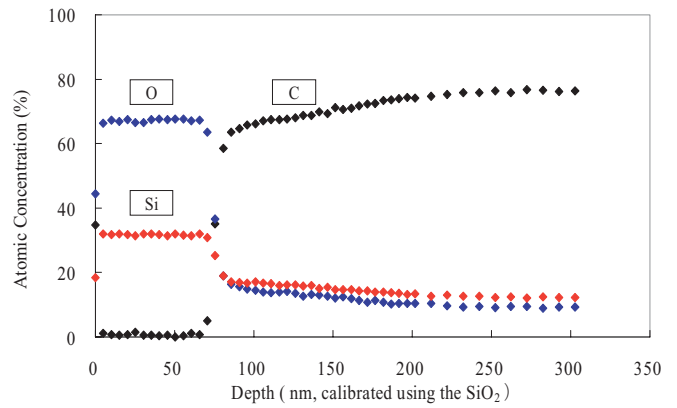


**Fig.9 Solar absorptance changes of Modified-PI on UV irradiation test**

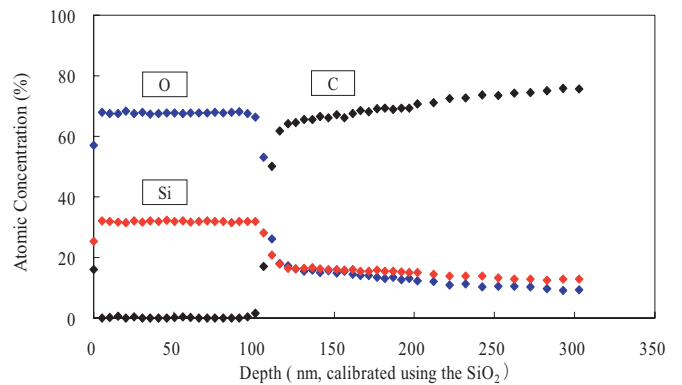
Figure 10 portrays XPS depth profiles of coated specimens. Carbon, oxygen, and silicon were the main elements detected. The outermost layer was apparently affected by ground contamination. Exposed specimens have a SiO<sub>2</sub> layer as a plateau area (homogeneous composition); the 315-day exposed specimens have a ca. 40 nm layer; the 865-day exposed specimens have a ca. 70-nm-thick SiO<sub>2</sub> layer.



(a) Not exposed



(b) 315 day exposed



(c) 865 day exposed

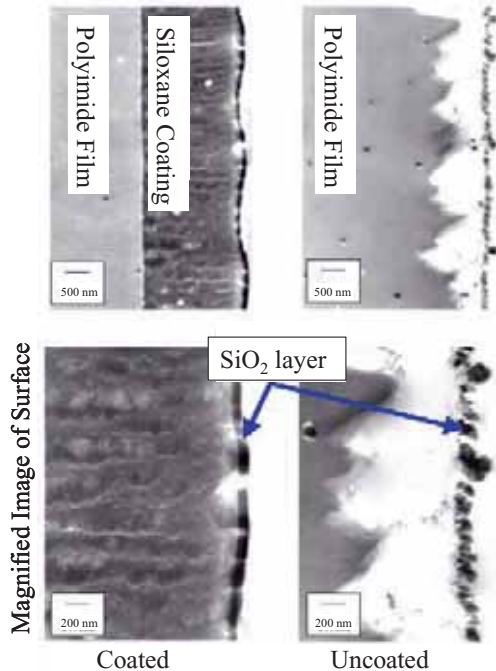
**Fig.10 XPS depth profile of Modified-PI**

Figure 11 presents TEM images of the flight specimens' cross-sections. Epoxy resin was embedded in the specimens. Coated specimens exhibited little erosion; uncoated specimens displayed considerable erosion.

The top layers of both specimens were identified as inorganic SiO<sub>2</sub> by XPS[10]. Interestingly, there was an eroded



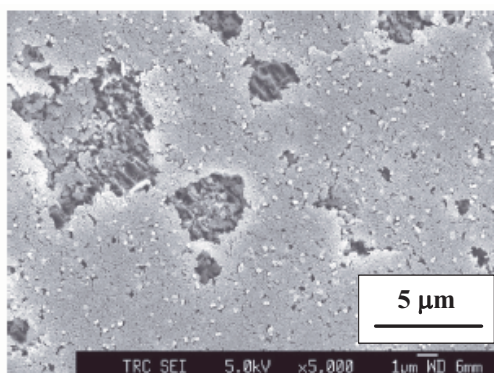
area underneath the thick and non-uniform  $\text{SiO}_2$  layer in the uncoated specimen, in contrast to the coated specimen. The  $\text{SiO}_2$  layer was observed as being afloat in the uncoated specimen, if that were true, they would break away during the embedding process. It is considered that the layer adheres to the film on several points.



**Fig.11 TEM images of cross-section for second retrieved Modified PI (coated and uncoated)**

Figure 12 is an FE-SEM image of uncoated specimen's surface with a porous layer and carpet-like matrix. Carpet-like geometry is typically found in AO-irradiated polyimide.

The silox layer's effective AO protection was confirmed in coated sample. The results of uncoated sample indicate that a  $\text{SiO}_2$  subjected to out-gassing siloxane contamination provided inadequate protection. Contamination environment of SM/SEED and condensed silicone evaluation are reported in reports [11,12].



**Fig.12 FE-SEM image of the second retrieved uncoated Modified PI surface**

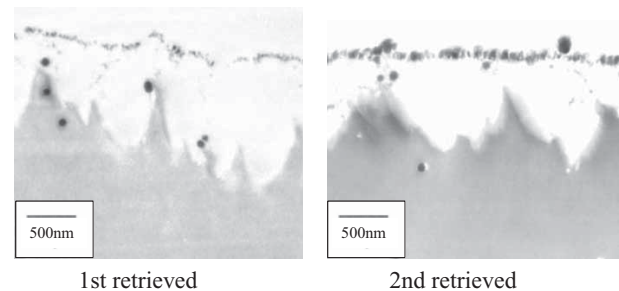
For detailed analysis of uncoated sample, mass loss, AO erosion rate and  $\alpha_S$  for SM/SEED retrieved specimens, ground AO irradiated specimen and the ESEM retrieved specimen [9] are compared in Table 5.

AO erosion rate of the second retrieved specimen (uncoated) was less than that of the first. The AO erosion rates calculated with  $\Delta M$  (mass change), estimated AO fluence, exposed area and density of UPILEX-R® were 0.10 to  $0.15 \times 10^{-24} \text{ cm}^3/\text{atom}$  and were quite small; in contrast, AO erosion rate of Kapton H polyimide film is around  $3 \times 10^{-24} \text{ cm}^3/\text{atom}$ . In  $\alpha_S$ , no differences were observed between flight specimens.

These results indicate that aging of polyimide material in mass and thermo-optical property slows during SM/SEED experiments aboard ISS. Figure 13 presents TEM images of the cross-section for second-retrieved samples. The second-retrieved uncoated sample's  $\text{SiO}_2$  layer created by outgassing siloxane contamination was thicker and more uniform than the first-retrieved one. For that reason, the contaminant silicone layer might increase during exposure and become a more effective barrier against AO. However, that depends on several factors that affect contamination condensation, such as the atmosphere (including outgassing), temperature, and active constituents of materials (AO, UV, EB, etc.). The contaminant barrier is uncertain and unreliable depending on individual missions, uncoated samples were inferior to the coated sample in solar absorptance stability in the SM/SEED experiment. A highly AO-tolerant material is necessary for the LEO environment.

**Table 5 Mass loss, AO erosion rate, and  $\alpha_S$  of the second retrieved Modified PI (uncoated)**

	Days	AO fluence (atom/cm <sup>2</sup> )	$\Delta M$ (mg)	AO erosion rate ( $\times 10^{-24} \text{ cm}^3/\text{atom}$ )	Erosion rate comparison with Kapton-H *
Uncoated 1st	315	$2.85 \times 10^{21}$	-1.9	0.15	1/20
Uncoated 2nd	865	$5.70 \times 10^{21}$	-2.5	0.10	1/30
Ground	-	$3.16 \times 10^{20}$	-4.0	2.9	Similar
ESEM	11.6	$4.4 \times 10^{23}$ $\sim 1.5 \times 10^{24}$	-1.4	2.1 ~ 7.3	same order
Coated 2nd, 3rd			> 0	-	



**Fig.13 TEM images of cross-sections for the first- and second-retrieved Modified PI (uncoated specimen)**

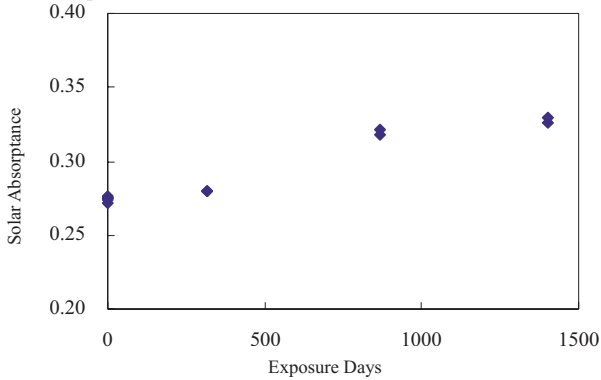
### 3.3 White paint

Solar absorptance and normal infrared emittance are depicted in Figure 14 and Figure 15. Although normal infrared emittance changed little during exposure, the solar absorptance increased corresponding to visible browning (Fig. 5). The solar absorptance value finally changed from 0.27 to 0.33. In Fig. 14, main changes in solar absorptance seem to have occurred from the 315-day to the 865-day exposure period; a slight change was apparent for 315-day-exposure; after the 865-day-exposure, it behaved as stable.

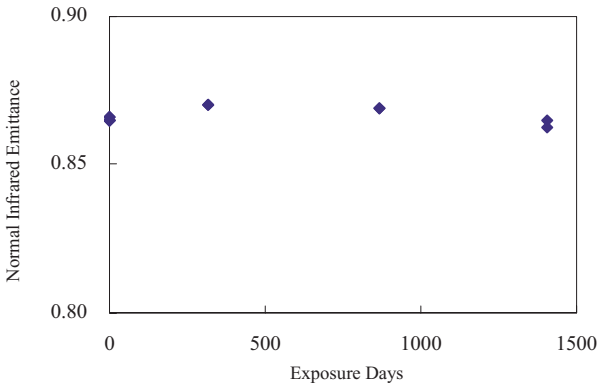
Figure 16 portrays the mass change in exposed specimens. The mass of white paints decreased gradually. Considering that the average of the paint film mass (deducting the aluminum plate weight) was 143 mg before exposure, only 0.3% of the original mass was lost in the 1403-day exposed specimen.

The white paint showed little mass loss in the SM/SEED experiment; the mass loss was inferred to have resulted from erosion by AO in LEO, which did not occur in the SM/SEED experiment. Solar absorptance was increased 0.06 for 1403-day exposure; the change was stable in later periods.

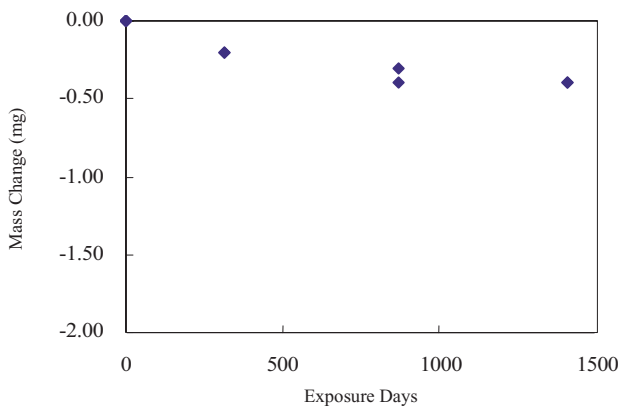
To clarify the solar absorptance change that occurred in SM/SEED experiments compared to ground test results, Fig. 17 shows AO irradiation; Fig. 18 shows UV irradiation test results for white paint.



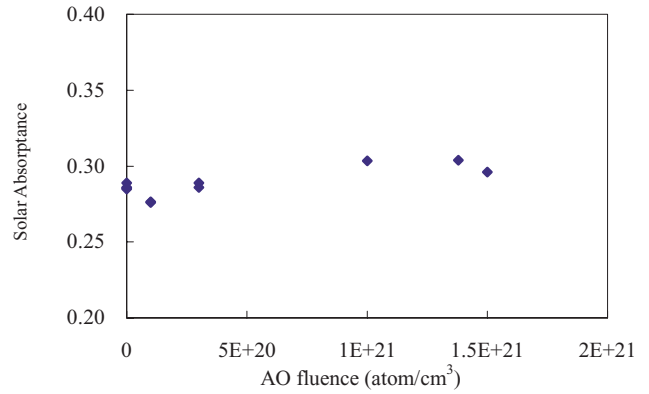
**Fig.14 Solar absorptance changes of white paint in the SM/SEED experiment**



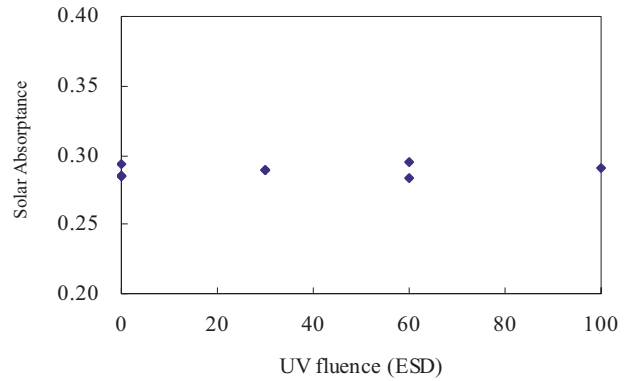
**Fig.15 Normal infrared emittance changes of white paint in the SM/SEED experiment**



**Fig.16 Mass change of white paint in the SM/SEED experiment**

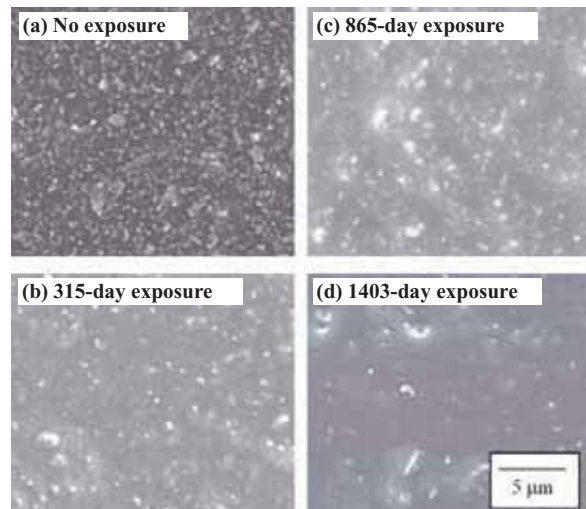


**Fig.17 Solar absorptance changes of white paint as measured from ground AO irradiation tests**



**Fig.18 Solar absorptance changes of white paint as measured from ground UV irradiation tests**

Referring to Table 2, fluences of the ground tests cover 315-day-exposure in UV, half of 315-day-exposure in AO of SM/SEED experiment condition analyzed using the SEES database. In both ground test results, white paint is stable against AO and UV irradiation. Furthermore, electron beam irradiation tests, which showed fluence of  $1.6 \times 10^{12}$  electrons/cm<sup>2</sup> corresponding to 315-day exposure, were conducted: the solar absorptance increase was only 0.003.

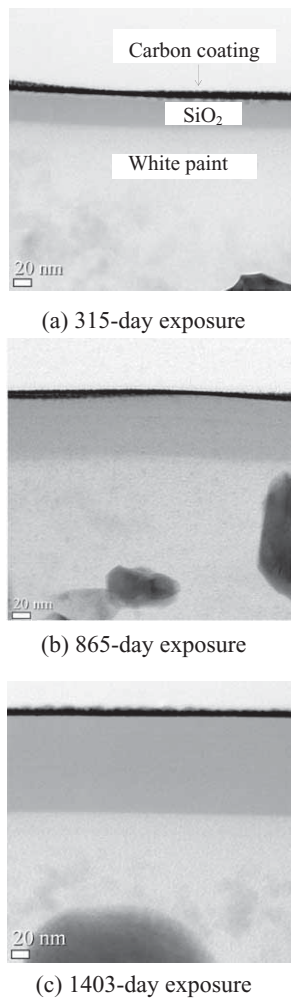


**Fig.19 FE-SEM images of a white paint surface in SM/SEED retrieval samples**

Figure 19 presents FE-SEM surface images of white paint specimens. White pigmentation was obviously identified on non-exposed samples. However, their vague profiles were observed on exposed specimens; the effects were apparent from longer exposure periods.

For detailed analyses of retrieved specimen surfaces, we performed cross-section observation using STEM, with focused ion beam (FIB) sample treatment. Shown in Fig. 20, a gray layer on white paint (white zone) surface is visible (the outermost black layer is conductive coating for observation). The gray area thickness increased during exposure.

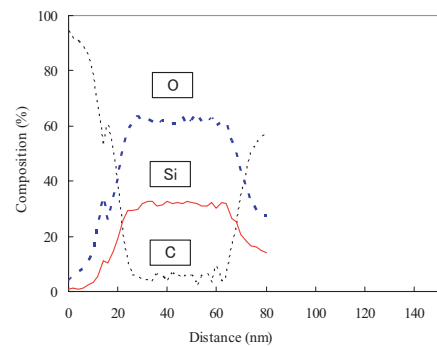
Figure 21 shows results of elemental depth analyses in the retrieved specimens' surface were coated with conductive carbon and conducted using EELS. A plateau area, a corresponding gray layer in STEM image, was detected in each retrieved specimen. The plateau area mostly comprises silicon and oxygen, with carbon in small quantities; the elemental ratio is approximately Si : O = 1 : 2; the gray layer was identified as silicon dioxide. From modified PI experimental results, this layer was formed through contaminant absorption and reaction with AO, which is considered as an AO-protection layer.



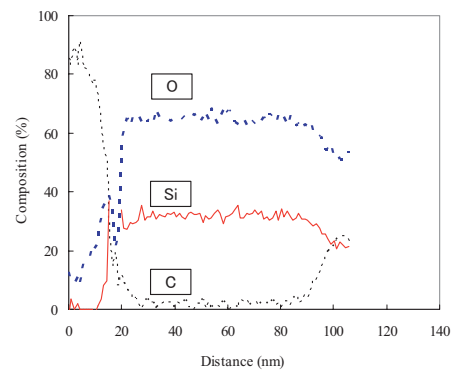
**Fig.20** Cross-section images of a white paint surface of SM/SEED retrieval samples

The origin of the silicon might be the white paint's resin and outgassing from other materials. It is probable that silicone outgassing deposition attributable to the thickness increased stably during exposure (Table 6). Several specimens in SM/SEED do not include silicone elements, but have a silicon-dioxide surface layer. In addition, the silicon dioxide layer thicknesses are almost identical to those of other SM/SEED specimens.

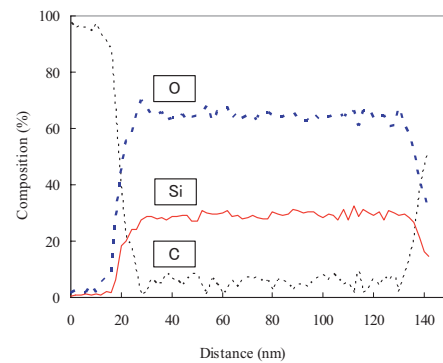
Silicon contamination and its reactant covered white pigments (high reflective) and possibly increased solar absorptance. Additional studies should be undertaken to examine contamination effects for thermo-optical properties specifically, along with synergetic effects such as AO, UV, irradiation, and thermal condition combinations.



(a) 315-day exposure



(b) 865-day exposure



(c) 1403-day exposure

**Fig.21** Depth profile of white paint surface in SM/SEED retrieval samples

**Table 6 Thicknesses of the silicon dioxide layer and thermo-optical properties of white paints**

	Exposure period (days)	SiO <sub>2</sub> thickness (nm)	Solar absorptance	Normal infrared emittance
No exposure	-	-	0.275	0.865
1st retrieval	315	40	0.280	0.870
2nd retrieval	865	70	0.320	0.869
3rd retrieval	1403	110	0.328	0.864

#### 4. SUMMARY

Observations and analyses of retrieved specimens from SM/SEED experiments, the aging behaviors of siloxane-coated polyimide film and silicone-based white paint were evaluated. The following results were obtained from this study.

##### (1) Modified PI

- The coated sample demonstrated its high AO tolerance.
- The solar absorptance of modified PI was increased, but it was less than that of the uncoated sample.
- An inorganic SiO<sub>2</sub> layer was observed on an uncoated sample. Although it originated from outgassing and was defective in shape, the layer reduced AO erosion.

##### (2) White paint

- Critical damage, such as peeling-off, cracks, and notable changes in thermo-optical properties, was not observed in any sample.
- Mass loss induced by AO erosion was quite small.
- Solar absorptance increased during the 315–865-day-exposure period; after 865-day exposure, it was stable.
- Silicon contamination deposited on the white paint surface probably affected the solar absorptance and increased AO protection.

We will continue to evaluate materials by preparing a JEM/MPAC&SEED experiment that will be placed on the front side of the ISS, where it is expected to experience less outgassing contamination. Thereby, we can clarify the white paint aging mechanisms in a LEO, where the ISS operates.

Through space materials exposure experiments and ground simulation tests, we will also continue to evaluate material aging and contaminant effects and to improve the tolerance of materials intended for space use.

#### References

- [1] F. Imai, M. Iwata, Y. Nakayama, and K. Imagawa: Characterization of newly-developed polymeric materials for spacecraft by Combined Space Effects Test Facility, *Proc. 23rd ISTS*, (2002) pp.646-651.
- [2] F. Imai, J. Ishizawa, R. Yokota, E. Sato, K. Imagawa, K. Umeda, S. Baba, Y. Uyama, K. Takahashi, and Y. Tajima: Newly Developed Polymeric Materials for Spacecraft Characterized by the Combined Space Effects Test Facility (II), *Proc. 24th ISTS*, (2004) (CD-ROM).
- [3] Y. Kimoto, J. Ishizawa, E. Miyazaki, and M. Suzuki: SM/MPAC & SEED Experiment Overview, *Proc. International Symposium on "SM/MPAC&SEED Experiment*, in press.
- [4] Y. Kitazawa, A. Fujiwara, T. Kadono, T. Noguchi, R. Yamanaka, Y. Kimoto, and M. Suzuki: Overview of the MPAC Experiment, *Proc. International Symposium on "SM/MPAC&SEED Experiment*, in press.
- [5] M. J. Neish, K. Imagawa, T. Inoue, J. Ishizawa, Y. Kitazawa, Y. Yamaura, A. Murakami, and Y. Ochi: Microparticle capture on the International Space Station using aerogel and polyimide foam, *Proc. 9th ISMSE*, (2003), pp.431-435.
- [6] <http://matdb.jaxa.jp/SpaceExperiment/>
- [7] Y. Kimoto, K. Yano, J. Ishizawa, and E. Miyazaki: Post Retrieval Analyses of Space Environment Monitoring Samples: Radiation Effects, UV, and Atomic Oxygen Fluence, *Proc. International Symposium on "SM/MPAC&SEED Experiment*, in press.
- [8] G.E. Caledonia, R.H. Krech, and B.D. Greent: A high flux source of energetic oxygen atoms for materials degradation studies, *AIAA J.*, 25, (1987) pp.59-63.
- [9] NASDA: Final Report of ESEM Experiments <http://matdb.jaxa.jp/SpaceExperiment/Image/MFD-ESE-M-E.pdf>
- [10] J. Ishizawa, K. Mori, F. Imai, I. Yamagata and M. Suzuki.: Results of the Space-Environment Exposure Experiment "SM/MPAC&SEED" on the International Space Station (2): Siloxane Coated Polyimide Films, and Silicone Based Paints and Adhesives, Proceedings of the 10th ISMSE, (2006) (CD-ROM).
- [11] N. Baba., M. Suzuki, I. Yamagata, and J. Ishizawa: External Contamination Observed on the SM/MPAC&SEED, *Proc. 10th ISMSE*, (2006) (CD-ROM).
- [12] N. Baba and Y. Kimoto: Contamination Effect on SM/MPAC&SEED Experiment, *Proc. International Symposium on "SM/MPAC&SEED Experiment*, in press.



**Publication list related SM/MPAC&SEED**

- [1] F. Imai, M.Iwata, Y.Nakayama, and K. Imagawa:  
Characterization of newly-developed polymeric materials for spacecraft by Combined Space Effects Test Facility, *Proc. 23rd ISTS*, (2002) pp.646-651.
- [2] F.Imai, J.Ishizawa, R.Yokota, E.Sato, K.Imagawa, K.Umeda, S.Baba, Y.Uyama, K.Takahashi, and Y. Tajima: Newly Developed Polymeric Materials for Spacecraft Characterized by the Combined Space Effects Test Facility (II), *Proc. 24th ISTS*, (2004) (CD-ROM).
- [3]J.Ishizawa, I.Yamagata, Y.Kimoto, N.Baba, E.Miyazaki, K.Mori, H.Shimamura, F.Imai, and M.Suzuki: Evaluation and Analysis of the Second Retrieved Space Environment Exposure Device (SM/MPAC&SEED), *Proc. of 25th ISTS*, (2006) (CD-ROM).
- [4]J.Ishizawa J, K.Mori, F.Imai, I.Yamagata, and M.Suzuki.: Results of the Space-Environment Exposure Experiment “SM/MPAC&SEED” on the International Space Station (2): Siloxane Coated Polyimide Films, and Silicone Based Paints and Adhesives, *Proc. of 10th ISMSE*, (2006) (CD-ROM).
- [5]J.Ishizawa, F.Imai, and I.Yamagata:Evaluation of Siloxane Coated Polyimide Films and Silicone Based Paints Exposed to Space Environment on ISS Russian Service Module / Space Environment Exposure Device, *Proc. of 51st Space Sciences and Technology Conference*, (2007) (CD-ROM).
- [6]J.Ishizawa: Improving Tolerance against Atomic Oxygen for Polyimide Film (in Japanese), *Proc. of 11th Japan Polyimide Conference*,(2007).
- [7]J.Ishizawa: Evaluation of White Paints Exposed to Space Environment on the ISS Russian Service Module / Space Environment Exposure Experiment (in Japanese), *Proc. of 26th ISTS*, (2008) (CD-ROM).

## EVALUATION OF F-OSR EXPOSED TO SPACE ON SM/SEED EXPERIMENT

Eiji MIYAZAKI, Junichiro ISHIZAWA and Hiroyuki SHIMAMURA

*Institute of Aerospace Technology, Japan Aerospace Exploration Agency,  
Tsukuba, Ibaraki 305-8505, Japan*

A Flexible Optical Solar Reflector (F-OSR) is a thermal control film for spacecraft. It provides low solar absorptance ( $\alpha_s$ ) and high infrared emittance ( $\varepsilon$ ) with flexibility. The F-OSR, which has a conductive layer and a mirror layer coated onto a polyetherimide base film, is a thermal control film material for spacecraft. Results indicate a mass increase: atomic oxygen does not erode F-OSR in low earth orbit. Thermo-optical properties show no marked change. In fact, F-OSR is verified as retaining its initial properties after exposure on ISS orbit for 46 months. Transmission electron microscopy (TEM) observation of cross-sections, including those of the exposed surface, showed that a new layer had formed over the flight sample. Qualitative analysis of the new layer indicates that the layer mainly comprises silicon and oxygen. The layer is chemically produced by deposited silicon contamination and atomic oxygen, which would be  $\text{SiO}_2$ . This experiment also provides actual quantitative contamination data on ISS, contributing to improvement of contamination control on ISS in the future.

**Keywords:** optical solar reflector, polyetherimide

### 1. Introduction

This report presents results of the Flexible Optical Solar Reflector (F-OSR) installed on SM/MPAC&SEED. The F-OSR is a thermal control film used for spacecraft. It has low solar absorptance ( $\alpha_s$ ) and high infrared emittance ( $\varepsilon$ ) with flexibility. The F-OSR is a five-layered and second-mirrored film with a polyetherimide (PEI) base film. It has a UV protection layer to protect the base film from UV degradation. The SM/SEED experiment can reveal whether the function of F-OSR can be maintained for a year-long-order period on orbit. For evaluation, the retrieved F-OSR samples were measured to determine their changes of mass and thermo-optical properties. Topographic analyses and qualitative analyses were also performed. Herein, we present results of those evaluations for F-OSR and discuss the influence of the space environment of the ISS orbit on the F-OSR for up to 46 months.

### 2. Sample preparation

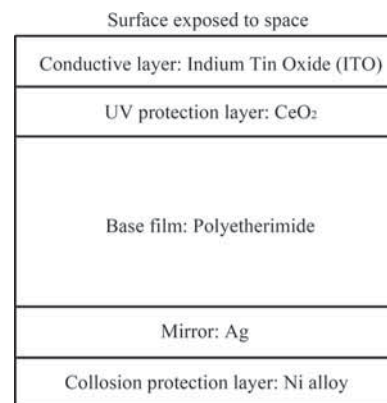
Actually, F-OSR, manufactured by Sumitomo Bakelite Co., Ltd., is a film with multilayered coatings for thermal control of spacecraft. As illustrated schematically in Fig. 1, F-OSR has five layers: a conductive layer, an ultraviolet ray (UV) protection layer, a base film polyetherimide (PEI), a mirror layer, and a corrosion protection layer. The maximum usage temperature of F-OSR is 150°C. The base film, polyetherimide, is UV degradable; for that reason,  $\text{CeO}_2$ , which is known to be UV-absorbent, is deposited. Silver is used as a second surface mirror; the layer is covered completely by Ni alloy to prevent corrosion.

With such features, F-OSR achieves low solar absorptance ( $\alpha_s$ ) and high infrared emittance ( $\varepsilon$ ) with good flexibility. The F-OSRs for SM/MPAC&SEED, with 100  $\mu\text{m}$ -thick base film, were cut into 25-mm-diameter circles, subsequently mounted on the sample holder with a frame opening a 20-mm-diameter window for exposure. Table 1 shows mass and thermo-optical properties of F-OSR provided for the SM/MPAC&SEED experiment. Two samples (A and B) were

mounted on each set (#1 – #3): six samples (#1-A – #3-B) were put on the ISS.

### 3. Evaluation

For mass measurement, we used a microbalance (readability 1  $\mu\text{g}$ , maximum load 5,100 mg, MX5; Mettler Toledo International Inc.). Solar absorptance ( $\alpha_s$ ) was measured using a JAXA custom-ordered spectrophotometer (Jasco Inc.). The value of  $\alpha_s$  is calculated by measured spectral reflectivity of a sample of 250–2500 nm and solar spectral irradiance.[1] The spectrum itself is also used for evaluation. Normal infrared emittance ( $\varepsilon_N$ ) was measured using a total-emittance reflectometer (DB-100; Gier Dunkle Instruments Inc.).



**Fig. 1 Cross-sectional illustration of F-OSR.**

**Table 1 Initial properties of F-OSR provided for the SM/MPAC&SEED experiment**

Mass (mg)	$\alpha_s$	$\varepsilon_N$
48.5	0.156	0.812

The cross-sectional microstructure was observed using transmission electron microscopy (TEM). The samples stained using  $\text{RuO}_4$  were sliced using ultramicrotomy to produce a cross-section including the exposed surface. Then TEM observation was performed at the acceleration voltage of 100 kV and magnification of  $\times 200,000$  to obtain microstructural information. Scanning TEM and Energy Dispersion X-ray Analysis (STEM-EDX) was conducted as qualitative analyses of small areas (ca. 1 nm diameter) in regions of interest identified in cross sectional images.

## 4. Results and discussion

### 4.1 Mass

Mass changes of exposed samples are depicted in Fig. 2, which shows the relationship between exposed duration and actual mass change. The results indicated a slight mass increase of less than 0.1 mg for all retrieved samples with 48.5 mg initial mass. In addition, the mass change shows a tendency of increase concomitant with the exposure duration, i.e., 0.04 mg gain for 10 months' exposure, 0.07 mg gain for 28 months, and 0.09 mg gain for 46 months. In general, the AO-attacked polymer material is eroded, resulting in mass loss. For instance, the third retrieved AO monitor polyimide sample "Vespel" lost 4.087 mg during exposure.[2] The F-OSR data suggest that erosion does not occur, i.e., it is verified that F-OSR has sufficient AO tolerance for almost 4 years on ISS orbit. On the other hand, such a mass increase suggests absorption or deposition of some substances during exposure. That point is discussed later using results of cross-sectional analysis.

### 4.2 Thermo-optical properties and spectral analysis

Changes of thermo-optical properties of the exposed samples during exposure are depicted in Figs. 3 and 4. No significant change of thermo-optical properties was observed, i.e.,  $\alpha_s$  increased 0.01 from the initial value of 0.156 for 46 months' exposure, which is almost within the uncertainty of the measuring device. For  $\epsilon_N$ , less than 0.005 changes were observed from the initial value of 0.812 for 46 months on orbit, which is also included in the uncertainty of the equipment. Figures 5–10 portray reflectance spectra obtained for  $\alpha_s$  measurement. In the UV region shorter than 400 nm, a change of reflectance by exposure is visible. However, the change depends on the sample, not the exposure duration. It might result from measurement error. No marked change was observed in other wavelength regions. Such a small change suggests that F-OSR has UV and radiation tolerance. Lack of UV protection might induce a color change of the base film, thereby changing  $\alpha_s$ .

On the other hand, some reports have described recovery: the degraded optical properties that have changed because of the space environment exposure are subsequently recovered by exposure to air.[3–4] In the present mission, it can not be confirmed that recovery occurred. Because of the retrieval procedure, air exposure before ground measurement is unavoidable. Compared to other SEED samples of the F-OSR, several samples show visible changes of the exposed surface. Although they might have recovered, such visible changes persist even after extended exposure to air on the ground. These results suggest that F-OSR can retain its beginning of life (BOL)

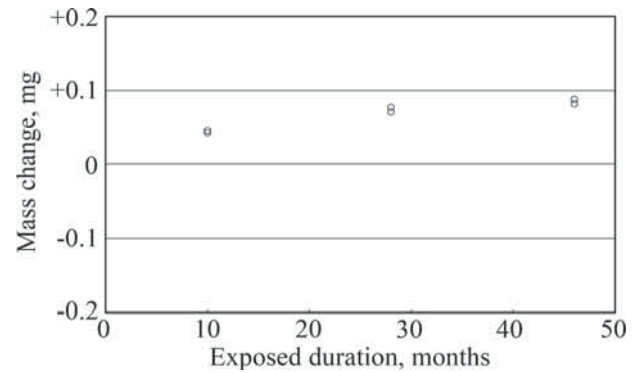


Fig. 2 Results of mass change of retrieved F-OSRs from SM/MPAC&SEED exposure.

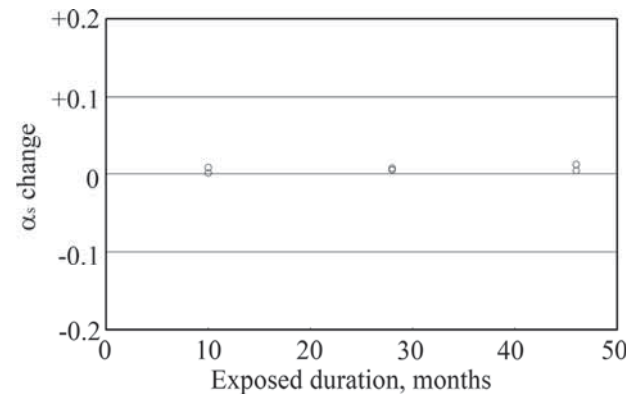


Fig. 3 Results of solar absorptance ( $\alpha_s$ ) change of retrieved F-OSRs from SM/MPAC&SEED exposure.

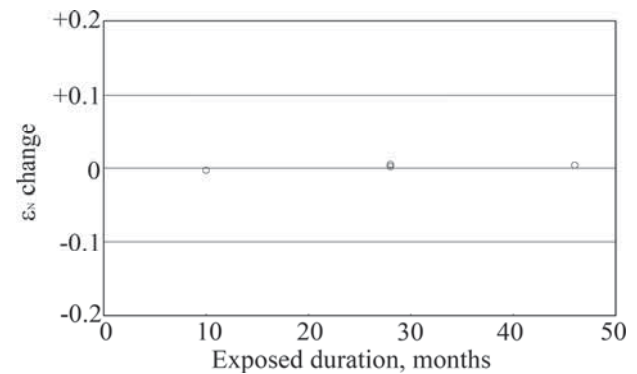
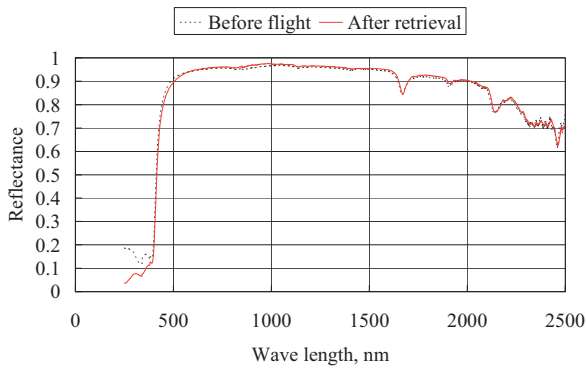
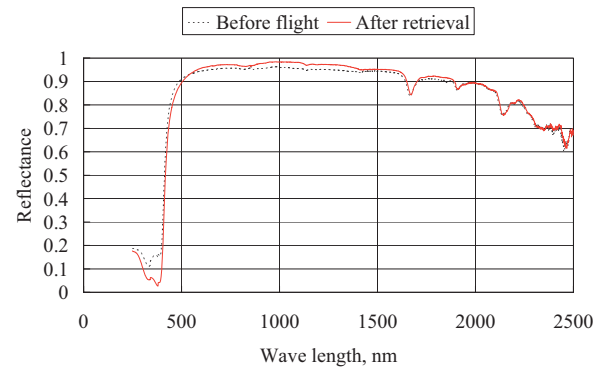


Fig. 4 Results of Normal Infrared Emittance ( $\epsilon_N$ ) change of retrieved F-OSRs from SM/MPAC&SEED exposure.

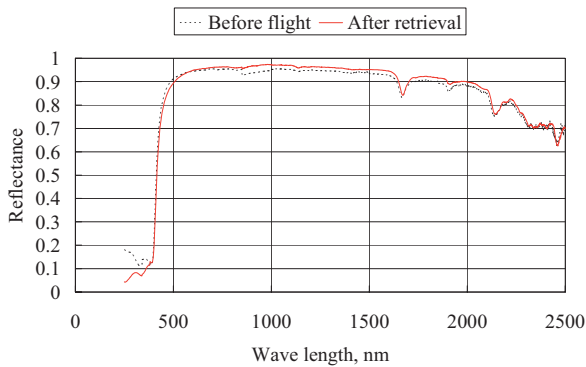
thermo-optical properties for 46 months on ISS orbit.



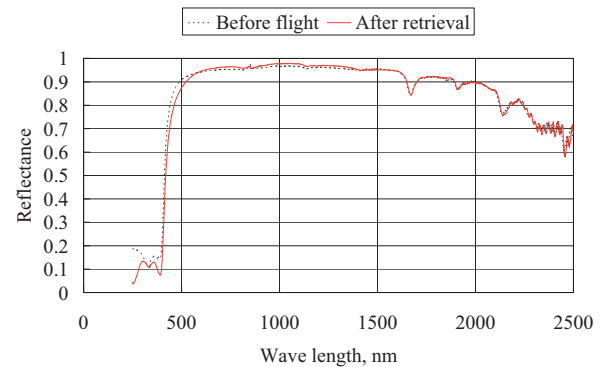
**Fig. 5** Measured results of spectral reflectance of F-OSR #1-A of SM/MPAC&SEED.



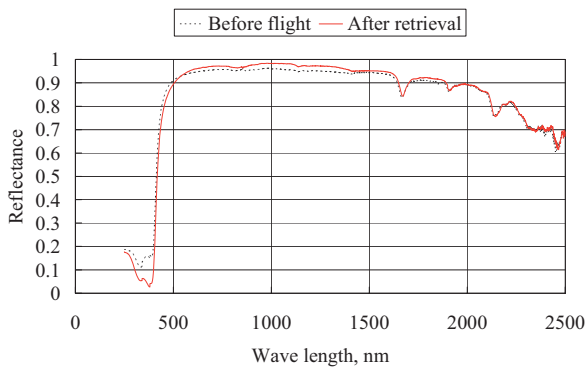
**Fig. 9** Measured results of spectral reflectance of F-OSR #3-A of SM/MPAC&SEED.



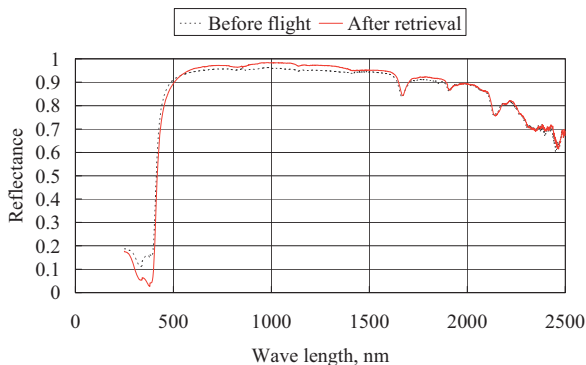
**Fig. 6** Measured results of spectral reflectance of F-OSR #1-B of SM/MPAC&SEED.



**Fig. 10** Measured results of spectral reflectance of F-OSR #3-B of SM/MPAC&SEED.



**Fig. 7** Measured results of spectral reflectance of F-OSR #2-A of SM/MPAC&SEED.



**Fig. 8** Measured results of spectral reflectance of F-OSR #2-B of SM/MPAC&SEED.

#### 4.3 Cross-sectional analysis of exposed surface

Cross-sectional TEM images of the near exposed surface are presented in Fig. 11. In those figures, the dark area appears in the lower is ITO/CeO<sub>2</sub> layer; a bright area appearing in the upper half is a mount material for TEM observation, which is not a part of F-OSR. These areas are visible in both blank sample and retrieved samples. A gray area is apparent between the dark area and the bright area only in images of retrieved samples. The gray area would be a new layer built during exposure and covering the flight samples. For the #1 sample presented in Fig. 11b, the new layer thickness can be estimated as ca. 20 nm. No marked change was observed on the original surface, i.e., the border between the new layer and ITO/CeO<sub>2</sub> layer, compared with the blank sample surface. The surface shape of the new layer, the border between the gray area and the bright area, is found to trace that of the original F-OSR's ITO/CeO<sub>2</sub> layer's surface. A cross section image of #2 sample is presented in Fig. 11c: the new layer thickness is ca. 80 nm. The original surface retains its original shape. The shape of the new layer surface does not trace finely but smoothly. Figure 11d portrays the cross section of the #3 sample: the thickness is ca. 120 nm; the new layer surface is smooth; and the original surface shows no obvious difference from its initial shape.

In general, the AO-attacked surface shows a distinctive shape with micrometer-sized asperity, a so-called carpet shape or needle-like shape. The F-OSR indicated neither apparent mass loss nor an AO-attacked shape at the original surface observed at



a magnification of nanometer nanometer-scale resolution. From the view, F-OSR might have tolerance against AO attack on the ISS orbit. Although the possibility exists that the new layer plays a role in protecting the surface from AO attack, such protection was not observed in the results for other retrieved polyimide films installed on the SM/MPAC&SEED unit, which were damaged by AO.[5] Results confirm that the tolerance of F-OSR itself against AO attack is sufficient.

Then, to examine the new layer, we performed STEM-EDX analysis in terms of investigating the layer qualitatively. For that analysis, the electron beam was focused around the center of the new layer in the depth direction, as presented in Fig. 12. The result shows detection of carbon, silicon, and oxygen, which are commonly observed in retrieved F-OSRs. The #3-A spectrum is shown as representative in Fig. 12. First, it could not be determined whether the detected carbon was derived from the exposure on orbit. Carbon was also detected in the ITO/CeO<sub>2</sub> layer, although the layer that was produced by deposition during manufacturing is not expected to contain carbon. Secondly, silicon and oxygen detected on the new layer are discussed. Because F-OSR contains no silicon, the silicon must originate from sources other than F-OSR, e.g., paints for thermal control, or adhesives used for solar arrays, containing silicon. Outgassed silicon from such sources would deposit on the other components on ISS including SM/MPAC&SEED. Silicon deposition is a known phenomenon occurring in spacecraft on orbit.[6] In the SM/MPAC&SEED mission, it was also observed and reported previously.[7] Oxygen originates from existing AO in the ISS orbit. The deposited silicon on the F-OSR surface is oxidized by collision with AO, resulting in silicon dioxide (SiO<sub>2</sub>) production. The processes of silicon deposition and oxidation would occur continuously on orbit.

Both mass measurements and thickness measurements of the new layer discovered by cross-sectional observation using TEM revealed mutual agreement, suggesting that the mass increase occurs because of new layer deposition. Figure 13 portrays the relationship between the measured mass increase per unit area and the exposure duration: the deposition is expected to become saturated as the exposure duration lengthens. This result suggests that such saturation might result from the outgassing rate behavior of the contaminant source.[8] The contamination deposition rate is calculable from the present result. Average rates are:  $1.7 \times 10^{-5}$  g/cm<sup>2</sup>/year for #1,  $1.0 \times 10^{-5}$  g/cm<sup>2</sup>/year for #2, and  $7.1 \times 10^{-6}$  g/cm<sup>2</sup>/year for #3. Those are higher than the required value: less than  $1.0 \times 10^{-6}$  g/cm<sup>2</sup>/year at a 300 K surface for molecular deposition.[9–10] Obtaining actually measured data will contribute to improvement of contamination control for ISS and other spacecraft in the future.

## 5. Conclusion

The F-OSR was exposed to the space environment as one SEED sample of the SM/MPAC&SEED mission carried out on ISS for 46 months from October 2001. The retrieved samples were investigated for their mass change and thermo-optical properties. Cross-sectional TEM observation and STEM-EDX analysis were also performed.

A slight mass gain of less than 0.1 mg was observed for all

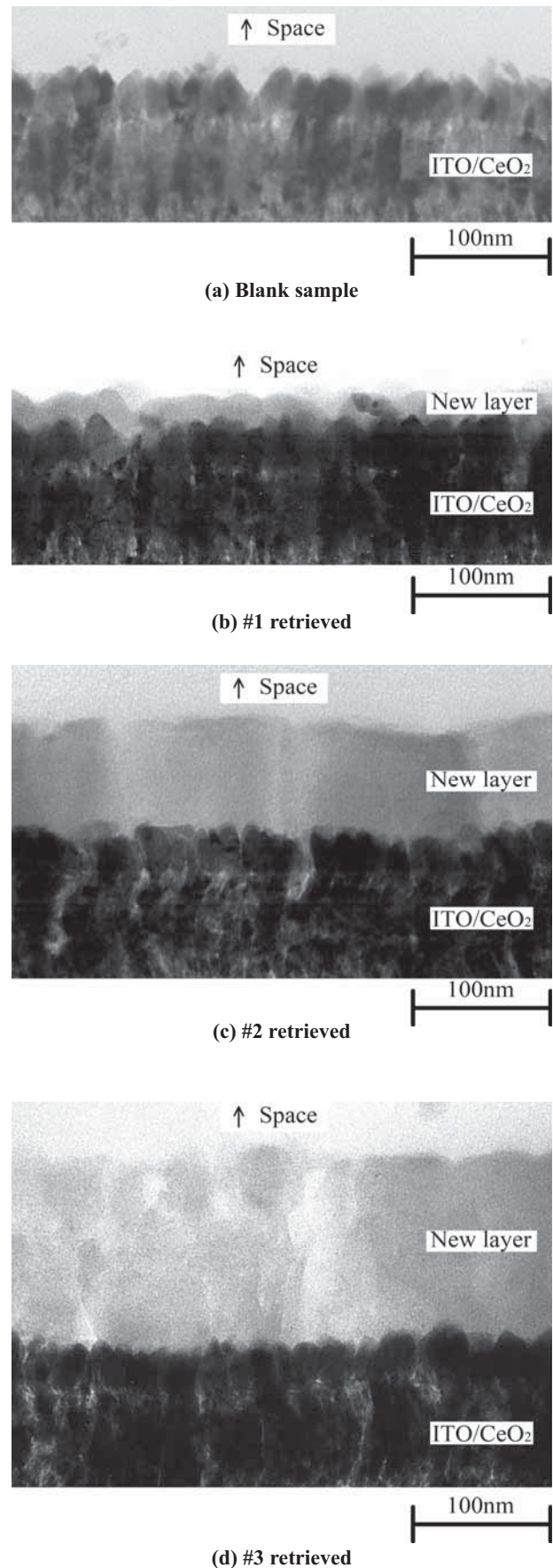
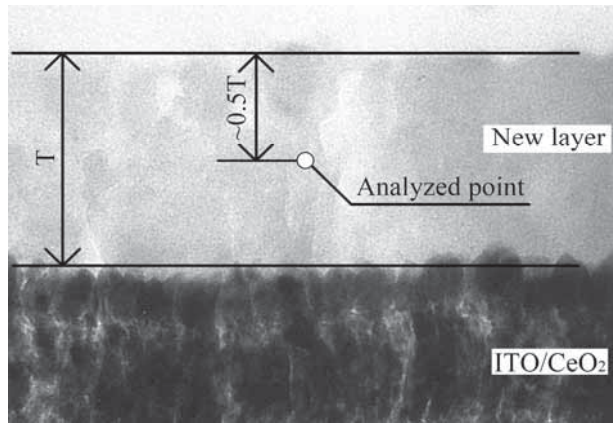
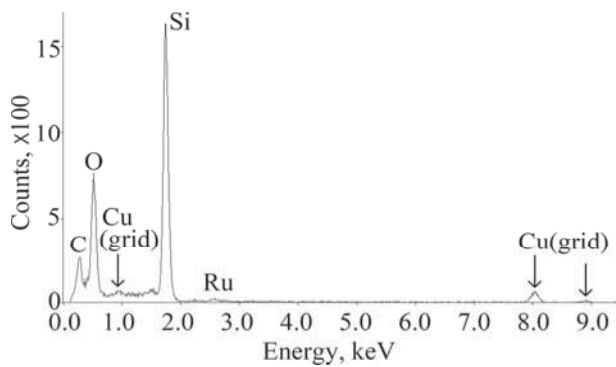


Fig. 11 Cross-sectional TEM images of F-OSRs for SM/MPAC&SEED.

retrieved samples, showing that F-OSR has tolerance against AO, i.e., erosion does not occur. The thermo-optical properties retained their initial values, although these results might also reflect recovery by exposure to air. Nevertheless, BOL thermo-optical properties of F-OSR were retained for 46 months in ISS orbit. Cross-sectional TEM observation revealed that a



(a) Analyzed point



(b) XPS spectrum obtained from #3-A

Fig. 12 Results of XPS analysis of F-OSR of SM/MPAC&SEED.

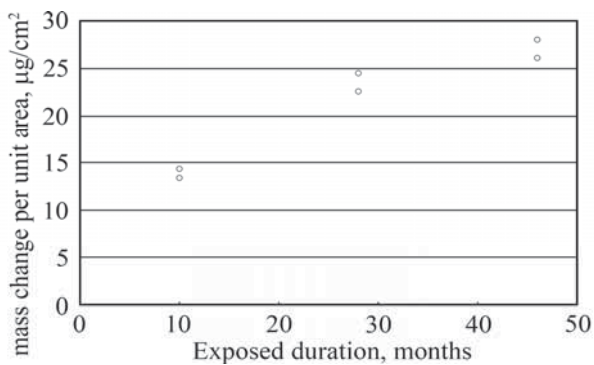


Fig. 13 Relationship between the measured mass increase per unit area and the exposure duration for F-OSR of SM/MPAC&SEED.

new layer, which does not exist on the blank sample, was built up on the exposed surface of F-OSR. The new layer thickness increased concomitantly with the exposure duration. A STEM-EDX analysis reveals that the new layer consists mainly of Si and O, which suggests that the new layer is silicon dioxide produced chemically from silicon contamination and AO.

This experiment verified F-OSR tolerance against space environments around the ISS for almost 4 years. It also provides actual contamination environmental data on ISS quantitatively, contributing to improvement of contamination control for ISS and other spacecraft in the future.

## References

- [1] ASTM E490, "Standard Solar Constant and Zero Air Mass Solar Spectral Irradiance Tables," ASTM International.
- [2] Y. Kimoto, I. Yamagata, J. Ishizawa, E. Miyazaki, N. Baba, and M. Kato, "Japanese Space Materials Exposure Experiment Utilizing International Space Station," *Proceedings of 57th International Astronautical Congress*, International Astronautical Federation (2006).
- [3] H. S. Choate, S. W. Johnson, and V. L. Mongold, "Analysis of Products Evolved from Selected Thermal Control Coating Materials during Ultraviolet Radiation in Vacuum," *AIAA Paper*, 69-640 (1969).
- [4] M. Iwata, F. Imai, K. Imagawa, N. Morishita, and T. Kamiya, "Fundamental Research to Establish Ground-Test Methodology of Thermal Control Film," *AIAA Paper*, 2003-3908 (2003).
- [5] J. Ishizawa, I. Yamagata, Y. Kimoto, N. Baba, E. Miyazaki, K. Mori, H. Shimamura, F. Imai, and M. Suzuki, "Evaluation and Analysis of the Second Retrieved Space Environment Exposure Device (SM/MPAC&SEED)," *Proceedings of The 25th International Symposium on Space Technology and Science*, ISTS 2006-r-2-28, Kanazawa, Japan (2006).
- [6] A. S. Levine, (ed.), "LDEF - 69 Months in Space, First Post-Retrieval Symposium," NASA CP-3134 (1991).
- [7] N. Baba, M. Suzuki, I. Yamagata, Y. Kimoto, and J. Ishizawa, "External Contamination Observed on the Micro-Particles Capturer and Space Environment Exposure Device," *Proc. 10th ISMSE*, ESA-SP-616 (2006).
- [8] D. H. Holkeboer, D. W. Jones, F. Pagano, and D. J. Santeler, "Vacuum Technology and Space Simulation," NASA SP-105, pp. 197-222 (1966).
- [9] NASA, "Space Station External Contamination Control Requirements," NASA SSP-30426, Rev. D (1994)
- [10] C. Soares, R. Mikatarijan, D. Schmidl, C. Pankop, and K. Smith, "External Contamination Environment of International Space Station Externally Mounted Payloads," *Proceedings of 56th International Astronautical Congress*, International Astronautical Federation (2005).

**Publication list related SM/MPAC&SEED**

E. Miyazaki and I. Yamagata: Results of the Space Environment Exposure Experiment “SM/MPAC&SEED” on the International Space Station: Flexible Optical Solar Reflector, *Proc. 10th ISMSE*, ESA-SP-616 (2006).

E. Miyazaki and I. Yamagata: Results of Space-Environment Exposure of the Flexible Optical Solar Reflector, *Journal of Spacecraft and Rockets* (to be published).

## EVALUATION OF SILICONE POTTING COMPOUND AND SILICONE ADHESIVE EXPOSED TO SPACE ON SM/SEED EXPERIMENT

Eiji MIYAZAKI, Kazuyuki MORI, Junichiro ISHIZAWA and Hiroyuki SHIMAMURA

*Institute of Aerospace Technology, Japan Aerospace Exploration Agency,  
Tsukuba, Ibaraki 305-8505, Japan*

JAXA has developed a silicone potting compound and adhesive. The samples were exposed to space on SM/SEED outside the ISS to evaluate their tolerance against a space environment. The developed silicone materials are fundamentally designed for interior use: exposed environments are not considered. This experiment was performed to evaluate whether the silicone materials have tolerance against space environments outside the ISS or not. The samples are two parts silicone potting compound and one part silicone adhesive, manufactured by Shin-Etsu Chemical Co. Ltd. Results show that the potting compound sample, the electrical properties, relative permittivity  $\epsilon$ , and dielectric tangent  $\tan\delta$  meet the requirements. Cross-sectional TEM revealed that the new layer, found as  $\text{SiO}_2$ , is built on the surface. The layer can be formed by atomic oxygen collision with silicone that is contained in the potting compound and contamination. For the adhesive, the fracture strength evaluated using a tensile lap-share test is 1.1–1.6 MPa, meeting the requirement that it be more than 1.0 MPa. The experiment verified that the silicone potting compound and adhesive can retain their performance for exposure to space on ISS orbit for up to 46 months.

**Keywords:** silicone, relative permittivity, dielectric tangent, tensile lap-share test

### 1. Introduction

To evaluate the tolerance of a silicone potting compound and adhesive developed by JAXA under a space environment, specimens of the developed silicone potting compound and adhesive were exposed to space outside ISS as SM/SEED samples. The silicone materials are fundamentally designed for inside use: exposed environments were not considered. For promotion of applications of the developed materials to outside use, this experiment was performed. The purpose was to evaluate whether the materials have tolerance against a space environment outside ISS or not by the SM/SEED mission.

This report presents test results for the silicone potting compound and the adhesive in separate sections because the samples have different properties to be evaluated: results for the silicone potting compound are described in section 2; those for the silicone adhesive are described in section 3.

### 2. Silicone potting compound

#### 2.1 Experimental

The sample is two-part silicone potting compound “KE-101A/B” manufactured by Shin-Etsu Chemical Co., Ltd. The general properties of KE-101A/B are shown in Table 1. The potting compound was applied 3-mm-thick onto aluminum substrates of  $20 \text{ mm} \times 20 \text{ mm} \times 1 \text{ mm}^t$  as an SM/SEED sample. The samples are set in holes made in the SM/MPAC&SEED hardware, held by holding plates with a  $16 \text{ mm} \times 16 \text{ mm}$  window: the area within the window is the actual exposed area.

The retrieved samples were evaluated as follows: macroscopic observation, mass, electrical properties (relative permittivity  $\epsilon$  and dielectric tangent  $\tan\delta$ ), and cross-sectional microscopic observation near surface. Evaluation items and methods are presented in Table 2.

Table 1 General properties of KE-101A/B

		KE-101A/B
Appearance		Clear and colorless
Hardness (Durometer A)		40
Breakdown voltage 1 mm		27 kV
Relative permittivity	1 Hz	2.5
	1 MHz	2.9
	10 MHz	3.5
Dielectric tangent	1 Hz	0.0010
	1 MHz	0.0007
	10 MHz	0.0010
Outgassing (ASTM-E595[1])	TML <sup>*1</sup>	0.357 %
	CVCM <sup>*1</sup>	0.057 %

Curing conditions: 23±2°C, 50±5%RH, 168 h (JIS K 6249)

\*1) TML: Total Mass Loss, CVCM: Collected Volatile Condensable Materials

Table 2 Evaluations of KE-101A/B

Item	Methods and equipment
Macroscopic observation	Digital CCD camera
Mass measurement	Microbalance (readability 1 $\mu\text{g}$ , maximum load 5100 mg, MX5; Mettler Toledo International Inc.)
Electrical properties	HP 4194A (Impedance/Gain-Phase Analyzer) Environment: R.T. in air Method: two terminal method
Dielectric tangent	
Microscopic observation	Cross-sectional TEM Samples stained using $\text{RuO}_4$ were sliced using ultramicrotomy to produce a cross-section including the exposed surface.



## 2.2 Results and discussion

### 2.2.1 Macroscopic observation

Figure 1 presents images of macroscopic observations. The difference of brightness between samples resulted from lighting while taking photographs. The difference is unrelated to a color change of the sample surface: a flat surface of the substrates beneath the potting compound is reflecting. The photographs show no marked change in potting compound, although a slight trace of the frame attached on the sample surface is visible on some samples: #1-A and #2-B.

### 2.2.2 Mass measurement

The mass changes of exposed samples are presented in Fig. 2, indicating that the mass decreases more as the exposure duration lengthens. The maximum mass loss was 1.3 mg for #2-A with initial mass of ca. 0.8 g, excluding the substrate. It is greater than that for #3. Outgassing might be one cause of such mass loss in TML: 0.396% of 0.8 g, or ca. 3 mg. The temperature is lower than the outgassing test condition. The level is reasonable. Some influential factor such as heating might occur.

For comparison, the mass loss of AO monitoring sample, VESPEL, is much greater than that of the potting compound[2]: 2.4 mg for VESPEL mounted on #1 exposed for 10 months. It is about 10 times greater than that of the potting compound.

### 2.2.3 Electric properties

Results of relative permittivity and the dielectric tangent are presented respectively in Figs. 3 and 4. The relative permittivity showed no significant change. It met the requirement of being less than 3.8. The dielectric tangent, however, showed a slight increase from the initial value. It can be said to be maintained within the requirement: less than 0.003.

### 2.2.4 Microscopic observation

Figure 5 presents cross-sectional TEM images of the sample surface. The vertical lines found in the retrieved samples are not related to the sample shape, but are made at making a specimen for TEM observation. The images revealed that a new layer was built up on the surface that was not found on the surface of the as-received sample. The layer thicknesses are: ca. 30 nm for #1, ca. 80 nm for #2, and ca. 150 nm for #3. Thicknesses of the new layers are comparable to the thickness observed for F-OSR[3]. Results show that the layer was SiO<sub>2</sub>. The layer can be formed by atomic oxygen collision with silicon contained in the potting compound and/or contamination deposited on orbit. Such a phenomenon is already known for silicone materials used on LEO spacecraft[4,5].

### 2.2.5 Discussion

As presented in Fig. 2, a mass loss occurred. For the silicone potting compound, a mass change, either a gain or loss, is attributable to outgassing, erosion by AO, or deposition of contamination. In terms of outgassing, its TML is 0.357%. The initial mass is 790 mg, i.e., the mass loss by outgassing can be expected up to 2.8 mg. According to ASTM-E595, the TML is measured by exposure in vacuum at 125°C for 24 h [1]. Unfortunately, the experimental condition of SM/SEED differs from the outgassing test condition, i.e., longer exposure at

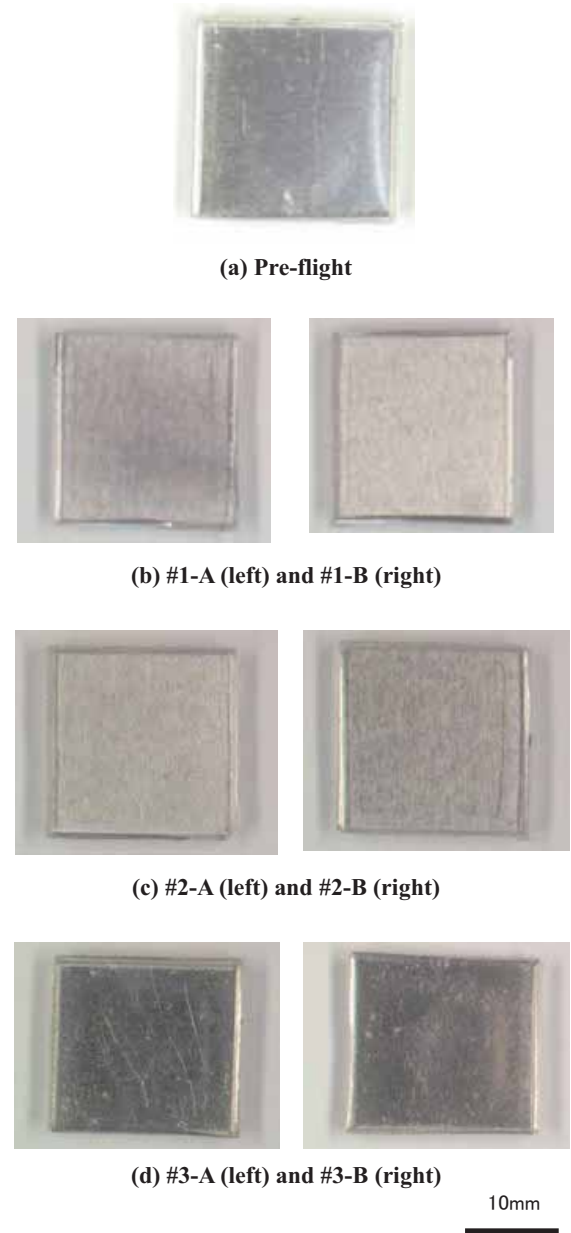


Fig. 1 Macroscopic images of Potting compound

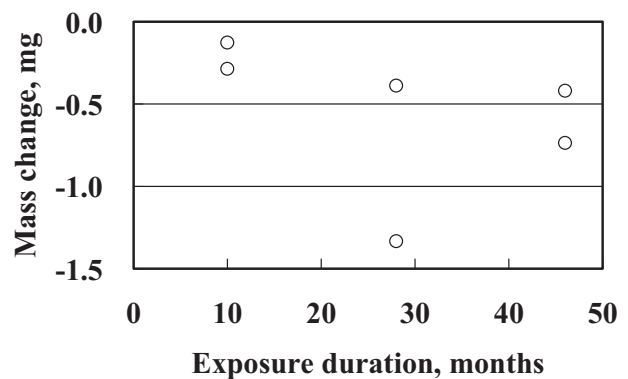


Fig. 2 Results of mass change of retrieved potting compound from SM/MPAC&SEED exposure.

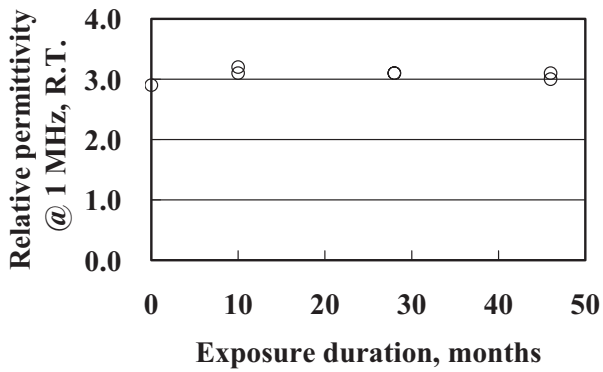


Fig. 3 Results of measured relative permittivity of retrieved potting compound from SM/MPAC&SEED

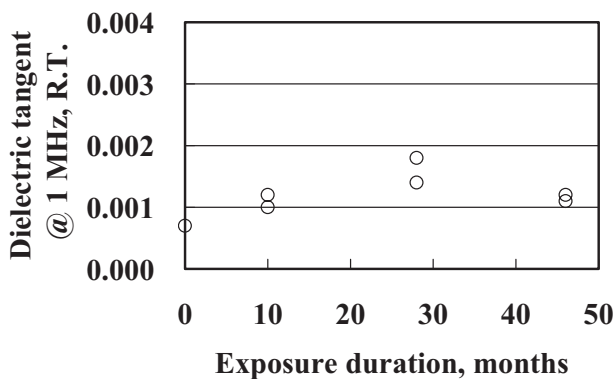


Fig. 4 Results of measured dielectric tangent of retrieved potting compound from SM/MPAC&SEED

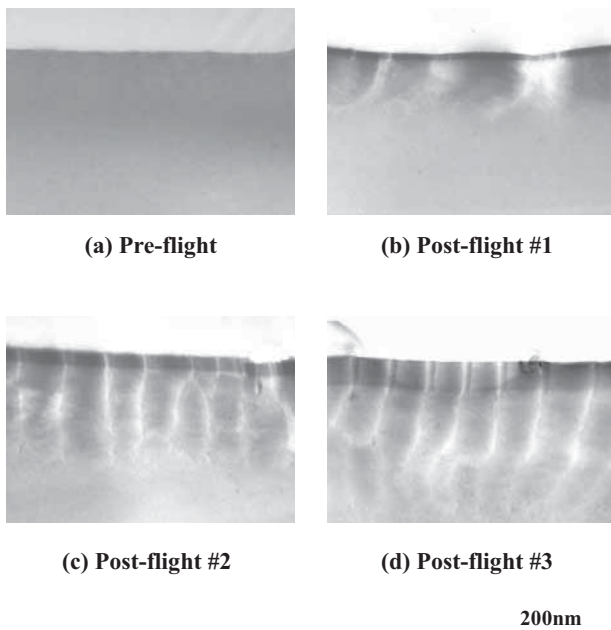


Fig. 5 Cross-sectional TEM images of potting compound for SM/MPAC&SEED

lower temperature. For that reason, it cannot be said that the actual mass loss was caused by outgassing for the retrieved sample. The second factor of mass change, erosion by AO, can contribute to mass loss initially at the time of exposure. As depicted in Fig. 5, the AO protective  $\text{SiO}_2$  layer was built up on the exposed surface. Once the layer is organized, the AO erosion is blocked: mass loss stops. The AO protective layer of ca. 10 nm is sufficiently thick[6]; it is organized before #1 retrieval because the layer's thickness of the #1 sample was ca. 30 nm. Therefore, the mass loss caused by AO erosion can occur only at the beginning of exposure. The third factor, deposition of contamination, also contributes to the mass change. Based on the result of F-OSR, a mass gain of up to 0.07 mg is expected, assuming that the same deposition occurred as F-OSR. It is sufficiently smaller than the total mass change of the potting compound sample. Therefore, it can be concluded that the mass loss is mainly caused by outgassing.

Electric properties are not affected by space environment exposure. It can be concluded that the tolerance of the potting compound is verified by the SM/MPAC&SEED experiment.

### 2.3 Conclusion

Results of this experiment verify that the JAXA-developed silicone potting compound can retain its properties within the requirement for 46 months' exposure on ISS. A new layer of  $\text{SiO}_2$  was observed on the retrieved sample surface, which is similar to other silicone materials collided with AO. Results of this investigation show that the mass loss is mainly the result of outgassing.

## 3. Silicone adhesive

### 3.1 Experimental

The sample is one part silicone adhesive (KE4908SC-T; Shin-Etsu Chemical Co. Ltd.). General properties of KE4908SC-T are portrayed in Table 3. The adhesive of  $13.2 \text{ mm}^L \times 25.4 \text{ mm}^W \times 2 \text{ mm}^t$  is cured between two  $83.2 \text{ mm} \times 25.4 \text{ mm} \times 1 \text{ mm}^t$  aluminum plates before flight, as depicted in Fig. 6. The specimen was tested for adhesive properties according to the standard test specification (JIS K 6850 – Adhesive – Determination of tensile lap-shear strength of rigid-to-rigid bonded assembly).[7] A schematic illustration of the installation to SM/MPAC&SEED hardware and the exposed area is portrayed in Fig. 7.

The retrieved samples are evaluated using macroscopic observation, mass measurement and adhesive characteristics test. The evaluation items and methods are presented in Table 4.

Table 3 General properties of KE4908SC-T

		KE4908SC-T
Appearance		Semi transparent
Hardness (Durometer A)		46
Lap share strength		1.7 MPa
Breakdown voltage 1 mm		26 kV
Relative permittivity	50 Hz	3.0
Dielectric tangent	50 Hz	0.0012
Outgassing (ASTM-E595)	TML <sup>*1</sup>	0.396 %
	CVCM <sup>*1</sup>	0.008 %

Curing conditions: 23±2°C, 50±5%RH, 168 h (JIS K 6249)

\*1)TML: Total Mass Loss, CVCM: Collected Volatile Condensable Materials

Table 4 Evaluations of the retrieved KE4908SC-T adhesive

Item	Methods and equipment
Macroscopic observation	Digital CCD camera
Mass measurement	Shimadzu AEL-160 readability : 1mg / maximum load : 160g
Adhesive characteristics test	Electric Hydraulic Fatigue Testing Machine EHF-EG-50kN-10L, Shimadzu Method: JIS K 6850 Adhesives – Determination of tensile lap-shear strength of rigid-to-rigid bonded assemblies Test speed: 9MPa/min

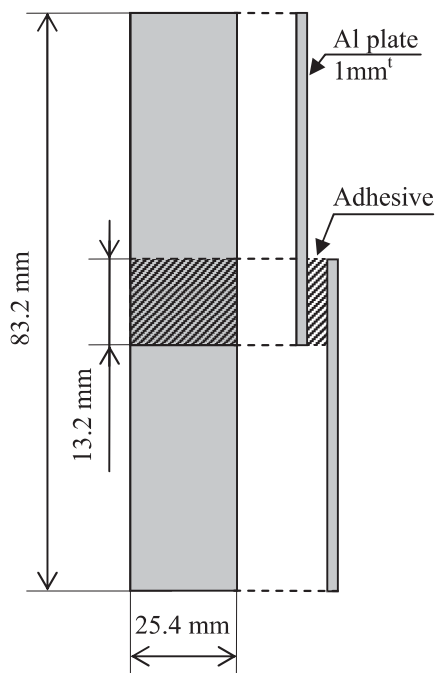


Fig. 6 Dimensions of adhesive specimen for SM/MPAC&amp;SEED

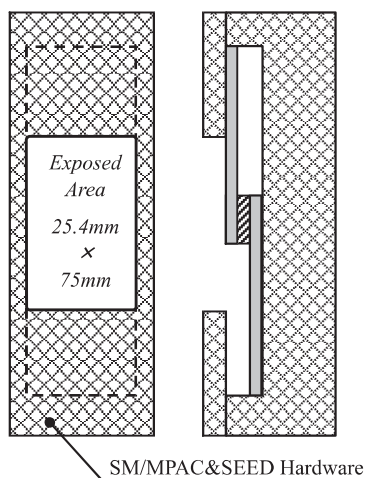


Fig. 7 Configuration of adhesive specimen installed on SM/MPAC&amp;SEED

## 3.2 Results

### 3.2.1 Macroscopic observation

Figure 8 portrays the surface appearance, including the exposure area. The adhesive sample is not visible in the figure: the sample is hidden by the upper substrate.

From the figure, semi-circular stains can be found near the adhesive sample on the lower substrate for retrieved samples. Apparently, some liquid oozed from the adhesive sample. The stain is very thin. In addition to the stains, color changed areas are visible for #2 and #3 retrieved samples along the shape of the exposure window.

### 3.2.2 Mass measurement

Figure 9 presents measured results of the differences in mass between pre-flight and post-flight conditions. The mass changes of exposed samples show complicated data: decreased samples are #1-B, -0.002 g and #2-B, -0.011 g; increased samples are #1-A, +0.014 g, #2-A, +0.003 g, #3-A, +0.014 g, and #3-B, +0.005 g.

### 3.2.3 Adhesive characteristics test

Figure 10 depicts the relationship between the crosshead displacement and the load obtained as ascertained through tensile lap-shear tests. The sample was fractured at the peak of each curve: the curve shown at the more displaced region beyond the fracture displacement is unrelated to actual test results. The pre-flight and post-flight slopes differ in shape. The pre-flight slope is not linear; the post-flight slopes are linear. The fracture lap shear strength and crosshead displacement are presented in Table 5. The lap shear fracture strength is 1.1–1.6 MPa. The values met the requirement of being greater than 1.0 MPa. No requirement value is set for the crosshead displacement. Therefore, it cannot be discussed in terms of meeting the requirement or not. The value of the crosshead displacement itself for retrieved samples is obviously lower than that of the pre-flight sample.

### 3.2.4 Discussion

The cured adhesive does not ooze any liquid, although outgassing can occur. If the stain had resulted from outgassing, the stain shape would not be natural, i.e., the shape must have full width along the sample and the edge of the far side from the sample must be unclear. Therefore, we infer that the stain might result from the residual sample. The protruded sample would be wiped out during manufacturing. A trace of it might be developed visually through exposure to the space environment.

The mass change data are confusing. The total mass of each specimen, i.e., the adhesive sample and two aluminum substrates, is ca. 13 g. The balance used for this study has 0.001 g readability. With a maximum change of 14 units of readability, it is difficult to determine the significance of the mass change.

The lap shear test result shows the change of ductility of the adhesive sample. The pre-flight sample can be said to have ductility from its nonlinear behavior at loading. All retrieved samples indicate linear behavior, i.e., elastic deformation is dominant. That result might be attributable to exposure to the space environment. Although such ductility is lost, the experiment verified that the required basic properties can be retained, even in the exposed environment on the ISS.

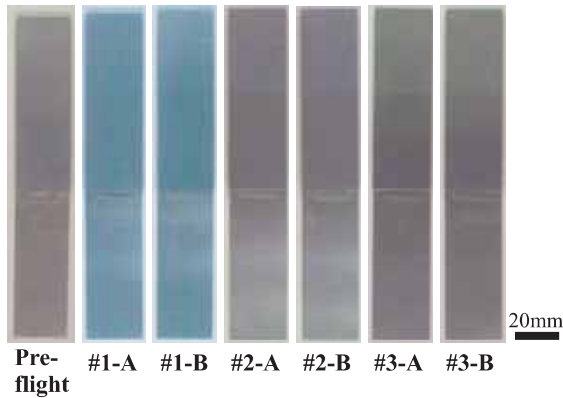


Fig. 8 Macroscopic images of adhesive specimens

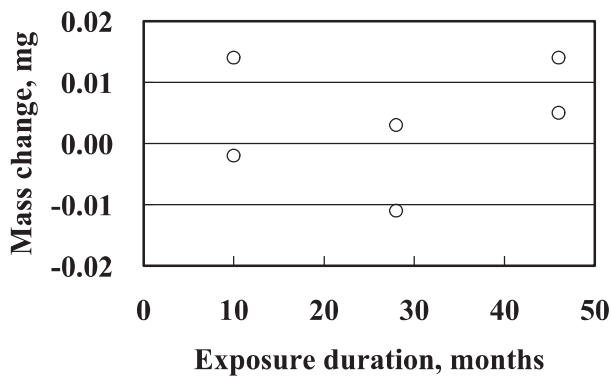


Fig. 9 Results of mass change of retrieved adhesive specimens from SM/MPAC&SEED exposure.

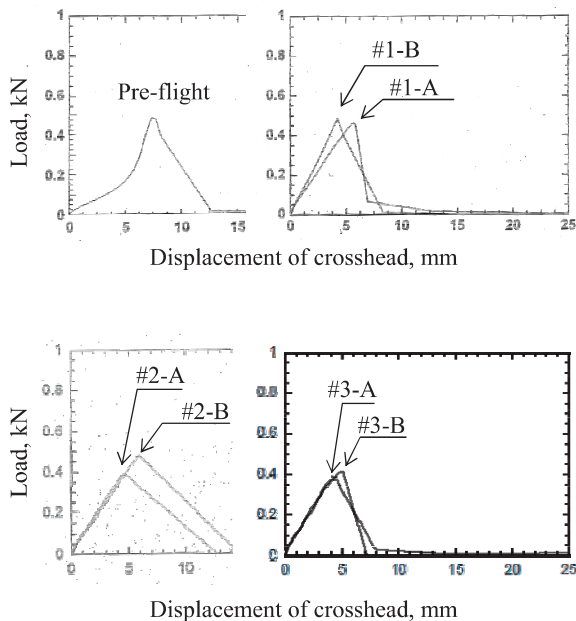


Fig. 10 Results of Lap-shear test of retrieved adhesive specimens from SM/MPAC&SEED

Table 5 Summary of adhesive characteristics test results

	Pre-flight	#1		#2		#3	
		A	B	A	B	A	B
Lap Shear Strength, MPa	1.57	1.38	1.55	1.13	1.41	1.15	1.19
Displacement, mm	7.3	5.6	4.3	4.3	5.9	4.1	4.9

### 3.3 Conclusion

Silicone adhesive (KE4908SC-T) was exposed for the 46 month-SM/SEED experiment. Degradation in elongation and loss of ductility were found, although the required properties are verified to be retained for up to 46 months' exposure on the ISS.

### References

- [1] ASTM E595, "Standard Test Method for Total Mass Loss and Collected Volatile Condensable Materials from Outgassing in a Vacuum Environment," ASTM International.
- [2] Yugo Kimoto, Keiichi Yano, Junichiro Ishizawa, Eiji Miyazaki, and Ichiro Yamagata, "Passive Measurement of Atomic Oxygen, UV Fluence, and Radiation Effect on the ISS Using the SEED experiment" , *Proc. 10th ISMSE*, ESA-SP-616 (2006).
- [3] Eiji Miyazaki and Ichiro Yamagata, "Results of Space-Environment Exposure of the Flexible Optical Solar Reflector," *Journal of Spacecraft and Rockets*, in press (2008)
- [4] United States Patent 5073607
- [5] R. I. Gonzalez, S. J. Tomezak, T. K. Minton, A. L. Brunsvold, and G. B. Hoflund, "Synthesis and Atomic Oxygen Erosion Testing of Space-Survivable POSS (Polyhedral Oligomeric Silsesquioxane) Polyimides," *Proceedings of the 9th International Symposium on "Materials in a Space Environment"*, ESA-SP-540, European Space Agency, pp. 113-120 (2003)
- [6] M. Tagawa, K. Yokota, N. Ohmae, and H. Kinoshita, "Volume diffusion of atomic oxygen in  $\alpha$ -SiO<sub>2</sub> protective coating," *High Performance Polymers*, Vol. 12, pp. 53-63 (2000).
- [7] JIS K 6850, "Adhesives – Determination of tensile lap-shear strength of rigid-to-rigid bonded assemblies," Japanese Industrial Standards

### Publication list related SM/MPAC&SEED

E. Miyazaki, and K. Mori, "Evaluation of Potting Compound Exposed to Space Environment on ISS Russian Service Module / Space Environment Exposure Device," *Proceedings of UKAREN 51*, 200



## MEDET IN-FLIGHT EXPERIMENT (MATERIALS EXPOSURE AND DEGRADATION EXPERIMENT) DESCRIPTION AND FIRST RESULTS

Virginie INGUIMBERT<sup>1</sup>, Sophie DUZELLIER<sup>1</sup>, Jean-Michel SIGUIER<sup>1</sup>, Adrian TIGHE<sup>2</sup> and Marc VAN EESBEEK<sup>2</sup>

<sup>1</sup> ONERA, 2, Avenue Edouard Belin, 31 055 Toulouse, France,

<sup>2</sup> ESA/ESTEC, PB 299, 2200 AG Noordwijk, The Netherlands

**Keywords:** Materials, exposure to space, degradation, contamination, MEDET, EUTeF, Columbus, ISS

### 1. Introduction

MEDET is a material experiment on board EuTEF/Columbus. It is a fruitful collaboration between ONERA, ESA, CNES and the University of Southampton. It combines seven sub-experiments devoted to the combined measure of the radiative space environment in low earth orbit and its associated effects on materials. It allows for real time characterization of the local ISS environment (radiation and contamination) and for the evaluation of material degradation such as thermal coatings, polymers for inflatable structures.... The mission is planned to start on February 2007 (Atlantis launch) and to last 1.5 years before the equipment return for post-flight investigation.

### 2. Objectives

The three main MEDET scientific objectives are:

- a) Evaluate the effect of the complex space environment on the optical and thermo-optical properties of materials to be considered for utilisation on LEO spacecraft. This includes the active measurement of thermo-optical properties (and more exactly, their variation as a function of space exposure) for a number of proposed spacecraft materials. Among these materials are anodizations, second surface mirrors (SSM) and new thermal paints externally used onboard the Space Station and LEO satellites.
- b) Assessment of the effects of the ISS environment on optical windows. Special emphasis will be placed upon the part of degradation that is due to molecular contamination. Contamination results from various sources, including outgassing and degradation of materials, manoeuvres of service vehicles, re-boost operations, firings of attitude control systems, dumps and EVA.
- c) Investigation of micro-particle and debris fluxes (especially their variation as a function of time) and, after retrieval, the origin of the debris and the detectors' behaviour.

In support of the above objectives, the local environment will

have to be characterised in terms of local pressure, contamination rate, Atomic Oxygen (AO), X rays and UV flux.

The experiment results are expected to give essential information to the spacecraft designer on:

- the mechanisms of space damage, discriminating between the effects of the individual components of the spacecraft environment, and detecting also possible synergistic effects,
- the long-term characteristics of these materials with the aim to indicate if they are appropriate for use in future space station applications or other missions,
- the validity of laboratory simulation results from comparison to the space data, laboratory simulation being considered as imperative for prediction of materials degradation in space.

### 3. Description

A schematic view of MEDET is given in figure 1 and a summary description of the experiments and systems in the flight segment is given in table 1. More detailed descriptions and diagrams are given in the following sections.

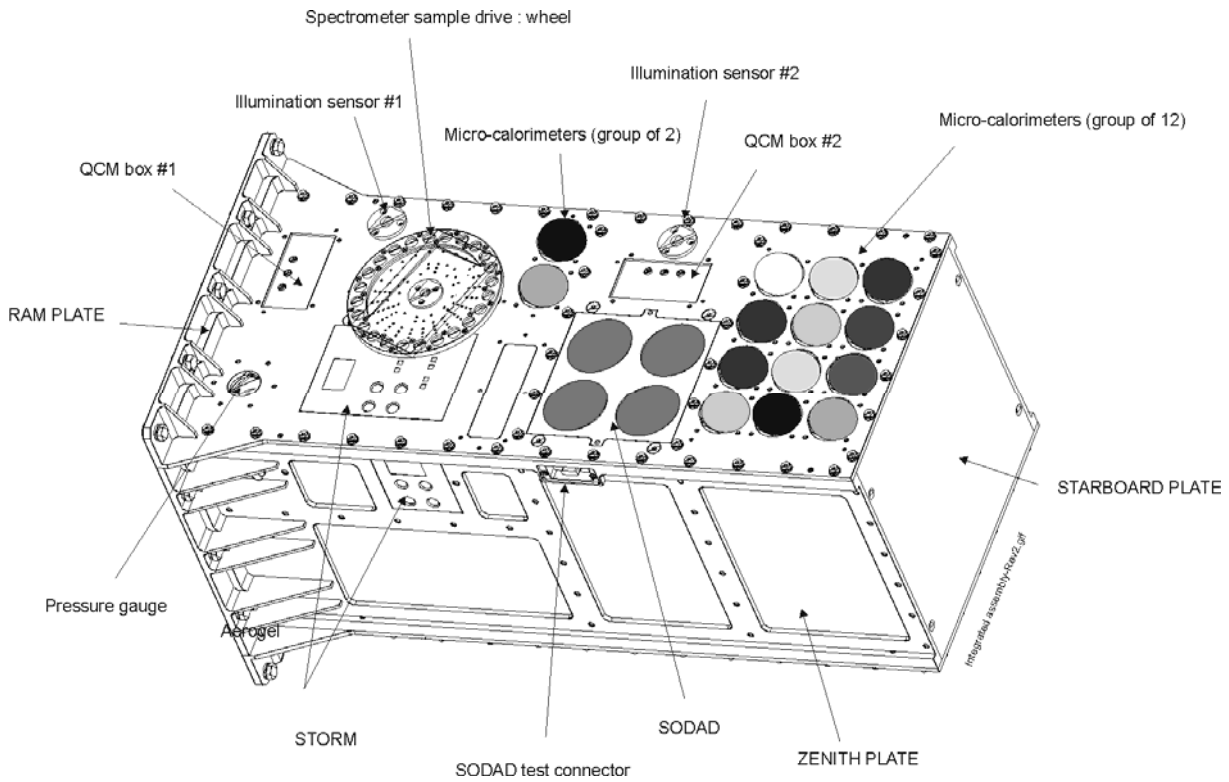


figure 1 : Schematics of MEDET experiment

Experiments	
<b>SODAD</b>	An active MOS type impact detector, to characterise the properties of micro meteoroids and orbital debris particles
<b>Spectrometer</b>	An active spectrometer system, to measure changes in the optical properties of transparent window materials.
<b>QCM</b>	A collection of active quartz crystal microbalances, to measure the atomic oxygen and contamination flux
<b>Pressure Gauge</b>	An active cold cathode type gauge, to measure the local pressure
<b>AEROGEL</b>	A passive detector, to capture micro meteoroid and orbital debris particles
<b>MicroCalorimeters</b>	A collection of active microcalorimeters, to measure the changes in the thermo-optical properties of thermal control coatings.
<b>Southampton Experiments (STORM)</b>	A collection of active detectors to measure the atomic oxygen, UV and X-ray flux

Sub-Systems	
<b>Mechanical support structure</b>	An aluminium box-type structure to provide the physical support for the sub-experiments and other sub-systems, and to attach MEDET to EuTEF.
<b>Data Acquisition and power control unit (DAPC)</b>	A central logic unit (LU), power supply (PDU) and associated electronics to control the operation of the sub-systems, store and transfer the data from the sub-systems to EuTEF and receive commands from the ground.
<b>Thermal control and monitoring system</b>	Used to keep the experiments and sub-systems within the specified temperature limits. Consists of radiators, multi layer insulation (MLI), thermal washers, temperature sensors, heaters and thermostats

Table 1 : Summary description of the MEDET sub-experiments and sub-system

### 3.1 SODAD

SODAD (Système Orbital de Détection Active de Débris) will be used to actively measure the micro meteoroid and debris flux in the vicinity of the ISS.

The detector works on the principle of monitoring the discharge of a parallel-plate capacitor containing a thin dielectric. The top electrode is made very thin and this surface is exposed to the impacting particles. The device is operated with an electrical potential (bias) applied across the capacitor plates : a charge is normally stored in the capacitor. When a high velocity particle impacts the exposed plate with enough energy, it can cause the dielectric to breakdown and results in a discharge of the capacitor.

The event is measured by monitoring the charge required to recharge the capacitor. After discharge the sensor is recharged to the nominal value within a short time. Evaporation of the electrode around the impact site usually prevents the occurrence of a permanent short. The sensitivity of the sensor depends mainly on the dielectric thickness, the top electrode material and thickness, the bias voltage, and also on the velocity of impacting particle. The device is best suited to the detection of particles with diameter ranging from 0.5  $\mu\text{m}$  to 100  $\mu\text{m}$ .

The electronics consists of a voltage doubler (providing the bias for the detector) and the circuits necessary for the detection of the discharge events and the monitoring of the detector status. The detection threshold is set at 95 % of the bias voltage. In the event of permanent short of the sensor, the measurement is automatically stopped if the leakage current is higher than 1100  $\mu\text{A}$ . Standard mounting plates (120 x 120 x 50 mm) accommodate 4 sensors with integrated electronics. Each sensor is divided into two independent parts in order to increase the detection rate.

### 3.2 SPECTROMETER

The spectrometer experiment is being developed specifically for the MEDET project.

It will be used to follow the degradation with time of several types of optical windows (including synthetic ultra-pure SiO<sub>2</sub> and other radiation stable materials). The optical spectral transmission of the samples will be measured by a system involving quartz optical fibres, two miniature spectrometer modules (to cover the solar spectrum from 200 to 1000 nm) and two illumination sensors.

The materials to be tested are placed on a rotating wheel, containing 24 apertures. A stepper motor is used to position each sample above the optical fibre entrance. The sun is used as the light source, so that measurements are allowed only when the sun is detected by the illumination sensor in a  $\pm 40^\circ$  acceptance angle. Only relative measurements are performed, comparing the spectra of the sunlight direct with the spectra of the sunlight observed through the tested materials. An encoder

system, consisting of photodiodes positioned under the wheel, is used to identify the location of the wheel with respect to the fibre optic at any given instant (see Figure 2).

The miniature spectrometer modules consist of a grating, optics and CCD detector. These are all rigidly housed within the same case. The module is based on a standard laboratory device (Zeiss MMS), has been adapted for space flight use. However, in order to be operated safely on MEDET, which is an external payload, the miniature spectrometer modules are mounted in a pressurised cylinder. For redundancy, 2 sets of pressurised cylinders (with 2 spectrometers in each) are mounted behind the filter wheel.

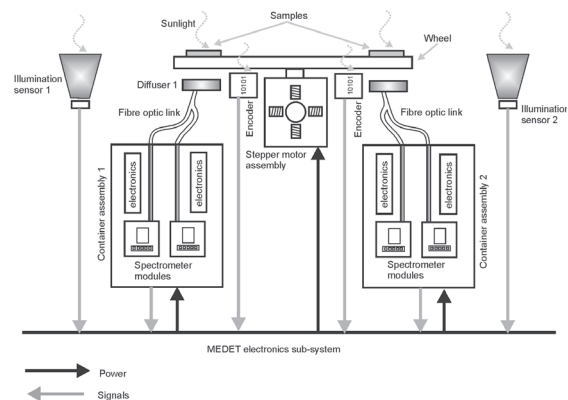


Figure 2 : Spectrometer experiment interface schematic

### 3.3 QCM

The Quartz Crystal Microbalance (QCM) experiment will be used to measure contamination levels and the atomic oxygen flux in the vicinity of the Space Station. The sensors are modified versions of commercially available miniature crystal oscillator packages. The package consists of a quartz crystal and an oscillator circuit contained within a metal housing. The quartz crystal is exposed to the space environment through a round hole in the housing directly above the crystal, and the oscillation frequency changes in relation to the changing mass and temperature of the crystal. The oscillator circuit provides an alternating voltage output.

To measure the contamination flux, a bare crystal is used, and the oscillation frequency decreases as contamination is deposited on the surface of the crystal and the mass of the crystal increases. To measure the atomic oxygen flux, a carbon coated crystal is used, and the oscillation frequency increases as the atomic oxygen erodes away the carbon layer and the mass of the crystal decreases. For both of these techniques, the relationship between the mass of the crystal and the oscillation frequency can depend on the temperature of the crystal. Therefore, a separate non coated crystal cut in the “Y-direction” is also used to independently monitor the crystal temperature, so that the mass data can be corrected for temperature dependent effects.

Three types of sensor will be flown on board MEDET :

- Type 1 : 10 MHz Crystal with Au electrode for contamination deposition measurements. The sensitivity is  $4.4 \times 10^{-9} \text{gcm}^{-2}\text{Hz}^{-1}$ .

- Type 2 : 10 MHz Crystal with C-coating, to measure Atomic Oxygen. The sensitivity is  $2.46 \times 10^{15} \text{O-atoms cm}^{-2} \text{Hz}^{-1}$ .

- Type 3 : 11 MHz Crystal with Au electrode, for temperature measurements. The sensitivity is 600 Hz/K. The output of this type of crystal will be used to correct for temperature variations in Type 1 and Type 2.

The response of each type of crystal is only linear within a limited frequency range. If a sudden large contamination deposit were to occur, perhaps due to a thruster firing in the local vicinity of MEDET, then the experiment would no longer be operable. Therefore, a heater and thermostat will also be placed directly underneath each crystal oscillator package, so that an attempt could be made to de-contaminate and regenerate the sensors by evaporating off the excess deposits (Figure 3 and Figure 4)

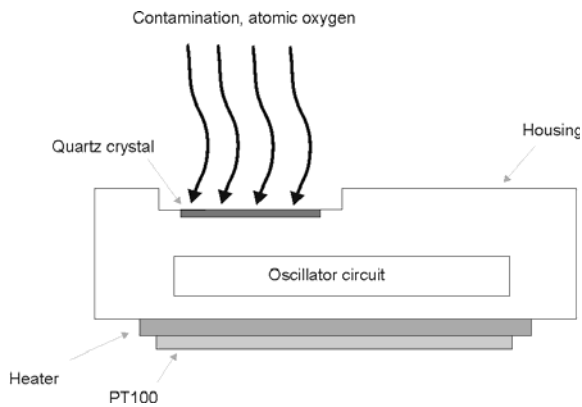


Figure 3 : QCM sensor in operational mode

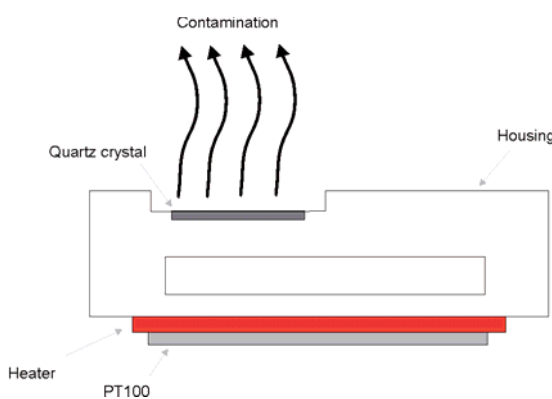


Figure 4 : QCM sensor in regenerate mode

### 3.4 Pressure Gauge

This sub-experiment will be used to actively measure changes in the concentration of gaseous products in the local vicinity of the Space Station. Gaseous products could be

produced as a result of transient events such as extra vehicular activities, spacecraft docking and waste dumps, as well as general outgassing and degradation of materials. It may be possible to correlate the pressure data with the contamination experiments on board MEDET, and the data will also be made available to other instruments on board EuTEF.

The experiment consists of a standard commercially available cold-cathode type pressure gauge, which has been adapted and qualified for space use. The operation of the cold-cathode pressure gauge is based on the ionisation of the residual gas molecules in the vacuum by electrons emitted from a cold cathode. The ions are collected and the measured current can be correlated with the pressure. The probability of an electron hitting a gas molecule can be increased by trapping the electrons in a electromagnetic field of the correct geometry. This has the effect of increasing the sensitivity of the device

### 3.5 AEROGEL

The aim of the aerogel experiment is to capture, in an intact state, residue from micro-particles so that they can be returned to earth for chemical and physical analysis. This will provide information about the origin of the particles i.e. whether they are natural micro-meteoroids or orbital debris. Such information cannot be derived from the present generation of active detectors. The experiment is passive in nature and consists of a block of Silica aerogel exposed directly to the space environment. Silica aerogel is made up of amorphous grains of  $\text{SiO}_2$ , with diameters of 4 – 10nm. It is a transparent, highly porous material, with ultra low density (ranging from 0.05 to 0.15  $\text{gcm}^{-3}$ ). On colliding with silica aerogel, particles travelling at orbital impact velocities can be slowed down in the material without completely vaporising, leaving solid residue at the bottom of the track. On return to earth, the residue can be analysed using a sectioning technique. The porous aerogel is filled with an epoxy and cured, after which it can be sectioned along the length of the particle tracks to reveal the residue. The length and shape of the track can also give some information about the original collision velocity and direction of the particle. Aerogel has been used before in space applications, such as on the Stardust comet mission and various Space Shuttle science experiments.

### 3.6 Microcalorimeters

This sub-experiment will be used to actively measure the changes in the thermo-optical properties of spacecraft materials and coatings. The experiment consists of an array of space qualified micro-calorimeters mounted on the ram face of MEDET. The calorimeter technique is based on a comparison between the temperature of a thermally insulated sample and the temperature of a black-body reference sample. Using a heat balance equation, the total emissivity and solar absorptance of the sample can be deduced.

The calorimeters which will be used on MEDET are based on a standard design which has been flown on many previous missions. The samples are attached to an insulated thin plate



using adhesive, painting or another form of bonding. The sample plate is held within a guard ring which has the same area and is coated with the same material as the sample. This minimises heat losses from the sample plate to the surrounding casing of the calorimeter. In addition, the sample plate and guard ring rest on thin Kapton cylinders, and layers of MLI are placed between the guard ring and the casing. The temperature of the sample is measured using a resistance thermometer mounted on the rear side of the sample plate (see Figure 6)

The black body reference calorimeter is of the same dimensions and basic construction as the standard calorimeters. However, the sample plate is covered by an array of thin edged blades packed tightly together, and the guard ring is painted with a black silicate based paint, to give the surface of the calorimeter an  $\alpha/\epsilon$  ratio close to 1.

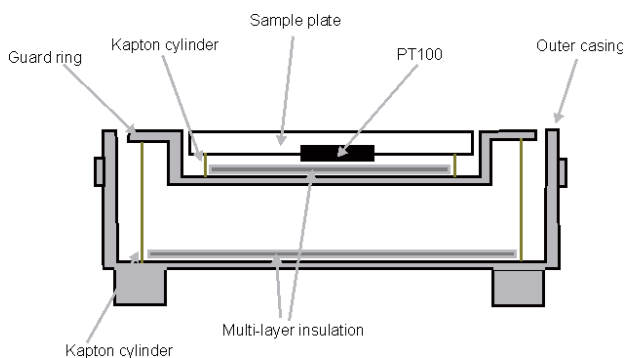


Figure 6 Micro-calorimeter schematic

### 3.7 STORM

The Southampton University Transient Oxygen and Radiation Monitor (STORM) consists of a package of sensors which will be used to measure Atomic Oxygen, UV and X-ray fluxes. STORM is being developed specifically for the MEDET experiment.

#### - AO sensors

Two AO sensor types are incorporated into STORM, based on carbon film actinometers and thin-film zinc oxide (ZnO) detectors. Both are located on the ram-face of MEDET in an area close to the rotating spectrometer wheel. The carbon actinometer instrument comprises four thin carbon films and an AD590 temperature sensor, all mounted on an alumina substrate. Incorporated onto the substrate is a low power heater element that will be used to stabilise the film temperature since carbon exhibits a temperature dependent erosion rate.

Zinc oxide is an n-type semiconductor material that is

sensitive to adsorbed atomic oxygen. Analysis of the non-steady response indicates that the initial rate of decrease of the conductivity of a fresh ZnO film exposed to atomic oxygen is proportional to the incident AO flux. However, after a relatively short exposure to AO the sensor becomes saturated and its response ceases. Nevertheless, the sensor offers the great advantage that, by heating to modest temperatures, the sensor can be refreshed (or "regenerated") and is then able to take further AO measurements. The ZnO sensor comprises four thin films, two of which will be shielded from AO attack by a thin overcoat of silicon monoxide (silica).

The carbon actinometer elements are fully exposed on the ram face, whereas the ZnO film array are partially covered by the spectrometer wheel. One sensor is permanently shadowed from direct exposure to AO by the wheel, whilst another is periodically covered/uncovered by the wheel. The other two sensors are fully exposed on the ram face. ZnO sensor regeneration will take place whilst the wheel covers two of the four sensors.

#### - X ray sensors

Four x-ray sensors are mounted on STORM. Two are located on the zenith face of MEDET and two placed on the ram face with one active and one redundant active sensor on each of the faces. The x-ray sensors consist of silicon PIN diodes. A beryllium window is placed over the diodes to filter out the signal from lower energy photons. X-ray fluxes will be measured continuously, but the most important data will be gathered during Solar x-ray flare events when the x-ray flux is at its highest and most damaging levels.

#### - UV sensors

Eight UV sensors are mounted on STORM, four on the MEDET ram face and four on the zenith. The UV sensors consist of solar-visible blind aluminium gallium nitride photodetectors. These detectors are sensitive to an UV light range from 120nm to 285nm, and this lower limit of the wavelength range is important to be able to detect the Lyman-alpha hydrogen line half the sensors (two on each face) are fitted with sapphire windows to cut out the UV spectrum below approximately 130nm.

## 4. Perspectives

At the time this paper is written, only MEDET commissioning was performed and the experiment has been working for only 3 days. The first sets of data are being acquired and will be analysed soon. The total duration of the mission is expected to be of 18 months.

## Status of JEM/MPAC&SEED Experiment Onboard SEDA-AP on KIBO Exposed Facility

Shoichi ICHIKAWA<sup>1</sup>, Yugo KIMOTO<sup>1</sup>, Eiji MIYAZAKI<sup>1</sup>, Kiyooki KUBO<sup>1</sup>, Keiichi YANO<sup>1</sup>, Koji MATSUMOTO<sup>2</sup>,  
Junichiro ISHIZAWA<sup>1</sup>, Hiroyuki SHIMAMURA<sup>1</sup>, Riyo YAMANAKA<sup>1</sup> and Mineo SUZUKI<sup>1</sup>

<sup>1</sup> *Institute of Aerospace Technology, Japan Aerospace Exploration Agency, Tsukuba, Ibaraki 305-8505, Japan*

<sup>2</sup> *Institute of Aerospace Technology, Japan Aerospace Exploration Agency, Chofu, Tokyo 182-8522, Japan*

### Abstract

To improve the lifetime and performance of spacecraft in a low-earth-orbit, it is very important to investigate space environment effects on materials applied to spacecraft. In a low-earth-orbit, atomic oxygen greatly affects spacecraft surfaces. It is produced by dissociation of molecular oxygen by solar ultraviolet (UV) rays. For investigation of degradation mechanisms of exposed materials and for accumulation of experimental data, a space-environment exposure experiment was planned for use with the Russian Service Module (SM) and Exposed Facility of the Japanese Experiment Module (JEM) of ISS. The exposure experiment at SM/MPAC&SEED has been completed. We are preparing the next experiment for JEM, which is scheduled for launch next year. Those experiments are expected to yield details of characteristic changes of exposed materials and mechanisms of their degradation by atomic oxygen, UV, and other radiation.

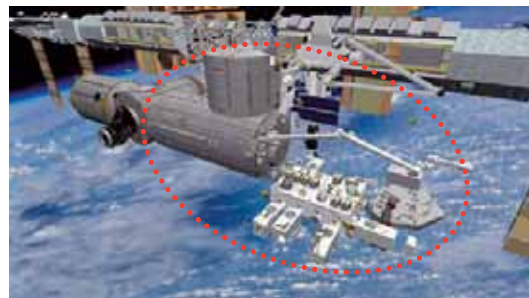
**Keywords:** MPAC&SEED, Space Exposure Experiment, Material, Space Environment, Low Earth Orbit, ISS, KIBO, Zvezda

### 1. Introduction

The Low Earth Orbit (LEO) altitude space environment affects the outside of spacecraft flying. It causes degradation from atomic oxygen, ultraviolet rays, radiation, etc. Past examinations of flight hardware show that atomic oxygen attacks organic materials of spacecraft; such materials are frequently used in spacecraft as thermal control material, paint, adhesive, etc. Carbon Fiber Reinforced Plastic (CFRP) is applied to the orbiter as a construction material. For improvement of the spacecraft lifetime and the performance, it is very important to obtain fundamental knowledge related to the compatibility of space materials with the LEO environment and to develop advanced materials having excellent resistance to space environments. In Japan, materials exposure experiments in space, Evaluation of Oxygen Interaction with Materials-3 (EOIM-3), Exposure Facility Flyer Unit (EFFU) [1], and Evaluation of Space Environment and effect on Materials (ESEM) [2] were conducted using space shuttles and satellite units. Nevertheless, the behavior of materials exposed to space environment has not been well understood. For that reason, the Japan Aerospace Exploration Agency (JAXA) has planned to perform exposure experiments in space using the Russian Service Module “Zvezda” and the Japanese Experiment Module “KIBO” of the International Space Station (ISS). Both KIBO and Zvezda are presented in Fig. 1.



(a) Russian Service Module “Zvezda”



(b) Japanese Experiment Module “KIBO”



(c) Positions of KIBO and SM on ISS

Figure 1 External views of KIBO and Zvezda

## 2. Purpose of experiments

These experiments are designed to elucidate characteristic change behaviors and to clarify degradation mechanisms of exposed materials to the LEO environment over a long period. Fig. 1 shows that the positions of the KIBO and the Zvezda differ on the ISS. In fact, the KIBO is situated in the front of the ISS, with the Zvezda in the back. They provide opportunities for exposure experiments in different space environments and orientations. Through on-orbit experiments, irradiation of atomic oxygen, ultraviolet rays, and electron beams will be performed on the ground as a reference experiment to establish an evaluation method of space environmental effects on materials [3].

## 3. SM/MPAC&SEED experiment

The experiment on the Zvezda is called the Service Module / Micro-Particles Capture and Space Environment Exposure Device (SM/MPAC&SEED). The orbital position of SM/MPAC&SEED on ISS is depicted in Fig. 2.

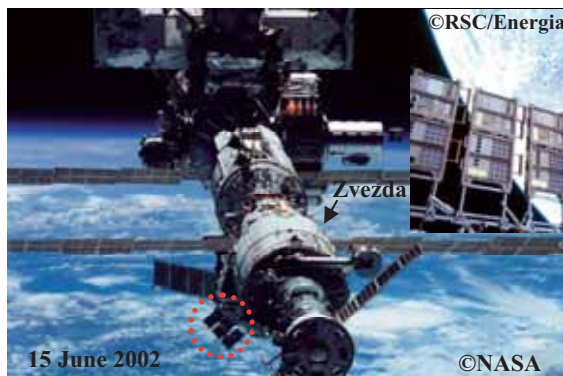


Figure 2 Orbital position of SM/MPAC&SEED

Actually, SM/MPAC&SEED includes both MPAC and SEED. The latter is a passive experiment designed simply to expose materials; it is shown in Fig. 3. The part enclosed in a red dotted line in the figure is MPAC. It is mounted on a collapsible frame that is 1 m long when open, which it shares with MPAC: it is a passive experiment designed to sample the micro-meteoroid and space-debris environment, and to capture particle residue for later chemical analysis using aerogel, polyimide foam, and 6061-T6 aluminum. More detailed descriptions of the MPAC and SEED on the Zvezda are reported elsewhere [4]–[7].

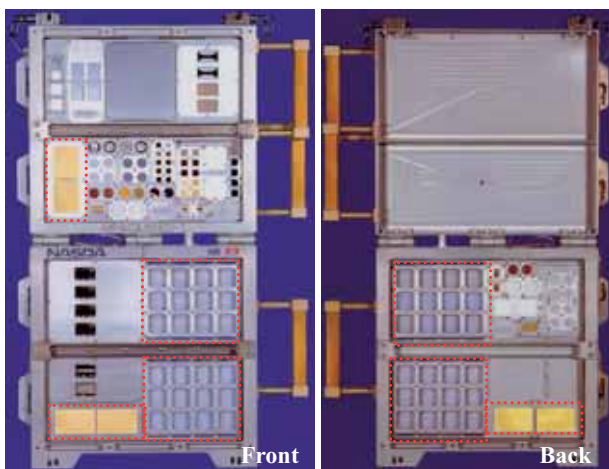


Figure 3 Photographs of SM/MPAC&SEED  
(570 (W)×900 (H)×156 (D) [mm])

Three identical SM/MPAC&SEED units (MPAC&SEED #1, #2, and #3) were attached to the Zvezda. The SM/MPAC&SEED was launched aboard a Progress M-45 on 21 August 2001. MPAC&SEED #1, was retrieved during EVA after 315 days of on-orbit exposure. Subsequently, MPAC&SEED #2 was retrieved on 26 February 2004 (after 865 days). Finally, MPAC&SEED #3 was retrieved on 18 August 2005 (after 1403 days).

## 4. JEM/MPAC&SEED experiment

### 4.1 Outline of KIBO

The experiment conducted on the KIBO is called the Japanese Experiment Module / Micro-Particles Capture and Space Environment Exposure Device (JEM/MPAC&SEED).

Here, the KIBO lightly is explained. The KIBO is composed of six main part; such as the Pressurized Module (PM), the Experiment Logistics Module-Pressurized Section (ELM-PS) in the pressurizing part, the Exposed Facility (EF), the Experiment Logistics Module-Exposed Section (ELM-ES) in the exposure part, the Remote Manipulator System (JEMRES) of the manipulator only for KIBO, and the Inter-orbit Communication System (ICS). These are presented in Fig. 4. The EF installs various experiment equipments. One of these experiment equipments is a experiment equipment that is called the Space Environment Data Acquisition Equipment-Attached Payload (SEDA-AP). JEM/MPAC&SEED is installed in the SEDA-AP.

The KIBO is divided into three parts, carried to the ISS respectively by the space shuttle, and assembled. The ELM-PS has already been launched by 1J/A mission (STS-123 mission). The PM and JEMRES will be launched by 1J mission (STS-124 mission) as follows. Finally, the EF and the ELM-ES will be launched by 2J/A mission (STS-127 mission).

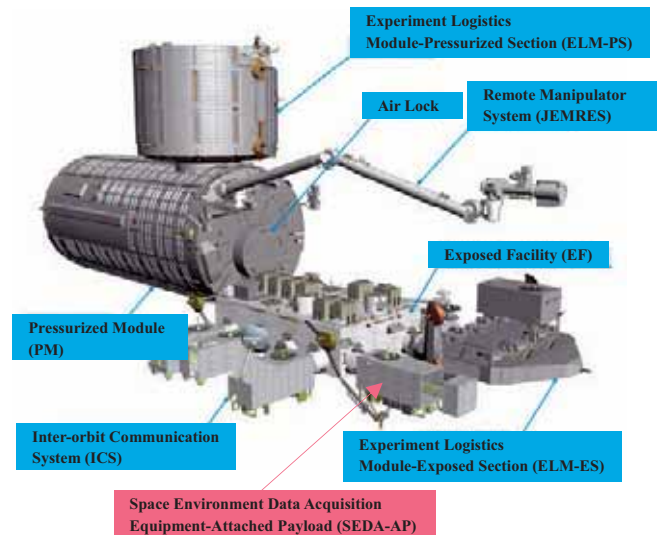


Figure 4 Composition of KIBO

### 4.2 Outline of SEDA-AP

The SEDA-AP has eight space environments and effect monitoring experiment sensors [8]: JEM/MPAC&SEED is one experiment component. Fig. 5 shows the composition of the SEDA-AP. To investigate interaction with the space environment and its effects on the KIBO/EF, SEDA-AP measures the space environment (neutrons, plasma, heavy ions high-energy light particles, atomic oxygen and MMOD) and



environmental effects on space materials and electronic devices. The sensors are the following: (1) NEutron Monitor (NEM), (2) Heavy Ion Telescope (HIT), (3) Plasma Monitor (PLAM), (4) Standard Dose Monitor (SDOM), (5) Atomic Oxygen Monitor (AOM), (6) Electronic Device Evaluation Equipment (EDEE), (7) MPAC, and (8) SEED. Also, JEM/MPAC&SEED comprises MPAC and SEED hardware.

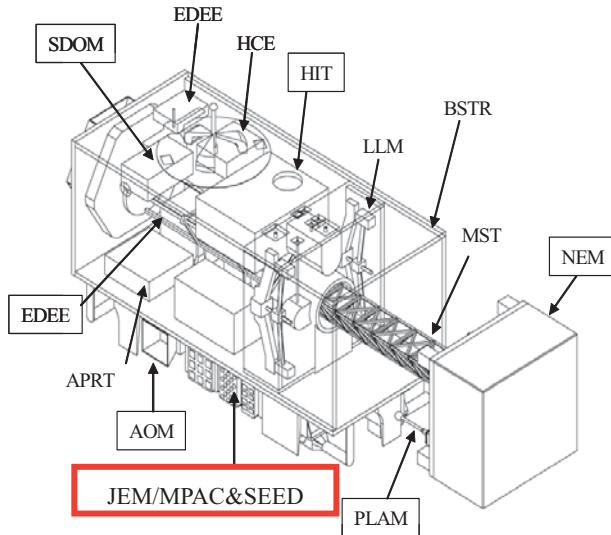


Figure 5 Composition of SEDA-AP

#### 4.3 Outline of JEM/MPAC&SEED

The positions of the SEED samples, including the space environment monitoring samples and silica aerogel and gold plate for MPAC are shown in Fig. 6 and Table 1. The MPAC and the SEED samples are installed on Sample assembly (Sample Units 1–3 etc.).



Figure 6 Photographs of JEM/MPAC&SEED  
((450 (W)×220 (H)×190 (D) [mm])

The MPAC has two functions; capturing space debris and micrometeoroids of 0.001–0.1 mm diameter and measuring their flux on orbit. Silica aerogel is used for MPAC on Sample Unit 1 to capture microparticles with minimum damage. Gold plate is used for MPAC on Sample Unit 2 to investigate the flux of impacts on it.

The SEED has holders to expose nine material samples (25.4 mm (1 inch) dia. and 32.3 mm (1.27 inch) dia) and space environment monitoring samples on Sample Units 2 and 3. Some SEED samples, MoS<sub>2</sub> on Ti-6Al-4V, white paint,

modified polyimide film and UPILEX-125S were also on board SM/MPAC&SEED. Degradation data from these materials will be compared with the SM/MPAC&SEED result. The sample newly installed is five of the following; such as Ge-coated Black Kapton, Black Kapton, BSF-30, ITO coated UPILEX-25S and Black paint (Only the black paint is not exposed to space.). Although it is a commercial polyimide that was not fundamentally intended for space use, BSF-30 is expected to have high durability against AO. This material is expected to be useful for applications for space use on LEO.

Actually, JEM/MPAC&SEED is exposed to the space environment attached on the SEDA-AP which is on the KIBO/EF. The exposure experiment period will be about ten months. After the exposure experiment end, the sample assembly is detached from the SEDA-AP, and returned to the ISS. The sample is scheduled for retrieval to the ground on the final shuttle flight (19A mission).

Table 1 SEED material list

SEED samples	SEED space environment monitoring samples
Solid lubricants / MoS <sub>2</sub> on Ti-6Al-4V	UV monitor / ITO coated DUS601 (Urethane Sheet)
White paint / NOVA 500 ASTRO WHITE	Dosimeter1 / RADFET
Black paint / NOVA 500 ASTRO BLACK	Dosimeter2 / ALANINE Dosimeter
Ge-coated Black Kapton	Dosimeter2 / TLD
Black Kapton	AO monitor / Vesplel
Polysiloxane-Block-Polyimide Film "BSF-30"	Temperature / Thermo Label
Modified Polyimide film /Siloxane Coated PI	
ITO coated UPILEX-25S	
UPILEX-125S	

#### 5. Ground Reference Experiment

For detailed clarification of the degradation mechanism of exposed materials, reference experiments will be conducted on the ground. Irradiation of atomic oxygen, ultraviolet rays, electron beams and their combined irradiation will be carried out under the same conditions as those in orbit. Irradiated materials will be measured for their changes of mass, solar absorptivity, emissivity, etc.; in addition, their irradiated surfaces will be observed. These results of ground reference experiments are effective to clarify damage mechanisms of irradiated materials by atomic oxygen, ultraviolet rays, and electron beams. It is also exposed such that not only the influences of each single irradiation to materials but also synergistic effect of combined irradiation to materials can be observed from results of ground reference experiments.

#### 6. Conclusion

The KIBO Exposed Facility is located on the front side of the ISS. There is no payload except for the ICS in the field of view of JEM/MPAC&SEED. For that reason, contamination effects are expected to be smaller than for SM/MPAC&SEED.



Degradation data from JEM/MPAC&SEED will be compared with results of SM/MPAC&SEED. In addition, a new finding is expected to be obtained according to the data new samples in JEM/MPAC&SEED. Moreover, the examination result of JEM/MPAC&SEED and SM/MPAC&SEED is expected to lead to the improvement of the experiment accuracy of Ground Reference Experiment.

### 7. Acknowledgment

We appreciate the work of all people involved in the development and operation of the SM/MPAC&SEED and JEM/MPAC&SEED projects.

### 8. References

- [1] <http://matdb.jaxa.jp/SpaceExperiment/Image/MFD-ESEM-E.pdf>
- [2] Tsutomu Fukatsu et al., "Post-flight Analysis of the exposed materials on the EFFU", Proc. of the 7th Symposium of Materials in a Space Environment, pp.287-292, 1997
- [3] Yoshiaki Tachi et al., "Outline of Space Environment Exposure Experiment on ISS", ISTS 2000-h-17
- [4] Ichiro Yamagata et al., "Overview of the Micro-Particles Capturer and Space Environment Exposure Device (MPAC&SEED) Experiment", Proc. of the 10th International Symposium on "Materials in a Space Environment" (ISMSE) and 8th International Space Conference on "Protection of Materials and Structures from the Space Environment" (ICPMSE), June 2006
- [5] Michael J. Neish et al., "Passive Measurement Of Dust Particles on the ISS Using MPAC: Experiment Summary, Particle Fluxes And Chemical Analysis", Proc. of the Fourth European Conference on Space Debris, Darmstadt, Germany, 18-20 April 2005 (ESA SP-587, August 2005)
- [6] Yugo Kimoto et al., "Passive measurement of atomic oxygen, UV fluence, and radiation effect on the ISS using the SEED experiment", Proc. of the 10th International Symposium on "Materials in a Space Environment" (ISMSE) and 8th International Space Conference on "Protection of Materials and Structures from the Space Environment" (ICPMSE), June 2006
- [7] Yugo Kimoto et al., "Japanese Space Materials Exposure Experiment Utilizing International Space Station", Proc. of the 59<sup>th</sup> International Astronautical Congress (IAC) 2006.
- [8] P. R. Young and W. S. Slemp, "Chemical Characterization of Selected LDEF Polymeric Materials", LDEF -69 Months in Space, NASA-CP-3134 1991

## FUTURE SPACE EXPOSURE EXPERIMENT BEYOND 2011 -ITS PROBLEMS AND NEW CHALLENGES-

Masahito TAGAWA

*Graduate School of Engineering, Kobe University, Kobe, Hyogo 657-8501, Japan*

In Japan, the largest material exposure program "SM/MPAC&SEED (Service Module/ Micro-Particles Capturer and Space Environment Exposure Device) Experiment" has been completed. This program is quite ambitious among the other Japanese materials exposure tests; 3 sets of samples have been exposed for 1, 2 and 3 years in orbit in order to discover the fluence dependence of the material responses. We have learned a lot of lessons from this program. Based on the lessons learned, the "Advanced Material Exposure Test Working Group" has been established by the Committee on Space Utilization in 2007. This working group discussed the current problems of the material exposure program (flight tests) and proposed the future direction of the experimental methodologies. In this presentation, problems and new challenges discussed in this working group will be discussed.

**Keywords:** MPAC&SEED, Space Exposure, Material, ISS, Space Environment, Low Earth Orbit

### 1. Introduction

The materials exposure program "SM/MPAC&SEED (Service Module/ Micro-Particles Capturer and Space Environment Exposure Device) Experiment" has been completed. This program is quite ambitious among the other materials exposure tests held in Japan; 3 sets of samples have been exposed for 1, 2 and 3 years in order to discover the fluence dependence of the material responses. Detail of the program is described in companion papers of this symposium. We have learned a lot of lessons from this program not only every material response, but also the methodology of a material test. Based on the lessons learned, the "Advanced Material Exposure Test Working Group" has been established with a permission of the Committee on Space Utilization in 2007. This working group discussed the current problems of the material exposure program in Japan and proposed the future direction of the experimental methodologies. The environment surrounding the space exposure tests is greatly changing. Building of the International Space Station (ISS) is in the final stage, and the Japanese Experimental Module (JEM or Kibo) will soon be operational which equips Exposure Facility (EF) usable for material exposure testing. As well as Kibo, US module and EU module of ISS compartment also equip their own EF at the outside of the module. It is, therefore, stated that the infrastructures for the material testing at ISS will soon be established. However, due to the delay of the construction schedule of ISS, another problem arises; space shuttle will be retired after the accomplishment of ISS in 2010. The major transportation system will not be available for material testing beyond 2011. New methods for material testing have to be developed to match the new circumstances of the flight tests.

In this talk, the discussion in the "Advanced Material Exposure Test Working Group" regarding new material exposure testing method suitable for Japan is reported.

### 2. Advanced material exposure test working group

#### 2.1 Purpose

The purpose of "Advanced Material Exposure Test Working Group" is to discuss the problems of the current "passive" in-orbit material exposure tests and to propose the methodologies for advanced material exposure tests including in-situ or acceleration test capabilities. A new protocol for ground-based simulation considering the effect on differences in environmental factors in space and on ground tests will also be discussed in this working group. The goal of this working group is to establish the methodologies for space exposure tests to develop the advanced space materials suitable for Japan.

#### 2.2 Member

The "Advanced Material Exposure Test Working Group" consists of nine Japanese researchers on the space environmental effect on space materials. Five members are from JAXA and four from Universities.

Masahito Tagawa	(Kobe University, Chair)
Mengu Cho	(Kyushu Institute of Technology)
Mineo Suzuki	(JAXA)
Rikio Yokota	(JAXA)
Minoru Iwata	(Kyushu Institute of Technology)
Koji Matsumoto	(JAXA)
Eiji Miyazaki	(JAXA)
Hiroyuki Shimamura	(JAXA)
Kumiko Yokota	(Kobe University)

This working group is the first attempt in Japan to reflect on the past material exposure mission from the viewpoint of mission design and management including outside opinion of JAXA.

### 3. Past Japanese flight missions

#### 3.1 Overview of the past missions

Three flight experiments have been performed in Japan to study material responses in actual space environment, i.e.,

**Table 1 Japanese material exposure missions.**

Mission	SFU/EFFU	MFD/ESEM	SM/MPAC&SEED
Launch date	Mar. 18, 1995 H2	Aug. 7, 1997 STS-85	Oct. 1, 2001 Progress
Retrieval date	Jan. 13, 1996 STS-72	Aug. 12, 1997 STS-85	Aug. 18, 2005 Soyuz
Exposure time	10 month	54 hour	315-1403 days
Altitude & Inclination	482 km 28.5 deg.	315 km 57 deg.	400 km 51.6 deg.
Samples	22	21	23

Space Flyer Unit/ Exposed Facility Flyer Unit (SFU/EFFU) [1], Manipulator Flight Demonstration/Evaluation Space Environment and Effects on Materials (MFD/ESEM) [2] and SM/MPAC&SEED [3]. SFU/EFFU experiment was flown by the Japanese satellite, and MFD/ESEM experiment was carried out in the cargo bay of the space shuttle orbiter. In contrast, SM/MPAC&SEED was done on ISS. Detail data of these flight experiments are summarized in Table 1. Exposure periods of these flight experiments are from 54 hours to 3 years.

Among these three missions, SM/MPAC&SEED is the most complicated mission, i.e., fluence dependence of the material responses to the space environmental factors such as atomic oxygen, radiation and ultraviolet were analyzed. Compared to the similar type of US mission (MISSE) [4], difference in mission concept is obvious. Namely, MISSE pallet carries wide variety of samples (more than 2000 samples), however the exposure period is not a primary point of interest. In contrast, SM/MPAC&SEED exposed only selected samples (approximately 20 samples) for multiple fluence conditions. This is probably due to the fact that the US has their own method to transfer the samples to/from ISS, but Japan does not have their own such a transportation method.

### 3.2 Lessons learned

In these past "successful" missions, we still have had some problems. It should be recorded somewhere and have to be used to improve the next flight mission. Unfortunately, the former attempt is not enough to share the past experiences among the scientists of the following missions. The author

believes this is the first official report in Japan on the problems of material exposure mission including the mission designing point of view.

One of the most important issues to be addressed is the contamination effect on the passive space exposure test. SFU/EFFU and SM/MPAC&SEED missions, sample surfaces were severely contaminated by the silicone vapor. Figure 1(a) and 1(b) show the X-ray photoelectron spectroscopic (XPS) data of the control and the 1-year-exposed samples of MoS<sub>2</sub> aboard SM/MPAC&SEED. After one year of exposure at Service Module of ISS, Mo3d (228 eV) and S2p (168 eV) signal almost disappeared and Si2s (151 eV) and Si2p (103 eV) signals became obvious. Figure 1(c) shows the XPS spectrum of the 3-year-exposed sample. Mo3d signal disappears and MoS<sub>2</sub> surface is completely covered by silicone contamination. Since Mo reacts to atomic oxygen and formed MoO<sub>3</sub>, which is not a volatile product, the MoS<sub>2</sub> surface could be covered by MoO<sub>3</sub> after atomic oxygen exposure. If this phenomenon is confirmed in this flight experiment, the predicted robustness of MoS<sub>2</sub> lubricant in an atomic oxygen environment could be proved in LEO [5, 6]. It is, however, SiO<sub>2</sub> contamination layer interferes this atomic oxygen reaction with Mo, and made it difficult to confirm the protection effect.

SiO<sub>2</sub> contamination layer blocks the atomic oxygen reaction not only with Mo, but also with polyimide which is the witness sample to measure atomic oxygen fluence. This makes the evaluation of atomic oxygen fluence difficult. Accuracy of atomic oxygen fluence measurement in SM/MPAC&SEED mission became low due to the presence of SiO<sub>2</sub> contamination. This is the major problem of

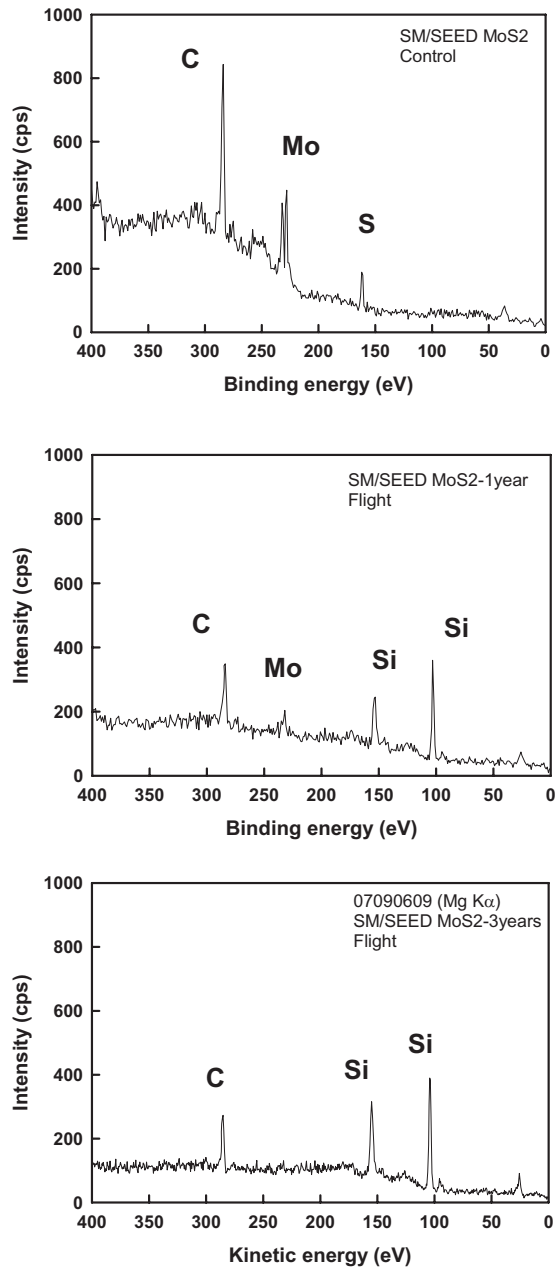


Fig.1 X-ray photoelectron spectra of control, 1-year and 3-year-exposed samples of MoS<sub>2</sub> aboard SM/MPAC&SEED.

material-related part of the SM/MPAC&SEED mission. The SiO<sub>2</sub> contamination may also influence UV and radiation monitor but has not been evaluated.

This contamination problem was not a new issue on SM/MPAC&SEED. Similar problem has been experienced in SFU/EFFU mission. In this first Japanese material exposure mission, many samples were covered by SiO<sub>2</sub> contamination. However, effective countermeasures were not taken in the following material exposure missions, even though the presence of contamination is expected. At least, the witness samples should be protected from contaminations.

#### 4. Current problems and solutions

##### 4.1 Too small chances to send the samples in orbit, too long preparation period and rigidity of the program

This is the common problem for all space programs. Because new functional materials are being developed, the requirements of space qualification test for such new materials are always arising. Due to the high-speed of the development of materials, preparation period of the material exposure test is 2-3 years at maximum. Otherwise, feedback of the exposure results to the material development process becomes impossible. Fast, cheap and better is the key for future material exposure mission. This is the same solution for the satellite system itself. The solution is also the same as satellite system, i.e., use of small, unmanned satellites for material exposure test. This will decrease the cost and time for material test and increase the chance to send samples to orbit as a piggyback mission. The unmanned mission can simplify the safety inspection process. It would solve the rigidity of the program. Also orbits other than ISS orbit can be used for the material test. It will be useful especially for the radiation test in polar orbit. On the other hand, in-situ monitoring technology has to be developed for this type of application. This is a technological challenge compared to the current "passive" experiment.

##### 4.2 Monitoring method of space environmental factors need to be reconstructed

Contamination control is a key for the passive material exposure test as described in Section 3. New monitoring methods (or device) for space environmental factors, including the methods for elimination of contamination, have to be developed. For the contamination control purpose, a hood or a skimmer system (Figure 2) would be effective, because atomic oxygen or UV in space is a directional beam but contamination is diffusive. Thus, a hood which restricts the field of view of the sample is a simple solution. Double skimmer system is the more appropriate but is weak for the misalignment from the velocity vector. These devices do not require any power and large mass attachment. It is worth trying in the future passive exposure test.

Witness samples of atomic oxygen, ultraviolet or radiation fluencies should be well-understood in its synergistic effect. For example, polyimide (or Kapton-H), which is widely used as

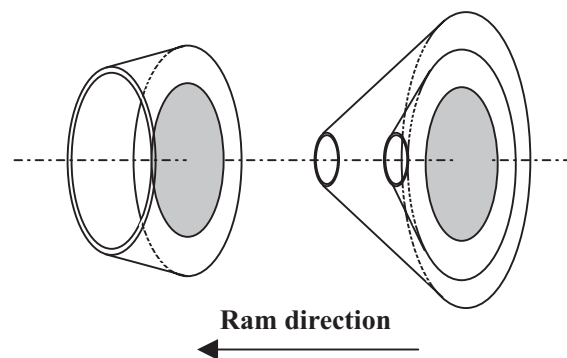


Fig.2 A hood (left) or a double skimmer system (right) for eliminating possible contamination.



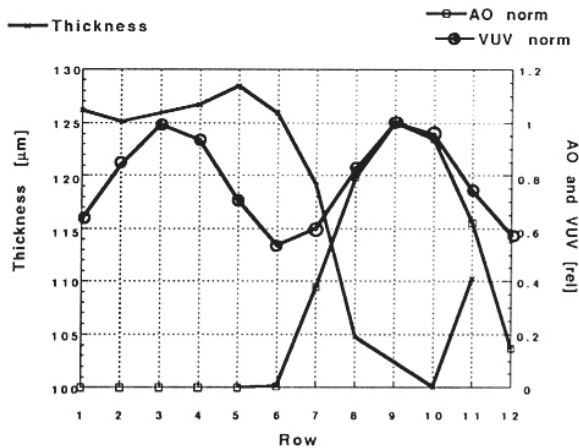


Fig.3 LDEF results regarding FEP Teflon degradation [8].

an atomic oxygen witness sample, show increase in mass loss with a certain environment which includes atomic oxygen and ultraviolet simultaneous exposure [7]. This leads to the overestimation of the atomic oxygen fluence; i.e., underestimation of the atomic oxygen effect on targeted materials. All of the witness samples, which measure the experimental parameter, should be well analyzed for their responses in a complicated space environment.

#### 4.3 Experimental data obtained by the past tests are not enough disclosed. A division that controls all of the material exposure programs must be established in Japan.

This might be a Japanese specific problem, but the results of the past material exposure test are not well disclosed even for the Japanese researchers. For improving the methods or materials for the next material exposure test, the past data should be disclosed for those who needed. At least, a division of JAXA should control all of the data and ready for the future requirement. According to the suggestion by the working group, the material group of JAXA will take this role.

#### 4.4 Main purpose of exposure program is not clear; screening test of space materials or reference data?

As pointed out in 4.1, opportunity of material exposure test in LEO is limited. It is not realistic to send all of the materials to space to evaluate their survivability in space environment. Only selected materials can be flown on the material exposure test. This limitation comes mainly from the fact that Japan does not have method to retrieve the samples. This may also reflect the difference in mission design of MISSE and SM/MPAC&SEED as described earlier. In such a situation, how should the materials be selected for the flight experiment in Japan? Newly developed materials will not have a chance to evaluate their survivability in space environment. Survivability of the materials will have to be evaluated through the ground-based simulation test. In that case, accuracy of the ground-based simulation test is quite important. In order to increase the accuracy of the ground-based simulation test, flight test should provide the reference data for the ground-based simulations. In order to obtain the reference data, passive

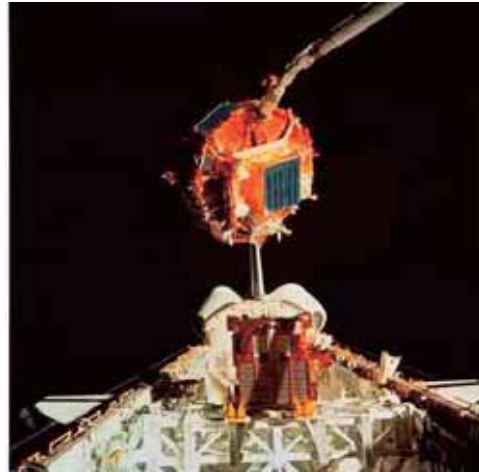


Fig.4 Retrieval of the SFU spacecraft by STS-72 mission.

experiment has a problem; only integrated data can be analyzed over the exposure period. Figure 3 represents the erosion of FEP Teflon obtained by LDEF [8]. Erosion of the FEP Teflon at the leading edge of LDEF satellite (ram direction) is clearly observed. This data can be implied that the degradation of FEP Teflon occurs on by atomic oxygen exposure or by the simultaneous exposure of atomic oxygen and ultraviolet; not by ultraviolet alone. However, due to the difficulty for atomic oxygen testing on the ground, this problem has not been clarified yet. The real-time measurement of erosion in space provides direct evidence on these problems. A quartz crystal microbalance (QCM) is a promising technique to provide these data. QCM has been applied in space to measure a contamination on satellites during its operation [9]. On the other hand, it has also been used for material degradation research on the ground. Thus, integration of these two examples easily realizes the real-time mass loss of the samples during the flight test. The advantage of this method will be demonstrated by MISSE-6 in 2008 [10].

#### 4.5 Methods to retrieve the exposed samples after the retirement of Shuttle are in the dark. Freedom of the flight experiment is quite limited by the capacity of the Soyuz spacecraft.

The retrieval of the exposed samples to Earth is made by the Space Shuttle in two of three past flight experiments in Japan (Figure 4). However, Space Shuttle is scheduled to be retired in 2010. After 2011, sample retrieval from the orbit has to be carried out by Soyuz. The capacity of Soyuz is limited and only small pallet can be retrieved. New exposure pallet should be designed to fit the capacity of Soyuz. It should be specially designed to maximize the spatial efficiency, i.e., sample density has to be increased significantly compared to SM/MPAC&SEED. However, due to the dimensional limitation, the complex equipment cannot be attached on the pallet. This restricts the freedom of the experimental design. For well-controlled exposure experiment, development of new transportation system with a large capacity is mandatory. With a marginal capacity of retrieval system, we can arrange some social experiments for next generation space scientists;

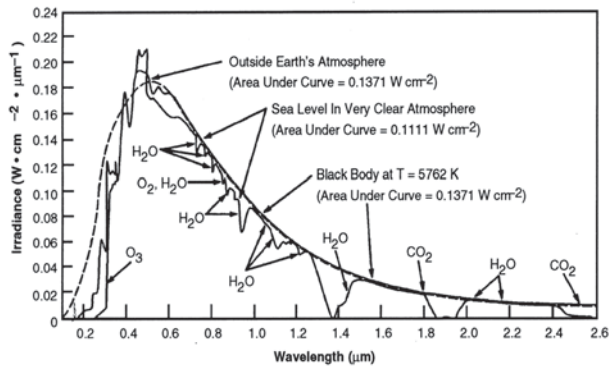


Fig.5 UV/VIS/IR spectrum in space [11].

for example, space-experienced rice seed distribution to all Japanese primary schools for growing experiment in biology.

### 5. Role of ground-based simulation

In order to evaluate the survivability of newly developed materials in space environment without sending the sample into space, the accuracy of the ground-based simulation test should be improved. Present technology of the ground-based space environmental simulation is not enough to predict the material response in real space environment. Absolute pressure and temperature in space can be simulated in the ground-based test. However, some other environmental factors are difficult to simulate in ground-based studies accurately. The inconsistency of the result of ground-based test with that of flight test is due mainly to the differences in experimental conditions between space and ground. Some examples of the experimental conditions which are difficult to simulate in ground-based experiments are listed below: (1) ultraviolet spectrum and intensity (Figure 5); (2) impact velocity of atomic oxygen both average and distribution, (Figure 6) and its peak flux; (3) energy spectrum and intensity of the radiation; and (4) the synergistic effects of these environmental factors.

In order to increase the accuracy of the predictions, differences in experimental conditions between space and ground should be considered quantitatively. This should be applied to the reference materials first. For example, temperature, angular and impact energy dependences on the atomic oxygen-induced etching of polyimide should be made clear. These erosion properties are necessary to measure the atomic oxygen fluence both in space and in ground-based simulations. The same data set is required to calculate the erosion depth of any material with computer code. Well-controlled ground-based experiment can only provide such basic properties of atomic oxygen erosion phenomenon [14, 15]. In the field of ground-based space environmental simulation, basic properties of material responses with space environmental factors have not been understood deeply. Sometimes, it is even difficult to judge whether the ground-based simulation is severer or milder compared to flight environment. Thus, improvement of the ground-based simulation technology is important even in the space-engineering field to assess the reliability of the materials.

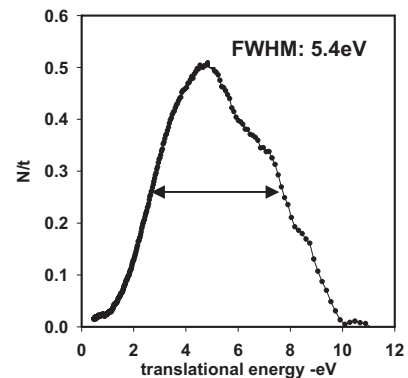
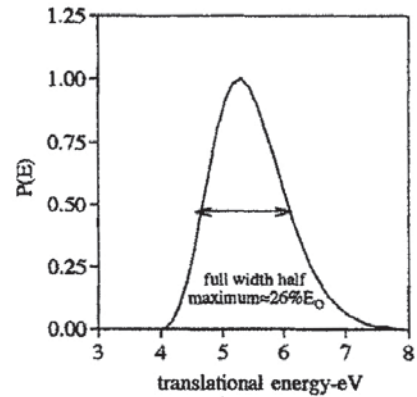


Fig.6 Translational energy distributions of atomic oxygen in LEO (upper panel) [12] and in the ground simulator (lower panel) [13].

### 6. Conclusions

The "Advanced Material Exposure Test Working Group" was established to overlook the past Japanese material exposure missions and to propose the future material exposure tests. From the lessons learned by the past missions, importance of contamination control to the "passive" material exposure test is addressed. In order to increase the freedom of experiment in space, use of unmanned small satellites is proposed. Due to the retirement of space shuttle, necessity of development new compact integrated pallet and new transportation system is also mandatory. Because of the limitation of the space exposure material test opportunity, increase in accuracy on the ground-based experiment has to be important.

### Acknowledgments

"Advanced Material Exposure Test Working Group" has been established by the Committee on Space Utilization. Stimulated discussion in the Working Group is appreciated for preparing this manuscript.

### References

- [1] T. Fukatsu, Y. Torii, Y. Koyari et. al.: Postflight Analysis of the Exposed Materials on EFFU, Proceedings of the 7th ISMSE, June 16-20, 1997.
- [2] Evaluation and Analysis of Parts and Materials installed on MFD-ESEM, ISSN 1345-7926, NASDA-ETR-020002 (NASDA-TMR-000011)

- [3] I. Yamagata, Y. Kimoto, E. Miyazaki, J. Ishizawa, H. Shimamura, N. Baba, K. Imagawa, and M. Suzuki: Overview of the Micro-Particles Capturer and Space Environment Exposure Device (MPAC&SEED) experiment, *Proc. 10th ISMSE*, ESA-SP-616 (2006) and papers in this proceeding book.
- [4] <http://misssl.larc.nasa.gov/>
- [5] M. Tagawa, K. Yokota, N. Ohmae, K. Matsumoto, M. Suzuki: Hyperthermal atomic oxygen interaction with MoS<sub>2</sub> lubricants relevance to space environmental effects in low earth orbit –atomic oxygen-induced oxidation-, *Tribology Letters*, Vol.17, No.4 (2004) pp.859-865.
- [6] M. Tagawa, M. Muromoto, S. Hachiue, K. Yokota, N. Ohmae, K. Matsumoto, M. Suzuki: Hyperthermal atomic oxygen interaction with MoS<sub>2</sub> lubricants relevance to space environmental effects in low earth orbit -effects on friction coefficient and wear life-, *Tribology Letters*, Vol.18, No.4 (2005) pp.437-443.
- [7] K. Yokota, N. Ohmae, M. Tagawa: Effect of relative intensity of 5 eV atomic oxygen and 172 nm vacuum ultraviolet in the synergism of polyimide erosion, *High Performance Polymers*, Vol.16, No.2 (2004) pp.221-234.
- [8] B. Weihs and M. V. Eesbeek: Secondary VUV Erosion Effects on Polymers in the ATOX Atomic Oxygen Exposure Facility, *Proceedings of the 6th International Symposium on Materials in a Space Environment*, ESA-SP368 (1994) pp. 277-283
- [9] D. A. Wallace, S. A. Wallace: High Mass Sensitivity Miniaturized Quartz Crystal Microbalances (QCMs) for Space Application, *Proceedings of the 7th International Symposium on Materials in a Space Environment*, ESA-SP368 (1994) pp. 161-168.
- [10] T. K. Minton, private communication,
- [11] B. J. Anderson, R. E. Smith: Natural Orbital Environment Guidelines for Use in Aerospace Vehicle Development, *NASA-TM 4527* (1994).
- [12] S. L. Koontz, L. J. Leger and J. T. Visentine: EOIM-III Mass Spectrometry and Polymer Chemistry, *Journal of Spacecraft and Rockets*, Vol. 32, No. 3 (1995) pp. 483-495.
- [13] K. Kishida, K. Yokota, M. Tagawa, to be published.
- [14] K. Yokota, M. Tagawa, N. Ohmae: Temperature dependence in erosion rates of polyimide under hyperthermal atomic oxygen exposures, *Journal of Spacecraft and Rockets*, Vol.40, No1, 2003 pp143-144
- [15] K. Yokota, M. Tagawa, N. Ohmae: Impingement angle dependence of erosion rate of polyimide in atomic oxygen exposures, *Journal of Spacecraft and Rockets*, Vol.39, No.1 (2002) 155-156.